BEILSTEIN JOURNAL OF ORGANIC CHEMISTRY

Antibiotic and cytotoxic peptides

Edited by Norbert Sewald

Imprint

Beilstein Journal of Organic Chemistry
www.bjoc.org
ISSN 1860-5397
Email: journals-support@beilstein-institut.de

The *Beilstein Journal of Organic Chemistry* is published by the Beilstein-Institut zur Förderung der Chemischen Wissenschaften.

Beilstein-Institut zur Förderung der Chemischen Wissenschaften
Trakehner Straße 7–9
60487 Frankfurt am Main
Germany
www.beilstein-institut.de

Beilstein Journal of Organic Chemistry

Antibiotic and cytotoxic peptides

Norbert Sewald

Editorial

Open Access

Address:
Bielefeld University, Department of Chemistry, Organic and Bioorganic Chemistry, Universitätsstr. 25, 33615 Bielefeld, Germany

Email:
Norbert Sewald - norbert.sewald@uni-bielefeld.de

Keywords:
antibiotic; cytotoxic; peptides

Beilstein J. Org. Chem. **2012,** *8,* 1144–1145.
doi:10.3762/bjoc.8.127

Received: 05 July 2012
Accepted: 06 July 2012
Published: 24 July 2012

This article is part of the Thematic Series "Antibiotic and cytotoxic peptides".

Guest Editor: N. Sewald

Through evolution, nature has provided practically all organisms with secondary metabolites: chemical compounds that provide the producing species with specific protective mechanisms or other advantages. Among these, there are, e.g., peptides that display antibiotic/antimicrobial activity. These have been isolated from plants, invertebrates, vertebrates, and humans, but also from microorganisms. Some antibiotic peptides are an essential part of innate immunity, which has evolved in most organisms to combat microbial challenge. In addition, antimicrobial peptides sometimes also display cytotoxicity against mammalian cells.

There are several good reasons for a Thematic Series in the *Beilstein Journal of Organic Chemistry* on "Antibiotic and cytotoxic peptides": The fight against bacterial infections is in a critical phase. The excessive application of antibiotics in human therapy, and also in livestock breeding, leads to the rapid development of highly virulent bacterial strains resistant to the conventionally applied antibiotics. Consequently, the search for new antibiotically active compounds is of premier importance. On the other hand, highly cytotoxic peptides and peptide analogues, such as monomethyl auristatin E, are used as the "warhead" in antibody–drug conjugates for tumor therapy, as approved recently by the FDA [1].

It is a privilege of synthetic chemists to be able to modify natural products by total synthesis. Many naturally occurring compounds are highly complex, and their efficient total synthesis often is out of reach. However, in frequent cases structural simplifications have proven amenable, and the resulting compounds have sometimes been shown to retain biological activity. The challenge of discovering new antibiotically active or cytotoxic compounds persists. Moreover, peptides have experienced a renaissance during recent years with respect to their application in Medicinal Chemistry [2].

This Thematic Series on "Antibiotic and cytotoxic peptides" presents contributions from synthetic chemists active in the fields of peptides, peptidomimetics, drug design, and method development, in order to promote the research area further and to disseminate the interdisciplinary research efforts to a broader audience.

Norbert Sewald

Bielefeld, July 2012

References

1. Sammet, B.; Steinkühler, C.; Sewald, N. *Pharm. Pat. Analyst* **2012,** *1,* 65–73. doi:10.4155/ppa.12.4
2. Hoffmann, T.; Metternich, R. *Angew. Chem.*, in press. doi:10.1002/ange.201201677

License and Terms

Beilstein Journal of Organic Chemistry

Similarity analysis, synthesis, and bioassay of antibacterial cyclic peptidomimetics

Workalemahu M. Berhanu[1], Mohamed A. Ibrahim[1,2,3], Girinath G. Pillai[1], Alexander A. Oliferenko[1], Levan Khelashvili[1], Farukh Jabeen[4], Bushra Mirza[5], Farzana Latif Ansari[4], Ihsan ul-Haq[5], Said A. El-Feky[2] and Alan R. Katritzky*[1,6]

Full Research Paper

Open Access

Address:
[1]Center for Heterocyclic Compounds, Department of Chemistry, University of Florida, Gainesville, FL 32611-7200, USA, [2]Department of Pharmaceutical Organic Chemistry, Faculty of Pharmacy, Zagazig University, Zagazig-44519, Egypt, [3]Department of Organic Chemistry, College of Pharmacy, Misr University for Science and Technology, Al-Motamayez District, P.O. Box: 77, Egypt, [4]Department of Chemistry, Quaid i Azam University, Islamabad 45320, Pakistan, [5]Department of Biochemistry, Quaid i Azam University, Islamabad 45320, Pakistan and [6]Department of Chemistry, King Abdulaziz University, Jeddah 21589, Saudi Arabia

Email:
Alan R. Katritzky* - katritzky@chem.ufl.edu

* Corresponding author

Keywords:
antibacterial; cluster analysis; *N*-acylbenzotriazoles; peptidomimetics; similarity

Beilstein J. Org. Chem. **2012,** *8,* 1146–1160.
doi:10.3762/bjoc.8.128

Received: 24 February 2012
Accepted: 01 June 2012
Published: 24 July 2012

This article is part of the Thematic Series "Antibiotic and cytotoxic peptides".

Guest Editor: N. Sewald

Abstract

The chemical similarity of antibacterial cyclic peptides and peptidomimetics was studied in order to identify new promising cyclic scaffolds. A large descriptor space coupled with cluster analysis was employed to digitize known antibacterial structures and to gauge the potential of new peptidomimetic macrocycles, which were conveniently synthesized by acylbenzotriazole methodology. Some of the synthesized compounds were tested against an array of microorganisms and showed antibacterial activity against *Bordetella bronchistepica*, *Micrococcus luteus*, and *Salmonella typhimurium*.

Introduction

Diverse cyclic peptides, both natural and synthesized, are potent antibiotics [1-3]. Gramicidin S, vancomycine, bacitracin, polymixin B, colistin, valinomycin, actinomycin, and many more, have been tested and used clinically as antimicrobial and antifungal agents: It is believed that cyclic peptides are more stable to proteolysis due to the lack of free N- and C-termini, as well as reduced conformational freedom. Stability can also be achieved by modifying peptides into “peptidomimetics” that

mimic and/or stabilize the secondary structure that modifies associated biological processes, thus affording opportunities for drug design and development.

One strategy to create peptidomimetics couples a small-molecule scaffold with a peptide. Such scaffolds include aromatic rings or heterocycles, which may be positioned in the interior of the peptide chain [4,5] or at the C- [6-8] or N-terminus [9]. Many reports describe the successful use of heterocycles as peptide-bond surrogates or as potential protein-recognition motifs to achieve superior potency in biological assays [10-14].

Pyridines are well-established as important heterocycles in medicinally and biologically active compounds and also as important structural elements. Pyridine scaffolds possess important antiviral [15], anti-inflammatory [16,17], anticonvulsant [18], antibacterial [19], and antitumor pharmacological activities [20,21].

Chiral macrocyclic ligands have found wide application in asymmetric synthesis and enantiomeric recognition [22,23]. Incorporation of amino acids in abiotic anion receptors can lead to systems that mimic the anion coordination properties of anion-binding proteins [24]. Introduction of cysteine subunits into a macrocycle facilitates receptor synthesis and allows control of the relative direction of the two chains attached to the cysteine residue. For example, one of the early cysteine-containing macrocycles was designed to mimic the cation binding ability of valinomycin [24].

Numerous literature approaches to the synthesis of 17-, 18- and 24-membered rings utilize: (i) acyl chlorides, (ii) active esters and (iii) coupling reagents. However, some of the published literature methods involve the utilization of complex procedures, protection/deprotection strategies, harsh reaction conditions, and long reaction times; provide only low yields; and are plagued with difficulties associated with product purification [25-29]. According to the literature [30,31], most antimicrobial cyclic peptides are active in their cationic form. Cationic peptides are considered advantageous, because they adhere better to the outer anionic parts of phospholipid membranes.

Although anionic peptides are less common in clinical practice, they are gaining momentum, because natural anionic peptides are a part of the innate immune system of living organisms (located in human, ovine, and bovine lungs) and also serve as immunomodulators [32]. The activity of anionic peptides can be enhanced when associated with zinc cations and/or surfactants [30-32]. Anionic peptides bind with lysozyme, an important cationic hydrolytic enzyme. It is believed that the lysozyme opens the cell wall, "allowing a small anionic peptide to penetrate". Topical administration of such anionic peptides is possible, for example in the form of nasal or throat sprays but, at least one anionic peptide, daptomycin, is administered intravenously.

The abundance of natural and synthetic antimicrobial peptides and peptidomimetics of varying structure and activity reported raises the question of how their similarity or dissimilarity can be quantified and how synthetic efforts can be focused towards novel active compounds. It would be beneficial to be able to draw practical conclusions (even if approximate) based solely on the chemical structures of existing agents. In the case of cyclic peptides, the complex cyclomatic structure, involving smaller rings and heteroatoms, as well as a limited conformational flexibility, makes it difficult to classify or compare such compounds by their ring sizes. Fortunately, chemical informatics provides formalized procedures for comparing chemical compounds based on composition and structure. While the principle of molecular similarity is quite simple, that is, "similar compounds have similar properties", the unambiguous and automated implementation of this principle needed to be backed with a solid mathematical background; this has been accomplished and has made it possible to develop efficient similarity measures [33]. The simplest similarity measure of two molecules would be the Euclidian distance between them in a descriptor space, which is an abstract *n*-dimensional space spanned by *n* molecular descriptors, or parameters. More elaborate measures have been developed, such as the Tanimoto coefficient or the Tversky index [34]. Although a well-established concept, molecular similarity has previously been used almost entirely in the design of small-molecule drugs, with very few applications in other chemical disciplines. To the best of our knowledge, despite their promise of consistent analysis and comparison, the principles of molecular similarity have never been used in the design of peptides.

The aim of the present work is thus three-fold: (i) To identify promising peptidomimetic scaffolds by using molecular similarity; (ii) to design a range of cyclic pyridine-containing peptidomimetics capable of facile synthesis; and (iii) to synthesize and biotest promising candidates. A synthetic route seems highly relevant, since *N*-acylbenzotriazoles have been reported elsewhere [35-37] to be stable, easy-to-handle acylating agents and have found numerous applications for advantageous N-, O-, C- and S-acylations.

Results and Discussion

Similarity analysis

Our literature search identified the thirty three cyclic peptides and peptidomimetic structures given in Table 1. All the

minimum inhibition constants (MIC) are pertinent to *Staphylococcus aureus*. These include (i) one 12-membered ring cyclic tetrapeptide, (ii) two 14-membered ring peptidomimetics each with two peptide links, (iii) two 18-membered ring peptidomimetics each with five peptide links, and (iv) twenty seven 16-membered ring pentapeptides. Table 1 demonstrates that compounds of group (iv) show the best antibacterial activity, with compounds **24** and **27** being the most active. The side-chain substitution clearly controls the antibacterial activity, as the cyclic scaffold is identical. The 18-membered ring scaffold **37**, accessible through the benzotriazole route, provides an excellent opportunity for introducing substituents economically, through the proper choice of the dicarboxylic starting materials. While scaffold **37** and the 16-membered ring scaffolds described in Table 1 seem to be visually different, we undertook analysis of their proximity in a multidimensional descriptor space to afford a more rigorous comparison. Such analysis takes into account not only structural similarity features, but also electronic, charge-distribution, and hydrogen-bond characteristics. We generated such a multidimensional descriptor space for all structures in Table 1 as well as for structures **37a**–**c**, using CODESSA-Pro software [38]. Clustering of the structures in such a multidimensional space is the natural choice for similarity analysis.

Table 1: Structures of cyclic peptides with their MIC values.

Structure	Cluster number	Observed MIC (μg/mL)	Ref.
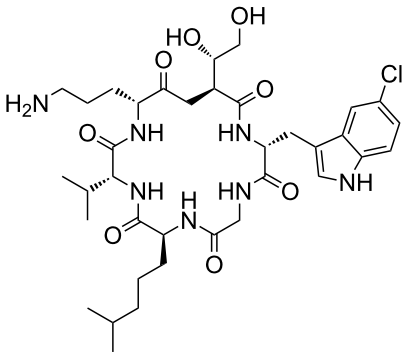 **1**	3	8.0	[39]
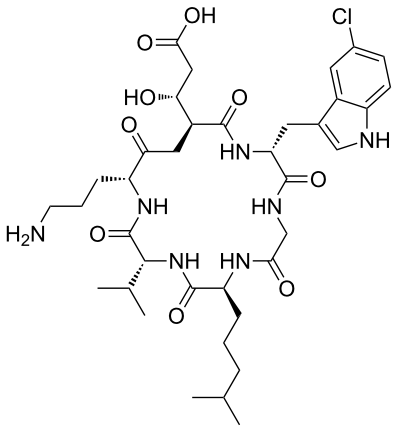 **2**	2	16	[39]
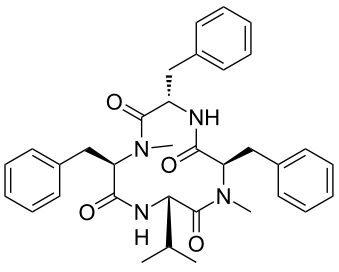 **3**	3	--	[40]

Table 1: Structures of cyclic peptides with their MIC values. (continued)

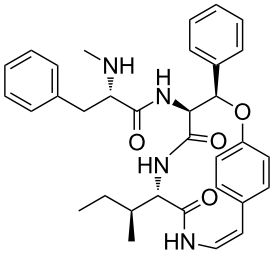 **4**	3	3.12	[41]
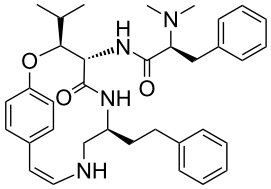 **5**	3	3.12	[42]
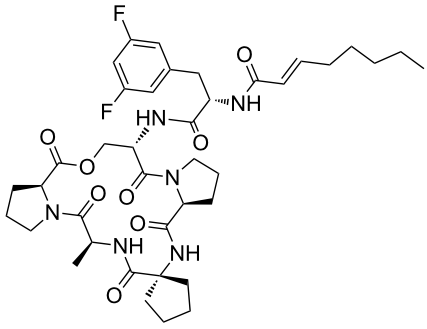 **6**	2	0.50	[43,44]
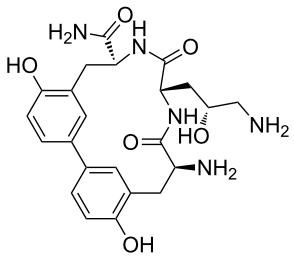 **7**	3	1.5	[44]
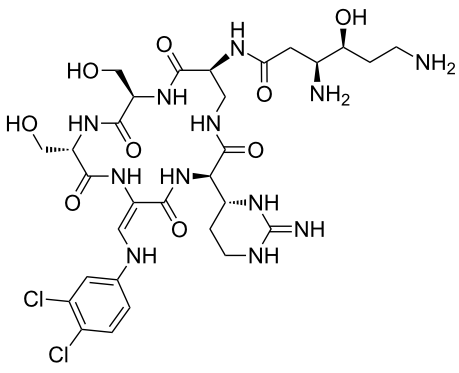 **8**	1	12.5	[45]

Table 1: Structures of cyclic peptides with their MIC values. (continued)

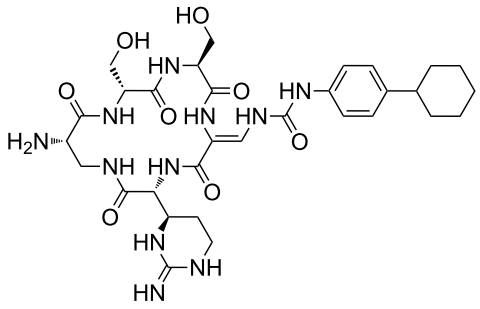 **9**	2	50	[45]
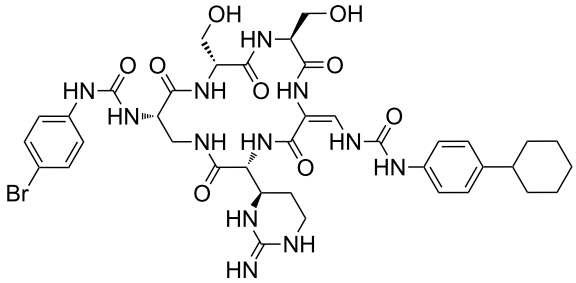 **10**	1	12.5	[45]
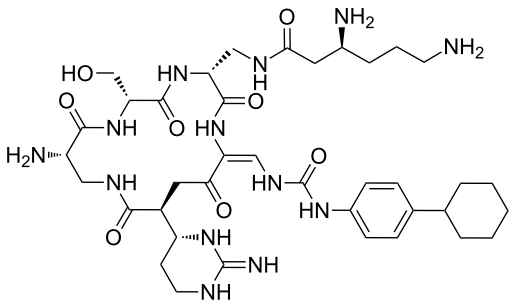 **11**	2	1.56	[45]
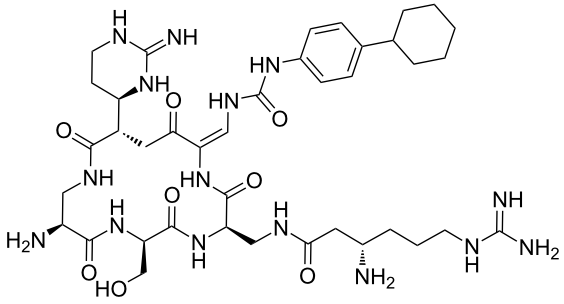 **12**	1	1.56	[45]
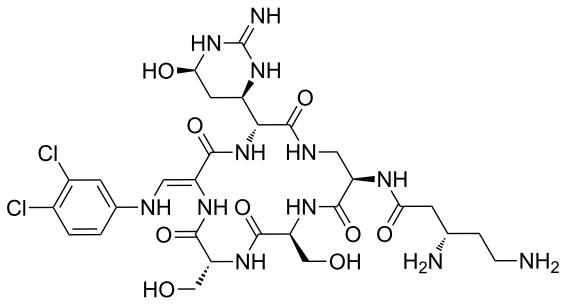 **13**	2	6.25	[46]

Table 1: Structures of cyclic peptides with their MIC values. (continued)

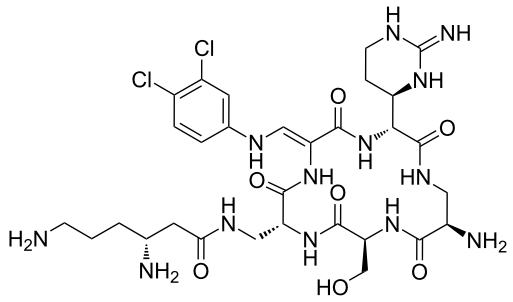 **14**	2	1.56	[46]
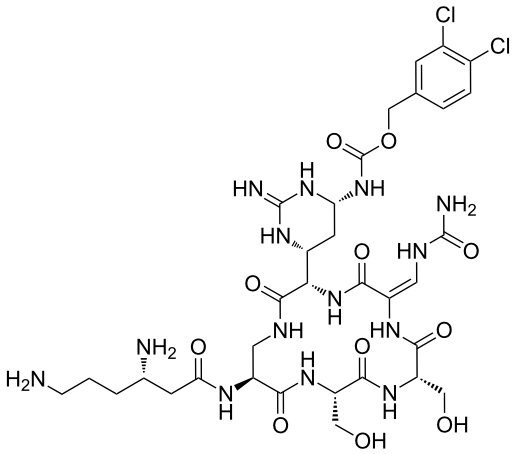 **15**	2	3.12	[47]
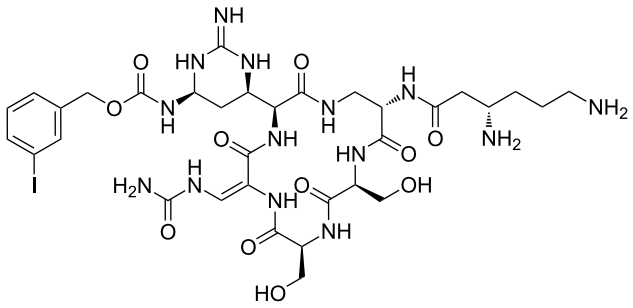 **16**	2	12.5	[47]
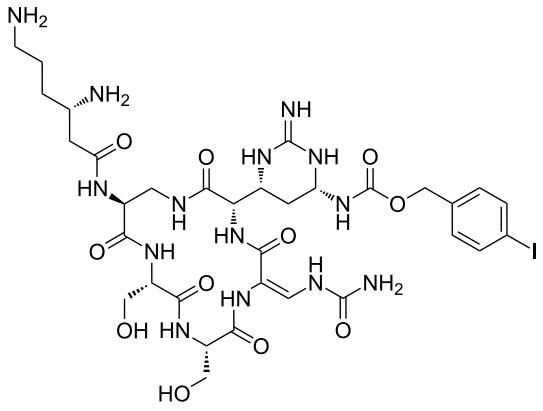 **17**	2	12.5	[47]

Table 1: Structures of cyclic peptides with their MIC values. (continued)

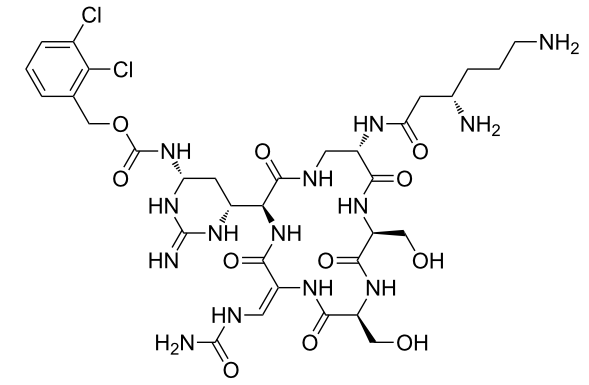 **18**	2	12.5	[47]
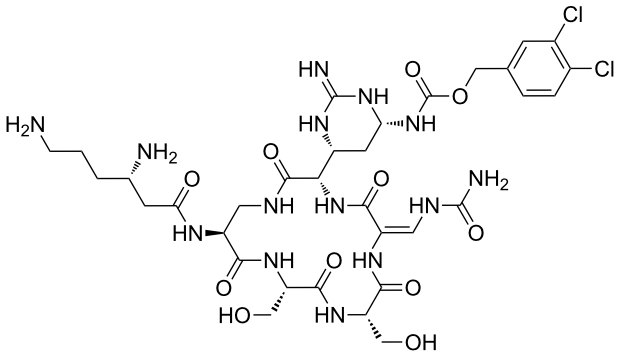 **19**	2	12.5	[47]
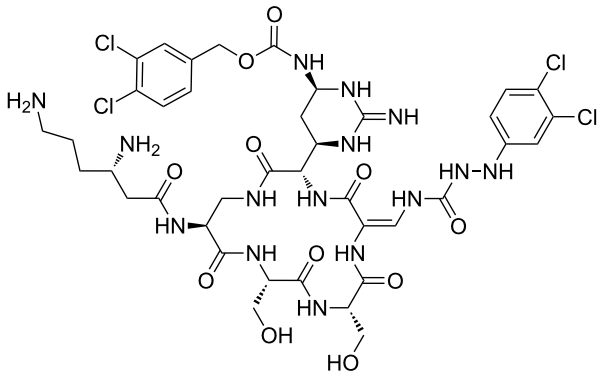 **20**	1	25.0	[47]
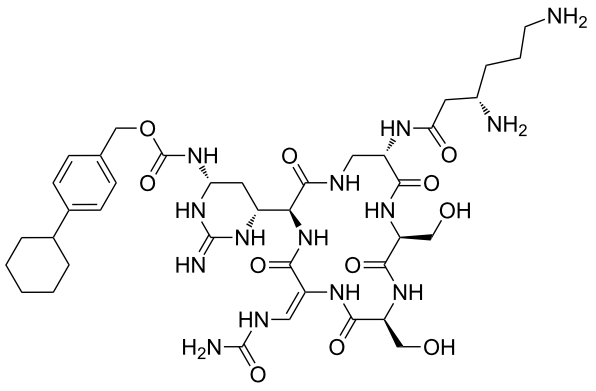 **21**	2	25.0	[47]

Table 1: Structures of cyclic peptides with their MIC values. (continued)

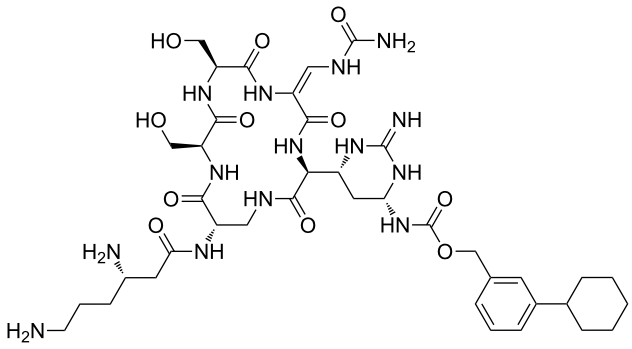 **22**	2	12.5	[47]
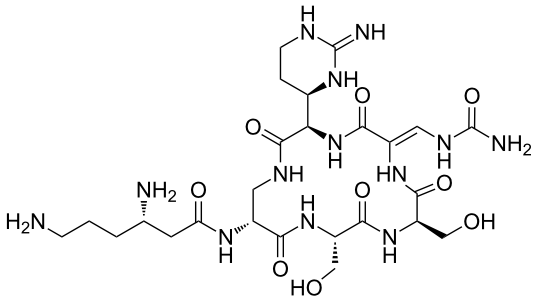 **23**	2	12.5	[47]
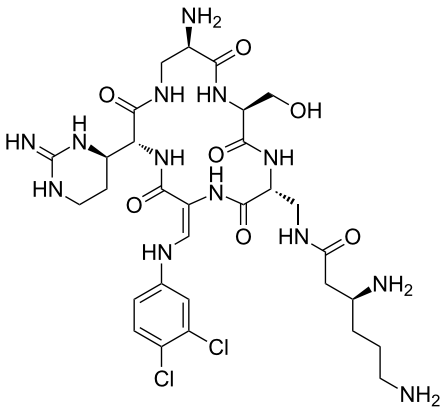 **24**	2	0.78	[48]
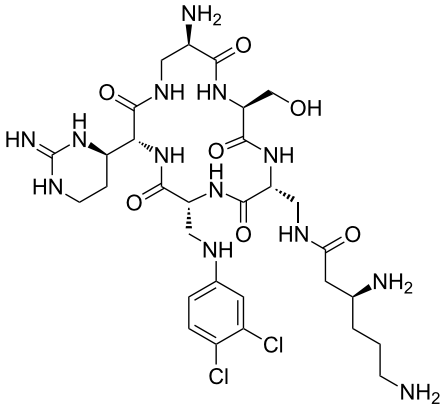 **25**	2	6.25	[48]

Table 1: Structures of cyclic peptides with their MIC values. (continued)

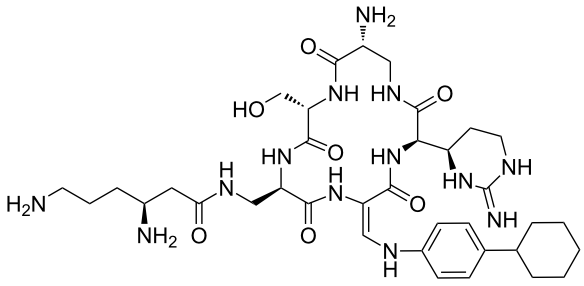 **26**	1	1.56	[48]
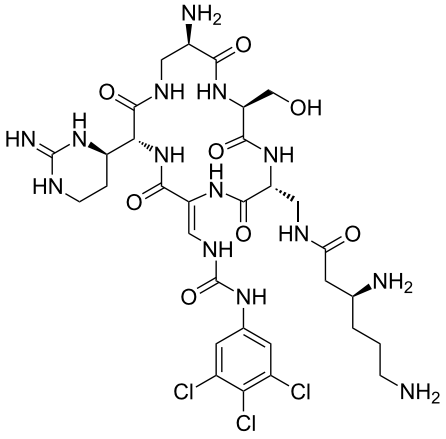 **27**	2	0.780	[48]
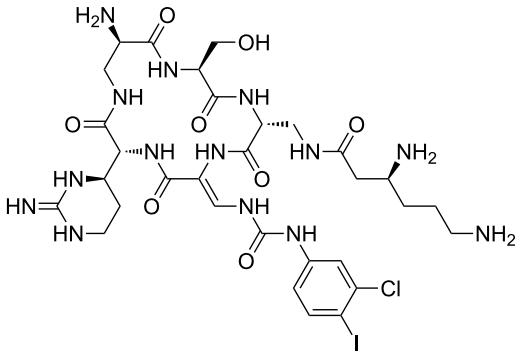 **28**	2	3.12	[48]
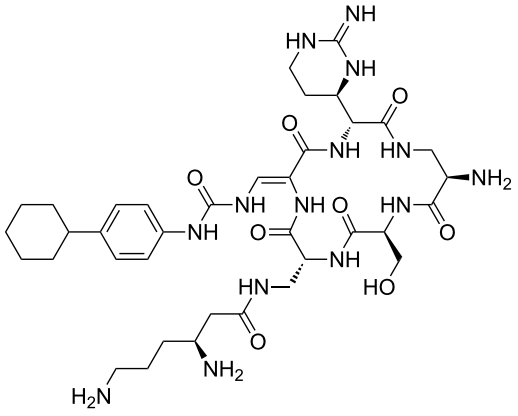 **29**	2	1.56	[48]

Table 1: Structures of cyclic peptides with their MIC values. (continued)

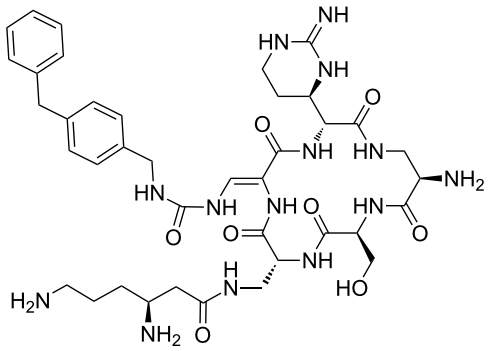 **30**	2	1.56	[48]
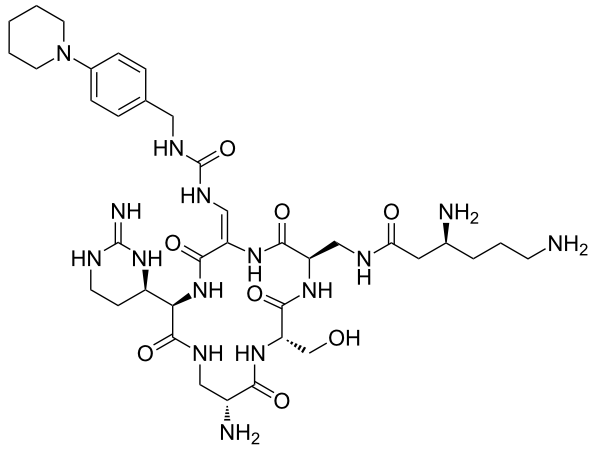 **31**	2	3.12	[48]
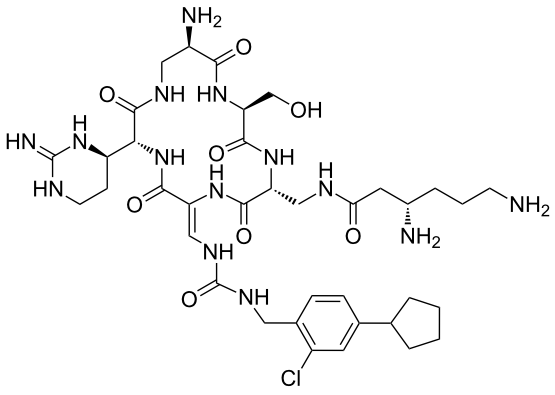 **32**	2	3.12	[48]
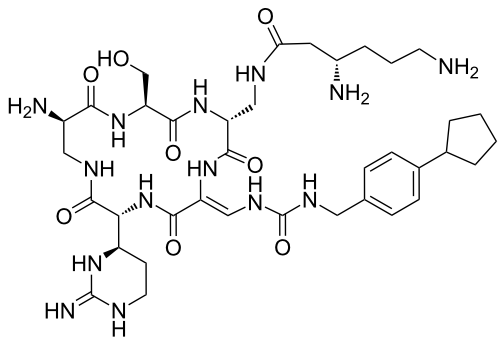 **33**	2	3.12	[48]

Clustering

Clustering is a widely used technique that has found application in the selection of compounds for screening, analysis of substructure search output, and the prediction of molecular properties [49]. The "*k*-means method" implemented in Statistica software is effective in clustering results for many practical applications, and was used to classify the current data set. All types of descriptors are calculated by using the CODESSA Pro program and the descriptor matrix is generated, which served as an input for the cluster-analysis module in STATISTICA software. The use of descriptors in this study can give differing clustering patterns [50]. The first step in the structure clustering is the generation of a matrix containing similarity values of descriptors for all pairs of compounds. Further, the matrix is converted to a hierarchical clustering tree by using single-linkage amalgamation and Euclidian distance measure. The single-linkage approach assigns sequential cluster labels to nearest-neighbor clusters. Then a series of clustering experiments was carried out with different cutoffs on the descriptor dependence, to clearly establish whether parameters produce realistic improvements in the quality of the results or not [51].

Analysis of the membership functions shows that the clusters are well-defined with each compound typically having one membership function, as shown in Figure 1 and Table 1. The cluster analysis results demonstrate that most of the studied compounds are clustered clusters. The peptidomimetics **37a**–**c** proposed for synthesis are located in cluster 1. Cluster 1 mainly consists of both cyclotetra- and cyclopentapeptides that are similar in ring size to **37a**–**c**; this cluster also includes those cyclic peptides that are highly potent as antibacterial agents (smallest MIC values). Clusters 1 and 2 contain structurally more diverse peptides. Thus, the majority of 12-membered ring-cyclic compounds were assigned to cluster 1, while the more branched structures with longer side chains were found in cluster 2. These assignments are chemically meaningful and thus bear witness to the validity of the clusterization method used.

The proximity of the cyclic peptidomimetics under study (**37a**–**c**) and the existing antibacterial cyclic peptides in such a rich descriptor space, in which all major structural, electronic, and intermolecular-interaction features are taken into account, attests to the feasibility of using the 17- and 18-membered ring scaffolds **37** as a main building block for designing novel antibacterial agents. This, along with the facile and economic synthetic route, renders scaffold **37** as a promising platform for further rational drug design.

Synthesis

Treatment of dicarboxylic acids **34a**–**c** by a standard method [36] using thionyl chloride and 1*H*-benzotriazole gave the corresponding benzotriazole derivatives in 37–54% yield (Scheme 1, see Supporting Information File 1 for experimental details).

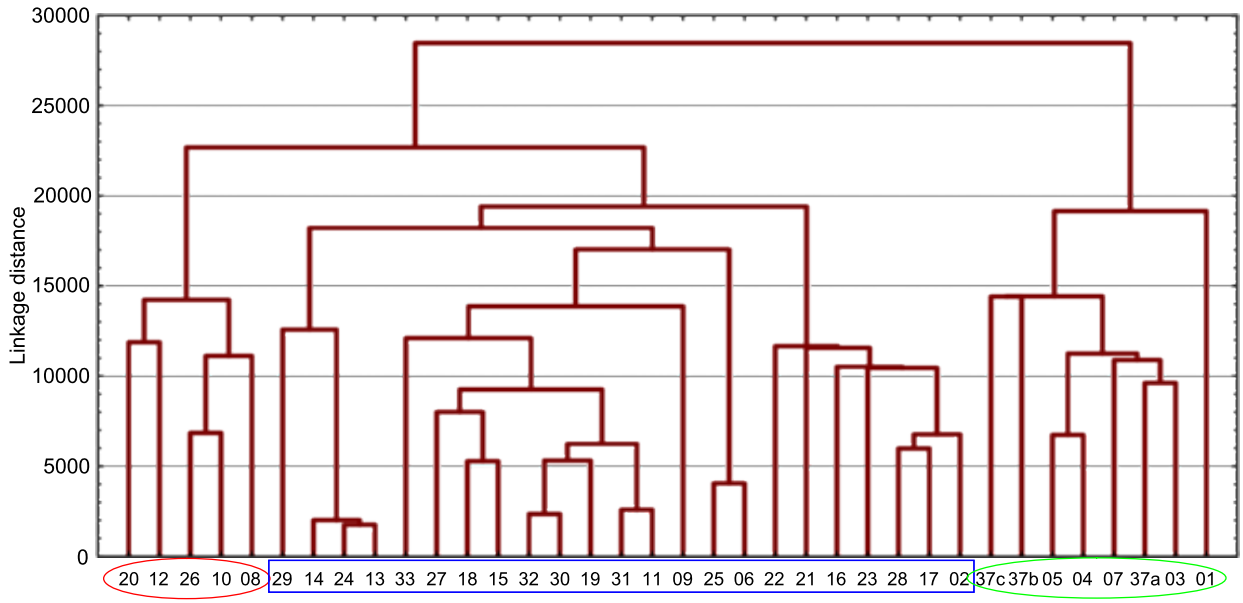

Figure 1: Molecular-descriptor-based cluster analysis; single-linkage Euclidean distances. Clustering of compounds in the descriptor space; a two-dimensional representation of chemical space being partitioned into clusters of similar compounds based on descriptors using a top-down (hierarchical) clustering method. Structures for compounds **37a**–**37c** are shown in Scheme 2. (Axis X denotes compounds and axis Y denotes linkage distance); the red oval, blue rectangle, and green oval represent cluster 1, cluster 2, and cluster 3, respectively.

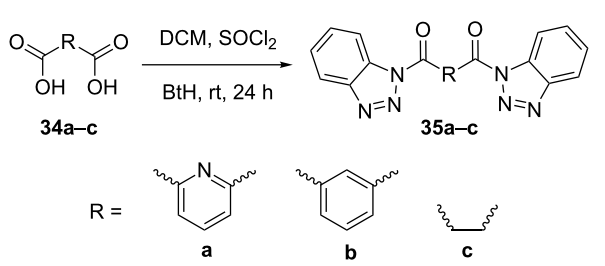

Scheme 1: Preparation of dicarboxylic benzotriazole derivatives.

The methodology used for the regioselective syntheses of *S*- and *N*-acylcysteines was developed recently in our group by using *N*-acylbenzotriazoles under mild reaction conditions [37]. Utilizing this methodology, **35a** was coupled with two equiv of free cysteine in aqueous acetonitrile at 20 °C over 12 h to give bis(*S*-acylcysteine) **36** in 64% yield. Compound **36** was then treated with 1 equiv of **35a–c** to synthesize cyclic enantiopure peptidomimetic products **37a–c** in 81–82% yield (Scheme 2, see Supporting Information File 1 for experimental details).

In a further application of this synthetic approach **35** was coupled with 2 equiv of L-Phe-OH in the presence of TEA in aqueous acetonitrile at room temperature over 3 h giving the bis N-acylated compound **38** in 88% yield. Compound **38** was converted to the corresponding benzotriazole derivative **39** and coupled with bis(*S*-acylcysteine) **36** forming the pyridine–cysteine-containing macrocycle **40** in 70% yield (Scheme 3, see Supporting Information File 1 for experimental details).

Bioassay

Screening for antibacterial activity was performed for two cyclic peptidomimetics belonging to scaffold **37**, namely **37a**

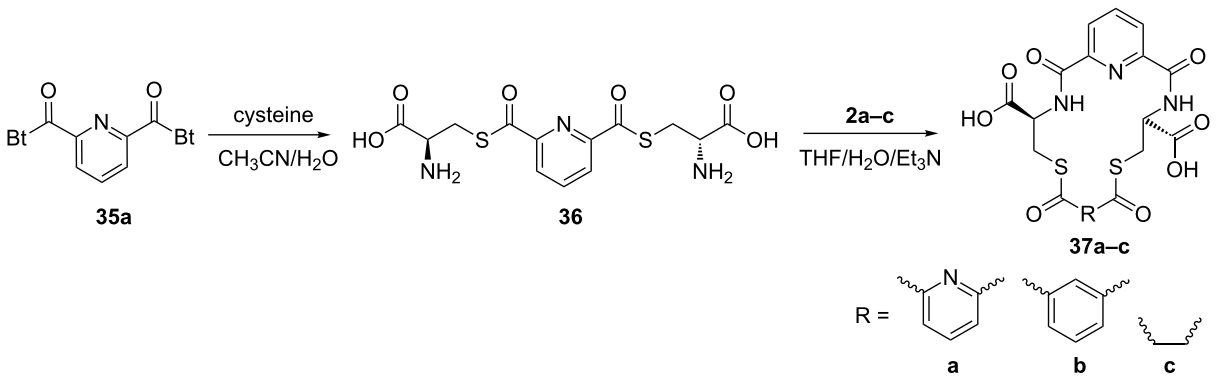

Scheme 2: Preparation of pyridine-based cysteine-containing macrocycles.

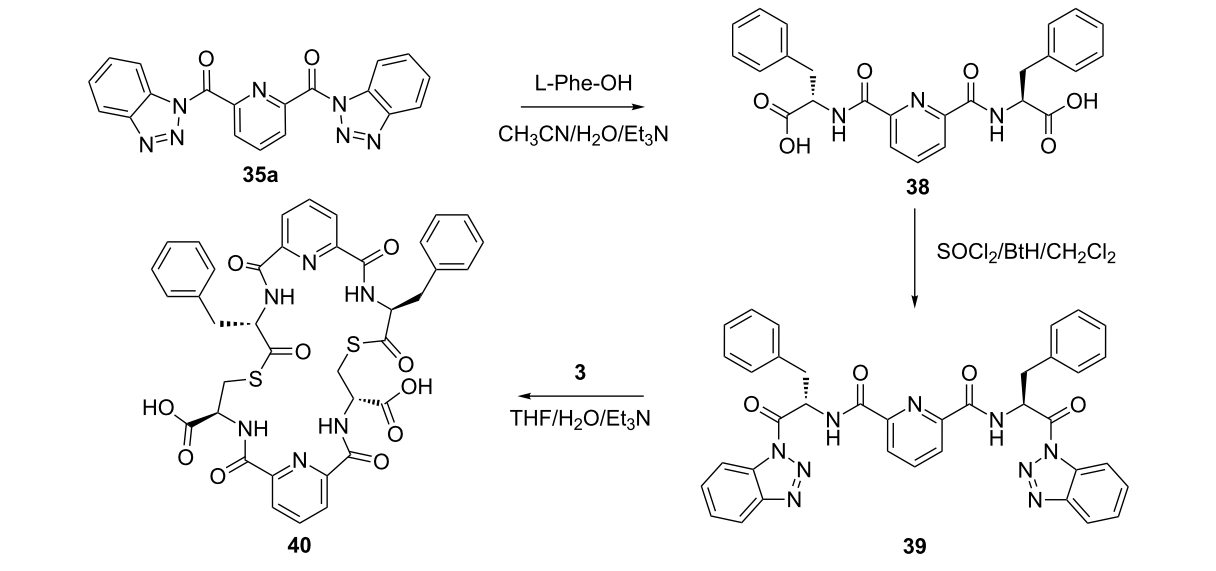

Scheme 3: Preparation of pyridine–cysteine-containing macrocycle **39**.

and **37b**, with the pyridine- and phenyl-linking fragments, respectively. The array of microbial strains assayed in this study included six pathogens listed in Table 2 (see Supporting Information File 1, for antibacterial testing protocol).

The in vitro data for **37a** and **37b** are given in Table 2. Reference antibiotics roxithromycin and cefixime were used as positive controls. It is seen that peptidomimetic **37b** exhibits moderate activity against *Bordetella bronchiseptica*, *Micrococcus luteus*, and *Salmonella typhimurium*. For a "bare" scaffold with no tailor-made substitution, this should be considered as an encouraging result and an indication of the possibility of more interesting results if the scaffold is furnished with appropriate functions.

Peptidomimetic **37a** showed no activity in this test, which can be explained by the formation of a zwitter-ionic structure due to protonation of the pyridine moiety by free carboxylic groups. It is reasonable to assume that such a zwitter-ionic structure alters the charge distribution and also eliminates hydrogen bonding in which the pyridine nitrogen atom acts as a H-bond acceptor. These factors increase hydrophobicity and thus deteriorate bioavailability, as reflected in the absence of activity of **37a**. Absence of data in Table 2 means that the sample is not active at the highest concentration tested.

Conclusion

Two new cyclic peptidomimetic scaffolds were identified by using similarity-based rational design. Their chemical similarity with existing antibacterial cyclic peptidomimetics was established in a huge descriptor space generated by Codessa-Pro software. At least one compound (**37b**) demonstrated a moderate antibacterial activity against three bacterial strains, which is a fairly promising result for a "bare" cyclic scaffold with no intentional functionalization. Given the successful scaffold identified, the next step will be to furnish it with appropriate functional groups and substituents by using rational design principles.

Experimental

Methodology

Molecular similarity

The potential of cyclic peptidomimetics, widely acknowledged as significant, arises because they are less prone to hydrolysis in vivo and can be synthesized rather inexpensively. The synthetic methodology that has been developed in our lab affords facile assembles of cyclic structures from dicarboxylic building blocks by using a benzotriazole methodology. Seventeen and eighteen-membered sulfur-containing rings can be synthesized readily if cysteine is used as the coupling agent. Such facile access to cyclic peptidomimetics is appropriate for the design of compounds expected to be biologically active as antibacterial agents. Exploring the molecular similarity of existing antibacterial cyclic peptides using the Tanimoto method in the Instant JChem software [52], and the peptidomimetics easily accessible through the benzotriazole route, should give structural insights and design criteria. Guidance for such a similarity-based design should be available by analysis of a reasonably sized dataset of existing analogues. As abundant data can be found in the literature for *Staphylococcus aureus,* this was chosen as a reference for antibacterial activity. SciFinder Scholar was used to retrieve the structures of 33 cyclic peptides with reported antibacterial activity (Table 1). The minimum growth inhibition constant (MIC) was used as the measure of antibacterial activity, and the data collected were converted where necessary to μg/mL. Three structures newly synthesized

Table 2: Antibacterial activity in vitro.

Microbial strain[a]	Inhibition zone (mm) at 200 μg/mL				MIC[b] (μg/mL)			
	37a	**37b**	Rox[c]	Cfx[d]	**37a**	**37b**	Rox[c]	Cfx[d]
Staphylococcus aureus (ATCC 6538)	0.0	0.0	30	40	–	–	12.5	6.25
Escherichia coli (ATCC 8739)	0.0	0.0	14.6	22.9	–	–	100	50
Bordetella bronchiseptica (ATCC 4617)	0.0	6.0	8	33	–	150	150	12.5
Micrococcus luteus (ATCC 10240)	0.0	6.0	30	40	–	150	12.5	12.5
Salmonella typhimurium (ATCC 14028)	0.0	6.0	12	40	–	150	100	6.25
Enterobacter aerogenes (ATCC 13048)	0.0	0.0	15	34	–	–	100	12.5

[a]*Bordetella bronchistepica*: Gram negative, relevant to veterinary science; *Micrococcus luteus*: Gram positive, not dangerous for humans; *Salmonella typhimurium*: Gram negative, relevant to veterinary science. [b]MIC = minimum inhibitory concentration. [c]Rox = roxithromycin. [d]Cfx = cefixime.

in our lab were also added to the general dataset (Table 1). All these structures were drawn with the Marvin Beans Suite program [52] and preoptimized using the molecular mechanics utility (MM2) [53] in Chem3D Ultra 12.0 software [54]. Final geometry optimization of the compounds was carried out by using the semiempirical quantum-mechanical AM1 parameterization [55].

Molecular descriptors

The optimized geometries of the compounds were loaded into CODESSA Pro software [38]. Overall, more than 800 theoretical descriptors were calculated including constitutional, geometrical, topological, electrostatic, quantum-chemical, and thermodynamic molecular descriptors [56,57].

Cluster analysis

Cluster analysis of the descriptor hyperspace was performed by using STATISTICA version 6 software [58], with Euclidean distance and other metrics used as similarity measures. Cluster analysis guided by the experimental MIC available for some compounds should help reveal structural features affording antibacterial activity and to identify hotspots in the descriptor hyperspace. Combinations of structural features in such hotspots can be used as guidelines for the rational design of cyclic peptide structures to achieve desirable levels of antibacterial activity.

Supporting Information

Supporting Information File 1

Experimental details, characterization data of synthesized compounds and antibacterial testing protocol.
[http://www.beilstein-journals.org/bjoc/content/supplementary/1860-5397-8-128-S1.pdf]

Acknowledgements

We thank the University of Florida, the Kenan Foundation and King Abdulaziz University, Jeddah, Saudi Arabia for financial support. We are grateful to Mr. Alexander Drijver, ChemAxon Kft. Hungary for a free academic license. The authors are grateful to Dr. C. D. Hall and Ms. Galyna Vakulenko for useful discussions and help.

References

1. Powers, J.-P. S.; Hancock, R. E. W. *Peptides* **2003,** *24,* 1681–1691. doi:10.1016/j.peptides.2003.08.023
2. Dartois, V.; Sanchez-Quesada, J.; Cabezas, E.; Chi, E.; Dubbelde, C.; Dunn, C.; Granja, J.; Gritzen, C.; Weinberger, D.; Ghadiri, M. R.; Parr, T. R., Jr. *Antimicrob. Agents Chemother.* **2005,** *49,* 3302–3310. doi:10.1128/AAC.49.8.3302-3310.2005
3. Epand, R. M.; Vogel, H. J. *Biochim. Biophys. Acta* **1999,** *1462,* 11–28. doi:10.1016/S0005-2736(99)00198-4
4. Singh, A.; Wilczynski, A.; Holder, J. R.; Witek, R. M.; Dirain, M. L.; Xiang, Z.; Edison, A. S.; Haskell-Luevano, C. *J. Med. Chem.* **2011,** *54,* 1379–1390. doi:10.1021/jm101425m
5. Bach, A.; Strømgaard, K. *Synthesis* **2011,** 807–815. doi:10.1055/s-0030-1258425
6. Biron, E.; Chatterjee, J.; Kessler, H. *Org. Lett.* **2006,** *8,* 2417–2420. doi:10.1021/ol0607645
7. Tornøe, C. W.; Sanderson, S. J.; Mottram, J. C.; Coombs, G. H.; Meldal, M. *J. Comb. Chem.* **2004,** *6,* 312–324. doi:10.1021/cc020085v
8. Saitton, S.; Kihlberg, J.; Luthman, K. *Tetrahedron* **2004,** *60,* 6113–6120. doi:10.1016/j.tet.2004.05.048
9. McComsey, D. F.; Hawkins, M. J.; Andrade-Gordon, P.; Addo, M. F.; Oksenberg, D.; Maryanoff, B. E. *Bioorg. Med. Chem. Lett.* **1999,** *9,* 1423–1428. doi:10.1016/S0960-894X(99)00197-3
10. Pedersen, D. S.; Abell, A. *Eur. J. Org. Chem.* **2011,** 2399–2411. doi:10.1002/ejoc.201100157
11. Appendino, G.; Bacchiega, S.; Minassi, A.; Cascio, M. G.; De Petrocellis, L.; Di Marzo, V. D. *Angew. Chem., Int. Ed.* **2007,** *46,* 9312–9315. doi:10.1002/anie.200703590
12. Tam, A.; Arnold, U.; Soellner, M. B.; Raines, R. T. *J. Am. Chem. Soc.* **2007,** *129,* 12670–12671. doi:10.1021/ja075865s
13. Brik, A.; Yang, Y.-Y.; Ficht, S.; Wang, C.-H. *J. Am. Chem. Soc.* **2006,** *128,* 5626–5627. doi:10.1021/ja061165w
14. Borg, S.; Vollinga, R. C.; Labarre, M.; Payza, K.; Terenius, L.; Luthman, K. *J. Med. Chem.* **1999,** *42,* 4331–4342. doi:10.1021/jm990197+
15. Balzarini, J.; Stevens, M.; De Clercq, E.; Schols, D.; Pannecouque, C. *J. Antimicrob. Chemother.* **2005,** *55,* 135–138. doi:10.1093/jac/dkh530
16. Haviv, F.; DeNet, R. W.; Michaels, R. J.; Ratajczyk, J. D.; Carter, G. W.; Young, P. R. *J. Med. Chem.* **1983,** *26,* 218–222. doi:10.1021/jm00356a018
17. Thirumurugan, P.; Mahalaxmi, S.; Perumal, P. T. *J. Chem. Sci.* **2010,** *122,* 819–832. doi:10.1007/s12039-010-0070-3
18. Phillips, O. A.; Knaus, E. E. *Drug Des. Delivery* **1991,** *4,* 279–286.
19. Reck, F.; Zhou, F.; Eyermann, C. J.; Kem, G.; Carcanague, D.; Ioannidis, G.; Illingworth, R.; Poon, G.; Gravestock, M. B. *J. Med. Chem.* **2007,** *50,* 4868–4881. doi:10.1021/jm070428+
20. Nassar, E. *J. Am. Sci.* **2010,** *6* (8), 463–471.
21. Liu, M. C.; Lin, T. C.; Sartorelli, A. C. *J. Med. Chem.* **1992,** *35,* 3672–3677. doi:10.1021/jm00098a012
22. Kim, G.-J.; Park, D.-W.; Tak, Y.-S. *Catal. Lett.* **2000,** *65,* 127–133. doi:10.1023/A:1019040532103
23. Li, Z.; Jablonski, C. *Chem. Commun.* **1999,** 1531–1532. doi:10.1039/a900018f
24. Kubik, S. *Chem. Soc. Rev.* **2009,** *38,* 585–605. doi:10.1039/b810531f
25. Ranganathan, D.; Thomas, A.; Haridas, V.; Kurur, S.; Madhusudanan, K. P.; Roy, R.; Kunwar, A. C.; Sarma, A. V. S.; Vairamani, M.; Sarma, K. D. *J. Org. Chem.* **1999,** *64,* 3620–3629. doi:10.1021/jo982472q
26. Ranganathan, D.; Haridas, V.; Gilardi, R.; Karle, I. L. *J. Am. Chem. Soc.* **1998,** *120,* 10793–10800. doi:10.1021/ja982244d
27. Pintér, Á.; Haberhauer, G. *Tetrahedron* **2009,** *65,* 2217–2225. doi:10.1016/j.tet.2009.01.047
28. Montero, A.; Albericio, F.; Royo, M.; Herradon, B. *Eur. J. Org. Chem.* **2007,** 1301–1308. doi:10.1002/ejoc.200600833
29. Wang, X.; Wang, Q.; Huang, X.; Wang, T.; Yu, X. *ARKIVOC* **2006,** *xi,* 1–7.

30. Hancock, R. E. W. *Lancet Infect. Dis.* **2001,** *1,* 156–164. doi:10.1016/S1473-3099(01)00092-5
31. Wu, M. H.; Hancock, R. E. W. *Antimicrob. Agents Chemother.* **1999,** *43,* 1274–1276.
32. Fales-Williams, A. J.; Gallup, J. M.; Ramirez-Romero, R.; Brogden, K. A.; Ackermann, M. R. *Clin. Diagn. Lab. Immunol.* **2002,** *9,* 28–32. doi:10.1128/CDLI.9.1.28-32.2002
33. Alastair, A. R. *Generalized Method of Moments;* Oxford University Press: Oxford, U.K., 2005.
34. Bender, A.; Glen, R. C. *Org. Biomol. Chem.* **2004,** *2,* 3204–3218. doi:10.1039/b409813g
35. Katritzky, A. R.; Khelashvili, L.; Mohapatra, P. P.; Steel, P. J. *Synthesis* **2007,** 3673–3677. doi:10.1055/s-2007-990889
36. Katritzky, A. R.; Angrish, P.; Todadze, E. *Synlett* **2009,** 2392–2411. doi:10.1055/s-0029-1217827
37. Katritzky, A. R.; Tala, S. R.; Abo-Dya, N. E.; Gyanda, K.; El-Gendy, B. E.-D. M.; Abdel-Samii, Z. K.; Steel, P. J. *J. Org. Chem.* **2009,** *74,* 7165–7167. doi:10.1021/jo900853s
38. *CODESSA Pro;* University of Florida: Gainesville, FL, USA, 2001.
39. von Nussbaum, F. V.; Anlauf, S.; Freiberg, C.; Benet-Buchholz, J.; Schamberger, J.; Henkel, T.; Schiffer, G.; Häbich, D. *ChemMedChem* **2008,** *3,* 619–626. doi:10.1002/cmdc.200700297
40. Morel, A. F.; Maldaner, G.; Ilha, V.; Missau, F.; da Silva, U. F.; Dalcol, I. I. *Phytochemistry* **2005,** *66,* 2571–2576. doi:10.1016/j.phytochem.2005.08.016
41. Morel, A. F.; Araujo, C. A.; da Silva, U. F.; Hoelzel, S. C. S. M.; Záchia, R.; Bastos, N. R. *Phytochemistry* **2002,** *61,* 561–566. doi:10.1016/S0031-9422(02)00287-X
42. Giacomelli, S. R.; Maldaner, G.; Gonzaga, W. A.; Garcia, C. M.; da Silva, U. F.; Dalcol, I. I.; Morel, A. F. *Phytochemistry* **2004,** *65,* 933–937. doi:10.1016/j.phytochem.2004.02.006
43. Socha, A. M.; Tan, N. Y.; LaPlante, K. L.; Sello, J. K. *Bioorg. Med. Chem.* **2010,** *18,* 7193–7202. doi:10.1016/j.bmc.2010.08.032
44. von Nussbaum, F.; Brands, M.; Hinzen, B.; Weigand, S.; Häbich, D. *Angew. Chem., Int. Ed.* **2006,** *45,* 5072–5129. doi:10.1002/anie.200600350
45. Linde, R. G., II; Birsner, N. C.; Chandrasekaran, R. Y.; Clancy, J.; Howe, R. J.; Lyssikatos, J. P.; MacLelland, C. P.; Magee, T. V.; Petitpas, J. W.; Rainville, J. P.; Su, W.-G.; Vu, C. B.; Whipple, D. A. *Bioorg. Med. Chem. Lett.* **1997,** *7,* 1149–1152. doi:10.1016/S0960-894X(97)00188-1
46. Norcia, L. J. L.; Silvia, A. M.; Dirlam, J. P.; Schnur, R. C.; Bergeron, J. M.; Retsema, J. A.; Hayashi, S. F. *J. Antibiot.* **1999,** *52,* 1007–1016. doi:10.7164/antibiotics.52.1007
47. Lyssikatos, J. P.; Chang, S.-P.; Clancy, J.; Dirlam, J. P.; Finegan, S. M.; Girard, A. E.; Hayashi, S. F.; Larson, D. P.; Lee, A. S.; Linde, R. G., II; MacLelland, C. P.; Petipas, J. W.; Seibel, S. B.; Vu, C. B. *Bioorg. Med. Chem. Lett.* **1997,** *7,* 1145–1148. doi:10.1016/S0960-894X(97)00187-X
48. Dirlam, J. P.; Belton, A. M.; Birsner, N. C.; Brooks, R. R.; Chang, S.-P.; Chandrasekaran, R. Y.; Clancy, J.; Cronin, B. J.; Dirlam, B. P.; Finegan, S. M.; Froshauer, S. A.; Girard, A. E.; Hayashi, S. F.; Howe, R. J.; Kane, J. C.; Kamicker, B. J.; Kaufman, S. A.; Kolosko, N. L.; LeMay, M. A.; Linde, R. G., II; Lyssikatos, J. P.; MacLelland, C. P.; Magee, T. V.; Massa, M. A.; Miller, S. A.; Minich, M. L.; Perry, D. A.; Petitpas, J. W.; Reese, C. P.; Seibel, S. B.; Su, W.-G.; Sweeney, K. T.; Whipple, D. A.; Yang, B. V. *Bioorg. Med. Chem. Lett.* **1997,** *7,* 1139–1144. doi:10.1016/S0960-894X(97)00186-8
49. Holliday, J. D.; Rodgers, S. L.; Willett, P.; Chen, M. Y.; Mahfouf, M.; Lawson, K. *J. Chem. Inf. Comput. Sci.* **2004,** *44,* 894–902. doi:10.1021/ci0342674
50. Stahl, M.; Mauser, H.; Tsui, M.; Taylor, N. R. *J. Med. Chem.* **2005,** *48,* 4358–4366. doi:10.1021/jm040213p
51. Adamson, G. W.; Bawden, D. *J. Chem. Inf. Comput. Sci.* **1981,** *21,* 204–209. doi:10.1021/ci00032a005
52. *Instant JChem 5.5.0; Marvin 5.6.0;* ChemAxon Kft.: Hungary, 2011.
53. Allinger, N. L. *J. Am. Chem. Soc.* **1977,** *99,* 8127–8134. doi:10.1021/ja00467a001
54. *ChemBioDraw Ultra,* Version 12.0.2; Cambridgesoft: Cambridge, MA, USA, 2010.
55. Dewar, M. J. S.; Zoebisch, E. G.; Healy, E. F.; Stewart, J. J. P. *J. Am. Chem. Soc.* **1985,** *107,* 3902–3909. doi:10.1021/ja00299a024
56. Karelson, M. *Molecular Descriptors in QSAR/QSPR;* Wiley Interscience: New York, 2000.
57. Katritzky, A. R.; Kuanar, M.; Slavov, S.; Hall, C. D.; Karelson, M.; Kahn, I.; Dobchev, D. A. *Chem. Rev.* **2010,** *110,* 5714–5789. doi:10.1021/cr900238d
58. *STATISTICA,* Version 6; StatSoft, Inc.: Tulsa, OK, USA, 2001.

License and Terms

Beilstein Journal of Organic Chemistry

Partial thioamide scan on the lipopeptaibiotic trichogin GA IV. Effects on folding and bioactivity

Marta De Zotti[1], Barbara Biondi[1], Cristina Peggion[1], Matteo De Poli[1], Haleh Fathi[1], Simona Oancea[2], Claudio Toniolo[1] and Fernando Formaggio[*1]

Full Research Paper

Open Access

Address:
[1]ICB, Padova Unit, CNR, Department of Chemistry, University of Padova, 35131 Padova, Italy and [2]Department of Biochemistry and Toxicology, Lucian Blaga University of Sibiu, 550012 Sibiu, Romania

Email:
Fernando Formaggio[*] - fernando.formaggio@unipd.it

* Corresponding author

Keywords:
bioactivity; conformation; peptaibiotic; peptide synthesis; peptides; thiopeptides

Beilstein J. Org. Chem. **2012,** *8,* 1161–1171.
doi:10.3762/bjoc.8.129

Received: 27 April 2012
Accepted: 21 June 2012
Published: 24 July 2012

This article is part of the Thematic Series "Antibiotic and cytotoxic peptides".

Guest Editor: N. Sewald

Abstract

Backbone modification is a common chemical tool to control the conformation of linear peptides and to explore potentially useful effects on their biochemical and biophysical properties. The thioamide, ψ[CS-NH], group is a nearly isosteric structural mimic of the amide (peptide) functionality. In this paper, we describe the solution synthesis, chemical characterization, preferred conformation, and membrane and biological activities of three, carefully selected, peptide analogues of the lipopeptaibiotic [Leu^{11}-OMe] trichogin GA IV. In each analogue, a single thioamide replacement was incorporated. Sequence positions near the N-terminus, at the center, and near the C-terminus were investigated. Our results indicate that (i) a thioamide linkage is well tolerated in the overall helical conformation of the [Leu^{11}-OMe] lipopeptide analogue and (ii) this backbone modification is compatible with the preservation of its typical membrane leakage and antibiotic properties, although somewhat attenuated.

Introduction

Since their first incorporation into peptides [1], backbone amide surrogates have attracted remarkable attention from organic and medicinal chemists. Not only may these modifications impart to a peptide an increased resistance to enzymatic hydrolysis as well as higher receptor affinity and specificity, but they may also influence its preferred secondary structure.

A ψ[CS-NH] thioamide group is one of the closest mimics of an amide (peptide) linkage. However, it exhibits significantly different chemical and physical properties, some of which are of great potential interest to peptide chemists [2-44]. Among these properties, we highlight the following: (i) The thioamide NH group is more acidic than that of its oxygenated counterpart and

consequently it is a stronger H-bonding donor. (ii) Its *cis*/*trans* isomerization can be phototriggered by irradiation at about 260 nm [absorption maximum of the -C(=S)NH- π→π* electronic transition]. (iii) It may act as a minimalist, effective quencher for any type of protein and nonprotein fluorophores.

Recently, based on the aforementioned characteristics of the ψ[CS-NH] thioamide bond, we started a program aimed at exploring how thiopeptide groups may affect folding and the related biophysical/biochemical activities of the membrane-active peptaibiotics [45]. This class of compounds represents a subject of long-standing, relevant, interest to our research group. In this paper, we describe our results on the syntheses by solution methods and characterizations of three thioamide-containing [Leu^{11}-OMe] analogues of the short helical lipopeptaibiotic trichogin GA IV [46-50] (Figure 1). We already found that the replacement of the native C-terminal 1,2-amino alcohol leucinol (Lol) by the corresponding α-amino methyl ester (Leu-OMe) alters only slightly the biophysical and biological properties of trichogin GA IV. Conversely, we showed that the N$^{\alpha}$-blocking fatty acyl moiety plays a major role in its membrane permeability and antibiotic activity.

In each analogue, the single ψ[CS-NH] group was strategically incorporated either at an internal position of the amino-acid sequence, **ψ[CS-NH]^5**, or near each of the two ends, **ψ[CS-NH]^2** and **ψ[CS-NH]^9**. Moreover, the preferred conformations of these analogues were investigated by circular dichroism (CD), FT-IR absorption, and NMR. Finally, we carried out fluorescence leakage experiments in model membranes and antibacterial assays on a large set of both Gram-positive and Gram-negative strains.

Results and Discussion

Peptide synthesis

The total syntheses of the three monothionated ψ[CS-NH] trichogin GA IV analogues at positions 2, 5, and 9, respectively, were accomplished by using the solution-phase method (Schemes 1–3). Both step-by-step and segment condensation approaches were utilized. The former strategy was used in the

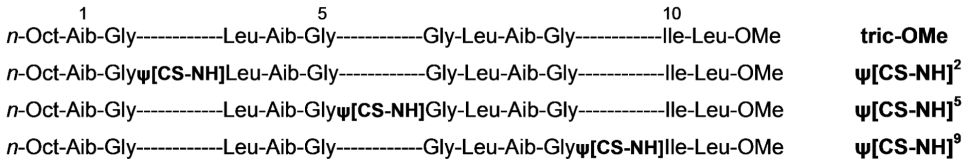

Figure 1: List of primary structures and abbreviations for the peptides studied in this work. The [Leu^{11}-OMe] trichogin GA IV is termed **tric-OMe** and its thionated derivatives at position 2, position 5, and position 9 are termed **ψ[CS-NH]^2**, **ψ[CS-NH]^5**, and **ψ[CS-NH]^9**, respectively.

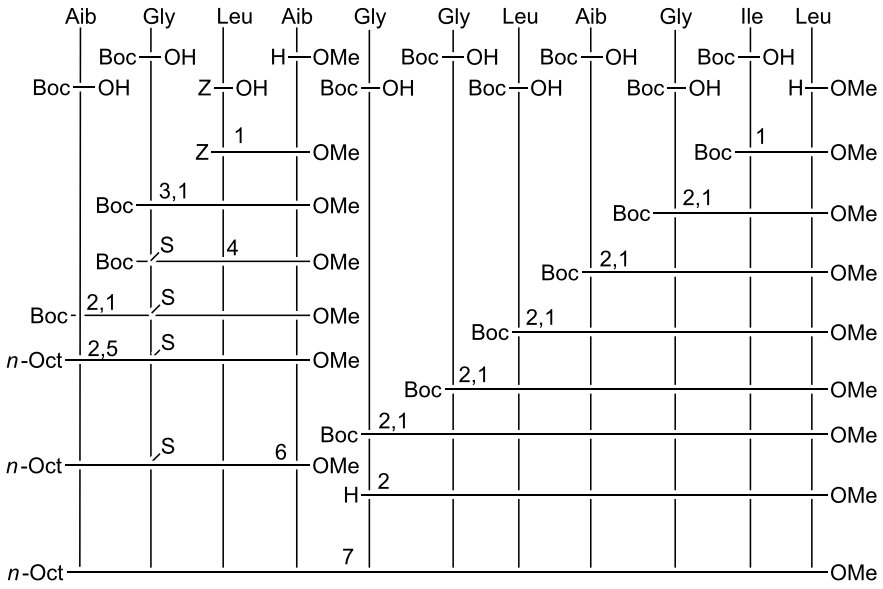

Scheme 1: Synthesis of **ψ[CS-NH]^2**. 1: Coupling in the presence of EDC/HOBt. 2: Deprotection by using TFA/DCM. 3: Deprotection by catalytic hydrogenation with Pd/C. 4: Thionation with Lawesson's reagent in THF. 5: Coupling with *n*-Oct-OH in the presence of EDC/HOBt. 6: Saponification with NaOH/MeOH. 7: Coupling in the presence of EDC/HOAt.

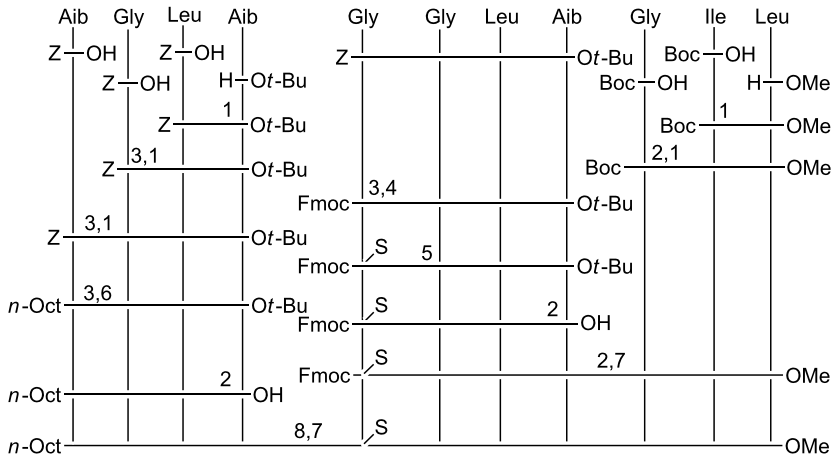

Scheme 2: Synthesis of **ψ[CS-NH]^5**. 1: Coupling in the presence of EDC/HOBt. 2: Deprotection by using TFA/DCM. 3: Deprotection by catalytic hydrogenation with Pd/C. 4: Coupling with Fmoc-OSu in 1,4-dioxane. 5: Thionation with Lawesson's reagent in THF. 6: Coupling with *n*-Oct-OH in the presence of EDC/HOBt. 7: Coupling in the presence of EDC/HOAt. 8: Deprotection with DEA in DCM.

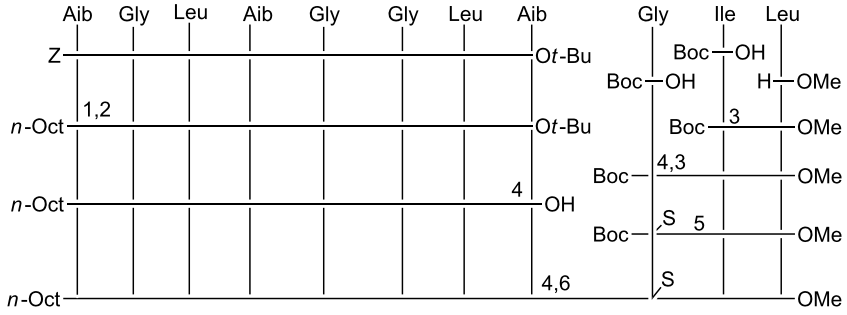

Scheme 3: Synthesis of **ψ[CS-NH]^9**. 1: Deprotection by catalytic hydrogenation with Pd/C. 2: Coupling with *n*-Oct-OH in the presence of EDC/HOBt. 3: Coupling in the presence of EDC/HOBt. 4: Deprotection by using TFA/DCM. 5: Thionation with Lawesson's reagent in THF. 6: Coupling in the presence of EDC/HOAt.

preparation of Boc-Gly^5-Gly-Leu-Aib-Gly-Ile-Leu^{11}-OMe (segment 5–11, for the synthesis of **ψ[CS-NH]^2**), Boc-Gly^9-Ile-Leu^{11}-OMe (segment 9–11), and *n*-Oct-Aib^1-Gly-Leu-Aib^4-O*t*-Bu (segment 1–4, for the synthesis of **ψ[CS-NH]^5**), and *n*-Oct-Aib^1-Gly-Leu-Aib-Gly-Gly-Leu-Aib^8-O*t*-Bu (segment 1–8, for the synthesis of **ψ[CS-NH]^9**). The latter strategy, which permits a faster preparation of multiple analogues, afforded (i) **ψ[CS-NH]^2** by condensation of the thionated 1–4 and the 5–11 segments; (ii) **ψ[CS-NH]^5** by condensation of the thionated 5–8 and the 9–11 segments followed by condensation of the 1–4 and the resulting, thionated, 5–11 segments; and (iii) **ψ[CS-NH]^9** by condensation of the 1–8 and the thionated 9–11 segments.

For the difficult coupling steps, in particular those involving the segment condensations, the *N*-[3-(dimethylamino)-propyl]-*N*'-ethylcarbodiimide (EDC)/7-aza-1-hydroxy-1,2,3-benzotriazole (HOAt) [51] activating method was used, while the EDC/1-hydroxy-1,2,3-benzotriazole (HOBt) [52] method turned out to be appropriate for the formation of the other peptide bonds. The yields of the segment condensation reactions were good (75–83%). An important feature, which makes trichogin GA IV a versatile synthetic platform, is the presence of as many as seven achiral (Aib or Gly) residues spread across its sequence, which allows one to design suitable segments each with an achiral residue at its C-terminus, thus reducing dramatically the usually considerable risk of epimerization during the coupling reactions.

For the best choice of the step involving treatment with the Lawesson's reagent [53], we decided to select the longest segment of our sequences, which, in principle, could permit complete regioselectivity between the peptide bond to be thionated and the other peptide bonds (in addition to the known regioselectivity versus the urethane and ester bonds) [53-56]. In this reaction, regioselectivity is known to be heavily governed by the steric hindrance of the two residues around the peptide

bond. Therefore, we synthesized Boc-Gly^{2}ψ[CS-NH]Leu-Aib^4-OMe (for the preparation of **ψ[CS-NH]^2**), Fmoc-Gly^{5}ψ[CS-NH]Gly-Leu-Aib^8-O*t*-Bu (for the preparation of **ψ[CS-NH]^5**), and Boc-Gly^{9}ψ[CS-NH]Ile-Leu^{11}-OMe (for the preparation of **ψ[CS-NH]^9**). Thionation of a peptide as short as a dipeptide is not recommended because a further synthetic step at the C-terminus of this compound would not take place satisfactorily, owing to the easy formation of a poorly reactive 1,3-thiazolidin-5-one. All thionation steps were conducted by use of the Lawesson's reagent under mild conditions (in tetrahydrofuran at room temperature) [53-56]. The only synthetic problem was identified in the preparation of the Fmoc-Gly^{5}ψ[CS-NH]Gly-Leu-Aib^8-O*t*-Bu, in which case the thionation selectivity on the Gly-Gly peptide bond was incomplete. Indeed, a limited production (about 10%) of the isomeric Fmoc-Gly-Gly^{6}ψ[CS-NH]Leu-Aib-O*t*-Bu, with its slightly more hindered, thionated Gly-Leu peptide bond, was observed. In this case, the desired monothionated peptide was separated from its isomer by means of flash chromatography.

For details of the synthetic procedures and characterizations of these analogues (and the synthetic precursor segments as well), see the Experimental section and Supporting Information File 1. Figure 2 gives the RP-HPLC profiles of the three monothionated trichogin GA IV analogues.

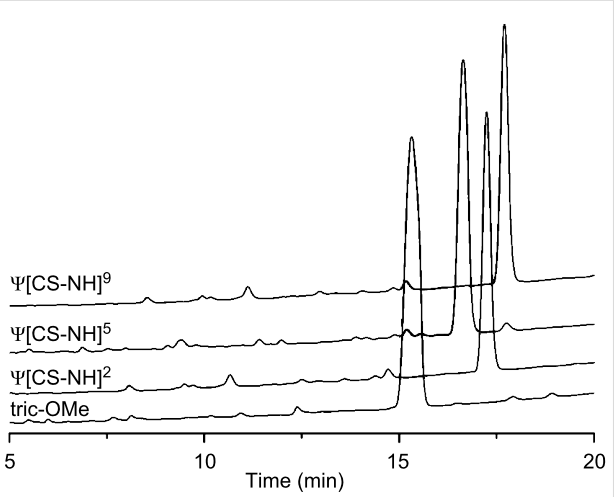

Figure 2: RP-HPLC profiles obtained for [Leu^{11}-OMe] trichogin GA IV (**tric-OMe**) and its **ψ[CS-NH]^2**, **ψ[CS-NH]^5**, and **ψ[CS-NH]^9** analogues.

Conformational analysis

A detailed analysis of the spectroscopic properties and conformational preferences of the three monothionated trichogin GA IV analogues synthesized in this work was performed by using CD, FT-IR absorption, and 2D NMR investigations in different solvents.

The far- (250–195 nm) and near-UV (400–250 nm) CD spectra of the three peptides, recorded in 2,2,2-trifluoroethanol (TFE) solution, are illustrated in Figure 3. In the near-UV region, in which the peptide chromophore is known not to absorb, both **ψ[CS-NH]^2** and **ψ[CS-NH]^9** display two well-separated Cotton effects at about 335 and 265 nm. The longer wavelength band is

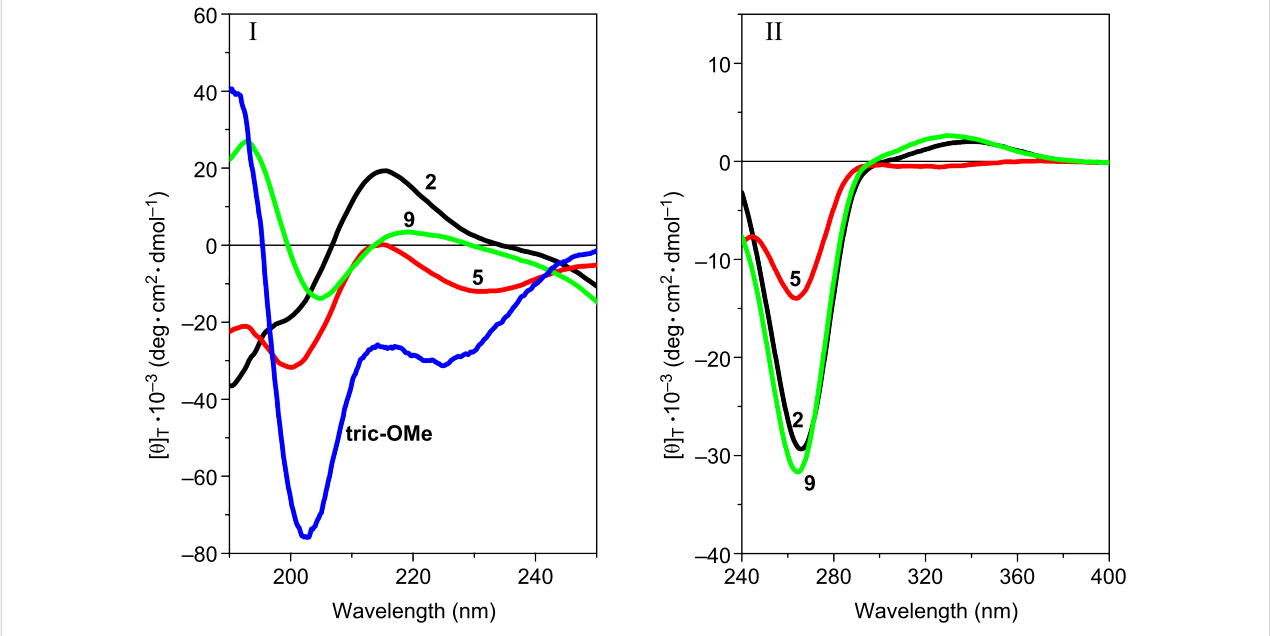

Figure 3: Far-UV (panel I) and near-UV (panel II) CD spectra of [Leu^{11}-OMe] trichogin GA IV (**tric-OMe**) and its **ψ[CS-NH]^2** (**2**), **ψ[CS-NH]^5** (**5**), and **ψ[CS-NH]^9** (**9**) analogues in TFE solution. Peptide concentration: 1 mM.

positive and weak, while the shorter wavelength band is negative and much more intense. Interestingly, the positive band is absent and the negative band is much weaker in **ψ[CS-NH]^5**. The spectral positions of these Cotton effects correspond to a very intense maximum (265 nm) and an extremely weak maximum (320 nm) found in the corresponding region of the UV absorption spectra (not shown) of our peptides in the same solvent. We assign the two bands to the π→π* and n→π* transitions, respectively, of thioamide chromophore [29,30,32-36,40,41,43]. We attribute the overall much less intense CD spectrum of **ψ[CS-NH]^5** in this region primarily to a thioamide chromophore positioned in this peptide between the two achiral Gly^5 and Gly^6 residues, i.e., it is significantly far apart from the nearest chiral center (the Leu^7 α-carbon).

In the far-UV region the CD spectra of all three analogues show multiple (negative/positive) Cotton effects of weak and medium intensities. Here, the bands (shoulders) of **ψ[CS-NH]^9** are the weakest. In our view, it is risky to attempt to extract any conclusive conformational information from the CD properties of these three isomeric peptides between 195 and 250 nm because, in addition to the expected Cotton effects of the peptide chromophores [57,58], the thioamide chromophore [34,35] is also known to contribute heavily in this spectral region. However, we can safely state that the shape of the CD spectrum of the [Leu^{11}-OMe] trichogin GA IV prototypical peptide [50,59] is most closely paralleled by that of its **ψ[CS-NH]^5** analogue, although the former is significantly more intense. This finding is not surprising in view of the above-mentioned low influence of the thioamide chromophore on the spectrum of this monothionated compound. It may also suggest that the overall conformation of the lipopeptaibiotic is disturbed by this specific oxygen-to-sulfur exchange only to a limited extent.

The preferred conformations of the three monothionated [Leu^{11}-OMe] trichogin GA IV analogues were more safely analyzed by means of FT-IR absorption and 2D NMR. In this study, we used $CDCl_3$, a solvent of low polarity. In the 3D-structurally informative 3550–3200 cm^{-1} region at 1.0 mM concentration, the FT-IR spectra of [Leu^{11}-OMe] trichogin GA IV and its analogues are similar and dominated by a broad and intense absorption at 3316–3328 cm^{-1} (Figure 4), assigned to the N–H stretching mode of the largely prevailing H-bonded peptide groups [60,61]. Additional, very weak bands are visible in the 3450–3400 cm^{-1} region, mostly attributed to free (solvated) peptide NH groups.

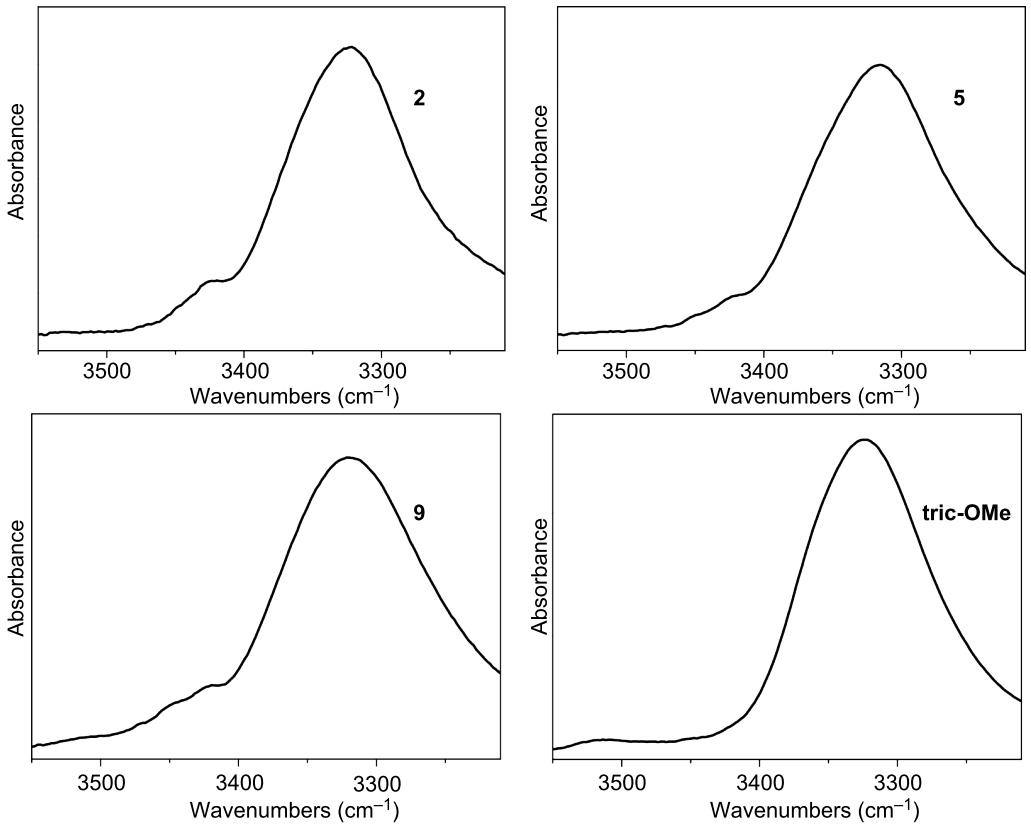

Figure 4: FT-IR absorption spectra (3550–3200 cm^{-1} region) in $CDCl_3$ solution of [Leu^{11}-OMe] trichogin GA IV (**tric-OMe**) and its **ψ[CS-NH]^2** (**2**), **ψ[CS-NH]^5** (**5**), and **ψ[CS-NH]^9** (**9**) analogues. Peptide concentration: 1 mM.

A nonnegligible dilution effect is observed in the spectra of the four peptides between 1.0 and 0.1 mM concentration (not shown). We ascribe this difference to the well-known tendency of trichogin GA IV and its analogues to self-associate above 1.0 mM concentration in $CDCl_3$ solution. We interpret the spectra at 0.1 mM concentration as arising almost exclusively from intramolecular C=O(S)···H–N interactions. It is clear that under these experimental conditions the preferred conformation of [Leu^{11}-OMe] trichogin GA IV [46-50] and its three analogues, all rich in the helix-supporting Aib residues, is highly folded and largely stabilized by intramolecular H-bonds. In the amide I (C=O stretching) region, the maximum of the absorption band of the four peptides is located between 1662 and 1656 cm^{-1} (not shown), close to the canonical positions of this band [61,62] in α- and 3_{10}-helical peptides [63].

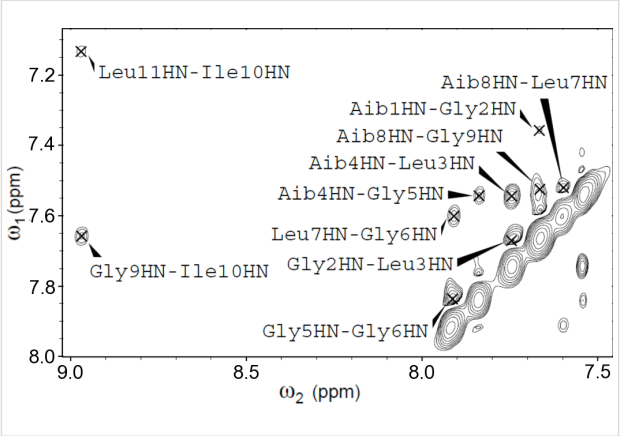

Figure 5: Region of the amide NH protons in the H/H-ROESY spectrum of **ψ[CS-NH]^9** (400 MHz, 1 mM in CD_3CN solution, 298 K).

A 2D NMR investigation was performed in CD_3CN solution for all of the ψ[CS-NH]-containing [Leu^{11}-OMe] trichogin GA IV analogues. The proton resonances were fully assigned following the Wüthrich procedure [64]. Regions of the ROESY spectrum acquired for **ψ[CS-NH]^9** are shown in Figures 5–7. The patterns of NH(i)–NH(i+1) connectivities (e.g., Figure 5) strongly suggest the onset of an overall helical structure for all analogues. More relevant 3D-structural information was extracted from the *fingerprint* regions of the ROESY spectra (e.g., Figure 6 and Figure 7), which show evidence for $d_{\alpha(\beta),N}$ (i, i+2), (i, i+3), and (i, i+4) medium-range connectivities, diagnostic of the presence of mixed 3_{10}-/α-helical conformations.

The conformational properties of **ψ[CS-NH]^9** were further investigated by simulated annealing (SA) and restrained molecular dynamics (MD) calculations. A total of 69 interproton distance restraints, derived from the related ROESY spectrum (Table S-I, Supporting Information File 1), were used in the SA protocol. The structures possessing violations to the NOE restraints lower than 0.5 Å were selected out of the 150 generated structures. The superposition of the 18 structures with a total energy <144 kcal/mol is shown in Figure S-I, Supporting Information File 1. All these structures converge to a well-defined, right-handed, mixed 3_{10}-/α-helical conformation throughout the sequence with a backbone average pairwise root-

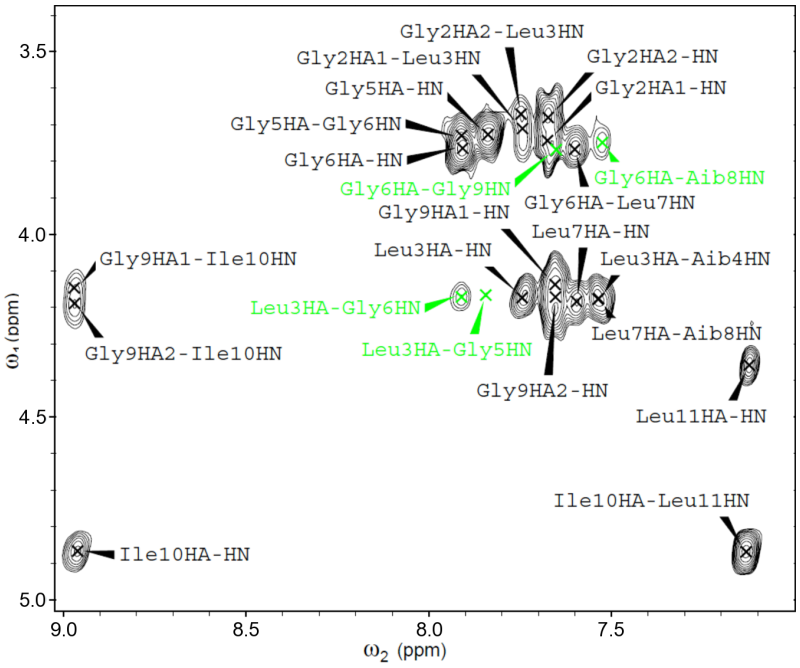

Figure 6: Fingerprint region of the H/H-ROESY spectrum of **ψ[CS-NH]^9** (400 MHz, 1 mM in CD_3CN solution, 298 K). The $C^{\alpha}H_i \rightarrow NH_{i+2}$, and $C^{\alpha}H_i \rightarrow NH_{i+3}$ cross peaks are highlighted in color.

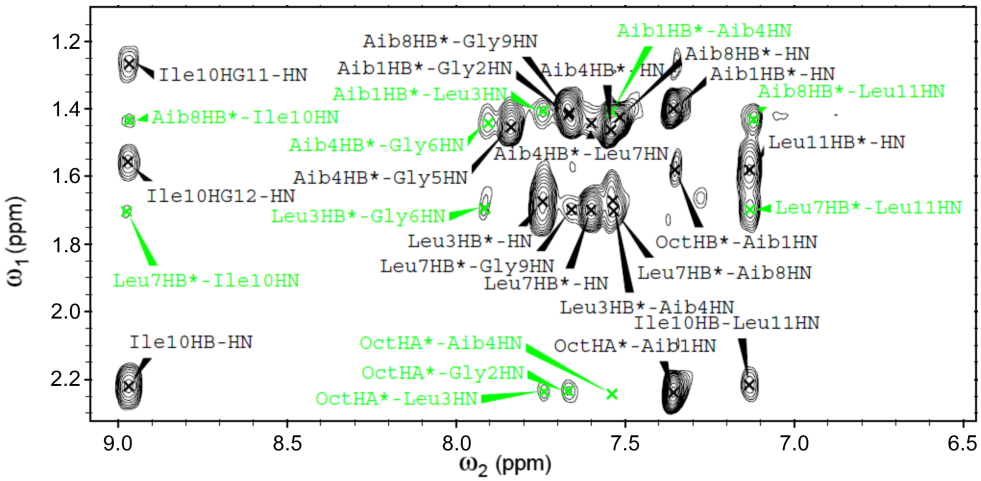

Figure 7: Fingerprint region of the H/H-ROESY spectrum of **ψ[CS-NH]^9** (400 MHz, 1 mM in CD_3CN solution, 298 K). The $C^{\beta}H_i \rightarrow NH_{i+2}$, $C^{\beta}H_i \rightarrow NH_{i+3}$, and $C^{\beta}H_i \rightarrow NH_{i+4}$ cross peaks are highlighted in color.

mean-square deviation of 0.49 ± 0.18 Å (deviations from idealized geometry and mean energies for the 18 lowest energy structures are listed in Table S-I, Supporting Information File 1). Due to heavily overlapped ROE signals, the helical structures originated from the MD calculations appear not to superimpose perfectly in correspondence with the first three residues of the sequence. Even with this experimental limit, the residues belonging to the central and C-terminal parts of the sequence showed values of torsion angles corresponding to those characteristic of right-handed helices (Table S-II, Supporting Information File 1). The helical structures are stabilized by intramolecular H-bonds throughout the sequence. H-bonds both of the α- ($i \leftarrow i+4$) and 3_{10}- ($i \leftarrow i+3$) helical types are present, although with a large predominance of the latter type (mean distance: 1.81 ± 0.17 Å; mean angle: 27.4 ± 3.7°), at the N-terminus. Conversely, only the former type (mean distance: 1.53 ± 0.02 Å; mean angle: 27.3 ± 2.9°) was detected at the C-terminus.

In conclusion, the MD calculations based on the restraints derived from the ROESY spectrum of **ψ[CS-NH]^9** reveal the marked preference of this analogue for a mixed α-/3_{10}- helical conformation, with a clear α-helical character at the C-terminus on which the thioamide bond is present. The lowest-energy 3D structure, shown in Figure 8, exhibits the slightly amphipathic character typical of the native peptide, with the poorly hydrophilic Gly residues aligned on the same face of the helix.

Membrane and biological activities

The membrane permeability properties of [Leu^{11}-OMe] trichogin GA IV and its monothionated analogues were tested by measuring the induced leakage of 5(6)-carboxyfluorescein (CF) entrapped in small unilamellar vesicles (SUVs) [65]. For this investigation, the overall negatively charged 1,2-dioleoyl-*sn*-glycero-3-phosphoethanolamine (DOPE)/1,2-dioleoyl-*sn*-glycero-3-phospho-(1'-*rac*-glycerol) (DOPG) model membrane was exploited. The extent of permeation induced by the three

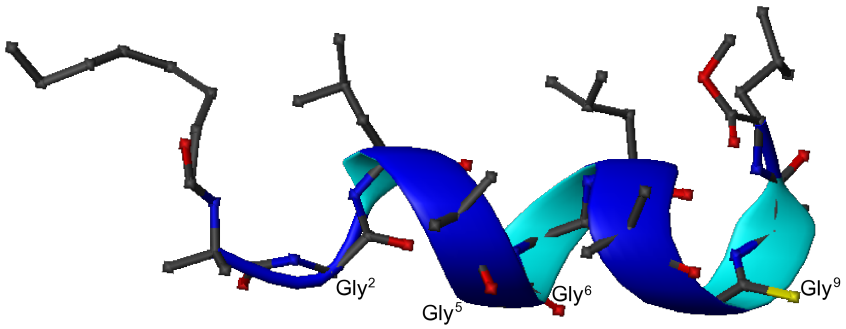

Figure 8: Ribbon representation of the lowest energy (138.7 kcal/mol) 3D structure obtained for **ψ[CS-NH]^9**. All amino acid side chains are shown. The yellow atom on Gly^9 refers to sulfur.

analogues is similar, although 30–40% lower than that of the parent peptaibiotic.

The antimicrobial activities were assessed on a large set of Gram-positive and Gram-negative bacterial strains. We found that [Leu^{11}-OMe] trichogin GA IV is active on the Gram-positive bacteria *Staphylococcus aureus* and *Streptococcus pyrogenes*, whereas the spectrum of action of its three analogues is more restricted, as they are not active on the latter strain. The activities of the analogues on *S. aureus* are comparable, but reduced by about 40% with respect to that of the parent peptaibiotic.

Conclusion

In this work, we performed a partial thioamide scan of the short lipopeptaibiotic [Leu^{11}-OMe] trichogin GA IV by synthesizing and studying three thioamide-containing analogues. The syntheses were accomplished in solution by using a combination of the step-by-step and segment condensation methods. Appropriate tri- and tetrapeptide segments were monothionated by treating the all-amide precursors with the Lawesson's reagent. Our CD, FT-IR absorption, and NMR conformational investigations show that all analogues maintain the mixed 3_{10}-/α-helical structure and the self-association propensity of the native lipopeptide. They also preserve, at least to a great extent, its well-established capability to interact with model phospholipid membranes and to exhibit activity against Gram-positive bacterial strains.

Experimental

All reagents and solvents, of analytical grade and purchased from commercial sources, were used without further purification. Melting points were measured by means of a capillary tube immersed in an oil bath (Tottoli apparatus, Büchi) and are uncorrected. Optical rotations $[\alpha]_D^{20}$ (given in units of 10^{-1} deg·cm^2·g^{-1}) were measured at 20 °C on a Perkin-Elmer PE241 polarimeter, with a 1 dm path length cell, at the D-wavelength of sodium (589 nm). The concentration of each compound (*c*) is given in mg/cL. Mass spectroscopy (electrospray ionization, ESIMS) was performed by using a PerSeptive Biosystem Mariner instrument (Framingham, MA). Analytical TLC and preparative column chromatography were performed on Kieselgel F 254 and Kieselgel 60 (0.040–0.063 mm) (Merck), respectively. The retention factor (R_f) values were determined by using three solvent mixtures as eluants: R_{f1}: chloroform/ethanol 9:1; R_{f2}: 1-butanol/acetic acid/water 3:1:1; R_{f3}: toluene/ethanol 7:1.

General procedure for thionation of peptides

To a solution of the peptide (1 mmol) in anhydrous tetrahydrofuran under nitrogen atmosphere, the Lawesson's reagent (0.6 mmol) was added. The reaction mixture was stirred at rt overnight. After removal of the solvent under reduced pressure, the crude product was purified by flash chromatography with a mixture of ethyl acetate and petroleum ether as eluant.

Peptides Boc-Ile-Leu-OMe [66], Z-Leu-Aib-OMe [67], Z-Leu-Aib-O*t*-Bu [68], Boc-Gly-Leu-Aib-OMe [69], Boc-Gly-Ile-Leu-OMe [66], Boc-Leu-Aib-Gly-Ile-Leu-OMe [66], Boc-Gly-Gly-Leu-Aib-Gly-Ile-Leu-OMe [66], Z-Gly-Gly-Leu-Aib-O*t*-Bu [59], and Z-Aib-Gly-Leu-Aib-Gly-Gly-Leu-Aib-O*t*-Bu [59] are known compounds. Chemical characterizations and selected NMR spectra for the other peptides reported in Schemes 1–3 are given in Supporting Information File 1.

Circular dichroism

The CD spectra were measured on a Jasco (Tokyo, Japan) model J-715 spectropolarimeter equipped with a Haake thermostat (Thermo Fisher Scientific, Waltham, MA). Baselines were corrected by subtracting the solvent contribution. Fused quartz cells of 1.0 mm and 10.0 mm path lengths (Hellma, Mühlheim, Germany) were used. The values are expressed in terms of $[\theta]_T$, the total molar ellipticity (deg·cm^2·dmol^{-1}). Spectrograde TFE and 99.9% MeOH (Acros Organic, Geel, Belgium) were employed as solvents.

FT-IR absorption

The FT-IR absorption spectra were recorded at 293 K by using a Perkin-Elmer model 1720X FT-IR spectrophotometer, nitrogen-flushed, equipped with a sample-shuttle device, at 2 cm^{-1} nominal resolution, averaging 100 scans. Solvent (baseline) spectra were recorded under the same conditions. For spectral elaboration, the software SPECTRACALC provided by Galactic (Salem, MA) was employed. Cells with path lengths of 1.0 and 10 mm (with CaF_2 windows) were used. Spectrograde deuterated chloroform (99.8%, *d*) was purchased from Merck (Darmstadt, Germany).

Nuclear magnetic resonance

All ^{1}H NMR experiments were performed on a Bruker AVANCE DMX-600, DRX-400 or AC200 spectrometer operating at 600, 400 or 200 MHz, respectively, using the TOPSPIN software package. Splitting patterns are abbreviated as (s) singlet, (d) doublet, (t) triplet, (q) quartet, (m) multiplet. The homonuclear 2D spectra of the three monothionated [Leu^{11}-OMe] trichogin GA IV analogues were recorded at 298 K, with CD_3CN as solvent. All spectra were acquired by recording 512 experiments, each one consisting of 64–80 scans and 2000 data points. The spin systems of protein amino acid residues were identified by using standard DQF-COSY [70] and CLEAN-TOCSY [71,72] spectra. In the latter case, the spin-lock pulse sequence was 70 ms long. A ROESY experiment was exploited

for sequence-specific assignment. The mixing time of the ROESY experiment acquired for **ψ[CS-NH]^9** (peptide concentration: 1.00 mM in CD_3CN) and used for interproton distance determination was 200 ms. Interproton distances were obtained by integration of the ROESY spectra using SPARKY 3.111. The calibration was based on the average of the integration values of the cross peaks due to the interactions between the sequential amide protons, set to a distance of 2.80 Å. When peaks could not be integrated because of partial overlap, a distance corresponding to the maximum limit of detection of the experiment (4.0 Å) was assigned to the corresponding proton pair.

MD calculations were carried out using the SA protocol of the XPLOR-NIH 2.9.6 program [73]. For distances involving equivalent or non-stereo-assigned protons, an r^{-6} averaging was used. The MD calculations involved a minimization stage of 100 cycles, followed by SA and refinement stages. The SA consisted of 30 ps of dynamics at 1,500 K (10,000 cycles, in 3 fs steps) and of 30 ps of cooling from 1,500 to 100 K in 50 K decrements (15,000 cycles, in 2 fs steps). The SA procedure, in which the weights of ROE and nonbonded terms were gradually increased, was followed by 200 cycles of energy minimization. In the SA refinement stage, the system was cooled from 1,000 to 100 K in 50 K decrements (20,000 cycles, in 1 fs steps). Finally, the calculations were completed with 200 cycles of energy minimization by using a NOE force constant of 50 kcal/mol. The generated structures were visualized with the MOLMOL [74] (version 2K.2) program.

Small unilamellar vesicles (SUVs) preparation

DOPE and DOPG were purchased from Avanti Polar Lipids, Inc. (Alabaster, AL). The preparation of SUVs was performed in a similar way as described in reference [59].

Leakage from lipid vesicles

The peptide-induced leakage from SUVs was measured at 293 K by using the CF-entrapped vesicle technique [65] and a Perkin Elmer model MPF-66 spectrofluorimeter. SUVs were prepared as described above. The phospholipid concentration was kept constant (0.06 mM), and increasing [peptide]/[lipid] molar ratios (R^{-1}) were obtained by adding aliquots of each non-hydrosoluble, monothionated peptide (or of trichogin GA IV, used as reference compound) as a MeOH solution, keeping the final MeOH concentration below 5% by volume. After rapid and vigorous stirring, the time course of fluorescence change corresponding to CF escape was recorded at 520 nm (6 nm band pass) with λ_{exc} 488 nm (3 nm band pass). The percentage of released CF at time t was determined as $100 \times (F_t - F_0)/(F_T - F_0)$, with F_0 = fluorescence intensity of vesicles in the absence of peptide, F_t = fluorescence intensity of vesicles at time t in the presence of peptide, and F_T = total fluorescence intensity determined by disrupting the vesicles by the addition of 50 μL of a Triton X-100 solution. The experiments were stopped at 20 min.

Antibacterial activity

Peptide antibacterial activity was tested against Gram-positive and Gram-negative bacteria by the standardized disk diffusion Bauer–Kirby method [75] using the Müller–Hinton culture medium at pH 7.2–7.4 as recommended by the National Committee for Clinical Laboratory Standards [76]. The antibacterial activity assay was performed in a similar way to that described in reference [77]. The activity of peptides was tested against clinical isolates of bacteria and reference bacterial strains: *Staphylococcus aureus* American Type Culture Collection strains (ATCC) 25923, *Streptococcus pyogenes* ATCC 19615, *Escherichia coli* ATCC 25922, *Pseudomonas aeruginosa* ATCC 27853, *Klebsiella pneumoniae* ATCC 13883, *Salmonella entereditis* 13076, and *Proteus mirabilis* ATCC 10975. The well-known antibiotics bacitracin and tetracyclin (10 μg/disk) were used as controls.

Supporting Information

Supporting Information File 1

Chemical characterization data for the peptides reported in Schemes 1–3.
[http://www.beilstein-journals.org/bjoc/content/supplementary/1860-5397-8-129-S1.pdf]

References

1. Spatola, A. F. Peptide backbone modifications: Structure–activity analysis of peptides containing amide bond surrogates. In *Chemistry and Biochemistry of Amino Acids, Peptides and Proteins;* Weinstein, B., Ed.; Dekker: New York, 1983; pp 267–357.
2. La Cour, T. F. M.; Hansen, H. A. S.; Clausen, K.; Lawesson, S.-O. *Int. J. Pept. Protein Res.* **1983,** *22,* 509–512. doi:10.1111/j.1399-3011.1983.tb02122.x
3. La Cour, T. F. M. *Int. J. Pept. Protein Res.* **1987,** *30,* 564–571. doi:10.1111/j.1399-3011.1987.tb03366.x
4. Jensen, O. E.; Lawesson, S.-O.; Bardi, R.; Piazzesi, A. M.; Toniolo, C. *Tetrahedron* **1985,** *41,* 5595–5606. doi:10.1016/S0040-4020(01)91361-4
5. Bardi, R.; Piazzesi, A. M.; Toniolo, C.; Jensen, O. E.; Omar, R. S.; Senning, A. *Biopolymers* **1988,** *27,* 747–761. doi:10.1002/bip.360270504
6. Bardi, R.; Piazzesi, A. M.; Toniolo, C.; Jensen, O. E.; Andersen, T. P.; Senning, A. *Tetrahedron* **1988,** *44,* 761–769. doi:10.1016/S0040-4020(01)86115-9
7. Lehmann, J.; Linden, A.; Heimgartner, H. *Tetrahedron* **1998,** *54,* 8721–8736. doi:10.1016/S0040-4020(98)00506-7
8. Pradeille, N.; Zerbe, O.; Möhle, K.; Linden, A.; Heimgartner, H. *Chem. Biodiversity* **2005,** *2,* 1127–1152. doi:10.1002/cbdv.200590084

9. Stamm, S.; Heimgartner, H. *Helv. Chim. Acta* **2006,** *89,* 1841–1855. doi:10.1002/hlca.200690178
10. Budzowski, A.; Linden, A.; Heimgartner, H. *Helv. Chim. Acta* **2008,** *91,* 1471–1488. doi:10.1002/hlca.200890160
11. Mawad, N.; Pour, F. G.-S.; Linden, A.; Heimgartner, H. *Helv. Chim. Acta* **2010,** *93,* 2326–2346. doi:10.1002/hlca.201000318
12. Liu, Z.; Mehta, S. J.; Lee, K.-S.; Grossman, B.; Qu, H.; Gu, X.; Nichol, G. S.; Hruby, V. J. *J. Org. Chem.* **2012,** *77,* 1289–1300. doi:10.1021/jo201753q
13. Hua, G.; Fuller, A. L.; Bühl, M.; Slawin, A. M. Z.; Woollins, J. D. *Eur. J. Org. Chem.* **2011,** 3067–3073. doi:10.1002/ejoc.201100226
14. Xie, J.; Okano, A.; Pierce, J. G.; James, R. C.; Stamm, S.; Crane, C. M.; Boger, D. L. *J. Am. Chem. Soc.* **2012,** *134,* 1284–1297. doi:10.1021/ja209937s
15. Chen, P.; Qu, J. *J. Org. Chem.* **2011,** *76,* 2994–3004. doi:10.1021/jo200403g
16. Tran, T. T.; Burgess, A. W.; Treutlein, H.; Perich, J. *J. Pept. Res.* **2001,** *58,* 67–78. doi:10.1034/j.1399-3011.2001.00898.x
17. Wood, P. A.; Pidcock, E.; Allen, F. H. *Acta Crystallogr., Sect. B* **2008,** *64,* 491–496. doi:10.1107/S0108768108015437
18. Tran, T. T.; Treutlein, H.; Burgess, A. W. *Protein Eng., Des. Sel.* **2006,** *19,* 401–408. doi:10.1093/protein/gzl024
19. Tran, T. T.; Zeng, J.; Treutlein, H.; Burgess, A. W. *J. Am. Chem. Soc.* **2002,** *124,* 5222–5230. doi:10.1021/ja011916o
20. Artis, D. R.; Lipton, M. A. *J. Am. Chem. Soc.* **1998,** *120,* 12200–12206. doi:10.1021/ja982398t
21. Alemán, C. *J. Phys. Chem. A* **2001,** *105,* 6717–6723. doi:10.1021/jp010198p
22. Choudhary, A.; Gandla, D.; Krow, G. R.; Raines, R. T. *J. Am. Chem. Soc.* **2009,** *131,* 7244–7246. doi:10.1021/ja901188y
23. Choudhary, A.; Raines, R. T. *ChemBioChem* **2011,** *12,* 1801–1807. doi:10.1002/cbic.201100272
24. Cervetto, V.; Pfister, R.; Kolano, C.; Bregy, H.; Heimgartner, H.; Helbing, J. *Chem.–Eur. J.* **2007,** *13,* 9004–9011. doi:10.1002/chem.200700396
25. Cervetto, V.; Pfister, R.; Helbing, J. *J. Phys. Chem. B* **2008,** *112,* 3540–3544. doi:10.1021/jp710611n
26. Cervetto, V.; Hamm, P.; Helbing, J. *J. Phys. Chem. B* **2008,** *112,* 8398–8405. doi:10.1021/jp801166q
27. Bregy, H.; Heimgartner, H.; Helbing, J. *J. Phys. Chem. B* **2009,** *113,* 1756–1762. doi:10.1021/jp8089402
28. Huang, Y.; Cong, Z.; Yang, L.; Dong, S. *J. Pept. Sci.* **2008,** *14,* 1062–1068. doi:10.1002/psc.1042
29. Wildemann, D.; Schiene-Fischer, C.; Aumüller, T.; Bachmann, A.; Kiefhaber, T.; Lücke, C.; Fischer, G. *J. Am. Chem. Soc.* **2007,** *129,* 4910–4918. doi:10.1021/ja069048o
30. Zhao, J.; Micheau, J.-C.; Vargas, C.; Schiene-Fischer, C. *Chem.–Eur. J.* **2004,** *10,* 6093–6101. doi:10.1002/chem.200400400
31. Bailey, P. D.; Boyd, C. A. R.; Collier, I. D.; Kellett, G. L.; Meredith, D.; Morgan, K. M.; Pettecrew, R.; Price, R. A. *Org. Biomol. Chem.* **2005,** *3,* 4038–4039. doi:10.1039/B513274F
32. Miwa, J. H.; Pallivathucal, L.; Gowda, S.; Lee, K. E. *Org. Lett.* **2002,** *4,* 4655–4657. doi:10.1021/ol027056d
33. Miwa, J. H.; Patel, A. K.; Vivatrat, N.; Popek, S. M.; Meyer, A. M. *Org. Lett.* **2001,** *3,* 3373–3375. doi:10.1021/ol0166092
34. Kajtár, M.; Hollósi, M.; Kajtár, J.; Majer, Z.; Kövér, K. E. *Tetrahedron* **1986,** *42,* 3931–3942. doi:10.1016/S0040-4020(01)87548-7
35. Hollósi, M.; Kollát, E.; Kajtár, J.; Kajtár, M.; Fasman, G. D. *Biopolymers* **1990,** *30,* 1061–1072. doi:10.1002/bip.360301107
36. Reiner, A.; Wildemann, D.; Fischer, G.; Kiefhaber, T. *J. Am. Chem. Soc.* **2008,** *130,* 8079–8084. doi:10.1021/ja8015044
37. Goldberg, J. M.; Batjargal, S.; Petersson, E. J. *J. Am. Chem. Soc.* **2010,** *132,* 14718–14720. doi:10.1021/ja1044924
38. Goldberg, J. M.; Wissner, R. F.; Klein, A. M.; Petersson, E. J. *Chem. Commun.* **2012,** *48,* 1550–1552. doi:10.1039/c1cc14708k
39. Satzger, H.; Root, C.; Gilch, P.; Zinth, W.; Wildemann, D.; Fischer, G. *J. Phys. Chem. B* **2005,** *109,* 4770–4775. doi:10.1021/jp045151t
40. Sifferlen, T.; Rueping, M.; Gademann, K.; Jaun, B.; Seebach, D. *Helv. Chim. Acta* **1999,** *82,* 2067–2093. doi:10.1002/(SICI)1522-2675(19991215)82:12<2067::AID-HLCA2067>3.0.CO;2-5
41. Bachmann, A.; Wildemann, D.; Praetorius, F.; Fischer, G.; Kiefhaber, T. *Proc. Natl. Acad. Sci. U. S. A.* **2011,** *108,* 3952–3957. doi:10.1073/pnas.1012668108
42. Mierke, D. F.; Geyer, A.; Kessler, H. *Int. J. Pept. Protein Res.* **1994,** *44,* 325–331. doi:10.1111/j.1399-3011.1994.tb01016.x
43. Otani, Y.; Hori, T.; Kawahata, M.; Yamagouchi, K.; Ohwada, T. *Tetrahedron* **2012,** *68,* 4418–4428. doi:10.1016/j.tet.2012.01.018
44. Banala, S.; Süssmuth, R. D. *ChemBioChem* **2010,** *11,* 1335–1337. doi:10.1002/cbic.201000266
45. Toniolo, C.; Brückner, H. *Peptaibiotics: Fungal Peptides Containing α-Dialkyl α-Amino Acids;* Wiley-VCH: Weinheim, Germany, 2009.
46. Toniolo, C.; Crisma, M.; Formaggio, F.; Peggion, C.; Epand, R. F.; Epand, R. M. *Cell. Mol. Life Sci.* **2001,** *58,* 1179–1188. doi:10.1007/PL00000932
47. Peggion, C.; Formaggio, F.; Crisma, M.; Epand, R. F.; Epand, R. M.; Toniolo, C. *J. Pept. Sci.* **2003,** *9,* 679–689. doi:10.1002/psc.500
48. Venanzi, M.; Gatto, E.; Bocchinfuso, G.; Palleschi, A.; Stella, L.; Formaggio, F.; Toniolo, C. *ChemBioChem* **2006,** *7,* 43–45. doi:10.1002/cbic.200500271
49. Venanzi, M.; Bocchinfuso, G.; Gatto, E.; Palleschi, A.; Stella, L.; Formaggio, F.; Toniolo, C. *ChemBioChem* **2009,** *10,* 91–97. doi:10.1002/cbic.200800617
50. De Zotti, M.; Biondi, B.; Formaggio, F.; Toniolo, C.; Stella, L.; Park, Y.; Hahm, K.-S. *J. Pept. Sci.* **2009,** *15,* 615–619. doi:10.1002/psc.1135
51. Carpino, L. A. *J. Am. Chem. Soc.* **1993,** *115,* 4397–4398. doi:10.1021/ja00063a082
52. König, W.; Geiger, R. *Chem. Ber.* **1970,** *103,* 788–798. doi:10.1002/cber.19701030319
53. Clausen, K.; Thorsen, M.; Lawesson, S.-O. *Tetrahedron* **1981,** *37,* 3635–3639. doi:10.1016/S0040-4020(01)98892-1
54. Lajoie, G.; Lépine, F.; Maziak, L.; Belleau, B. *Tetrahedron Lett.* **1983,** *24,* 3815–3818. doi:10.1016/S0040-4039(00)94282-5
55. Cava, M. P.; Levinson, M. I. *Tetrahedron* **1985,** *41,* 5061–5087. doi:10.1016/S0040-4020(01)96753-5
56. Ozturk, T.; Ertas, E.; Mert, O. *Chem. Rev.* **2007,** *107,* 5210–5278. doi:10.1021/cr040650b
57. Goodman, M.; Toniolo, C. *Biopolymers* **1968,** *6,* 1673–1689. doi:10.1002/bip.1968.360061202
58. Sreerama, N.; Woody, R. W. Circular dichroism of peptides and proteins. In *Circular Dichroism: Principles and Applications,* 2nd ed.; Berova, N.; Nakanishi, K.; Woody, R. W., Eds.; Wiley-VCH: New York, 2000; pp 601–620.
59. De Zotti, M.; Biondi, B.; Peggion, C.; Formaggio, F.; Park, Y.; Hahm, K.-S.; Toniolo, C. *Org. Biomol. Chem.* **2012,** *10,* 1285–1299. doi:10.1039/c1ob06178j
60. Palumbo, M.; da Rin, S.; Bonora, G. M.; Toniolo, C. *Makromol. Chem.* **1976,** *177,* 1477–1492. doi:10.1002/macp.1976.021770519

61. Moretto, V.; Crisma, M.; Bonora, G. M.; Toniolo, C.; Balaram, H.; Balaram, P. *Macromolecules* **1989,** *22,* 2939–2944. doi:10.1021/ma00197a010
62. Kennedy, D. F.; Crisma, M.; Toniolo, C.; Chapman, D. *Biochemistry* **1991,** *30,* 6541–6548. doi:10.1021/bi00240a026
63. Toniolo, C.; Benedetti, E. *Trends Biochem. Sci.* **1991,** *16,* 350–353. doi:10.1016/0968-0004(91)90142-I
64. Wüthrich, K. *NMR of Proteins and Nucleic Acids;* Wiley: New York, 1986.
65. Auvin-Guette, C.; Rebuffat, S.; Prigent, Y.; Bodo, B. *J. Am. Chem. Soc.* **1992,** *114,* 2170–2174. doi:10.1021/ja00032a035
66. Gurunath, R.; Balaram, P. *Biopolymers* **1995,** *35,* 21–29. doi:10.1002/bip.360350104
67. Iida, A.; Yoshimatsu, S.; Sanekata, M.; Fujita, T. *Chem. Pharm. Bull.* **1990,** *38,* 2997–3003. doi:10.1248/cpb.38.2997
68. Brückner, H.; Koza, A. *Amino Acids* **2003,** *24,* 311–323. doi:10.1007/s00726-002-0401-x
69. Nagaraj, R.; Balaram, P. *Tetrahedron* **1981,** *37,* 1263–1270. doi:10.1016/S0040-4020(01)92061-7
70. Rance, M.; Sørensen, O. W.; Bodenhausen, G.; Wagner, G.; Ernst, R. R.; Wüthrich, K. *Biochem. Biophys. Res. Commun.* **1983,** *117,* 479–485. doi:10.1016/0006-291X(83)91225-1
71. Bax, A.; Davis, D. G. *J. Magn. Reson.* **1985,** *65,* 355–360. doi:10.1016/0022-2364(85)90018-6
72. Griesinger, C.; Otting, G.; Wüthrich, K.; Ernst, R. R. *J. Am. Chem. Soc.* **1988,** *110,* 7870–7872. doi:10.1021/ja00231a044
73. Schwieters, C. D.; Kuszewski, J. J.; Tjandra, N.; Clore, G. M. *J. Magn. Reson.* **2003,** *160,* 65–73. doi:10.1016/S1090-7807(02)00014-9 (based on X-PLOR 3.851 by A. T. Brunger).
74. Koradi, R.; Billeter, M.; Wüthrich, K. *J. Mol. Graphics* **1996,** *14,* 51–55. doi:10.1016/0263-7855(96)00009-4
75. Bauer, A. W.; Kirby, W. M.; Sherris, J. C.; Turck, M. *Am. J. Clin. Pathol.* **1966,** *45,* 493–496.
76. *Performance Standards for antimicrobial Disk Susceptibility Tests; Approved Standard–Sixth Edition;* CLSI: Wayne, PA, 1997; CLSI document M02–A06.
77. Oancea, S.; Hilma, G.; Peggion, C.; Formaggio, F.; Toniolo, C. *Chem. Biodiversity* **2008,** *5,* 681–692. doi:10.1002/cbdv.200890065

License and Terms

Beilstein Journal of Organic Chemistry

Design of a novel tryptophan-rich membrane-active antimicrobial peptide from the membrane-proximal region of the HIV glycoprotein, gp41

Evan F. Haney, Leonard T. Nguyen, David J. Schibli[§] and Hans J. Vogel[*¶]

Full Research Paper

Open Access

Address:
Department of Biological Sciences, University of Calgary, 2500 University Drive NW, Calgary, Alberta, Canada, T2N 1N4

Email:
Hans J. Vogel[*] - vogel@ucalgary.ca

* Corresponding author
§ Current address: Ontario Genomics Institute, MaRS Centre, Heritage Building, 101 College Street, Suite HL50, Toronto, Ontario, Canada, M5G 1L7
¶ Phone: 1-403-220-6006

Keywords:
antimicrobial peptides; cytotoxic peptides; NMR solution structure; membrane interactions; peptides structure–function relationship

Beilstein J. Org. Chem. **2012,** *8,* 1172–1184.
doi:10.3762/bjoc.8.130

Received: 10 April 2012
Accepted: 21 June 2012
Published: 24 July 2012

This article is part of the Thematic Series "Antibiotic and cytotoxic peptides".

Guest Editor: N. Sewald

Abstract

A number of physicochemical characteristics have been described which contribute to the biological activity of antimicrobial peptides. This information was used to design a novel antimicrobial peptide sequence by using an intrinsically inactive membrane-associated peptide derived from the HIV glycoprotein, gp41, as a starting scaffold. This peptide corresponds to the tryptophan-rich membrane-proximal region of gp41, which is known to interact at the interfacial region of the viral membrane and adopts a helical structure in the presence of lipids. Three synthetic peptides were designed to increase the net positive charge and amphipathicity of this 19-residue peptide. Ultimately, the peptide with the greatest degree of amphipathicity and largest positive charge proved to be the most potent antimicrobial, and this peptide could be further modified to improve the antimicrobial activity. However, the other two peptides were relatively ineffective antimicrobials and instead proved to be extremely hemolytic. This work demonstrates a novel approach for the design of unexplored antimicrobial peptide sequences but it also reveals that the biological and cytotoxic activities of these polypeptides depend on a number of interrelated factors.

Introduction

Antimicrobial peptides (AMPs) continue to attract significant attention as potential alternatives to conventional antibiotics. A large number of AMP sequences have been reported in the literature, ranging from diverse peptides isolated from different natural sources to synthetic peptides generated with high-throughput screening methods. From this large sample size, a

number of characteristics have been identified that all contribute to the antimicrobial potency of these polypeptides. In this study, we attempted to design a novel AMP using a helical peptide scaffold known to interact at the surface of phospholipid bilayers. Using this template, a series of derivatives were synthesized to augment many of the important antimicrobial factors, with the goal of generating a novel peptide sequence with enhanced antimicrobial potency and weak cytotoxic activity.

The first step in this process was to select an appropriate sequence to serve as the peptide scaffold. Many linear AMPs are unstructured in aqueous solution and only adopt a well-defined structure in the presence of a lipid bilayer [1]. This binding event is integral to the mechanism of action of the peptide, either through direct damage to the phospholipid bilayer or by allowing the peptide to cross the bacterial membrane to reach intracellular targets [2]. A number of AMPs form amphipathic α-helices when bound to lipid bilayers with the hydrophilic residues clustering on one face of the peptide, while hydrophobic residues appear on the opposite face [3]. This amphipathic structure allows the peptide to embed itself into the interfacial region of a phospholipid membrane and it anchors the peptide to the surface of the bilayer.

Another common feature of several AMPs is an unusually high proportion of specific amino acids [4]. Our group has been particularly interested in AMPs rich in tryptophan and cationic amino acids [5,6]. The cationic residues (Arg and Lys) are thought to mediate the initial electrostatic attraction to the negatively charged bacterial cell surface [7]. On the other hand, Trp residues have the unique property that they bind in the interfacial region of a membrane [8,9], thereby anchoring the peptide to the bilayer surface.

Based on these properties, we sought a Trp-rich, membrane-associated region of a protein that does not possess intrinsic antimicrobial activity. Peptides derived from the envelope HIV-1 glycoproteins, gp120 and gp41, have previously been examined for their antimicrobial activity [10] and we chose to use the membrane-proximal region of gp41 as our starting peptide scaffold. This region of the gp41 protein is of particular interest, because it contains five Trp residues, is believed to bind at the surface of the viral membrane [11] and plays an important role in fusing the viral membrane to the target cell membrane. The solution structure of the 19-residue peptide (gp41w) bound to micelles was previously reported by our group [12], and it was shown that this peptide adopts a well-defined helix in the presence of detergent micelles, with four of the five Trp residues distributed in a plane along the length of the peptide. Therefore, this peptide satisfies two of the features that we were looking for, i.e., helical structure and high Trp content. It follows from our current understanding of structure–function relationships of AMPs that adding positive charges and increasing the degree of amphipathicity of this membrane-associated peptide could generate a peptide sequence with potent antimicrobial activity.

Three derivatives were synthesized based on the amino-acid sequence of gp41w (Figure 1). The first peptide, gp41w-4R, has the polar uncharged amino acids in gp41w replaced with Arg residues. These mutations increased the net charge of the peptide from +3 to +7 and should increase the electrostatic attraction to bacterial cells, which are characterized by a negative surface charge [7]. The second derivative, gp41w-KA, is based on the helical-wheel representation of gp41w and has mutations in the sequence to increase both the net positive charge and amphipathicity of the peptide, while maintaining the

A

Peptide	Sequence
gp41w	KWASLWNWFNITNWLWYIK-NH_2
gp41w-4R	KWA**R**LW**R**WF**R**IT**R**WLWYIK-NH_2
gp41w-KA	KWA**KK**W**K**WF**AKAA**W**K**WY**K**K-NH_2
gp41w-FKA	K**F**A**KKFK**WF**AKAAFKFFK**K-NH_2

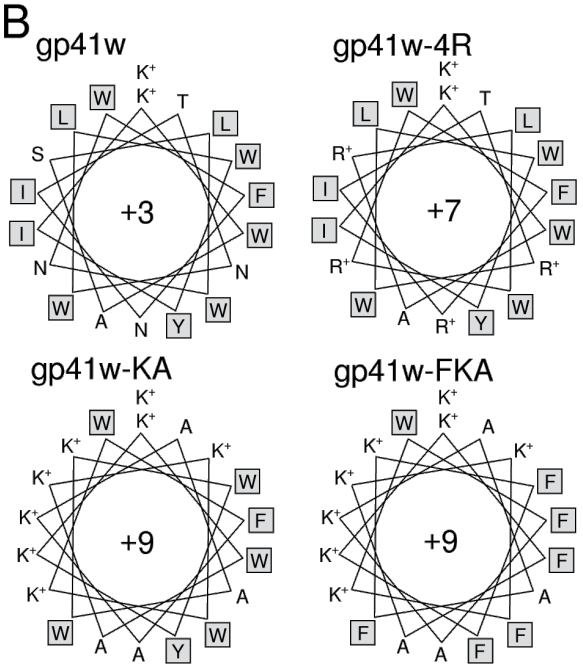

Figure 1: (A) Names and sequences of the gp41w-derived peptides. (B) Helical-wheel projections of gp41w, gp41w-4R, gp41w-KA and gp41w-FKA showing the hydrophobic and large aliphatic side chains in grey boxes. These helical wheels show the amphipathicity of the gp41w derivatives as the hydrophobic residues are increasingly segregated from the hydrophilic and charged residues.

relative positions of the bulky hydrophobic residues. Compared to the helical-wheel projection of gp41w-4R, the gp41w-KA peptide removes two of the positive charges from the hydrophobic Trp-rich face of the peptide and replaces them with Ala. In addition, the aliphatic Ile and Leu residues are removed from the hydrophilic surface and are replaced with cationic residues. This generates a peptide with a large net positive charge (+9) and if it can still adopt a helical conformation, then it will be highly amphipathic. The final gp41w derivative, gp41w-FKA, has the same sequence as gp41w-KA except that all of the Trp residues, apart from Trp8, have been replaced by Phe residues. Because the Trp and Phe amino-acid side chains insert in a different manner into membranes, it is interesting to examine the effect of replacing the interface-binding indole groups [13] with the more hydrophobic and deeper penetrating phenyl moieties [8].

Results

Antimicrobial and hemolytic activities

The antimicrobial activity for gp41w and its derivatives was determined against Gram-negative *E. coli* and Gram-positive *S. aureus* strains (Table 1). Three of the peptides, gp41w, gp41w-4R and gp41w-KA, were inactive at the concentrations tested. Only gp41w-FKA displayed significant antimicrobial activity against the two bacterial strains, with bacteriostatic and bactericidal effects observed at concentrations ranging from 10–50 μg/mL. The effect of adding gp41w to red blood cells caused minimal hemolysis, indicating that the parent peptide is not particularly cytotoxic. However, the mutation of four residues to cationic Arg residues resulted in a dramatic increase in the hemolytic activity, with significant hemolysis occurring at gp41w-4R concentrations as low as 7 μg/mL. For gp41w-KA and gp41w-FKA, the hemolytic activity was stronger than gp41w, but the effect was not as pronounced as seen with gp41w-4R. Gp41w-KA was hemolytic at a peptide concentration of 42 μg/mL, while gp41w-FKA lysed red blood cells at a concentration of 195 μg/mL. In the case of gp41w-FKA, the hemolytic concentration was substantially higher than the minimum inhibitory concentration (MIC) and minimum bactericidal concentration (MBC) values (Table 1).

Tryptophan fluorescence spectroscopy

Tryptophan emission fluorescence of all the gp41w derivatives was performed to examine the microenvironment surrounding the Trp side chains. The emission spectra of the four peptides in aqueous buffer are shown in Figure 2. It is evident that the behaviour of the gp41w peptide is very different from the other peptides. The wavelength of the maximum emission for gp41w occurs at 342 nm, while the other three peptides have maximum

A

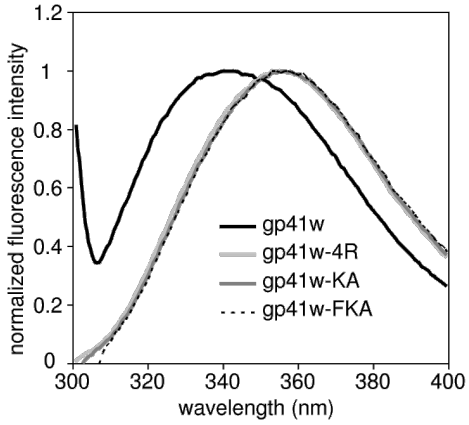

B

Peptide	SDS	DPC	ePC:ePG	ePE:ePG	ePC:ePE
gp41w	8	1	3	3	1
gp41w-4R	16	11	15	13	11
gp41w-KA	20	12	16	14	3
gp41w-FKA	18	5	3	3	0

Figure 2: (A) Normalized Trp emission spectra of the gp41w derivatives in buffer. The spectra have been normalized to the fluorescence intensity value measured at the wavelength of the emission maximum. (B) Blue shifts (nm) in the Trp maximum-emission wavelength for gp41w, gp41w-4R, gp41w-KA and gp41w-FKA in the presence of micelles and large unilamellar vesicles (LUVs) of varying composition. All wavelengths of the maxima are based on average values from three separate scans. Abbreviations for the detergents and lipids are: SDS, sodium dodecylsulfate; DPC, dodecylphosphocholine; ePC, egg-derived L-α-phosphatidylcholine; ePE, egg-derived L-α-phosphatidylethanolamine; ePG, egg-derived L-α-phosphatidylglycerol; Chol, cholesterol.

Table 1: Antimicrobial and hemolytic activities of the gp41w-derived peptides. All concentrations are presented as μg/mL.

Peptide	MIC[a] *E. coli*	MBC[b] *E. coli*	MIC[a] *S. aureus*	MBC[b] *S. aureus*	Hemolysis EC_{50}[c]
gp41w	>100	>100	>100	>100	550
gp41w-4R	>100	>100	>100	>100	7–14
gp41w-KA	>100	>100	>100	>100	42
gp41w-FKA	10–30	40–50	<10	20–30	195

[a]Minimum inhibitory concentrations (MIC); [b]minimum bactericidal concentrations (MBC); [c]effective concentration for 50% hemolysis.

emission wavelengths at ~356 nm. The value of 356 nm is normal for an exposed Trp side chain in aqueous solution. Apparently, the environments surrounding the Trp residues of the parent gp41w are significantly different from the three derivative peptides, resulting in a blue shift in the wavelength of the emission maximum. A shift towards lower wavelengths is usually interpreted as the Trp residue residing in a more hydrophobic environment, which may be due to the gp41w peptides oligomerizing in solution.

The addition of detergent micelles and large unilamellar vesicles (LUVs) to the peptide solutions caused substantial blue shifts of the maximum wavelength in the Trp emission spectra (Figure 2B). The maximum wavelength of the gp41w-4R samples blue shifted in all the lipid environments, with the largest changes occurring in the presence of anionic LUVs and detergents. Gp41w-KA also displayed large blue shifts in the presence of negatively charged lipid species, while only small blue shifts were seen with zwitterionic ePC:ePE LUVs. Gp41w-FKA displayed similar behaviour to gp41w-KA except that the blue shifts were not as pronounced for the negatively charged lipids and there was almost no blue shift seen when the peptide was added to neutral LUVs. The helical-wheel projection of gp41w-FKA places Trp8 in the hydrophilic face of the helix (Figure 1) and the NMR structure, determined in the cosolvent mixture of chloroform, methanol and water, places the indole side chain at the interface of the charged and hydrophobic sides of the helix (see below). Therefore, Trp8 likely does not penetrate as deeply into the acyl chains of the vesicles. The blue shifts seen in the gp41w samples were also comparatively small, but this is likely due to the unusual emission maximum measured for this particular peptide in aqueous buffer. Therefore, the smaller blue shifts for gp41w can be attributed to the peptide dissociating from the oligomeric form followed by peptide insertion into the bilayer.

Acrylamide quenching experiments were performed for the four peptides to examine the accessibility of the Trp fluorophores in the various membrane environments. If a Trp side chain inserts into the hydrophobic core of the bilayer, it becomes less accessible to the effects of the soluble acrylamide quencher. The quenching of Trp fluorescence is directly related to the concentration of quencher, so a titration with the neutral acrylamide allows for the calculation of the Stern–Volmer constant (K_{sv}), which quantitatively measures the accessibility of the Trp residues in various lipid environments.

The K_{sv} values for the gp41w peptides are summarized in Figure 3. Consistent with the other fluorescence results, the K_{sv} for gp41w in buffer is significantly smaller than the K_{sv} values calculated for the other peptides under the same conditions. This suggests that the Trp residues in gp41w are not as accessible to the acrylamide molecules and further supports the idea that this peptide is present in an oligomeric state in aqueous solution. When detergent micelles or LUVs were added to the gp41w peptide, all of the calculated K_{sv} were lower than the values determined in buffer, indicating that gp41w binds to both micelles and LUVs with the Trp residues inserting into the membrane.

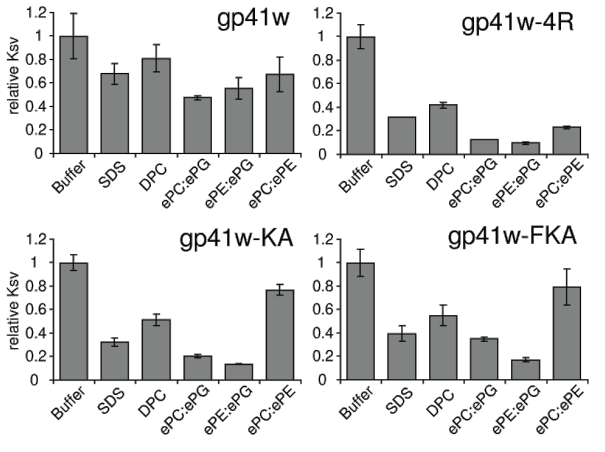

Figure 3: Relative K_{sv} values calculated for gp41w, gp41w-4R, gp41w-KA and gp41w-FKA in buffer and in the presence of detergent micelles and phospholipid LUVs. Error bars represent the standard deviation of three separate trials. Values are reported as relative values compared to the K_{sv} determined in buffer. The numerical values of the buffer K_{sv}s were 10.3, 27.8, 16.4 and 17.9 for gp41w, gp41w-4R, gp41w-KA and gp41w-FKA, respectively.

All of the gp41w derivatives have large K_{sv} values in buffer, which is expected if the Trp fluorophores are exposed to the aqueous buffer. In the presence of detergent micelles and LUVs, all of the calculated K_{sv} values for gp41w-4R decreased dramatically, consistent with this peptide binding to the bilayer and the Trp side chains burying into the membrane. This effect was most pronounced in the presence of anionic liposomes, but all of the mixtures resulted in strong decreases in the calculated K_{sv} values (Figure 3).

The other two peptides, gp41w-KA and gp41w-FKA, demonstrate a preference for anionic lipids and detergents, as the K_{sv} values determined in the presence of SDS micelles and LUVs containing ePG lipids are much lower than those determined in the presence of DPC or zwitterionic liposomes (Figure 3). When the peptides were added to ePC:ePE LUVs, there was only a small decrease in the calculated K_{sv}. This suggests that these two peptides interact only weakly with the neutral liposomes. The decrease in K_{sv} observed in the presence of DPC

micelles is likely due to the high concentration of detergent used in these samples. These conditions shift the equilibrium of the free-floating peptide in solution to the micelle-bound form, resulting in the insertion of the Trp side chain into the hydrophobic core of the micelle.

Calcein leakage

All four peptides were tested for their ability to induce the release of the self-quenching fluorescent dye, calcein, from calcein-encapsulated LUVs [14,15]. All of the peptides caused calcein release from negatively charged LUVs composed of ePC:ePG or ePE:ePG, and the percentage of calcein released was similar to that induced by melittin, a known lytic peptide [16]. Interestingly, the amount of leakage induced by each of the gp41 peptides was roughly equivalent, indicating that all of these derivatives disrupt negatively charged liposomes to the same extent (Figure 4A and Figure 4B). When the peptides were added to zwitterionic LUVs composed of ePC:ePE lipids, there was a larger difference in the amount of calcein released from the LUVs. Gp41w-4R caused significant leakage, similar to the effect of melittin, while the gp41w peptide also caused leakage, but not to the same extent. Gp41w-KA and gp41w-FKA caused membrane disruption of the zwitterionic LUVs, but only ~70% leakage was observed at the highest peptide:lipid ratio tested. This demonstrates that these two peptides do not disrupt bilayer organization in neutral liposomes to the same extent as gp41w or gp41w-4R (Figure 4C).

Differential scanning calorimetry

The gp41w derivatives were added to 1,2-dipalmitoyl-*sn*-glycero-3-phosphocholine (DPPC) and 1,2-dipalmitoyl-*sn*-glycero-3-phospho-(1'-*rac*-glycerol) (DPPG) lipid suspensions and the resulting lipid and peptide mixtures were examined by differential scanning calorimetry (DSC) to determine the effect of the peptides on the thermotropic phase behaviour of phospholipids. Eukaryotic membranes typically have a high phosphatidylcholine content, while bacterial membranes are characterized by phosphatidylethanolamine and anionic phosphatidylglycerol head groups [7]. Therefore, the DPPC lipids serve as a simple model for a eukaryotic membrane, while the anionic DPPG lipids are representative of the negatively charged bacterial membrane.

When added to DPPC lipid suspensions, gp41w and gp41w-FKA had very little effect on the phase transitions of DPPC lipids (Figure 5). The main phase transition of DPPC, seen at 41 °C, is unaffected by the addition of peptide, while the pretransition at ~34 °C is slightly broadened and shifts to a lower temperature. When gp41w-4R and gp41w-KA were added to the DPPC lipid suspensions, the resulting thermograms showed that these peptides had very drastic effects on the organization of DPPC bilayers (Figure 5). The final heating scan of gp41w-4R mixed with DPPC phospholipids shows a sharp transition at ~36 °C with a broad shoulder between 37–40 °C. This large temperature shift compared to the main phase transition of DPPC indicates that the gp41w-4R peptide destabilizes zwitterionic bilayers more effectively than any of the other gp41w derivatives. For gp41w-KA, there are a number of peaks at temperatures below the phase-transition temperature of pure DPPC, including a sharp transition at ~40 °C, suggesting that this peptide also destabilizes the transition of DPPC from the lamellar-gel to the liquid-crystalline phase. The ability of the gp41w derivatives to disrupt DPPC bilayers correlates with the observed hemolytic activity, and this may explain why gp41w-4R and gp41w-KA readily lyse red blood cells in vitro.

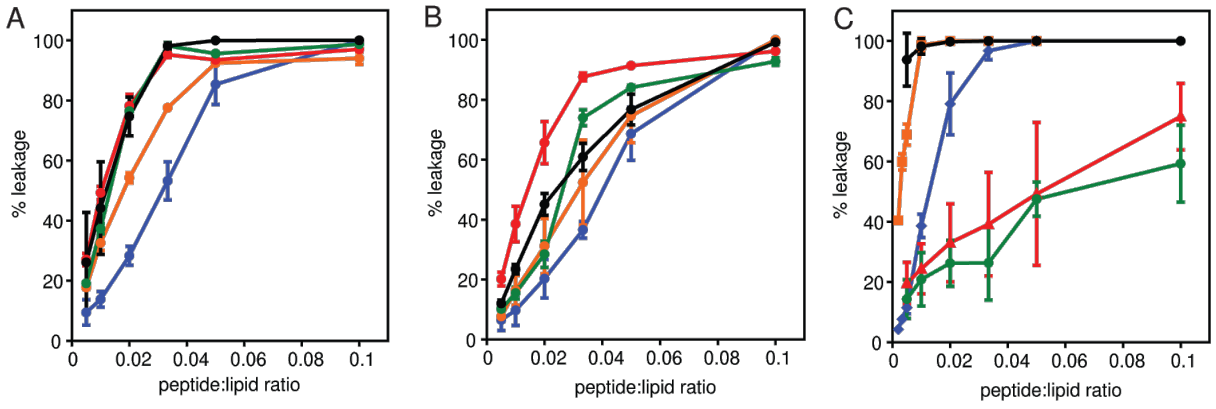

Figure 4: Percent calcein leakage induced by the gp41 derivatives. Gp41w (blue), gp41w-4R (orange), gp41w-KA (red) and gp41w-FKA (green) were added to calcein encapsulated LUVs composed of (A) ePC:ePG, (B) ePE:ePG and (C) ePC:ePE at different peptide:lipid ratios. Melittin (black), a known lytic peptide from honey-bee venom was used as a positive control. All experiments were carried out in triplicate at 37 °C.

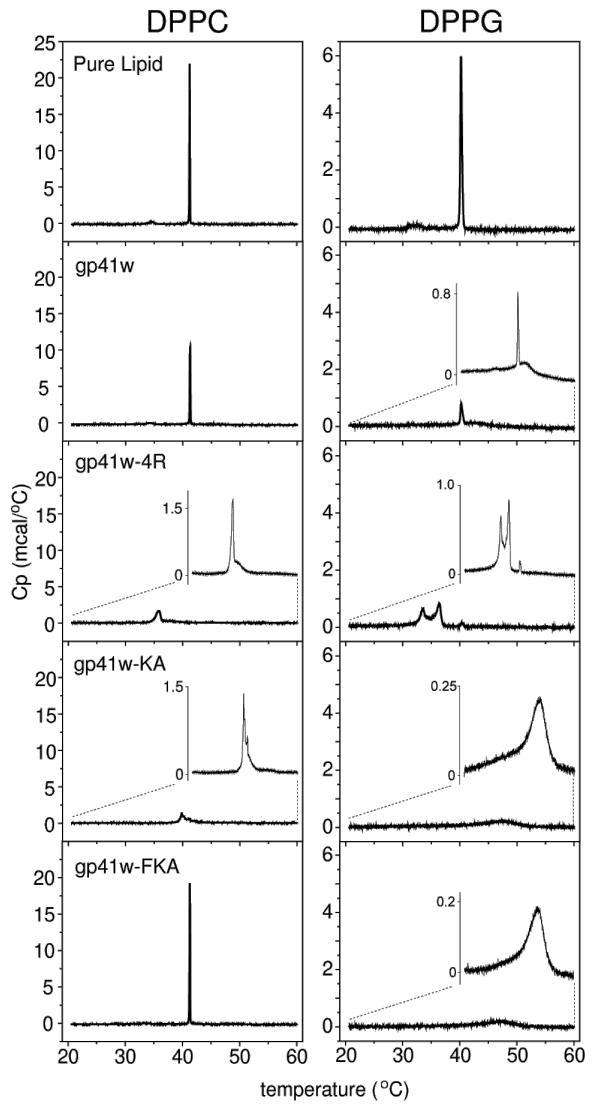

Figure 5: DSC thermograms of pure zwitterionic DPPC (left) and anionic DPPG (right) lipid suspensions compared to lipids mixed with gp41w, gp41w-4R, gp41w-KA and gp41w-FKA. A peptide-to-lipid molar ratio of 1:10 was maintained in all of the samples. The insets are a magnification of the thermogram to show the distribution and shape of the peaks.

The DSC results of the gp41w derivatives mixed with DPPG lipids demonstrate that all the peptides induce changes in the thermotropic phase behaviour of negatively charged lipids. The pretransition at ~33 °C seen in the DSC trace of pure DPPG lipids disappears in the presence of all the gp41w peptides. For gp41w added to DPPG lipid suspensions, the peak at 40 °C indicates that there is some unbound DPPG that behaves like the pure lipid suspension. However, the emergence of a broad transition at ~43 °C is likely due to the formation of peptide–lipid aggregates. The addition of gp41w-4R to DPPG yields peaks in the thermogram at 33 and 36 °C, suggesting that when gp41w-4R binds to negatively charged liposomes, it destabilizes the organization of the bilayer. Apparently, some unbound DPPG remains as well because there is still a small peak at ~40 °C. The addition of gp41w-KA and gp41w-FKA to DPPG gave remarkably similar DSC results. The main phase transition at 40 °C is abolished in the presence of either peptide and is replaced by a broad transition centered at 47 °C. This could be due to the formation of peptide–lipid aggregates that produce the high-temperature transitions in the thermogram. Interestingly, the degree to which the gp41w derivatives disrupt DPPG lipids does not correlate with the observed antimicrobial activity, suggesting that interaction with negatively charged lipids is not sufficient to explain the observed antimicrobial effects.

Circular dichroism spectroscopy

The backbone conformations of all of the gp41 peptide derivatives were examined by using far-UV circular dichroism (CD) spectroscopy. The resulting CD spectra of the peptides in buffer, SDS, DPC and 50% trifluoroethanol (TFE) are shown in Figure 6. Two of the peptides, gp41w and gp41w-4R, generated unique CD spectra for AMPs dissolved in aqueous solution. Typically, linear AMPs are unstructured in aqueous buffer, resulting in CD spectra with a characteristic minimum at ~200 nm. For gp41w-4R, there is a consistent signal from 235 to 205 nm and a maximum peak at ~195 nm, suggesting that this peptide already adopts a partially helical conformation in aqueous buffer. The CD spectra of gp41w are even more intriguing as there are strong minima observed at 230 and 208 nm. The peak at 208 nm is likely due to the presence of α-helical structure, while the band at ~230 nm can be attributed to stacking interactions between nearby aromatic rings [17]. This is in agreement with the fluorescence results and suggests that the gp41w backbone adopts a regular secondary structure when oligomerized in solution.

The addition of SDS or DPC micelles to gp41w caused a conformational change in the peptide, likely due to the peptide multimers disassociating followed by peptide binding to the micelles. When micelles were mixed with gp41w-4R, an increase in the mean residue ellipticity at 208 and 222 nm was observed, consistent with the formation of an α-helix. When compared to the curve of gp41w-4R in 50% TFE, the traces from the micelle-containing samples show little difference, indicating that the conformation of gp41w-4R is similar in all these environments. In the presence of 50% TFE, gp41w also adopts a largely α-helical conformation, but in the presence of micelles there may be other structural elements that contribute to the CD spectra, as evidenced by the strong minima at ~218 nm seen in both the SDS and DPC traces. However, the micelle samples still have minima at 208 nm and maximum

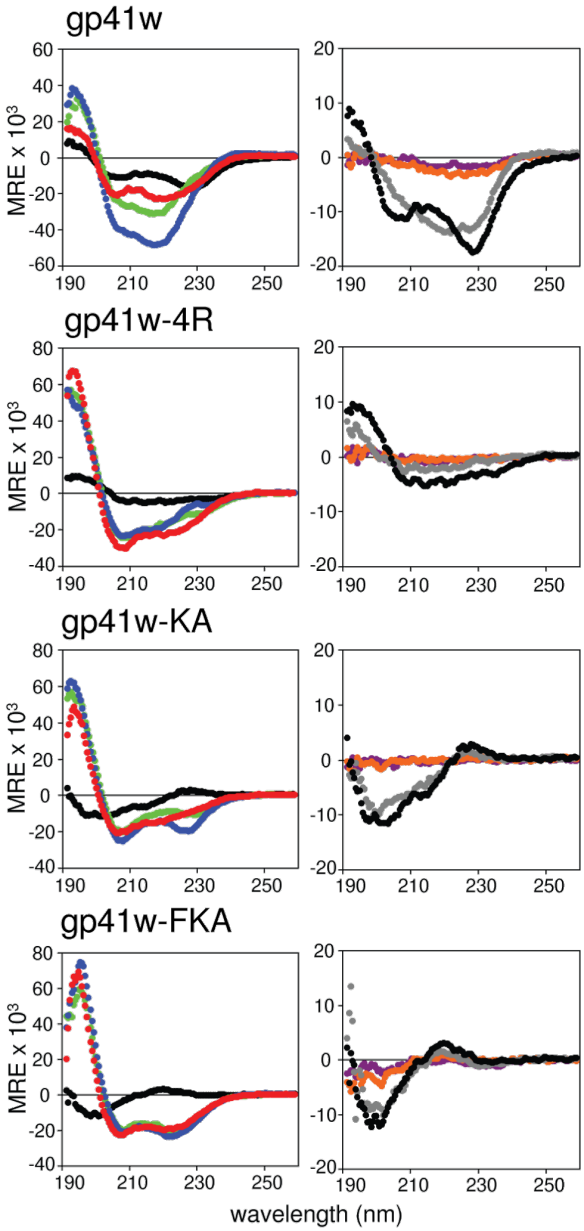

Figure 6: Far-UV CD spectra of gp41w and the three derivative peptides. The panel on the left shows the peptides in phosphate buffer (black), 25 mM SDS (green), 25 mM DPC (yellow) and 50% TFE (red). The panel on the right is the peptides in the presence of LUVs composed of ePC:ePG (violet), ePE:ePG (orange) or ePC:ePE (gray). All data are reported in units of mean residue ellipticity (MRE) with units of deg cm^2 $dmol^{-1}$ res^{-1}.

values at 195 nm, both of which are characteristic of helical structure. Therefore, it appears that a large portion of gp41w forms a helix when bound to SDS and DPC micelles.

The CD spectra for gp41w-KA and gp41w-FKA are more typical for AMPs. Both peptides are unstructured in aqueous solution, with strong minima at 200 nm. The addition of micelles or TFE induces a conformational change in the peptides consistent with the formation of helical structure. The micelle-bound conformation of gp41w-KA has another minimum at 227 nm, which may be due to interactions among the Trp side chains [18]. The fact that the CD spectra of gp41w-FKA in the presence of SDS, DPC and 50% TFE overlap almost perfectly with each other suggests that this peptide adopts equivalent structures in all three environments.

The conformations of the gp41w derivatives in the presence of LUVs of varying composition were also examined with CD spectroscopy (Figure 6). In the presence of zwitterionic ePC:ePE LUVs, a slight conformational change was observed for the gp41w peptide while the intensity of the CD signal from gp41w-4R decreased significantly. In the case of gp41w, this is likely due to a minor conformational change as the peptide reorients itself to interact with the LUVs. There was evidence of lipid aggregation in the gp41w-4R sample; therefore the spectral change likely arises from the formation of peptide–lipid aggregates, which no longer absorb the circularly polarized light. Only minor changes were seen in the CD values measured for gp41w-KA and gp41w-FKA compared to the spectra obtained in buffer, suggesting that these two peptides do not readily interact with neutral liposomes.

Peptide–lipid aggregates were observed in all the CD samples containing anionic LUVs composed of ePC:ePG or ePE:ePG, and the intensity of the measured CD signals virtually disappeared for all the peptide samples (Figure 6). This was accompanied by a corresponding decrease in the absorbance values measured by the spectropolarimeter (data not shown). In addition, precipitates could be seen in the cuvette, suggesting that all the gp41w peptides interact strongly with negatively charged lipid species leading to the formation of insoluble peptide–lipid complexes. Unfortunately, due to the loss of CD signal in these samples, it is impossible to determine what type of secondary structure is present in these aggregates.

NMR solution structure

All the gp41w derivatives were examined by nuclear magnetic resonance (NMR) spectroscopy to determine the high-resolution structure in a membrane mimetic environment. The structure of gp41w was previously determined in the presence of DPC micelles [12]. However, when the three derivatives were tested with SDS and DPC micelles, the resulting NMR spectra were poorly resolved and not suitable for structural analysis (data not shown). Consequently, we chose to use a cosolvent mixture consisting of four parts deuterated chloroform, four parts deuterated methanol and one part water [19,20]. The 2D ^{1}H NOESY spectra obtained in this solvent mixture were very

well resolved, allowing for identification of all of the backbone atoms and virtually all the side-chain atoms in gp41w-4R, gp41w-KA and gp41w-FKA (Supporting Information File 1, Figure S1). The nuclear Overhauser effect (NOE) patterns of the connections between protons in the gp41w-derived peptides are highly indicative of helical structure (Supporting Information File 1, Figure S2). Interestingly, when gp41w was added to the cosolvent mixture, the peptide did not readily dissolve and there was evidence of aggregation. These aggregates persisted at higher temperatures and the NMR spectra acquired with these samples were of poor quality. As a result, the solution structure of gp41w was not determined in the cosolvent mixture. Structural statistics from the ARIA calculations are shown in the Supporting Information File 1, Table S1.

As expected, similar to gp41w [12], the solution structures of gp41w-4R, gp41w-KA and gp41w-FKA were found to be largely helical, but there are significant differences in the charge distribution and amphipathicity of these peptides, which must be related to the observed biological effects. The solution structure of gp41w-4R forms a well-defined helix across the length of the peptide with a backbone root-mean-square deviation (RMSD) of 0.630 Å (Figure 7). It appears that the structure is slightly bent, especially in the N-terminal region, which lies well below the plane of the helix formed by residues 7–19. The side-chain distribution of gp41w-4R in the cosolvent solution shows that the peptide does not form a distinct amphipathic structure. The hydrophobic side chains and the charged Arg and Lys residues are relatively evenly distributed across the surface of the peptide.

The structure of gp41w-KA in the cosolvent mixture also forms a very well defined helix with a backbone RMSD of 0.389 Å (Figure 7). In agreement with the structure of gp41w-4R, the N-terminal region of gp41w-KA is not aligned with the C-terminal helix formed across residues 7–19 and these first six residues appear to form a slightly extended conformation. This may be an important structural feature of this peptide but could also be due to a low number of intramolecular contacts between the side-chain protons in this region of the peptide. Different from the structure of gp41w-4R, the well-defined helical region of gp41w-KA is largely amphipathic, with the positively charged Lys residues at positions 7, 11, 15, 18 and 19 all appearing on the same face of the peptide, while the opposite face has many of the large hydrophobic residues, including Phe9, Trp16 and Tyr17. In addition, the side chains of Trp6, Trp8 and Trp14 are all found in the same plane of the peptide, which separates the charged Lys surface from the hydrophobic face. The amphipathic structure of gp41w-KA is highly suggestive of a membrane-bound orientation in which the

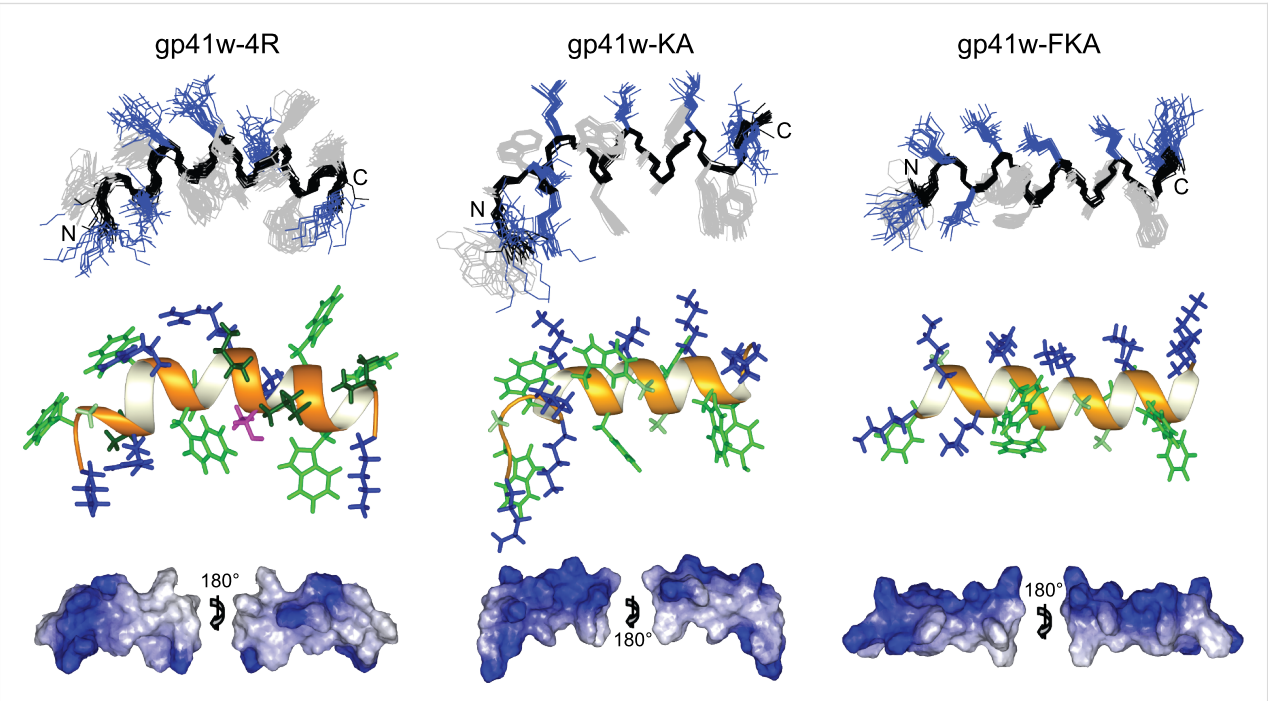

Figure 7: NMR solution structure of gp41w-4R, gp41w-KA and gp41w-FKA in the cosolvent mixture. Overlay of the 20 lowest-energy structures reveals a well-defined backbone conformation for all three peptides (top panel). All the peptides adopt a largely helical conformation as seen in the ribbon diagrams (middle panel). The hydrophobic residues (green) and the cationic residues (blue) are shown along with Thr12 (magenta) in gp41w-4R. The gp41w-4R peptide lacks distinct amphipathicity, while gp41w-KA and gp41w-FKA have much more pronounced amphipathic character across the length of the helix (bottom panel, positively charged regions are indicated in blue).

hydrophobic face inserts into the hydrophobic core of the bilayer while the positively charged residues interact with the charged lipid head groups. Based on this model, the N-terminal region of gp41w-KA would then be oriented into the bilayer, which would bring the Lys residues at positions 1, 4 and 5 into the hydrophobic core of the bilayer. This may be related to the membrane-destabilizing properties of the gp41w-KA peptide.

The gp41w-FKA peptide has a similar primary sequence to the gp41w-KA except that all of the Trp residues in gp41w-KA (except Trp8) have been mutated to Phe residues. These changes did not affect the ability of the gp41w-FKA peptide to adopt a helical conformation in the cosolvent mixture of chloroform, methanol and water. The peptide formed a very well defined α-helix across the length of the peptide with a backbone RMSD of 0.426 Å (Figure 7). The side-chain distribution of gp41w-FKA creates the most amphipathic structure of any of the gp41w derivatives. Only Lys1 and Lys5 are not part of the positively charged face formed by the remaining Lys residues. Most of the hydrophobic Phe residues are found opposite the charged face, with the side chain of Trp8 once again located equidistant from the charged surface and the hydrophobic face. A closer examination of the surface-charge distribution of this peptide reveals an uninterrupted hydrophobic face stretching from Phe1 to Phe17, suggesting that gp41w-FKA binds at the interfacial region of a phospholipid bilayer.

Discussion

AMPs are often considered as potential therapeutic agents because of their selectivity towards bacterial cells and the perceived difficulty associated with bacteria in developing resistance to these molecules [21]. Using an inactive membrane-associated Trp-rich peptide as a scaffold, we attempted to generate a novel AMP based on some of the simple characteristics that have been outlined for AMPs, such as hydrophobicity, amphipathicity, net charge, helical structure and phospholipid bilayer interactions [22]. The results obtained with the gp41w-derived peptides reveal a complex relationship between the structural factors that contribute to the antibacterial activity and the features that determine the hemolytic activity.

A large proportion of AMPs are unstructured in solution, and they adopt amphipathic α-helices when bound to a phospholipid bilayer [3,23]. This binding to the bacterial membrane is often related to a membrane-destabilizing mode of action, which ultimately leads to bacterial cell death [24]. However, recent evidence suggests that membrane binding may be a part of a more complex mode of action involving multiple targets of inhibition [21,25]. In addition to their membrane-binding properties, many AMPs are typified by a high proportion of Trp and cationic amino acids [5,6]. The Trp residues are unique because of their preference for the interfacial region of biological membranes [8,9], while the cationic residues are responsible for the initial electrostatic attraction to the negatively charged bacterial cell [7,22]. In this work, the membrane proximal region of gp41 was chosen as a starting point from which to design a novel AMP sequence. This 19-residue peptide adopts a helical structure with partial amphipathic character in the presence of DPC micelles [12] and contains five Trp residues, four of which form a plane along the helix axis. A model for the membrane interaction of gp41w was proposed wherein the peptide inserts into the interfacial region of the outer leaflet of the viral membrane and this Trp plane resides at the lipid–water interface. The net positive charge of the native gp41w peptide is relatively small (+3). Three peptide derivatives were synthesized to increase the overall charge of the peptide as well as enhance the amphipathicity of the helix with the ultimate goal of generating a novel AMP sequence.

It was expected that the gp41w peptide would have weak antimicrobial and hemolytic activity. Indeed this was the case as no antimicrobial activity was observed against *E. coli* and *S. aureus* at gp41w concentrations below 100 μg/mL, and hemolysis was not observed at peptide concentrations lower than 500 μg/mL. The fluorescence spectroscopy results demonstrate that gp41w interacts with lipid bilayers and the Trp residues embed themselves into the membrane. The DSC data indicate that gp41w interacts with both DPPC and DPPG lipids, since the shape of the main phase-transition peak is significantly different compared to the pure lipid. However, it appears that gp41w does not dramatically alter the bilayer organization, since the melting temperature of the main phase transition remains unchanged. The calcein leakage results suggest that gp41w is membrane active, since it causes leakage of vesicle contents, but it appears that vesicle leakage does not correlate with antimicrobial activity. It could be related to the relatively low positive charge of gp41w, but this seems unlikely since gp41w-4R has four additional positive charges and is also antimicrobially inactive.

The lack of antimicrobial activity may be related to the fact that the gp41w peptide appears to oligomerize in solution. When found in the HIV-1 Env glycoprotein complex, gp41 is known to exist as a trimer [26], and previous attempts to resolve the NMR structure of gp41w in aqueous solution or 40% TFE were unsuccessful because of peptide aggregation or poor solubility [12]. In terms of the antimicrobial activity, gp41w oligomers may be too large to pass through the peptidoglycan layer surrounding Gram-positive bacteria. Additionally, they would have to disassociate into monomers before they could insert themselves into the bacterial membrane. Recent artificial-neural-network prediction models of antimicrobial peptides

have found that peptide aggregation in solution indeed contributes to a low antimicrobial activity [27]. Interestingly, the addition of cationic residues to peptides that tend to aggregate in solution has been shown to inhibit aggregation while improving the antimicrobial potency at the same time [28].

The gp41w-4R derivative of the gp41w peptide has the three Asn residues and Ser8 mutated to cationic Arg residues. Arginine residues seem to be preferred over Lys residues in short Trp- and Arg-rich AMPs obtained through combinatorial chemistry [29]. Interestingly, the gp41w-4R peptide did not show any increased antimicrobial activity despite the high content of Trp and cationic residues. Instead, the gp41w-4R peptide unexpectedly demonstrated extremely high hemolytic activity. The solution structure of gp41w-4R in the cosolvent mixture is largely α-helical, but the peptide is not particularly amphipathic. This is consistent with the helical wheel projection of gp41w-4R (Figure 1), which predicted that the positively charged residues would be evenly distributed around the circumference of the helix axis.

The biophysical experiments reveal that gp41w-4R readily interacts with membranes, irrespective of the composition of the head groups in the phospholipids. The effect of gp41w-4R on zwitterionic liposomes is substantial in comparison to the other peptides, especially in the calcein leakage and DSC results, and this behaviour is likely directly related to the strong hemolytic activity of this peptide. The positively charged Arg and Lys side chains in gp41w-4R would prefer to reside in an aqueous environment; however, gp41w-4R also possesses a large number of hydrophobic amino acids, which readily insert into the interfacial region of the bilayer and into the hydrophobic acyl chains [8,30]. Therefore, if the hydrophobic residues penetrate into the hydrophobic core of a membrane, this would also introduce positive charges into the bilayer, thereby destabilizing the membrane. A model such as this can explain the hemolytic activity of gp41w-4R, but the lack of antimicrobial activity suggests that the gp41w-4R peptide does not reach the bacterial cytoplasmic membrane in the presence of bacterial cells.

Amphipathicity is often cited as an important factor that contributes to the effectiveness of AMPs [3,4,23,31-33] and this may explain why the gp41w-4R peptide has poor antimicrobial activity since it is not overly amphipathic. Additionally, the CD spectra of gp41w-4R in buffer suggests that this peptide is somewhat structured in aqueous solution, so a conformational rearrangement of gp41w-4R may be required for membrane destabilization of bacterial cells.

The gp41w-KA and gp41w-FKA peptides are significantly different in primary sequence compared to gp41w, but the common feature of these peptides is the positioning of the bulky hydrophobic residues. The positively charged residues in gp41w-KA and gp41w-FKA were engineered to appear on one side of the helix axis to improve the overall amphipathicity of the α-helix. Indeed, the NMR solution structures of gp41w-KA and gp41w-FKA were found to be largely amphipathic (Figure 7). The C-terminal region in both peptides adopts a well-defined helical structure and only the N-terminal residues appear to deviate from this conformation. Interestingly, the increased amphipathicity appears to be inversely related to the hemolytic activity of these peptides and the interactions with zwitterionic ePC:ePE LUVs or DPPC lipids suspensions are not as substantial as the effects seen with gp41w-4R. In addition, the selectivity for negatively charged membranes over zwitterionic lipids is enhanced in these two peptides, particularly for gp41w-FKA.

The stronger antimicrobial potency of the gp41w-FKA peptide compared to gp41w-KA was unexpected because Trp residues have long been implicated as being important for the activity of AMPs [5,6]. While Trp residues preferentially sit at the interfacial region of a membrane [8,9] and Phe residues show a preference for the interior of the membrane [8,30], our group previously observed an increase in the antimicrobial activity of tritrpticin analogues, wherein the three Trp residues were mutated to Phe [34]. This was accompanied by a decrease in hemolytic concentration of tritrpticin as well. Conversely, mutating Trp residues to Phe residues decreased the antimicrobial potency of indolicidin [35] while increasing the hemolytic activity of this peptide.

At this point, it is unclear why gp41w-FKA is a more potent antibacterial than gp41w-KA. The fluorescence results demonstrate that both peptides preferentially interact with anionic lipids and the calcein leakage profiles of both peptides are similar in the presence of anionic and neutral liposomes. The DSC traces of DPPG mixed with both peptides are virtually identical and the only large difference between the two peptides is that gp41w-KA has a strong effect on DPPC lipid suspensions, which only explains the stronger hemolytic effect of this peptide. Evidently, the antimicrobial mechanism of action of gp41w-FKA involves more than a simple disruption of the bacterial cytoplasmic membrane. Alternatively, gp41w-KA and gp41w-4R may not reach the bacterial cytoplasmic membrane through some unknown interactions with molecules on the surface of the bacterial cell.

Other de novo strategies for generating AMPs have been reported in the literature. For instance, Lee et al. recently published a study wherein they synthesized short peptides (5-11 residues) composed of only three amino acids: Lys, Leu and

Trp [36]. Their results support the notion that the antimicrobial activity of a peptide is related to peptide amphipathicity and helicity as well as to the location of the Trp residues. However, their most potent peptide (LKWLLKWLL-NH_2) also displayed significant hemolytic activity, indicating that further refinement of these peptide sequences is required to optimize their use as antimicrobials.

This study demonstrates that de novo generation of AMPs is still not a trivial endeavour and our current understanding of AMPs is insufficient to predict the antimicrobial potency of novel peptide sequences. Be that as it may, the methodology described here was successful in generating an AMP (gp41w-FKA) with comparatively low cytotoxicity from an intrinsically inactive membrane-associated peptide sequence. With further modifications, the gp41w-FKA peptide can be taken as a starting point to create a potent AMP.

Experimental

Peptide synthesis and chemical reagents

Gp41w, gp41w-4R, gp41w-KA, gp41w-FKA were synthesized by Anaspec Inc. (Fremont, CA) to >95% purity. Peptide concentrations were determined from absorbance measurements at 280 nm and theoretical extinction coefficients obtained from Protparam on the EXPASY web server [37]. Powdered dodecylphosphocholine (DPC) and stock chloroform solutions of 1,2-dipalmitoyl-*sn*-glycero-3-phosphocholine (DPPC), 1,2-dipalmitoyl-*sn*-glycero-3-phospho-(1'-*rac*-glycerol) (DPPG), egg-derived L-α-phosphatidylcholine (ePC), egg-derived L-α-phosphatidylethanolamine (ePE), egg-derived L-α-phosphatidylglycerol (ePG) and cholesterol were purchased from Avanti Polar Lipids, Inc. (Alabaster, AL). Deuterated methanol used in the NMR samples was obtained from Cambridge Isotopes Laboratories, Inc. (Andover, MA). Deuterated chloroform ($CDCl_3$) was obtained from Norell, Inc. (Landisville, NJ). All other chemicals were purchased from Sigma Aldrich (St. Louis, MO).

Biological activity

Minimum inhibitory concentrations (MIC) and minimum bactericidal concentrations (MBC) were determined for *E. coli* and *S. aureus* as described previously [38]. Hemolytic activity was also determined by using red blood cells from healthy volunteers, as described previously [38].

Large unilamellar vesicle preparation

Lipid mixtures consisting of 1:1 weight ratios of ePC, ePG and ePE were prepared from stock lipid solutions in chloroform. The organic solvent was evaporated under a stream of nitrogen gas and the resulting lipid cake was placed under vacuum for ~2 h then stored at −20 °C until ready for use. Large unilamellar vesicles (LUVs) were prepared by warming the lipid film to room temperature followed by resuspension in buffer (10 mM Tris, 150 mM NaCl, 1 mM EDTA, pH 7.4) with vigorous vortexing. The lipid suspension was subjected to five rounds of freezing and thawing in liquid nitrogen followed by 15 passes through two 100 nm polycarbonate filters using the Avanti Mini-Extruder apparatus. The lipid concentration in the LUV samples was determined by measuring the phosphate concentration using the assay described by Ames [39].

Tryptophan emission fluorescence

Intrinsic tryptophan fluorescence of the peptides was measured on a Cary Eclipse Fluorimeter (Agilent Technologies, Victoria, Australia) equipped with a temperature control unit set at 25 °C. Emission spectra were recorded between 300 and 400 nm with an excitation wavelength of 295 nm. Excitation and emission slits were kept at 5 and 10 nm, respectively, for all the peptides except for gp41w-FKA, which has a single Trp residue, and for which both slit widths were maintained at 10 nm. The concentration of SDS and DPC in the fluorescence samples was 25 mM, while the lipid concentration in the LUV samples was 30 μM. Acrylamide titrations were performed to determine K_{sv} [40] by adding five aliquots of a 4 M acrylamide solution to the sample and recording an emission spectra using the parameters described above. K_{sv} was calculated by using the formula $F_0/F = 1 + K_{sv}/[Q]$, Where F_0 is the initial fluorescence and F is the fluorescence intensity after the addition of soluble quencher (Q).

Calcein leakage

Calcein leakage was performed according to established protocols [41]. Melittin, the principal component of bee venom and a known lytic peptide, was used as a positive control. Calcein leakage was measured for LUVs made from lipid mixtures of ePC:ePG, ePE:ePG or ePC:ePE.

Differential scanning calorimetry

Lipid films of 0.5 mg pure DPPC or DPPG were prepared as described above and stored at −20 °C until needed. Lipid films and buffer were heated to 55 °C for 15 min and then hydrated with buffer (20 mM phosphate buffer, 130 mM NaCl, pH 7.4) and vortexed vigorously. Following resuspension, stock solutions of peptides in water were added to achieve a final lipid:peptide molar ratio of 10:1. The final lipid concentration in each sample was 0.5 mg/mL. Differential scanning calorimetry was performed on a MicroCal high sensitivity VP-DSC machine (GE Healthcare, Piscataway, NJ). Five cycles of heating between 20 and 60 °C, at a scan rate of 10 °C/h were performed and the peptide–lipid mixture was added as the cells cooled between the first and second scans. Since the peptide was added exogenously to the lipid suspensions, the four

remaining heating and cooling cycles allowed the peptide to equilibrate amongst all the lipid molecules. In all cases, the final scan was virtually identical to the previous scan, indicating that equilibrium had been reached.

Circular dichroism spectroscopy

CD spectra were collected at room temperature on a Jasco J815 spectropolarimeter by using a 0.1 cm path length cuvette. Far-UV spectra of 50 μM peptide solutions were collected between 190–260 nm with a 0.5 nm step resolution, a 200 nm/min scan speed, a response time of 0.5 s and a bandwidth of 1 nm. CD spectra were acquired for the peptide in buffer (25 mM sodium phosphate, pH 7.4) and in buffered solutions containing 25 mM SDS, 25 mM DPC and 50% 2,2,2-trifluoroethanol. Spectra were also recorded for peptides in the presence of LUVs composed of ePC:ePG, ePE:ePG, and ePC:ePE. The lipid concentration in each of the LUV samples was maintained at 0.5 mM. Each spectra represents the average of 10 scans, and a blank spectra, lacking peptide, was subtracted in the final analysis. Data was converted to mean residue ellipticity according to Wallace and Janes [42].

NMR structure determination

The solution structures of gp41w-4R, gp41w-KA and gp41w-FKA were determined in the 4:4:1 cosolvent mixture of $CDCl_3$:methanol-d_3:H_2O previously used by our group to study the NMR solution structures of other AMPs [19,20,43]. NMR samples were prepared by dissolving 1–2 mg of lyophilized peptide powder in 500 μL of the miscible cosolvent solution, and then the samples were flame sealed in an NMR tube to avoid evaporation of the organic solvents. Two-dimensional NOESY, TOCSY and COSY spectra were collected at 298 K on a Bruker Avance 700 MHz spectrometer. Mixing times in the NOESY and TOCSY experiments were 100 ms and 120 ms, respectively. Spectra were acquired with 4096 × 600 data points in the F1 and F2 dimensions at a spectral width of 8992.806 Hz. Water suppression was achieved by using excitation sculpting [44].

All of the spectra were processed with NMRPipe [45]. The 2D data was zero-filled once in each dimension and Fourier transformed with a shifted sine-bell function. Spectra were analyzed with NMRView [46] and chemical shifts were assigned according to Wuthrich [47]. Starting structures of the gp41 peptides were generated with CNS [48] and broad dihedral restraints were placed on the backbone *phi* and *psi* angles to maintain these angles in allowable regions of the Ramachandran plot [49]. Solution structures were calculated based on the NOESY-derived distance restraints by using the simulated annealing protocol in ARIA1.2 [50]. Nine iterations of the simulated annealing protocol were performed with 20 structures generated in the first seven iterations followed by 40 and 100 in the final two iterations. The 20 lowest energy structures from the final iteration were analysed with Procheck [51] and visualized with MOLMOL [52].

Supporting Information

Supporting Information File 1

NMR spectra and peptide connectivity analysis based on the observed NOEs and structural statistics for the calculated NMR structures.
[http://www.beilstein-journals.org/bjoc/content/supplementary/1860-5397-8-130-S1.pdf]

Acknowledgements

This work is dedicated to the memory of Dr. Deane McIntyre who was instrumental in the training and education of students and researchers at the University of Calgary. The authors would also like to Dr. Howard N. Hunter for assistance with the NMR experiments. This work was supported by the Canadian Institutes of Health Research program for "Novel Alternatives to Antibiotics". HJV is an Alberta Innovates – Health Solutions Scientist.

References

1. Bhattacharjya, S.; Ramamoorthy, A. *FEBS J.* **2009,** *276,* 6465–6473. doi:10.1111/j.1742-4658.2009.07357.x
2. Nguyen, L. T.; Haney, E. F.; Vogel, H. J. *Trends Biotechnol.* **2011,** *29,* 464–472. doi:10.1016/j.tibtech.2011.05.001
3. Haney, E. F.; Hunter, H. N.; Matsuzaki, K.; Vogel, H. J. *Biochim. Biophys. Acta* **2009,** *1788,* 1639–1655. doi:10.1016/j.bbamem.2009.01.002
4. Epand, R. M.; Vogel, H. J. *Biochim. Biophys. Acta* **1999,** *1462,* 11–28. doi:10.1016/S0005-2736(99)00198-4
5. Chan, D. I.; Prenner, E. J.; Vogel, H. J. *Biochim. Biophys. Acta* **2006,** *1758,* 1184–1202. doi:10.1016/j.bbamem.2006.04.006
6. Vogel, H. J.; Schibli, D. J.; Jing, W.; Lohmeier-Vogel, E. M.; Epand, R. F.; Epand, R. M. *Biochem. Cell Biol.* **2002,** *80,* 49–63. doi:10.1139/o01-213
7. Lohner, K. The role of membrane lipid composition in cell targeting of antimicrobial peptides. *Development of novel antimicrobial agents: Emerging strategies;* Horizon Scientific Press: Norfolk, England, 2001; pp 149–165.
8. Wimley, W. C.; White, S. H. *Nat. Struct. Mol. Biol.* **1996,** *3,* 842–848. doi:10.1038/nsb1096-842
9. Killian, J. A.; von Heijne, G. *Trends Biochem. Sci.* **2000,** *25,* 429–434. doi:10.1016/S0968-0004(00)01626-1
10. Cole, A. M.; Liao, H.-I.; Ganz, T.; Yang, O. O. *FEBS Lett.* **2003,** *535,* 195–199. doi:10.1016/S0014-5793(02)03860-7
11. Salzwedel, K.; West, J. T.; Hunter, E. *J. Virol.* **1999,** *73,* 2469–2480.
12. Schibli, D. J.; Montelaro, R. C.; Vogel, H. J. *Biochemistry* **2001,** *40,* 9570–9578. doi:10.1021/bi010640u
13. Yau, W.-M.; Wimley, W. C.; Gawrisch, K.; White, S. H. *Biochemistry* **1998,** *37,* 14713–14718. doi:10.1021/bi980809c

14. Matsuzaki, K.; Fukui, M.; Fujii, N.; Miyajima, K. *Biochim. Biophys. Acta* **1991,** *1070,* 259–264. doi:10.1016/0005-2736(91)90173-6
15. Matsuzaki, K.; Harada, M.; Handa, T.; Funakoshi, S.; Fujii, N.; Yajima, H.; Miyajima, K. *Biochim. Biophys. Acta* **1989,** *981,* 130–134. doi:10.1016/0005-2736(89)90090-4
16. Pandey, B. K.; Ahmad, A.; Asthana, N.; Azmi, S.; Srivastava, R. M.; Srivastava, S.; Verma, R.; Vishwakarma, A. L.; Ghosh, J. K. *Biochemistry* **2010,** *49,* 7920–7929. doi:10.1021/bi100729m
17. Ladokhin, A. S.; Selsted, M. E.; White, S. H. *Biochemistry* **1999,** *38,* 12313–12319. doi:10.1021/bi9907936
18. Grishina, I. B.; Woody, R. W. *Faraday Discuss.* **1994,** *99,* 245–262. doi:10.1039/fd9949900245
19. Hunter, H. N.; Demcoe, A. R.; Jenssen, H.; Gutteberg, T. J.; Vogel, H. J. *Antimicrob. Agents Chemother.* **2005,** *49,* 3387–3395. doi:10.1128/AAC.49.8.3387-3395.2005
20. Haney, E. F.; Nazmi, K.; Bolscher, J. G. M.; Vogel, H. J. *Biochim. Biophys. Acta* **2012,** *1818,* 762–775. doi:10.1016/j.bbamem.2011.11.023
21. Brogden, K. A. *Nat. Rev. Microbiol.* **2005,** *3,* 238–250. doi:10.1038/nrmicro1098
22. Teixeira, V.; Feio, M. J.; Bastos, M. *Prog. Lipid Res.* **2012,** *51,* 149–177. doi:10.1016/j.plipres.2011.12.005
23. Hwang, P. M.; Vogel, H. J. *Biochem. Cell Biol.* **1998,** *76,* 235–246. doi:10.1139/o98-026
24. Lohner, K. *Gen. Physiol. Biophys.* **2009,** *28,* 105–116. doi:10.4149/gpb_2009_02_105
25. Hale, J. D. F.; Hancock, R. E. W. *Expert Rev. Anti-Infect. Ther.* **2007,** *5,* 951–959. doi:10.1586/14787210.5.6.951
26. Root, M. J.; Steger, H. K. *Curr. Pharm. Des.* **2004,** *10,* 1805–1825.
27. Torrent, M.; Andreu, D.; Nogués, V. M.; Boix, E. *PLoS One* **2011,** *6,* e16968. doi:10.1371/journal.pone.0016968
28. Torrent, M.; Valle, J.; Nogués, M. V.; Boix, E.; Andreu, D. *Angew. Chem., Int. Ed.* **2011,** *50,* 10686–10689. doi:10.1002/anie.201103589
29. Blondelle, S. E.; Houghten, R. A. *Trends Biotechnol.* **1996,** *14,* 60–65. doi:10.1016/0167-7799(96)80922-X
30. MacCallum, J. L.; Bennett, W. F. D.; Tieleman, D. P. *Biophys. J.* **2008,** *94,* 3393–3404. doi:10.1529/biophysj.107.112805
31. Dempsey, C. E.; Hawrani, A.; Howe, R. A.; Walsh, T. R. *Protein Pept. Lett.* **2010,** *17,* 1334–1344.
32. Bechinger, B.; Lohner, K. *Biochim. Biophys. Acta* **2006,** *1758,* 1529–1539. doi:10.1016/j.bbamem.2006.07.001
33. Reddy, K. V. R.; Yedery, R. D.; Aranha, C. *Int. J. Antimicrob. Agents* **2004,** *24,* 536–547. doi:10.1016/j.ijantimicag.2004.09.005
34. Schibli, D. J.; Nguyen, L. T.; Kernaghan, S. D.; Rekdal, Ø.; Vogel, H. J. *Biophys. J.* **2006,** *91,* 4413–4426. doi:10.1529/biophysj.106.085837
35. Ryge, T. S.; Doisy, X.; Ifrah, D.; Olsen, J. E.; Hansen, P. R. *J. Pept. Res.* **2004,** *64,* 171–185. doi:10.1111/j.1399-3011.2004.00177.x
36. Lee, S.-H.; Kim, S.-J.; Lee, Y.-S.; Song, M.-D.; Kim, I.-H.; Won, H.-S. *Regul. Pept.* **2011,** *166,* 36–41. doi:10.1016/j.regpep.2010.08.010
37. Gasteiger, E.; Hoogland, C.; Gattiker, A.; Duvaud, S.; Wilkins, M. R.; Appel, R. D.; Bairoch, A. Protein Identification and Analysis Tools on the ExPASy Server. In *The Proteomics Protocols Handbook;* Walker, J. M., Ed.; Humana Press: Totowa, NJ., 2005; pp 571–601. doi:10.1385/1-59259-890-0:571
38. Haney, E. F.; Lau, F.; Vogel, H. J. *Biochim. Biophys. Acta* **2007,** *1768,* 2355–2364. doi:10.1016/j.bbamem.2007.04.018
39. Ames, B. N.; Neufeld, E. F.; Ginsberg, V. Assay of inorganic phosphate, total phosphate and phosphatases. *Meth. Enzymol.;* Academic Press: New York, 1966; pp 115–118.
40. Lakowicz, J. R. Quenching of Fluorescence. *Principles of Fluorescence Spectroscopy;* Kluwer Academic: New York, 1999; Vol. 2, pp 237–265.
41. Nguyen, L. T.; Schibli, D. J.; Vogel, H. J. *J. Pept. Sci.* **2005,** *11,* 379–389. doi:10.1002/psc.629
42. Wallace, B. A.; Janes, R. W. An Introduction to Circular Dichroism and Synchrotron Radiation Circular Dichroism Spectroscopy. In *Modern Techniques for circular dichroism and synchrotron radiation circular dichroism spectroscopy;* Haris, P. I., Ed.; IOS Press: Amsterdam, 2009; pp 1–18.
43. Nguyen, L. T.; Chan, D. I.; Boszhard, L.; Zaat, S. A. J.; Vogel, H. J. *Biochim. Biophys. Acta* **2010,** *1798,* 1062–1072. doi:10.1016/j.bbamem.2009.11.021
44. Hwang, T. L.; Shaka, A. J. *J. Magn. Reson., Ser. A* **1995,** *112,* 275–279. doi:10.1006/jmra.1995.1047
45. Delaglio, F.; Grzesiek, S.; Vuister, G. W.; Zhu, G.; Pfeifer, J.; Bax, A. *J. Biomol. NMR* **1995,** *6,* 277–293. doi:10.1007/BF00197809
46. Johnson, B. A. *Methods Mol. Biol.* **2004,** *278,* 313–352. doi:10.1385/1-59259-809-9:313
47. Wüthrich, K. *NMR of Proteins and Nucleic Acids;* John Wiley & Sons Inc.: New York, 1986.
48. Brünger, A. T.; Adams, P. D.; Clore, G. M.; DeLano, W. L.; Gros, P.; Grosse-Kunstleve, R. W.; Jiang, J.-S.; Kuszewski, J.; Nilges, M.; Pannu, N. S.; Read, R. J.; Rice, L. M.; Simonson, T.; Warren, G. L. *Acta Crystallogr., Sect. D: Biol. Crystallogr.* **1998,** *54,* 905–921. doi:10.1107/S0907444998003254
49. Ramachandran, G. N.; Ramakrishnan, C.; Sasisekharan, V. *J. Mol. Biol.* **1963,** *7,* 95–99. doi:10.1016/S0022-2836(63)80023-6
50. Linge, J. P.; O'Donoghue, S. I.; Nilges, M. *Methods Enzymol.* **2001,** *339,* 71–90. doi:10.1016/S0076-6879(01)39310-2
51. Laskowski, R. A.; Rullmann, J. A. C.; MacArthur, M. W.; Kaptein, R.; Thornton, J. M. *J. Biomol. NMR* **1996,** *8,* 477–486. doi:10.1007/BF00228148
52. Koradi, R.; Billeter, M.; Wüthrich, K. *J. Mol. Graphics* **1996,** *14,* 51–55. doi:10.1016/0263-7855(96)00009-4

License and Terms

Beilstein Journal of Organic Chemistry

Binaphthyl-anchored antibacterial tripeptide derivatives with hydrophobic C-terminal amino acid variations

John B. Bremner[*1], Paul A. Keller[*1], Stephen G. Pyne[*1], Mark J. Robertson[1], K. Sakthivel[1], Kittiya Somphol[1], Dean Baylis[2], Jonathan A. Coates[2], John Deadman[3], Dharshini Jeevarajah[2] and David I. Rhodes[4]

Full Research Paper

Open Access

Address:
[1]School of Chemistry, University of Wollongong, Wollongong, NSW 2522, Australia, [2]Avexa Ltd, 576 Swan St, Richmond, Vic 3121, Australia, [3]Chemocopeia Pty Ltd, 114 Kay St, Carlton, Melbourne, Vic 3053, Australia and [4]JDJ Bioservices Pty Ltd, 576 Swan St, Richmond, Vic 3121, Australia

Email:
John B. Bremner[*] - jbremner@uow.edu.au; Paul A. Keller[*] - keller@uow.edu.au; Stephen G. Pyne[*] - spyne@uow.edu.au

* Corresponding author

Keywords:
antibacterials; binaphthyls; cationic peptides; peptides; resistance; VISA; VRE

Beilstein J. Org. Chem. **2012,** *8,* 1265–1270.
doi:10.3762/bjoc.8.142

Received: 31 March 2012
Accepted: 12 July 2012
Published: 09 August 2012

This article is part of the Thematic Series "Antibiotic and cytotoxic peptides".

Guest Editor: N. Sewald

Abstract

The facile synthesis of seven new dicationic tripeptide benzyl ester derivatives, with hydrophobic group variations in the C-terminal amino acid component, is described. Moderate to good activity was seen against Gram-positive bacteria in vitro. One cyclohexyl-substituted compound **2c** was tested more widely and showed good potency (MIC values ranging from 2–4 μg/mL) against antibiotic-resistant strains of *Staphylococcus aureus* and Enterococci (VRE, VSE), and against *Staphylococcus epidermidis*.

Introduction

Among the most pressing challenges in current healthcare is the resistance of bacterial human pathogenic organisms to antibiotics [1,2], and of particular concern is the resistance to the cationic glycopeptide, vancomycin [3,4]. This challenge is being addressed in a number of ways, which include both detailed studies aimed at the further understanding of the mechanism of this resistance, as well as the development of new large glycopeptide analogues containing amine sites that can be protonated, such as telavancin, oritavancin and dalbavancin [5]. An alternative approach to meeting this resistance challenge, at least in part, is through the design and synthesis of smaller cationic peptidic compounds incorporating features that could circumvent the vancomycin resistance mechanism. In much of our work we have been concerned with binaphthyl-based dicationic peptide derivatives, for example the acyclic tripeptides of type **1** (Figure 1; for example A = $CH_2CH{=}CH_2$,

B = CH_2Ph, R = $CH_2CH_2CH(CH_3)_2$, MIC against *S. aureus* 4 μg/mL [6]), which show significant promise as antibacterials [6-8]. In the development of these antibacterials, it became apparent that the nature of the C-terminal amino acid derivative was significant, with indications that the hydrophobic groups at the terminus (Figure 1, group B) [6] and at the α-carbon of the amino acid moiety (Figure 1, group A) [6,7] were important. In further exploration of the structural space in the latter area, while maintaining benzyl ester functionality at the terminus itself (a free carboxylic acid unit at the C-terminal was deleterious to activity [8]), we envisaged the introduction of two alkyl substituent units incorporated in a ring system at this carbon, resulting in the target compounds **2a**–**d**. Two further compounds based on a β–alanine unit with disubstitution at the α- or β-carbons of this unit, **2f** and **2e** respectively, were accessed with a view to assessing the effect of variation in the spatial disposition of the cycloalkyl or oxacycloalkyl ring on antibacterial activity. The conformationally less restricted *gem* diethyl-substituted compound **2g** was also targeted in order to make antibacterial activity comparisons with the five-membered ring analogue **2b**. The results of these synthetic and antibacterial testing studies are reported in this paper.

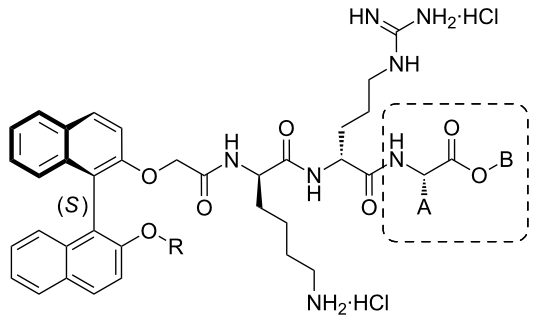

1

Figure 1: Binaphthyl-anchored tripeptide derivatives **1**.

Results and Discussion

A concise and flexible approach to all the target compounds **2a**–**g** was used, starting from the commercially available amino acid derivatives **3** and proceeding via the amino benzyl esters **4** (Scheme 1), with the exception of the synthesis of **2c** in which the commercially available **4c** was used as the starting material. Addition of the protected central arginine unit by diimide- or BOP-induced amide bond formation, followed by selective Fmoc removal from the respective intermediates **5**, then provided access to the key intermediate amines **6a**–**g** (Scheme 1). Diimide-mediated coupling of the previously reported lysine containing (*S*)-binaphthyl acid derivative **7** [8] then afforded the protected tripeptides **8a**–**g**. Removal of the Pmc (or Pbf) and Boc protecting groups in one pot was then achieved by exposure to trifluoroacetic acid, followed by trifluoroacetate/chloride ion exchange on treatment with an excess of HCl in diethyl ether, and finally evaporation to afford the salts **2a**–**g** in good overall yields.

The structures of the final compounds were supported by ^1H and ^{13}C NMR spectroscopy and high-resolution mass spectrometry. Details of the synthesis and spectral data are given in the experimental section for the representative compound **2c**. The experimental and spectroscopic data for all the other compounds are included in Supporting Information File 1.

The peptidic dihydrochloride salts **2a**–**g** were tested against the Gram-positive bacteria *Staphylococcus aureus* (ATCC 6538) and four clinical isolates of vancomycin-resistant (and sensitive) enterococci (VRE; *Enterococcus faecium*), and the results are shown in Table 1; some compounds were also tested against *Staphylococcus epidermidis* (ATCC 12228). Vancomycin was used as a positive control, and showed a rounded MIC (minimum inhibitory concentration) value of 2–3 μg/mL against *S. aureus* and MIC values of 2, >25, >25 and 3 μg/mL against the vancomycin sensitive and partially resistant enterococci

Table 1: MIC values (μg/mL) against *S. aureus*, *S. epidermidis* and Enterococci of the tripeptide benzyl ester derivatives **2a**–**g** and **9** [6] as their dihydrochloride salts.[a]

Compound	*S. aureus*	*S. epidermidis*	VRE_{243}	VRE_{449}	VRE_{820}	VRE_{987}
2a	4	–	62	31	31	62
2b	3	–	62	31	31	62
2c	2	–	31	16	16	31
2d	3	3	>25	>25	>25	>25
2e	3	3	>25	>25	>25	>25
2f	3–6	3	25	25	12	25
2g	2	2	16	16	16	31
9	4	–	16	16	8	16
Vancomycin	2–3	3	2	>25	>25	3

[a]All MIC values have been rounded to whole numbers.

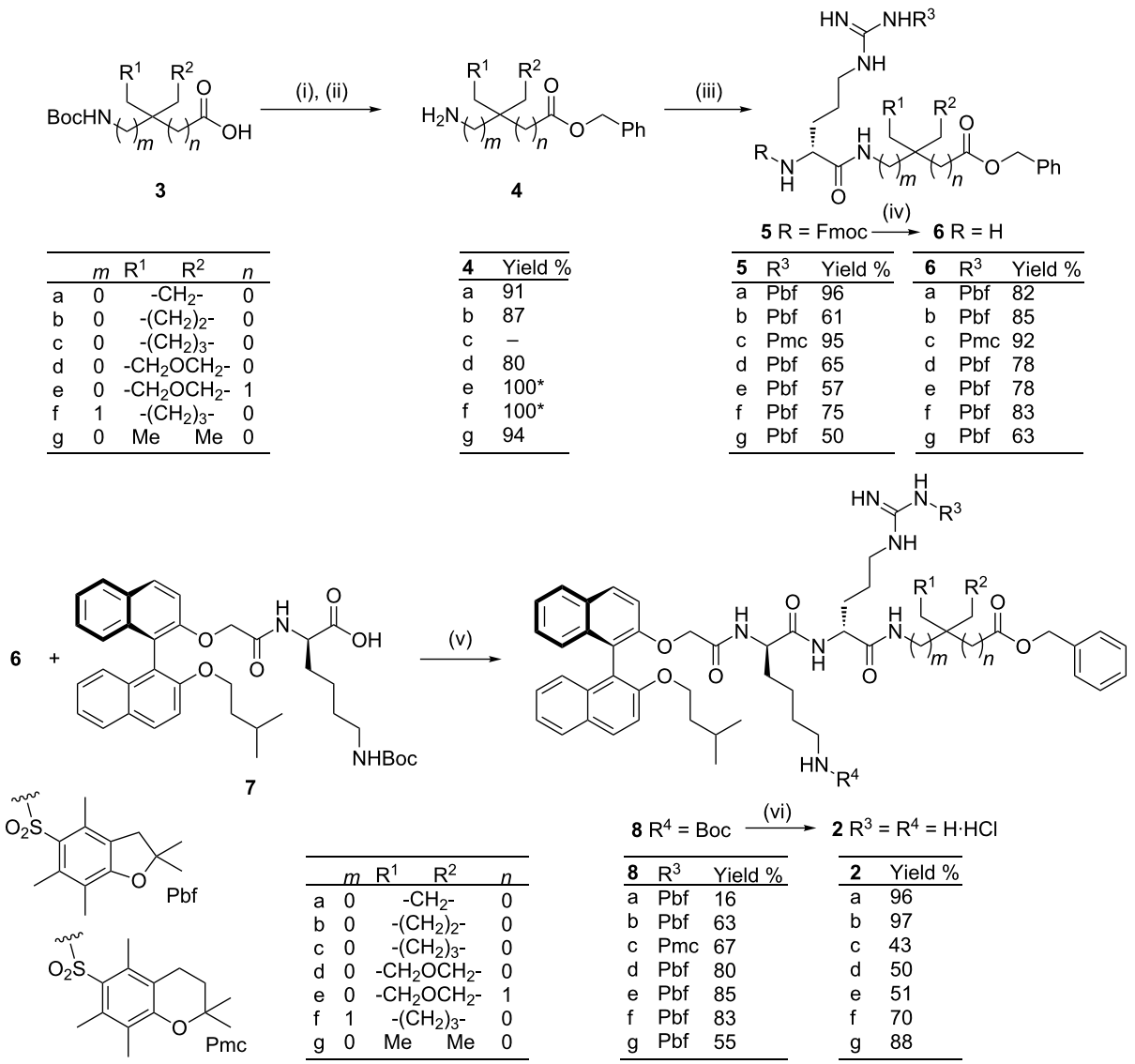

	m	R1	R2	n
a	0		-CH2-	0
b	0		-(CH2)2-	0
c	0		-(CH2)3-	0
d	0		-CH2OCH2-	0
e	0		-CH2OCH2-	1
f	1		-(CH2)3-	0
g	0	Me	Me	0

4	Yield %
a	91
b	87
c	–
d	80
e	100*
f	100*
g	94

5	R3	Yield %
a	Pbf	96
b	Pbf	61
c	Pmc	95
d	Pbf	65
e	Pbf	57
f	Pbf	75
g	Pbf	50

6	R3	Yield %
a	Pbf	82
b	Pbf	85
c	Pmc	92
d	Pbf	78
e	Pbf	78
f	Pbf	83
g	Pbf	63

	m	R1	R2	n
a	0		-CH2-	0
b	0		-(CH2)2-	0
c	0		-(CH2)3-	0
d	0		-CH2OCH2-	0
e	0		-CH2OCH2-	1
f	1		-(CH2)3-	0
g	0	Me	Me	0

8	R3	Yield %
a	Pbf	16
b	Pbf	63
c	Pmc	67
d	Pbf	80
e	Pbf	85
f	Pbf	83
g	Pbf	55

2	Yield %
a	96
b	97
c	43
d	50
e	51
f	70
g	88

Scheme 1: Synthesis of compounds **2a**–**g**. Reagents and conditions: (i) **2a**–**b**,**d**–**g**, BnBr, acetone or THF, K_2CO_3, reflux, 3–12 h; (ii) TFA, DCM, rt, 1–2 h, 2 M HCl/Et_2O (HCl salts); (iii) **5a**–**f**: (DIPEA), Fmoc-(*R*)-Arg(Pmc)-OH (**5c**) or Fmoc-(*R*)-Arg(Pbf)-OH (**5a**–**b**, **d**–**f**), EDCI, HOBt, CH_3CN, rt, 3–16 h; **5g**: DIPEA, Fmoc-(*R*)-Arg(Pbf)-OH, BOP, CH_3CN, rt, 3–16 h (iv) piperidine, CH_3CN, rt, 3–12 h; (v) EDCI, HOBt, CH_3CN, rt, 3–72 h; (vi) TFA/CH_2Cl_2 (1:1), rt, 2–16 h, then 2 M HCl/Et_2O. *Isolated as the HCl salt.

strains, VRE_{243}, VRE_{449}, VRE_{820} and VRE_{987}, respectively (Table 1). For comparison purposes, data for the previously reported [6] isobutyl-substituted analogue **9** (Table 2) are also included.

While MIC micromolar values should be used for comparative analysis of activities, the more commonly used concentration of micrograms per milliliter is retained in this case. The micromolar values are barely different from the latter, as the molecular weights for all of the compounds are similar (959–1001; vancomycin·HCl, 1486). In most cases, incorporation of a hydrophobic alkyl ring in the chain adjacent to the ester functionality results in good activity against *S. aureus* and *S. epidermidis*, but a greater variation of activity was seen with the enterococcal strains. The systems with four- and five-membered cycloalkyl rings (**2a** and **2b**) displayed similar activities, while the cyclohexyl analogue **2c** was somewhat better. Reducing the hydrophobicity while increasing the hydrophilicity of the six-membered ring in **2c** through inclusion of a ring oxygen atom, as in **2d**, had a significant detrimental effect on the activity against the vancomycin-resistant strains VRE_{449} and VRE_{820}. Interestingly, the placement of an extra methylene group in the chain, either on the carboxylic ester side (**2e**) or the amino side (**2f**), had no or little effect on antibacterial activity,

Table 2: MIC values of compounds **2c** and **9** against Gram-positive isolates.

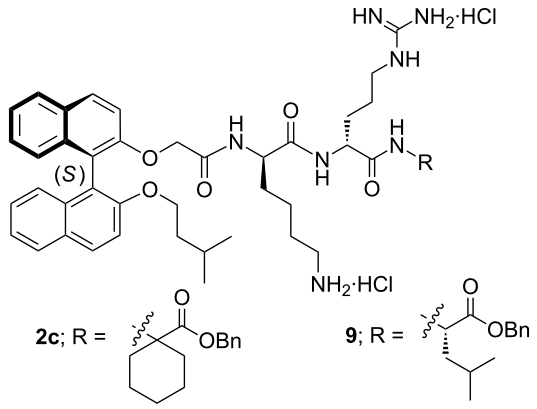

Strain[a]	MIC_{50} (range) or MIC [μg/mL][b]		
	2c	**9** [6]	Vancomycin
S. aureus			
MSSA (8)	2–4	6	1–2
MRSA (7)	2–4	6	1–2
VISA (1)	4	6	6–8
S. epidermidis (3)	2	3	2–3
E. faecium			
VRE (4)	4	2	>32
VSE (4)	2–4	16	2–8

[a]Compound **2c** was tested against a variety of strains (number in brackets) of *S. aureus*, *S. epidermidis* and *E. faecium*, while compound **9** was tested against only one strain of each organism. Where the MIC was the same for each strain, no range is given. [b]Where only one strain was tested, the value given is a MIC. *S. epidermidis* = *Staphylococcus epidermidis*; *E. faecium* = *Enterococcus faecium*; MSSA = methicillin-sensitive *S. aureus*; MRSA = methicillin-resistant *S. aureus*; VISA = vancomycin-intermediate *S. aureus*; VRE = vancomycin-resistant enterococci; VSE = vancomycin-sensitive enterococci. MIC = minimum inhibitory concentration [μg/mL; rounded to whole numbers].

regardless of whether a ring oxygen atom was present or not. It appeared that moving the hydrophobic ring substituent position by a small amount in the terminal amino acid unit could be tolerated in these systems.

The diethyl-substituted peptide derivative **2g** was more active than the constrained ring comparator compound **2b** against the enterococci, including the vancomycin resistant isolates VRE_{449} and VRE_{820}, but both had similarly good potencies against *S. aureus*. In contrast, compound **2c** with the cyclohexyl ring was somewhat more active than the isobutyl-substituted analogue **9**. It would thus appear that greater coverage of the hydrophobic space available in this region is required for good to moderate activity against both the staphylococci and enterococci.

As a result of its promising initial activity profile, the tripeptide derivative **2c** was subjected to further evaluation (Table 2). It was tested against methicillin-sensitive (MSSA), methicillin-resistant (MRSA) and vancomycin-intermediate (VISA) *S. aureus*, *S. epidermis* and vancomycin-resistant (VRE) and vancomycin-sensitive (VSE) enterococci. The test compound **2c** showed good activity against all these Gram-positive bacteria with MIC values in the range of 2–4 μg/mL. Again, for comparison purposes, results for the published analogue **9** [6], containing a single isobutyl group in place of the cyclohexyl group, are also included in Table 2. This tripeptide derivative **9** showed similar, if slightly weaker, antibacterial activity against these strains, apart from VSE, against which it was significantly less potent than **2c**.

Although the mode of action of the tripeptide derivatives has not been established, our earlier results on compounds of type **1** (Figure 1) and related cyclic systems implicated the possibility of more than one mode of action [8]. As noted for other cationic peptide derivatives [9-12], cell membrane damage could well be one of these actions, together with some more specific interactions. Dual-action type behaviour has been shown for the vancomycin analogue telavancin, which affects cell wall synthesis and the integrity of the cell membrane [13].

Conclusion

In conclusion, seven novel binaphthyl-anchored tripeptide derivatives have been prepared and tested for antibacterial activity against *S. aureus* and four clinical enterococcal strains. The dicationic derivatives **2c** and **2g** showed the best overall activities. In addition, compound **2c** with a hydrophobic cyclohexyl substituent originating from the α-position of the C-terminal amino acid ester, showed good activity against *S. epidermidis* and MSSA, MRSA, VISA and VRE organisms. Our results confirmed the positive contribution to good Gram-positive antibacterial activity, engendered by filling of a hydrophobic area close to the C-terminus of these acyclic tripeptide derivatives.

Experimental

General notes were those detailed previously in the supporting information for reference [8].

Benzyl 1-((*R*)-3-amino-1-aza-6-(3,4-dihydro-2,2,5,7,8-pentamethyl-2*H*-1-benzopyran-6-yl)sulfonyl]guanidino)-2-oxohexan)cyclohexanecarboxylate (6c). This compound was prepared in two steps. To a solution of the amine **4c** [14] (115 mg, 0.49 mmol) in CH_3CN (5 mL) at rt was added HOBt (1.2 equiv), EDCI (1.2 equiv) and the acid Fmoc-(*R*)-Arg(Pmc)-OH [8] (318 mg, 0.48 mmol). The mixture was stirred for ca. 3 h, then the solvent was removed under reduced pressure, and

the resulting residue was subjected to silica gel column chromatography (MeOH/CH_2Cl_2, 1:99–4:96 as the eluent) to afford the Fmoc-protected precursor **5c** as a white foamy solid (402 mg, ESIMS *m*/*z*: $[M + H]^+$ 877.9 (100%)). This precursor **5c** (200 mg, 0.238 mmol) was then directly deprotected by being stirred in 1 equiv of piperidine/acetonitrile (5 mL per 0.1 mmol of substrate) for 12 h at rt. The solvent was removed under reduced pressure, and the crude product was purified by flash column chromatography (silica gel; CH_2Cl_2/MeOH 15:1) to afford the desired amine **6c** as a white solid (141 mg, 87% two steps). ^{1}H NMR (500 MHz, $CDCl_3$) δ 1.19–1.44 (m, 16H), 1.30 (s, 6H, $2CH_3$ (Pmc)), 2.34 (br s, NH_2), 2.10 (s, 3H, CH_3 (Pmc)), 2.57 (s, 3H, CH_3 (Pmc)), 2.58 (s, 3H, CH_3 (Pmc)), 2.61 (t, *J* = 6.5 Hz, 2H, CH_2 (Pmc)), 3.05–3.29 (m, 2H, CH_2N), 3.39–3.50 (m, 1H, CH (Arg)), 5.06 (ABq, *J* = 12.6 Hz, 1H), 5.09 (ABq, *J* = 12.6 Hz, 1H), 6.41 (s, NH), 7.26–7.41 (m, 5H, ArH), 7.80 (s, NH); ^{13}C NMR (125 MHz, $CDCl_3$) δ 12.0, 17.4, 18.4, 21.3, 24.5, 25.0, 25.3, 26.7, 26.75, 31.6, 31.9, 32.4, 32.7, 40.5, 54.1, 57.8, 58.4, 66.7, 73.5, 117.8, 123.9, 127.9, 128.1, 128.4, 133.3, 134.6, 135.3, 135.8, 153.4, 156.3, 174.0, 174.4; ESIMS *m*/*z*: $[M + H]^+$ 656.3 (100%).

Benzyl 1-((3*R*,6*R*)-3-(3-[(3,4-dihydro-2,2,5,7,8-pentamethyl-2*H*-1-benzopyran-6-yl)sulfonyl]guanidinopropyl)-9-((*S*)-2'-(3-methylbutoxy)-1,1'-binaphth-2-yloxy)-6-(4-(*tert*-butoxycarbonylamino)butyl)-1,4,7-triaza-2,5,8-trioxononan)cyclohexanecarboxylate (8c). To a solution of the amine **6c** (140 mg, 0.213 mmol) in CH_3CN (10 mL) at rt was added HOBt (1.2 equiv), EDCI (1.2 equiv) and the binaphthyl acid **7** [8] (122 mg, 0.190 mmol). The mixture was stirred for ca. 3 h. The solvent was then removed under reduced pressure and the resulting residue subjected to silica gel chromatography (MeOH/CH_2Cl_2 1:99–4:96 as the eluent) to yield **8c** as a white solid (163 mg, 67%). $[\alpha]_D^{24}$ −18.6 (*c* 2.0, MeOH); ^{1}H NMR (300 MHz, $CDCl_3$) δ 0.49 (d, *J* = 6.4 Hz, 3H), 0.54 (d, *J* = 6.4 Hz, 3H), 0.66–0.84 (m, 2H), 0.85–1.03 (m, 2H), 1.05–1.62 (m, 16H), 1.29 (s, 6H), 1.44 (s, 9H), 1.64–1.88 (m, 4H), 1.89–2.14 (m, 1H), 2.09 (s, 3H), 2.54–2.64 (m, 2H), 2.55 (s, 3H), 2.57 (s, 3H), 2.84–2.96 (m, 2H), 2.97–3.22 (m, 2H), 3.76–3.94 (m, 1H), 4.00–4.07 (m, 2H), 4.36 and 4.54 (ABq, *J* = 14.6 Hz, 2H), 4.39–4.48 (m, 1H), 4.78–4.82 (m, NH), 5.06 (s, 2H), 6.14 (br s, NH) 6.36 (br s, NH), 7.11–7.46 (m, 12H), 7.44 (d, *J* = 9.1 Hz, 1H), 7.84 (d, *J* = 8.9 Hz, 1H), 7.86 (d, *J* = 7.9 Hz, 1H), 7.92 (d, *J* = 8.8 Hz, 1H), 7.95 (d, *J* = 7.6 Hz, 1H); ESIMS *m*/*z*: $[M + H]^+$ 1280.3 (100%); HRMS–ESI *m*/*z*: $[M + H]^+$ calcd for $C_{72}H_{94}N_7O_{12}S$, 1280.6676; found, 1280.6627.

Benzyl 1-((3*R*,6*R*)-6-aminobutyl-3-(3-guanidinopropyl)-9-((*S*)-2'-(3-methylbutoxy)-1,1'-binaphth-2-yloxy)-1,4,7-triaza-2,5,8-trioxononan)cyclohexanecarboxylate dihydrochloride (2c). The protected amine **8c** (106 mg, 0.083 mmol) in 1:1 CH_2Cl_2/TFA (6 mL/0.10 mmol) solution was stirred for 12 h at rt. The solvent was removed under reduced pressure, and the residue was resuspended in a minimal volume of methanol. The solution was then treated with an excess of 2 M HCl/diethyl ether solution (2 mL, 0.01 mmol) and the solvent evaporated. The crude product was purified by precipitation from MeOH by addition of diethyl ether to yield **2c** as an off white solid (35 mg, 43%). $[\alpha]_D^{24}$ −10.9 (*c* 3.4, MeOH); ^{1}H NMR (300 MHz, CD_3OD) δ 0.50 (d, *J* = 6.4 Hz, 3H), 0.56 (d, *J* = 6.4 Hz, 3H), 0.84–1.02 (m, 2H), 1.03–3.15 (m, 21H), 2.68–2.92 (m, 2H), 2.96–3.20 (m, 2H), 3.91–3.98 (m, 1H), 4.09–4.16 (m, 2H), 4.24–4.36 (m, 1H), 4.42 and 4.54 (ABq, *J* = 14.6 Hz, 2H), 5.02 and 5.09 (ABq, *J* = 12.3 Hz, 2H), 7.06 (t, *J* = 5.5 Hz, 2H), 7.17–7.22 (m, 2H), 7.27–7.36 (m, 7H), 7.44 (d, *J* = 8.8 Hz, 1H), 7.53 (d, *J* = 9.1 Hz, 1H), 7.90 (t, *J* = 7.0 Hz, 2H), 8.00 (dd, *J* = 2.3 and 9.1 Hz, 2H), 8.09 (s, NH); ^{13}C NMR (75 MHz, CD_3OD) δ 22.5, 22.6, 22.8, 23.0, 25.6, 26.2, 26.3, 27.7, 30.0, 32.3, 32.9, 33.7, 39.3, 40.3, 42.0, 53.3, 54.3, 60.3, 67.8, 69.0, 69.1, 115.9, 116.9, 120.5, 121.7, 124.8, 125.2, 125.9, 126.4, 127.5, 127.6, 129.1, 129.2, 129.6, 130.7, 130.9, 131.4, 135.0, 135.2, 137.4, 154.0, 155.9, 158.5, 170.7, 173.1, 173.6, 175.4; ESIMS *m*/*z*: $[M + H]^+$ 915.0 (10%), $[M + 2H]^{2+}$ 457.9 (100); HRMS–ESI *m*/*z*: $[M + H]^+$ calcd for $C_{53}H_{68}N_7O_7$, 914.5175; found, 914.5130 (100%). HPLC analysis of this compound was also undertaken with a gradient system comprised of H_2O containing 10% CH_3CN and 0.1% TFA 90:10:0.5 (A), and CH_3CN containing 0.1% TFA (B). The gradient profile was 0–3 min, linear gradient 0 to 50% B; 4–13 min, linear gradient 50 to 80% of B; 14–15 min, linear gradient 80 to 100% B; t_R = 6.1 min, 96% pure.

Determination of minimum inhibitory concentration (MIC)

MIC studies (Table 1) were performed on *Staphylococcus aureus* wild type (ATCC 6538P), and *Staphylococcus epidermidis* (ATCC 12228) in Mueller–Hinton broth (Oxoid Ltd, England) supplemented with 50 mg/L $CaCl_2$. As in [6], MIC determinations for clinical isolates of *Enterococcus faecium* were conducted by growth in Enterococcosal broth (Becton Dickinson Microbiology Systems). Briefly, overnight stationary phase cultures were diluted 1:1000 into fresh media and then incubated with two-fold dilutions of compounds in media, typically with a highest concentration of 128 μg/mL, in a 96-well plate. Plates were incubated overnight at 37 °C and the MIC was recorded as the highest concentration at which bacterial growth was observed.

Compound **2c** (Table 2) was tested at JMI Laboratories through Ordway Research Institute (USA) on *Staphylococcus aureus* (MSSA; MRSA; VISA), *S. epidermidis* and *E. faecium* (VRE and VSE). The microdilution reference methods (M7-A6 (2003)

and M11-A6 (2004)) of the CLSI/NCCLS were used. Quality control ranges for the selected control agent vancomycin from CLSI/NCCLS M100-S15 (2005) were used. Panels were produced in volumes of 100 µL/well over a concentration of 0.03–32 µg/mL. A growth control was included for each dilution series. MIC results were produced by using the M7-A6 and M11-A6 CLSI/NCCLS procedures in cation-adjusted Mueller–Hinton broth media with supplements as required for the test species. The compounds were initially dissolved in DMSO and then diluted.

Supporting Information

Supporting Information File 1

Experimental procedures and associated spectroscopic data (NMR and MS) for the syntheses of compounds **2a**–**b** and **2d**–**g**.
[http://www.beilstein-journals.org/bjoc/content/supplementary/1860-5397-8-142-S1.pdf]

Acknowledgements

We thank the former Amrad Operations Pty Ltd and Avexa Limited, the University of Wollongong and the National Health and Medical Research Council (Development Grants 303415 and 404528) for their support. We also thank Dr A. McCracken for assistance, Dr S. Cox for her support in the initial development of this project, and T. R. Fritsche, D. J. Biedenbach and R. N. Jones of JMI Laboratories, North Liberty, Iowa and M. H. Miller, M. S. Howe, P. Ambrose and S. Bhavnani from Ordway Research Institute, New York (USA) for the provision of some assays.

References

1. French, G. L. *Int. J. Antimicrob. Agents* **2010,** *36* (Suppl. 3), S3–S7. doi:10.1016/S0924-8579(10)70003-0
2. Fischbach, M. A.; Walsh, C. T. *Science* **2009,** *325,* 1089–1093. doi:10.1126/science.1176667
3. Rong, S. L.; Leonard, S. N. *Ann. Pharmacother.* **2010,** *44,* 844–850. doi:10.1345/aph.1M526
4. Werner, G.; Strommenger, B.; Witte, W. *Future Microbiol.* **2008,** *3,* 547–562. doi:10.2217/17460913.3.5.547
5. Guskey, M. T.; Tsuji, B. T. *Pharmacotherapy* **2010,** *30,* 80–94. doi:10.1592/phco.30.1.80
6. Bremner, J. B.; Keller, P. A.; Pyne, S. G.; Boyle, T. P.; Brkic, Z.; David, D. M.; Robertson, M.; Somphol, K.; Baylis, D.; Coates, J. A.; Deadman, J.; Jeevarajah, D.; Rhodes, D. I. *Bioorg. Med. Chem.* **2010,** *18,* 2611–2620. doi:10.1016/j.bmc.2010.02.033
7. Bremner, J. B.; Keller, P. A.; Pyne, S. G.; Boyle, T. P.; Brkic, Z.; Morgan, J.; Somphol, K.; Coates, J. A.; Deadman, J.; Rhodes, D. I. *Bioorg. Med. Chem.* **2010,** *18,* 4793–4800. doi:10.1016/j.bmc.2010.05.005
8. Bremner, J. B.; Keller, P. A.; Pyne, S. G.; Boyle, T. P.; Brkic, Z.; David, D. M.; Garas, A.; Morgan, J.; Robertson, M.; Somphol, K.; Miller, M. H.; Howe, A. S.; Ambrose, P.; Bhavnani, S.; Fritsche, T. R.; Biedenbach, D. J.; Jones, R. N.; Buckheit, R. W., Jr.; Watson, K. M.; Baylis, D.; Coates, J. A.; Deadman, J.; Jeevarajah, D.; McCracken, A.; Rhodes, D. I. *Angew. Chem., Int. Ed.* **2010,** *49,* 537–540. doi:10.1002/anie.200904392
9. Haug, B. E.; Stensen, W.; Kalaaji, M.; Rekdal, Ø.; Svendsen, J. S. *J. Med. Chem.* **2008,** *51,* 4306–4314. doi:10.1021/jm701600a
10. Flemming, K.; Klingenberg, C.; Cavanagh, J. P.; Sletteng, M.; Stensen, W.; Svendsen, J. S.; Flægstad, T. *J. Antimicrob. Chemother.* **2009,** *63,* 136–145. doi:10.1093/jac/dkn464
11. Fjell, C. D.; Hiss, J. A.; Hancock, R. E. W.; Schneider, G. *Nat. Rev. Drug Disc.* **2012,** *11,* 37–51. doi:10.1038/nrd3591
12. Sundriyal, S.; Sharma, R. K.; Jain, R.; Bharatam, P. V. *J. Mol. Model.* **2008,** *14,* 265–278. doi:10.1007/s00894-008-0268-1
13. Higgins, D. L.; Chang, R.; Debabov, D. V.; Leung, J.; Wu, T.; Krause, K. M.; Sandvik, E.; Hubbard, J. M.; Kaniga, K.; Schmidt, D. E., Jr.; Gao, Q.; Cass, R. T.; Karr, D. E.; Benton, B. M.; Humphrey, P. P. *Antimicrob. Agents Chemother.* **2005,** *49,* 1127–1134. doi:10.1128/aac.49.3.1127-1134.2005
14. Tailleur, P.; Berlinguet, L. *Can. J. Chem.* **1961,** *39,* 1309–1320. doi:10.1139/v61-165

License and Terms

Beilstein Journal of Organic Chemistry

A macrolactonization approach to the total synthesis of the antimicrobial cyclic depsipeptide LI-F04a and diastereoisomeric analogues

James R. Cochrane, Dong Hee Yoon, Christopher S. P. McErlean and Katrina A. Jolliffe*

Full Research Paper

Open Access

Address:
School of Chemistry, The University of Sydney, 2006, NSW, Australia; Tel: +61-2-93512297; Fax: +61-2-93513329

Email:
Katrina A. Jolliffe* - kate.jolliffe@sydney.edu.au

* Corresponding author

Keywords:
antifungal; cyclic depsipeptide; epimerization; lipopeptide; macrolactonization; peptides

Beilstein J. Org. Chem. **2012,** *8,* 1344–1351.
doi:10.3762/bjoc.8.154

Received: 02 May 2012
Accepted: 16 July 2012
Published: 21 August 2012

This article is part of the Thematic Series "Antibiotic and cytotoxic peptides".

Guest Editor: N. Sewald

Abstract

The cyclic peptide core of the antifungal and antibiotic cyclic depsipeptide LI-F04a was synthesised by using a modified Yamaguchi macrolactonization approach. Alternative methods of macrolactonization (e.g., Corey–Nicolaou) resulted in significant epimerization of the *C*-terminal amino acid during the cyclization reaction. The D-stereochemistry of the alanine residue in the naturally occurring cyclic peptide may be required for the antifungal activity of this natural product.

Introduction

The LI-F or fusaricidin class of cyclic depsipeptides are produced by a number of strains of *Bacillus* (*Paenebacillus*) and exhibit antifungal and antibacterial activity against a range of clinically relevant species, including *Candida albicans*, *Cryptococcus neoformans*, *Staphylococcus aureus* and *Micrococcus luteus* [1-7]. These compounds have a cyclic hexadepsipeptide core, in which three amino acids, L-Thr, D-*allo*-Thr and D-Ala are conserved throughout the series, while there are slight variations in the other three amino acids. In LI-F04a these are D-Asn, L-Val and D-Val. A unique 15-guanidino-3-hydroxypentadecanoyl (GHPD) side chain is appended to the cyclic peptide core through the nitrogen atom of the L-Thr residue. There has been recent interest in the synthesis of the LI-F family of cyclic depsipeptides due to their antifungal activity. Biosynthetic processes have been employed to this end, although these provide mixtures of depsipeptides, which makes it difficult to determine structure–activity relationships [7,8]. More recently, the solid-phase synthesis of a number of

analogues of the fusaricidins has been reported. However, in all cases, the side chain 3-hydroxy group was not incorporated into the structure [9]. By total synthesis of both side-chain epimers of this structure we have recently established that the absolute configuration of this side-chain hydroxy group is (*R*) in the naturally occurring LI-F04a **1** [10]. We employed a late-stage coupling of the cyclic peptide core **2** with the GHDP side chain **3** to enable ready access to both side-chain epimers (Scheme 1). While macrocyclization to give the core **2** could be performed at any of the amide or ester bonds [10], we chose to use a macrolactonization approach to enable ready access to analogues of the LI-F04a core through straightforward Fmoc solid-phase peptide synthesis of the linear precursors. We report here our optimization of these macrolactonization conditions, together with the synthesis of several analogues of LI-F04a using this approach, and an investigation of the antifungal activity of these synthetic lipodepsipeptides.

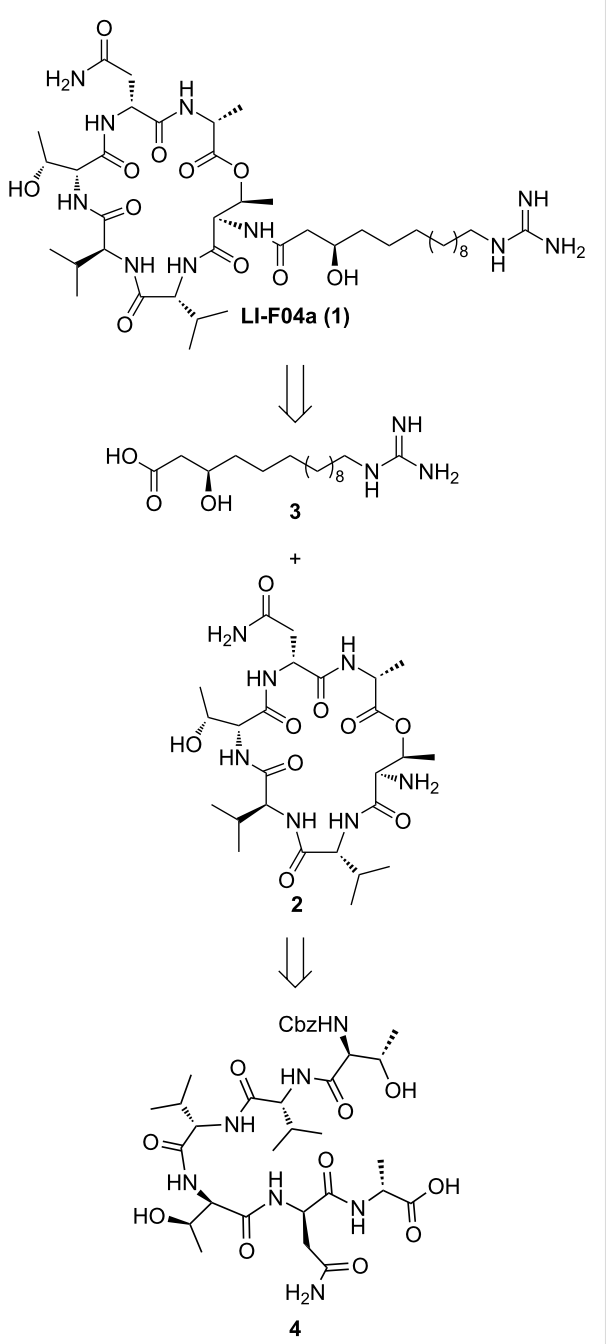

Scheme 1: Retrosynthetic strategy.

Results and Discussion

The required linear precursor for the synthesis of **2** by a macrolactonization approach is **4** (Scheme 1), in which the *N*-terminal amino group of the L-Thr residue is protected while the side-chain hydroxy group is free. The Cbz group was chosen as a suitable protecting group for the *N*-terminus. The D-Asn and D-*allo*-Thr residues were the only amino acids requiring side-chain protection. Given previous reports that 2,2-dimethylated pseudoprolines ($\Psi^{Me,Me'}$Pros) [11-13] are useful turn-inducers for improving yields of macrolactamization reactions [14-17], we chose to prepare two linear precursors, **5** and **6** (Scheme 2), in which the D-*allo*-Thr protecting group was either *tert*-butyl or $\Psi^{Me,Me'}$Pro, respectively, to investigate whether a turn-inducer might assist the macrolactonization reaction. Linear peptides **5** and **6** were prepared by standard Fmoc solid-phase peptide synthesis protocols using PyBOP/Hünigs base as the activation reagent and 2-chlorotritylchloride resin to allow cleavage of the peptide from the solid support with side-chain protecting groups intact. In the case of **6**, the $\Psi^{Me,Me'}$Pro was introduced by coupling the known dipeptide Fmoc-Val-D-*a*-Thr($\Psi^{Me,Me'}$Pro)-OH [18] into the growing peptide chain.

While there are a large number of methods available for macrolactonization reactions, those most commonly employed include the Corey–Nicolaou [19], Boden–Keck [20] and Yamaguchi [21] lactonization procedures. We initially chose to screen these three procedures for the macrolactonization of **5**. In all three cases (Table 1, entries 1–3), analysis of the crude product mixtures showed that mixtures of cyclic diastereoisomers were obtained, indicating that the *C*-terminal amino acid underwent epimerization during the macrolactonization reactions (see Supporting Information File 1 for full experimental details) [22]. However, the ratio of the two diastereoisomers differed significantly under the three sets of conditions, with the major diastereomer formed under the Yamaguchi conditions differing from the major product obtained in the other reactions.

In order to establish which set of conditions gave the highest ratio of the desired product **7**, the mixture of cyclic depsipeptides **7** and **8** obtained from macrolactonization under the highest yielding conditions (Corey–Nicolaou) was separated, and the major diastereomer was subjected to hydrolysis upon

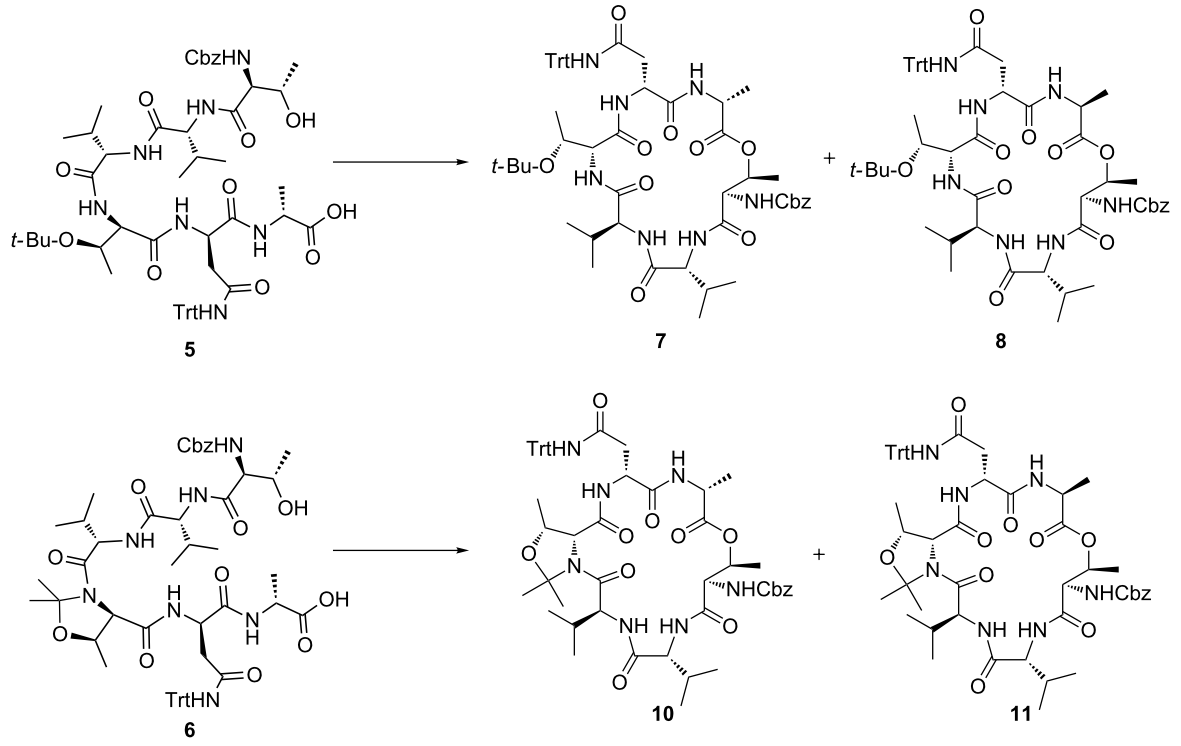

Scheme 2: Macrolactonization reactions of seco acids **5** and **6** (for reagents and yields see Table 1 and Table 2).

treatment with MeOH/H_2O/aq NH_4OH (4:1:1 v/v/v). Comparison of the crude peptide, so obtained, to authentic samples of both **5** and the *C*-terminal epimer **9** (which was independently prepared by solid-phase peptide synthesis), indicated that the major product obtained upon macrolactonization of **5** under the Corey–Nicolaou conditions was the undesired cyclic depsipeptide **8**, in which the *C*-terminal Ala residue had epimerized (Figure 1). Since the Yamaguchi conditions gave improved ratios of the desired/epimerized cyclic depsipeptides, subsequent optimization of the macrolactonization conditions focussed on this and related procedures (Table 1). The best yields of the desired cyclic depsipeptide **7** (58% isolated yield, with 5–12% of epimer **8** also observed) were obtained using a modification of Yonemitsu's conditions [23] in which linear peptide **5** was added slowly to a solution of DMAP, 2,4,6-trichlorobenzoyl chloride and triethylamine in toluene at room temperature. Similar yields and low epimerization (52% isolated yield, 6% epimer observed) were obtained using 2-methyl-6-nitrobenzoic anhydride (MNBA) [24] as the activating agent in place of 2,4,6-trichlorobenzoyl chloride.

Table 1: Reaction conditions for macrocyclization of **5**.

entry	reaction conditions	yield of major isomer[a]	ratio of **7**:**8**[b]
1	dithiopyridine, triphenylphosphine, MeCN, 80 °C	56%	13:87
2	DCC, DMAP, camphorsulfonic acid, CH_2Cl_2	14%	45:55
3	2,4,6-trichlorobenzoyl chloride, DMAP, NEt_3, toluene, 110 °C	20%	61:39
4	2,4,6-trichlorobenzoyl chloride, DMAP, iPr_2NEt, toluene, 80 °C	33%	69:31
5	2,4,6-trichlorobenzoyl chloride, DMAP, NEt_3, toluene, 25 °C	33%	89:11
6	2,4,6-trichlorobenzoyl chloride, DMAP, NEt_3, THF, 25 °C	16%	82:18
7	2,4,6-trichlorobenzoyl chloride, DMAP, NEt_3, toluene, 25 °C, slow addition of **5**	58%	92:8[c]
8	2-methyl-6-nitrobenzoic anhydride, DMAP, NEt_3, toluene, 25 °C, slow addition of **5**	52%	94:6
9	cyanuric chloride, MeCN, 25 °C	30%	80:20

[a]Isolated yield; [b]as determined by integration of analytical HPLC traces of the crude reaction mixtures; [c]average value (5–12% epimerization was observed upon repeat reactions).

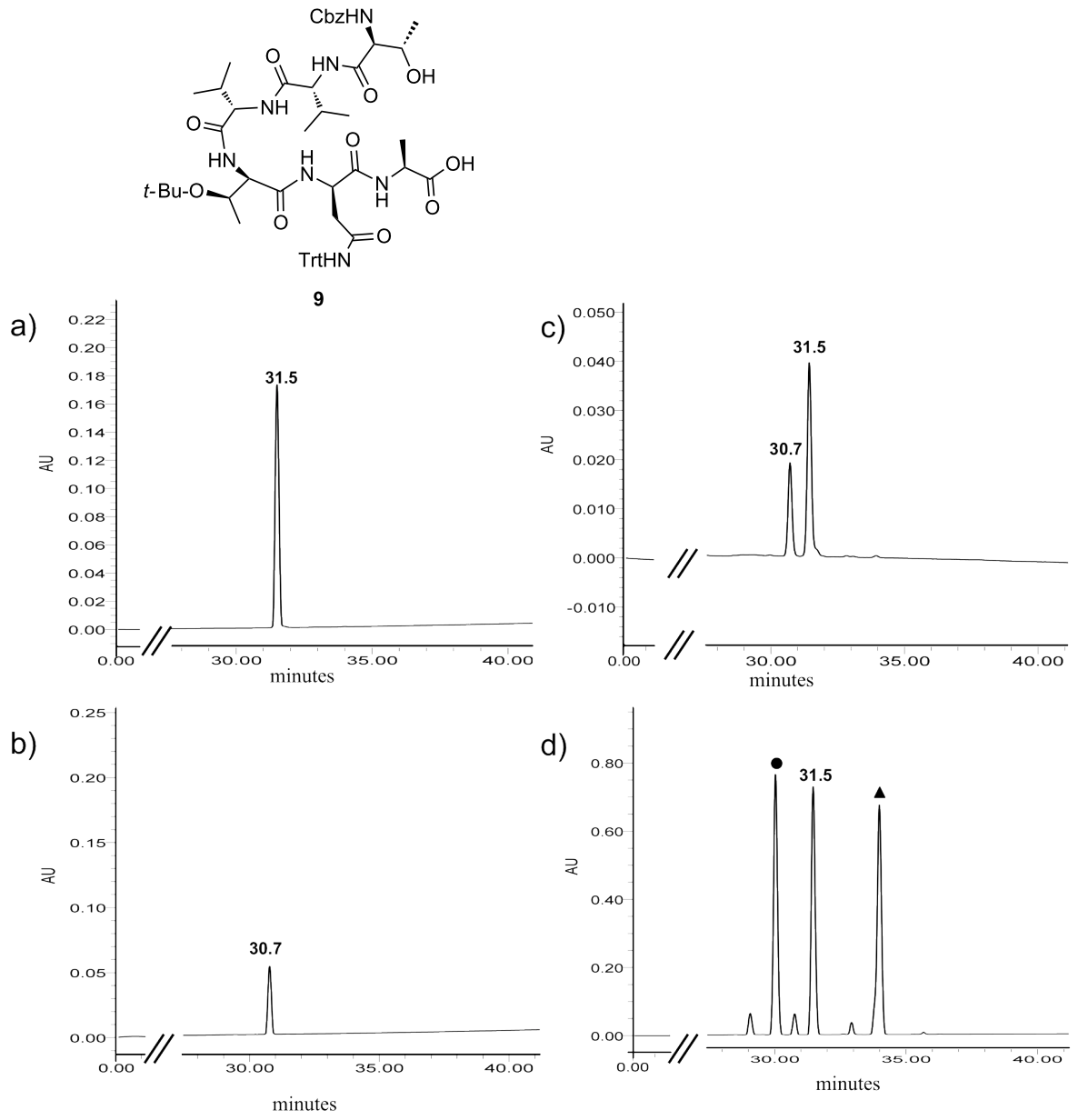

Figure 1: Analytical HPLC traces of linear peptides. (a) Compound **9** (retention time = 31.5 min); (b) Compound **5** (retention time = 30.7 min); (c) co-injection of mixture of **9** and **5** (2:1); (d) Crude reaction mixture after hydrolysis of major cyclic peptide from Corey–Nicolaou cyclization, indicating that the major product of hydrolysis is **9**; ▲ indicates the unreacted cyclic peptide (retention time = 34.0 min) and ● is a peak attributed to hydrolysis of both the cyclic peptide ester bond and Cbz protecting group (LCMS m/z = 902 $[M + H]^+$).

To investigate whether the $\Psi^{Me,Me'}$Pro would assist macrolactonization, linear precursor **6** was subject to cyclization under a range of conditions (Table 2). However, in all cases, the cyclization yields were found to be lower for the $\Psi^{Me,Me'}$Pro-containing peptide than for the *tert*-butyl protected precursor **5**, with higher amounts of *C*-terminal epimerization also observed, except in the case of cyclization using cyanuric chloride [25]. Unfortunately, the yield could not be improved above 17% in this case, so all further reactions were performed using the Thr(O-*t*-Bu) protected cyclic peptides **7** and **8**. With cyclic peptides **7** and **8** in hand, we chose to attach the GHPD side chain to both compounds to enable the effect of peptide stereochemistry on the biological activity of the LI-F cyclic peptides to be assessed. Additionally, to investigate the effect of the 3-hydroxy group of the GHPD side chain on the biological activity of this class of cyclic peptide, we prepared the dehydroxy side-chain analogue **12** for attachment to the cyclic peptide core (Scheme 3). Notably, a previously synthesised

Table 2: Reaction conditions for macrocyclization of **6**.

entry	reaction conditions	yield of major isomer[a]	ratio of **10**:**11**[b]
1	dithiopyridine, triphenylphosphine, MeCN, 80 °C	24%	<5 to >95
2	2,4,6-trichlorobenzoyl chloride, DMAP, NEt_3, toluene, 110 °C	19%	50:50
3	2,4,6-trichlorobenzoyl chloride, DMAP, NEt_3, toluene, 25 °C	7%	80:20
4	2,4,6-trichlorobenzoyl chloride, DMAP, NEt_3, toluene, 25 °C, slow addition of **5**	24%	79:21
5	cyanuric chloride, MeCN, 25 °C	17%	>95 to <5

[a]Isolated yield; [b]as determined by integration of analytical HPLC traces of the crude reaction mixtures.

LI-F04a analogue with a twelve-carbon side chain lacking the hydroxy group has been observed to have antimicrobial activity [9]. Thus, hydrolysis of pentadecanolide **13** [26] was followed by esterification to give the methyl ester **14** in excellent yield. Reaction of **14** with di(*tert*-butoxycarbonyl)guanidine under Mitsunobu conditions [27] proceeded smoothly to give **15** in 86% yield. Hydrolysis of the methyl ester followed by acidic work up to enable extraction of the resulting carboxylic acid gave **12**, in which one of the guanidino Boc protecting groups was also removed.

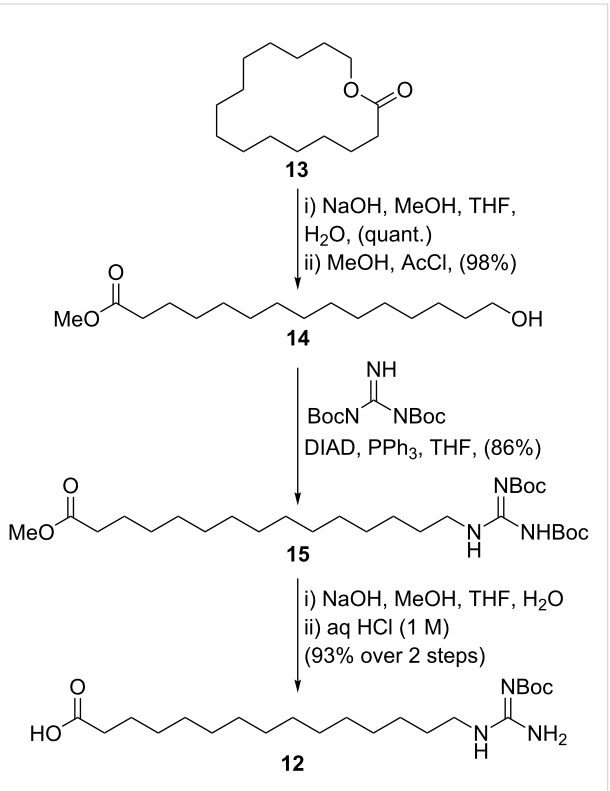

Scheme 3: Synthesis of the dehydroxy side chain **12**.

Hydrogenolysis of the Cbz protecting groups of **7** and **8** gave the corresponding amines **16** and **17**, respectively (Scheme 4). These were coupled with the previously synthesised side chains **18**, **19** [10] and **12**, by using HATU as the coupling agent. The resulting compounds were not isolated but immediately subjected to global deprotection upon treatment with trifluoroacetic acid/CH_2Cl_2/H_2O (90:5:5 v/v/v) to give LI-F04a (**1**), side-chain epimer **20**, dehydroxy analogue **21** and the two side-chain epimers of the L-Ala derivative, **22** and **23**.

The antifungal activity of **1** and **20**–**23** was evaluated by using a standardised serial dilution sensitivity assay [28] against reference strains of *Candida albicans*, *Cryptococcus neoformans* and *Aspergillus fumigatus* (Table 3). Synthetic LI-F04a was found to exhibit good activity against both *C. albicans* and *C. neoformans*, but only modest activity against *A. fumigatus*, consistent with the previously reported activity of the natural product [1,3,5]. The side-chain epimer **20** exhibited significantly lower activity than **1** against *C. albicans* and *C. neoformans*, indicating that the stereochemistry of the side-chain hydroxy group is important for the antifungal activity of the compounds. Removal of the hydroxy group, as in **21**, resulted in a further small decrease in activity against these species. Notably, compounds **22** and **23**, prepared from the *C*-terminal-epimerised cyclic peptide did not exhibit antifungal activity against any of the species tested. This suggests that the conformation of the cyclic peptide core is important in determining the antifungal activity of these compounds, since inversion of the stereocentre of one of the amino acids in the macrocycle is expected to result in a significantly different peptide conformation [29]. Modelled structures of the side-chain-acylated cyclic peptides **24** and **25** obtained by using Monte Carlo conformational searches in Macromodel [30] suggest that these cyclic peptides adopt significantly different conformations with different arrangements of hydrogen bonds (Figure 2). The temperature dependence of the chemical shifts of the signals attributable to the amide NHs of **1** in d_6-DMSO was determined experimentally and confirmed the involvement of the D-Ala and D-Asn amide protons in hydrogen bonds [31] as suggested by the modelling studies of the acetamide analogue (see Supporting Information File 1 for details). This indicates that these hydrogen bonds may be important in locking the cyclic depsipeptide into a biologically active conformation.

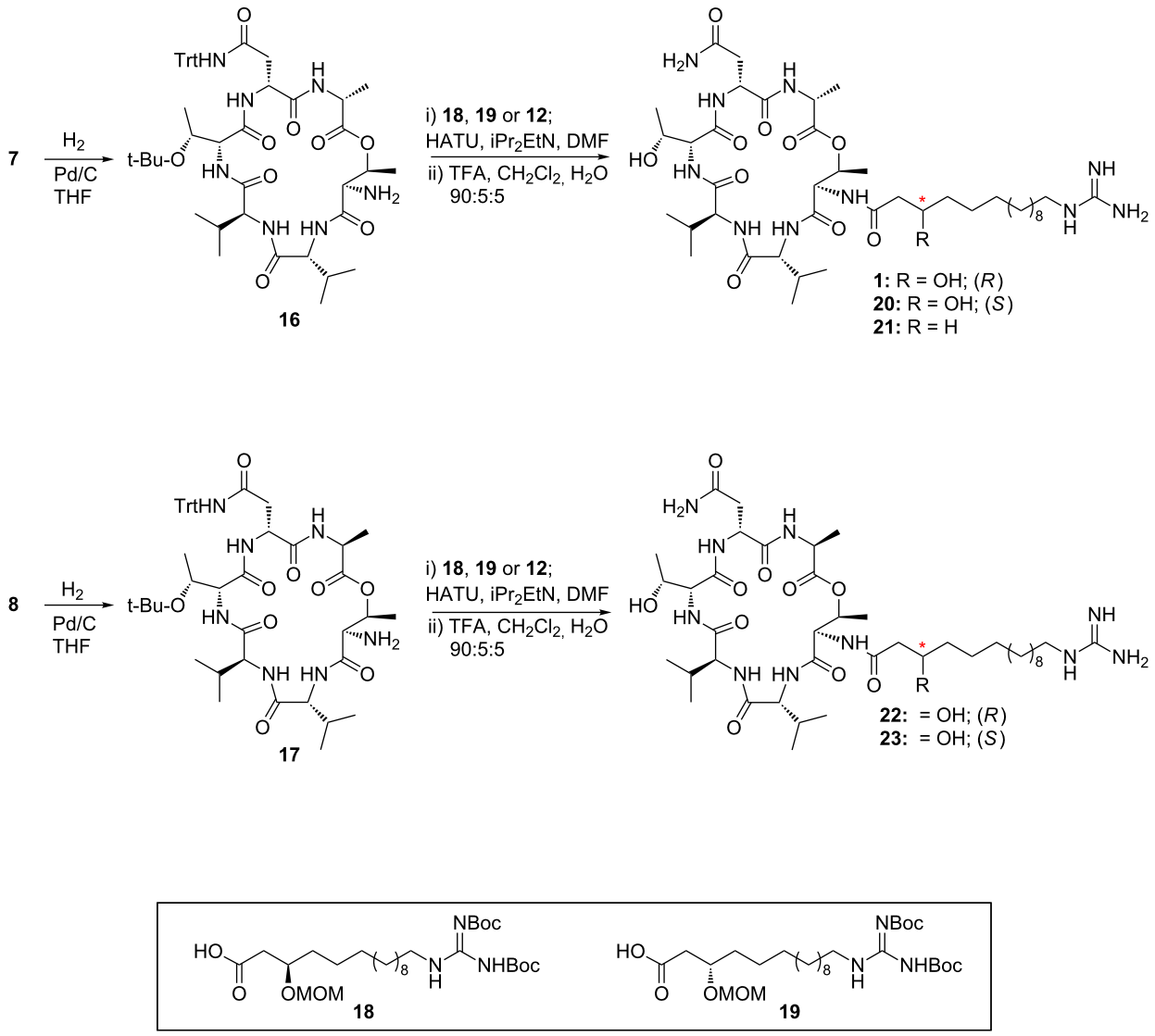

Scheme 4: Synthesis of LI-F04a (**1**) and analogues **20**–**23**.

Table 3: Antifungal activity.

compound	*C. albicans* ATCC 10231 (MIC μM)[a]	*C. neoformans* ATCC 90112 (MIC μM)[a]	*A. fumigatus* ATCC 204305 (MIC μM)[a]
1	5.5	2.8	44
20	22	11	22
21	44	22	22
22	>88	>88	>88
23	>88	>88	>88

[a]MICs for amphotericin B: *C. albicans* 0.35 μM; *C. neoformans* 0.35 μM; *A. fumigatus* 0.70 μM.

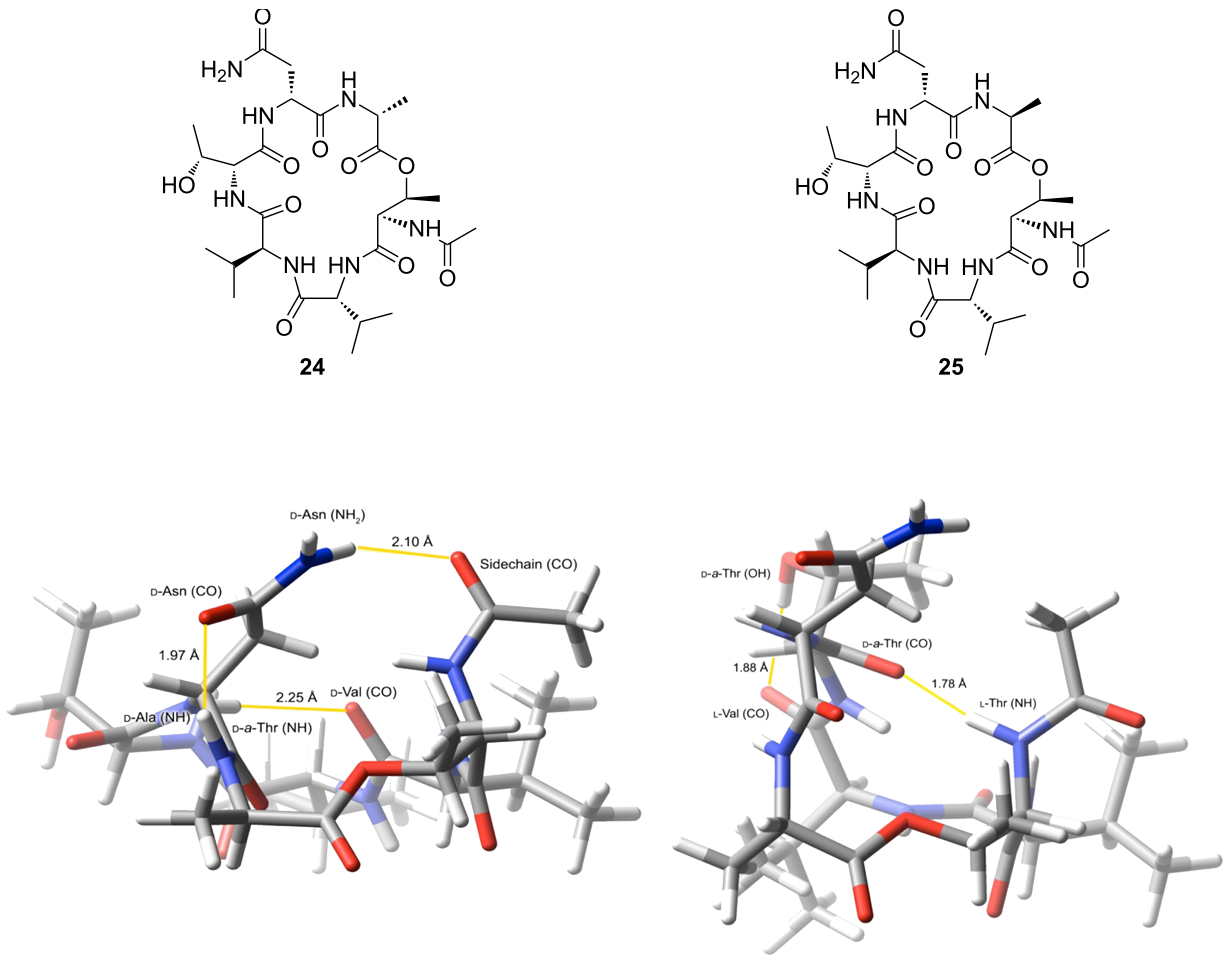

Figure 2: Structures and lowest-energy conformers of **24** (left) and **25** (right) obtained using Macromodel. Hydrogen bonding is highlighted in yellow.

Conclusion

In summary, macrolactonization to form the cyclic depsipeptide core of LI-F04a was achieved in good yields by using either modified Yonemitsu conditions or similar conditions, in which the 2,4,6-trichlorobenzoyl chloride activating agent was replaced with MNBA. Slow addition of the linear seco-acid to the activating agents was found to be the key factor to minimizing epimerization of the *C*-terminal amino acid during the macrolactonization reaction. Synthetic LI-F04a was found to exhibit similar antifungal activity to that reported for the naturally occurring material. The antifungal activity of **1** was reduced upon either inversion of the stereochemistry, or deletion of the side-chain hydroxy group. Inversion of the D-Ala residue in the cyclic depsipeptide core resulted in complete loss of antifungal activity, indicating that the cyclic peptide conformation may be important in the biological activity of this class of cyclic lipodepsipeptide.

Supporting Information

Supporting Information File 1

Experimental details for all new compounds.
[http://www.beilstein-journals.org/bjoc/content/supplementary/1860-5397-8-154-S1.pdf]

Supporting Information File 2

^{1}H, ^{13}C and 2D NMR data for all new compounds.
[http://www.beilstein-journals.org/bjoc/content/supplementary/1860-5397-8-154-S2.pdf]

Acknowledgements

We thank the University of Sydney for financial support and the award of a postgraduate scholarship to JRC; and Prof. Tania Sorrell and Dr. Julianne Djordjevic (Centre for Infectious

Diseases and Microbiology, Westmead Hospital, University of Sydney) for assistance with the antifungal assays.

References

1. Kurusu, K.; Ohba, K.; Arai, T.; Fukushima, K. *J. Antibiot.* **1987,** *40,* 1506–1514. doi:10.7164/antibiotics.40.1506
2. Kajimura, Y.; Sugiyama, M.; Kaneda, M. *J. Antibiot.* **1995,** *48,* 1095–1103. doi:10.7164/antibiotics.48.1095
3. Kajimura, Y.; Kaneda, M. *J. Antibiot.* **1996,** *49,* 129–135. doi:10.7164/antibiotics.49.129
4. Kajimura, Y.; Kaneda, M. *J. Antibiot.* **1997,** *50,* 220–228. doi:10.7164/antibiotics.50.220
5. Kuroda, J.; Fukai, T.; Konishi, M.; Uno, J.; Kurusu, K.; Nomura, T. *Heterocycles* **2000,** *53,* 1533–1549. doi:10.3987/COM-00-8922
6. Kaneda, M.; Kajimura, Y. *Yakugaku Zasshi* **2002,** *122,* 651–671.
7. Choi, S.-K.; Park, S.-Y.; Kim, R.; Lee, C.-H.; Kim, J. F.; Park, S.-H. *Biochem. Biophys. Res. Commun.* **2008,** *365,* 89–95. doi:10.1016/j.bbrc.2007.10.147
8. Li, J.; Beatty, P. K.; Shah, S.; Jensen, S. E. *Appl. Environ. Microbiol.* **2007,** *73,* 3480–3489. doi:10.1128/AEM.02662-06
9. Bionda, N.; Stawikowski, M.; Stawikowska, R.; Cudic, M.; López-Vallejo, F.; Treitl, D.; Medina-Franco, J.; Cudic, P. *ChemMedChem* **2012,** *7,* 871–882. doi:10.1002/cmdc.201200016
10. Cochrane, J. R.; McErlean, C. S. P.; Jolliffe, K. A. *Org. Lett.* **2010,** *12,* 3394–3397. doi:10.1021/ol101254m
11. Wöhr, T.; Wahl, F.; Nefzi, A.; Rohwedder, B.; Sato, T.; Sun, X.; Mutter, M. *J. Am. Chem. Soc.* **1996,** *118,* 9218–9227. doi:10.1021/ja961509q
12. Dumy, P.; Keller, M.; Ryan, D. E.; Rohwedder, B.; Wöhr, T.; Mutter, M. *J. Am. Chem. Soc.* **1997,** *119,* 918–925. doi:10.1021/ja962780a
13. Keller, M.; Sager, C.; Dumy, P.; Schutkowski, M.; Fischer, G. S.; Mutter, M. *J. Am. Chem. Soc.* **1998,** *120,* 2714–2720. doi:10.1021/ja973966s
14. Skropeta, D. S.; Jolliffe, K. A.; Turner, P. *J. Org. Chem.* **2004,** *69,* 8804–8809. doi:10.1021/jo0484732
15. Sayyadi, N.; Skropeta, D.; Jolliffe, K. A. *Org. Lett.* **2005,** *7,* 5497–5499. doi:10.1021/ol0522891
16. Fairweather, K. A.; Sayyadi, N.; Luck, I. J.; Clegg, J. K.; Jolliffe, K. A. *Org. Lett.* **2010,** *12,* 3136–3139. doi:10.1021/ol101018w
17. Wong, M. S. Y.; Jolliffe, K. A. *Aust. J. Chem.* **2010,** *63,* 797–801. doi:10.1071/CH09643
18. Clegg, J. K.; Cochrane, J. R.; Sayyadi, N.; Skropeta, D.; Turner, P.; Jolliffe, K. A. *Aust. J. Chem.* **2009,** *62,* 711–719. doi:10.1071/CH09151
19. Corey, E. J.; Nicolaou, K. C. *J. Am. Chem. Soc.* **1974,** *96,* 5614–5616. doi:10.1021/ja00824a073
20. Boden, E. P.; Keck, G. E. *J. Org. Chem.* **1985,** *50,* 2394–2395. doi:10.1021/jo00213a044
21. Inanaga, J.; Hirata, K.; Saeki, H.; Katsuki, T.; Yamaguchi, M. *Bull. Chem. Soc. Jpn.* **1979,** *52,* 1989–1993. doi:10.1246/bcsj.52.1989
22. Atherton, E.; Sheppard, R. C. *Solid Phase Peptide Synthesis: A Practical Approach;* IRL Press: Oxford, New York, 1989.
23. Hikota, M.; Sakurai, Y.; Horita, K.; Yonemitsu, O. *Tetrahedron Lett.* **1990,** *31,* 6367–6370. doi:10.1016/S0040-4039(00)97066-7
24. Shiina, I.; Kubota, M.; Ibuka, R. *Tetrahedron Lett.* **2002,** *43,* 7535–7539. doi:10.1016/S0040-4039(02)01819-1
25. Venkataraman, K.; Wagle, D. R. *Tetrahedron Lett.* **1980,** *21,* 1893–1896. doi:10.1016/S0040-4039(00)92809-0
26. Nesmeyanov, A. N.; Zakharkin, L. I.; Kost, T. A.; Friedlina, R. K. *Russ. Chem. Bull.* **1960,** *9,* 195–199. doi:10.1007/BF00942889
27. Dodd, D. S.; Kozikowski, A. P. *Tetrahedron Lett.* **1994,** *35,* 977–980. doi:10.1016/S0040-4039(00)79943-6
28. Reference Method for Broth Dilution Susceptibility Testing of Yeasts: Approved Standard. NCCLS document M27-A (ISBN 1-56238-186-5). National Committee for Clinical Laboratory Standards, Pennsylvania, USA, 1997; Reference Method for Broth Dilution Susceptibility Testing of Filamentous Fungi: Approved Standard. NCCLS document M38-A (ISBN 1-56238-186-5). National Committee for Clinical Laboratory Standards, Pennsylvania, USA, 2002.
29. Haubner, R.; Finsinger, D.; Kessler, H. *Angew. Chem., Int. Ed. Engl.* **1997,** *36,* 1374–1389. doi:10.1002/anie.199713741
30. Mohamadi, F.; Richards, N. G. J.; Guida, W. C.; Liskamp, R.; Lipton, M.; Caufield, C.; Chang, G.; Hendrickson, T.; Still, W. C. *J. Comput. Chem.* **1990,** *11,* 440–467. doi:10.1002/jcc.540110405
31. Kessler, H. *Angew. Chem., Int. Ed. Engl.* **1982,** *21,* 512–523. doi:10.1002/anie.198205121

License and Terms

Beilstein Journal of Organic Chemistry

Synthetic studies towards bottromycin

Stefanie Ackermann[1], Hans-Georg Lerchen[2], Dieter Häbich[2], Angelika Ullrich[1] and Uli Kazmaier[*1]

Full Research Paper

Open Access

Address:
[1]Institute of Organic Chemistry, Saarland University, P.O. Box 151150, 66041 Saarbrücken, Germany and [2]Bayer Pharma Aktiengesellschaft, Aprather Weg 18a, 42113 Wuppertal, Germany

Email:
Uli Kazmaier[*] - u.kazmaier@mx.uni-saarland.de

* Corresponding author

Keywords:
amidines; antibiotics; bottromycin; peptides; thiopeptides; Ugi reactions

Beilstein J. Org. Chem. **2012,** *8,* 1652–1656.
doi:10.3762/bjoc.8.189

Received: 16 July 2012
Accepted: 28 August 2012
Published: 01 October 2012

This article is part of the Thematic Series "Antibiotic and cytotoxic peptides".

Guest Editor: N. Sewald

Abstract

Thio-Ugi reactions are described as an excellent synthetic tool for the synthesis of sterically highly hindered endothiopeptides. *S*-Methylation and subsequent amidine formation can be carried out in an inter- as well as in an intramolecular fashion. The intramolecular approach allows the synthesis of the bottromycin ring system in a straightforward manner.

Introduction

Natural products are excellent sources as lead structures for the development of new antibiotics. Over millions of years microorganisms, such as bacteria and fungi, developed efficient defense strategies against their bacterial competitors [1-3]. Not surprising, a wide range of common antibiotics such as penicillin or vancomycin are natural products or derivatives thereof.

In 1957 Waiswisz et al. reported a new antibiotic peptide isolated from the fermentation broth of *Streptomyces bottropensis*, called bottromycin [4-6]. This antibiotic inhibits the growth of a wide range of microorganisms by interfering with their protein biosynthesis [7-12]. In 1965 Nakamura et al. isolated closely related antibiotics from the strain *Streptomyces* No. 3668-L2, named bottromycin A and B [13,14]. Acidic hydrolysis provided a mixture of all-(*S*)-configured amino acids containing 3-methylphenylalanine [15], *tert*-leucine, valine, β-(2-thiazolyl)-β-alanine [16] and glycine. While also proline was found in bottromycin B, *cis*-3-methylproline is a component in bottromycin A [17]. Originally Nakamura postulated a linear *N*-acylated iminohexapeptide structure, a proposal which was revised after synthetic studies [18] as well as NMR spectroscopic investigations by Takita et al., which proposed a cyclic iminopeptide structure [19]. This proposal was verified by Schipper [20] and Kaneda [21], based on detailed NMR studies. According to them, the bottromycins are cyclic tetrapeptides, connected to a tripeptidic side chain through an amidine struc-

ture. The different bottromycins differ only in the substitution pattern of the proline (Figure 1). The three-dimensional structure was reported recently by Gouda et al. [22]. This structure is quite unusual, not only because of the amidine moiety but also because most amino acids are found in β-methylated form (*tert*-leucine can be seen as β-methylvaline).

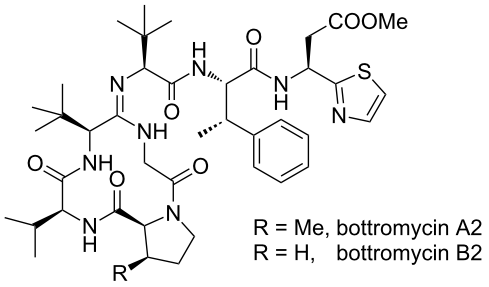

Figure 1: Bottromycins.

Although a series of synthetic studies towards linear bottromycin sequences have been published [23,24], no total synthesis was reported for a long time. The first and only synthesis so far was described by Sunazuka and Ōmura et al. in 2009 [25]. Their synthesis was based on the formation of the amidine structure by reaction of the tripeptide side chain with an endothiopeptide and ring closure between proline and glycine. The same group also undertook some modifications on the natural product [26].

Results and Discussion

Our group is also involved in the synthesis of peptide-based natural products [27-32], and of course the structure of bottromycin is highly fascinating from a synthetic point of view. In our previous investigations we observed that for the synthesis of sterically demanding peptides, especially those containing *N*-alkylated amide bonds, Ugi reactions are especially suited [33,34]. For *N*-unsubstituted peptides the Ugi reactions should be carried out with ammonia as the amine component, which is a protocol that is often accompanied by a range of side reactions. But in general the yields are good if sterically demanding aldehydes, such as pivaldehyde are used [35,36]. With thiocarboxylic acids as acid components, this approach allows also the synthesis of endothiopeptides [37-40], and therefore this protocol should be extremely suitable for the synthesis of bottromycins.

To prove this option, we reacted Boc-protected (*S*)-thiovaline [41] with pivaldehyde, ethyl isocyanoacetate, and a 2 M NH_3 solution in CH_3OH. In trifluoroethanol, which is the best solvent for ammonia Ugi reactions [35], the expected endothiopeptide **1** was formed in high yield as a 1:1 diastereomeric mixture (Scheme 1). With this building block in hand, we were interested to see whether we would be able to generate the required cyclic endothiopeptide and if we could even subsequently connect the side chain.

Therefore, we prolonged the peptide chain **2** under standard peptide coupling conditions and tried to activate the linear

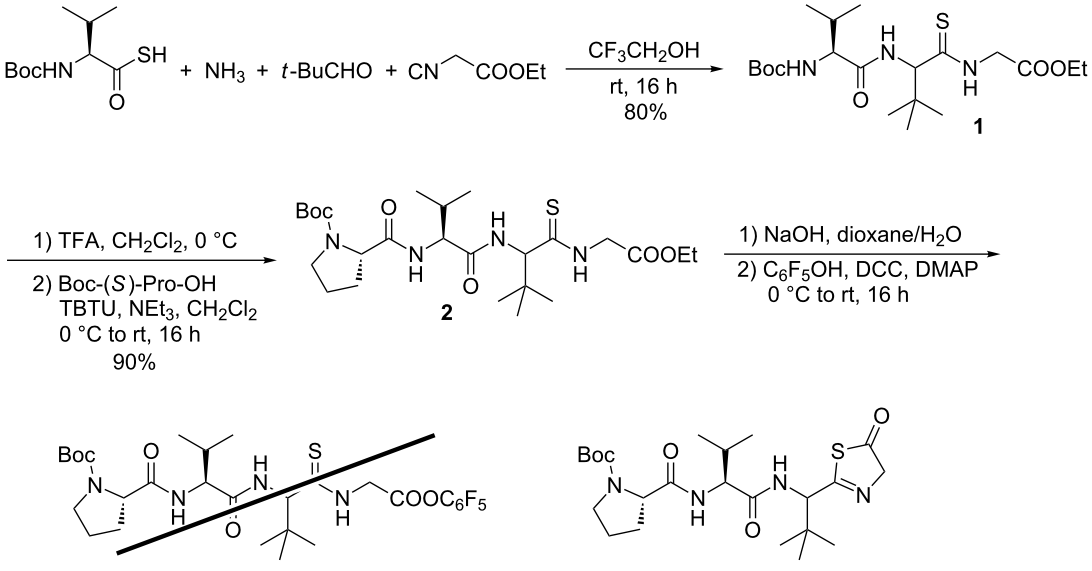

Scheme 1: Syntheses of endothiopeptides by thio-Ugi reaction.

peptide chain. We chose the pentafluorophenylester protocol developed by Schmidt et al. for cyclization [42]. But unfortunately this approach failed (as did all other activations investigated) because of the formation of thiazolone side product, which could not be cyclized.

In parallel, we tried to figure out if the amidine formation is possible with sterically hindered endothiopeptides (Scheme 2). As a model substrate we chose thiopeptide **3** [37], easily obtained by thio-Ugi reaction in excellent yield. The reaction was very fast and was finished already after 15 min, and peptide **3** crystallized directly from the reaction mixture. Because our first attempts to couple **3** directly with amines to the corresponding amidine **5** failed [43], we decided to convert **3** into the corresponding thioimidate **4**, which was reacted with (*S*)-valine methyl ester as an amine component in the presence of Hg salts [44]. $Hg(OCOCF_3)_2$ was found to be more suitable than $Hg(OCOCH_3)_2$ (Table 1, entries 1 and 2) and from the different solvents tested, THF was the solvent of choice. With a twofold excess of the amine component a yield of up to 72% of **5** could be obtained as a 1:1 diastereomeric mixture. The diastereomers could be separated by flash chromatography, but unfortunately these reaction conditions could not be transferred to the thioimidoester obtained from endothiopeptide **2**. Here, the expected amidine was only formed in a trace amount, and a range of side products was obtained.

Therefore, we decided to change our strategy and to replace the intermolecular amidine formation by an intramolecular one. In this case the peptide ring should be formed in the amidination step. For this approach we first needed the isocyanide **7** derived from (*S*)-*tert*-leucine methyl ester. According to Ugi et al. this isocyanide was obtained in enantiomerically pure form from the corresponding formamide **6** by dehydration with $POCl_3/NEt_3$ (Scheme 3).

Table 1: Optimization of amidine formation.

entry	Hg salt	equiv (*S*)-Val-OMe	solvent	yield (%)
1	$Hg(OCOCH_3)_2$	1.3	MeCN	0
2	$Hg(OCOCF_3)_2$	1.3	MeCN	24
3	$Hg(OCOCF_3)_2$	1.3	CH_2Cl_2	50
4	$Hg(OCOCF_3)_2$	1.3	THF	61
5	$Hg(OCOCF_3)_2$	2.0	THF	72

This isocyanide was subjected to a thio-Ugi reaction as described before, and the expected sterically highly demanding endothiopeptide **8** was obtained in high yield as a 1:1 diastereomeric mixture. In this case, the diastereomers could not be separated. Elongation of the peptide chain under standard peptide coupling conditions provided the linear precursor **10** for the ring-closing amidination. After removal of the Boc-protecting group the resulting salt showed a low solubility in THF, and therefore we had to run the amidination in CH_3CN, although this was not the solvent of choice in our model system.

The amidination was carried out under high-dilution conditions. The peptide salt was dissolved in CH_3CN and was added slowly through a syringe to a solution of $Hg(OCOCF_3)_2$ in CH_3CN at 50 °C over a period of 10 h. Interestingly, the best result was obtained not with the free peptide amine but with the hydrochloride salt. Here the cyclic amidine was obtained in 51% yield.

Conclusion

In conclusion, we could show that thio-Ugi reactions are an excellent synthetic tool for the synthesis of highly sterically hindered endothiopeptides. *S*-Methylation and subsequent amidine formations can be carried out in an inter- as well as in

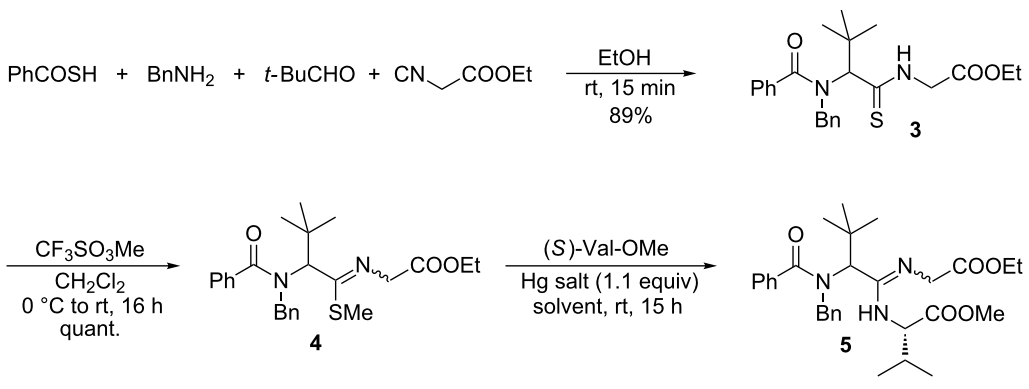

Scheme 2: Synthesis of amidine **5** by thio-Ugi reaction.

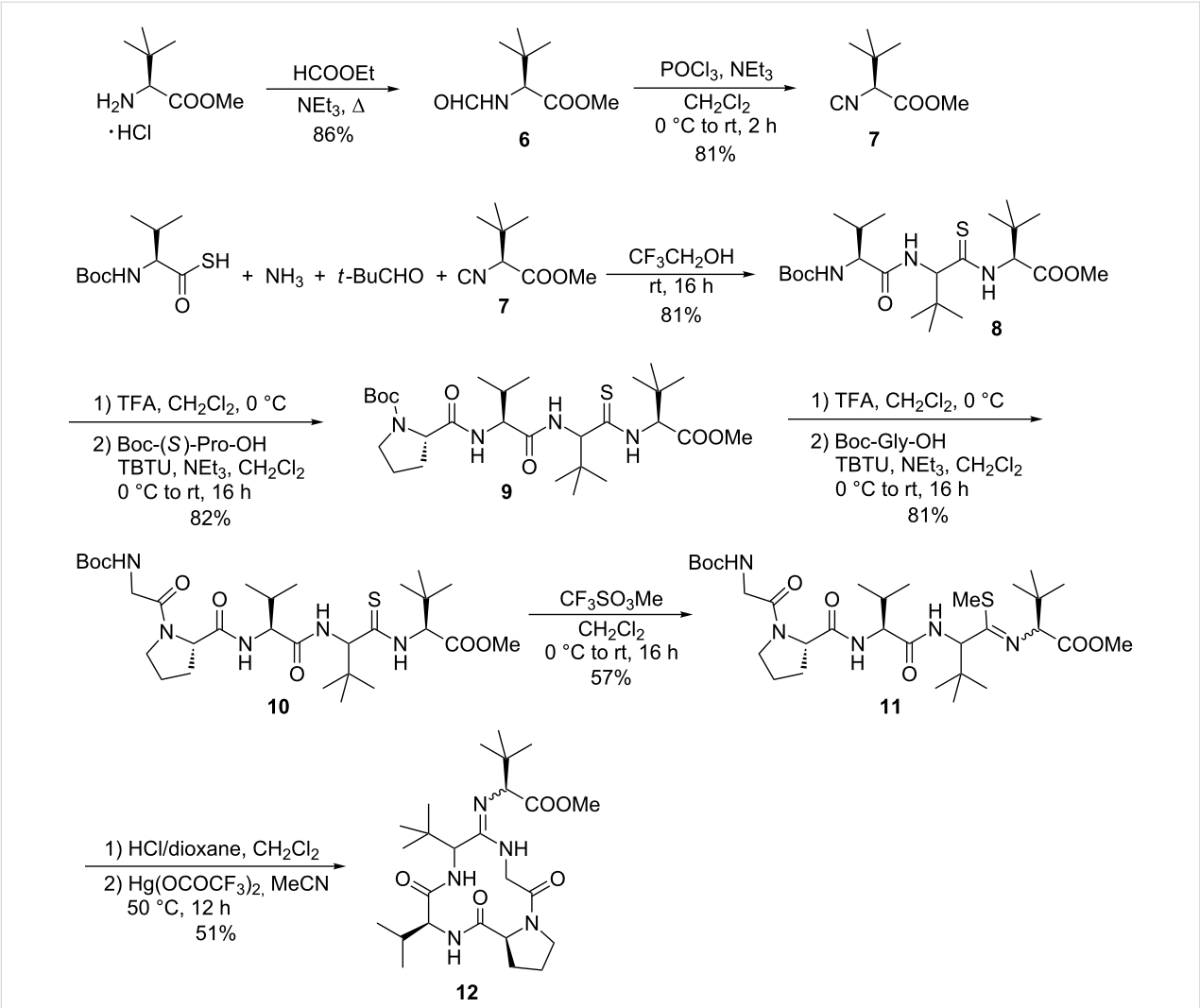

Scheme 3: Synthesis of the bottromycin ring system **12** by thio-Ugi reaction.

an intramolecular fashion. The intramolecular approach allows the synthesis of the bottromycin ring system in a straightforward manner. The synthesis of the bottromycins and derivatives thereof is currently under investigation.

Supporting Information

Supporting Information File 1

Detailed experimental procedures, NMR and analytical data of all compounds.
[http://www.beilstein-journals.org/bjoc/content/supplementary/1860-5397-8-189-S1.pdf]

Acknowledgements

This work was supported by the Deutsche Forschungsgemeinschaft and Bayer Health Care.

References

1. Gräfe, U. *Biochemie der Antibiotika;* Spektrum Akademischer Verlag: Heidelberg, Germany, 1992.
2. Eberle, A. E. *Chimia* **1991,** *45,* 145–153.
3. von Nussbaum, F.; Brands, M.; Hinzen, B.; Weigand, S.; Häbich, D. *Angew. Chem.* **2006,** *118,* 5194–5254. doi:10.1002/ange.200600350 *Angew. Chem., Int. Ed.* **2006,** *45,* 5072–5129. doi:10.1002/anie.200600350
4. Waisvisz, J. M.; van der Hoeven, M. G.; van Peppen, J.; Zwennis, W. C. M. *J. Am. Chem. Soc.* **1957,** *79,* 4520–4521. doi:10.1021/ja01573a072
5. Waisvisz, J. M.; van der Hoeven, M. G.; Hölscher, J. F.; te Nijenhuis, B. *J. Am. Chem. Soc.* **1957,** *79,* 4522–4524. doi:10.1021/ja01573a073
6. Waisvisz, J. M.; van der Hoeven, M. G.; Te Nijenhuis, B. *J. Am. Chem. Soc.* **1957,** *79,* 4524–4527. doi:10.1021/ja01573a074
7. Nakamura, S.; Chikaike, T.; Karasawa, K.; Tanaka, N.; Yonehara, H.; Umezawa, H. *J. Antibiot.* **1965,** *18,* 47–52.
8. Tanaka, N.; Sashika, K.; Yamaguchi, H.; Umezawa, H. *J. Biochem.* **1966,** *60,* 405–410.

9. Nakamura, S.; Yajima, T.; Lin, Y.-C.; Umezawa, H. *J. Antibiot.* **1967,** *20,* 1–5.
10. Tanaka, N.; Lin, Y.-C. *J. Biochem.* **1968,** *63,* 1–7.
11. Otaka, T.; Kaji, A. *J. Biol. Chem.* **1976,** *251,* 2299–2306.
12. Otaka, T.; Kaji, A. *FEBS Lett.* **1983,** *153,* 53–59. doi:10.1016/0014-5793(83)80118-5
13. Nakamura, S.; Chikaike, T.; Karasawa, K.; Tanaka, N.; Yonehara, H.; Umezawa, H. *J. Antibiot.* **1965,** *9,* 1860–1861.
14. Nakamura, S.; Umezawa, H. *Chem. Pharm. Bull.* **1966,** *14,* 981–986. doi:10.1248/cpb.14.981
15. Arold, H.; Eule, M.; Reissmann, S. *Z. Chem.* **1969,** *9,* 447–448.
16. Seto, Y.; Torii, K.; Bori, K.; Inabata, K.; Kuwata, S.; Watanabe, H. *Bull. Chem. Soc. Jpn.* **1974,** *47,* 151–155. doi:10.1246/bcsj.47.151
17. Nakamura, S.; Chikaike, T.; Yonehara, H.; Umezawa, H. *Chem. Pharm. Bull.* **1965,** *13,* 599–602. doi:10.1248/cpb.13.599
18. Yamada, Y.; Takashima, K.; Miyazawa, T.; Kuwata, S.; Watanabe, H. *Bull. Chem. Soc. Jpn.* **1978,** *51,* 878–883. doi:10.1246/bcsj.51.878
19. Takahashi, Y.; Naganawa, H.; Takita, T.; Umezawa, H.; Nakamura, S. *J. Antibiot.* **1976,** *29,* 1120–1123. doi:10.7164/antibiotics.29.1120
20. Schipper, D. *J. Antibiot.* **1983,** *36,* 1076–1077. doi:10.7164/antibiotics.36.1076
21. Kaneda, M. *J. Antibiot.* **1992,** *45,* 792–796. doi:10.7164/antibiotics.45.792
22. Gouda, H.; Kobayashi, Y.; Yamada, T.; Ideguchi, T.; Sugawara, A.; Hirose, T.; Ōmura, S.; Sunazuka, T.; Hirono, S. *Chem. Pharm. Bull.* **2012,** *60,* 169–171. doi:10.1248/cpb.60.169
23. Kataoka, Y.; Seto, Y.; Yamamoto, M.; Yamada, T.; Kuwata, S.; Watanabe, H. *Bull. Chem. Soc. Jpn.* **1976,** *49,* 1081–1084. doi:10.1246/bcsj.49.1081
24. Yamada, T.; Miyazawa, T.; Kuwata, S.; Watanabe, H. *Bull. Chem. Soc. Jpn.* **1977,** *50,* 1827–1830. doi:10.1246/bcsj.50.1827
25. Shimamura, H.; Gouda, H.; Nagai, K.; Hirose, T.; Ichioka, M.; Furuya, Y.; Kobayashi, Y.; Hirono, S.; Sunazuka, T.; Ōmura, S. *Angew. Chem., Int. Ed.* **2009,** *48,* 914–917. doi:10.1002/anie.200804138
26. Kobayashi, Y.; Ichioka, M.; Hirose, T.; Nagai, K.; Matsumoto, A.; Matsui, H.; Hanaki, H.; Masuma, R.; Takahashi, Y.; Ōmura, S.; Sunazuka, T. *Bioorg. Med. Chem. Lett.* **2010,** *20,* 6116–6120. doi:10.1016/j.bmcl.2010.08.037
27. Quirin, C.; Kazmaier, U. *Eur. J. Org. Chem.* **2009,** 371–377. doi:10.1002/ejoc.200800890
28. Ullrich, A.; Chai, Y.; Pistorius, D.; Elnakady, Y. A.; Herrmann, J. E.; Weissman, K. J.; Kazmaier, U.; Müller, R. *Angew. Chem.* **2009,** *121,* 4486–4489. doi:10.1002/ange.200900406
Angew. Chem., Int. Ed. **2009,** *48,* 4422–4425. doi:10.1002/anie.200900406
29. Ullrich, A.; Herrmann, J.; Müller, R.; Kazmaier, U. *Eur. J. Org. Chem.* **2009,** 6367–6378. doi:10.1002/ejoc.200900999
30. Gawas, D.; Kazmaier, U. *Org. Biomol. Chem.* **2010,** *8,* 457–462. doi:10.1039/b917589j
31. Burkhart, J. L.; Müller, R.; Kazmaier, U. *Eur. J. Org. Chem.* **2011,** 3050–3059. doi:10.1002/ejoc.201100155
32. Deska, J.; Hähn, S.; Kazmaier, U. *Org. Lett.* **2011,** *13,* 3210–3213. doi:10.1021/ol201120k
33. Hebach, C.; Kazmaier, U. *Chem. Commun.* **2003,** 596–597. doi:10.1039/b210952b
34. Kazmaier, U.; Hebach, C.; Watzke, A.; Maier, S.; Mues, H.; Huch, V. *Org. Biomol. Chem.* **2005,** *3,* 136–145. doi:10.1039/b411228h
35. Kazmaier, U.; Hebach, C. *Synlett* **2003,** 1591–1594. doi:10.1055/s-2003-40987
36. Pick, R.; Bauer, M.; Kazmaier, U.; Hebach, C. *Synlett* **2005,** 757–760. doi:10.1055/s-2005-863722
37. Kazmaier, U.; Ackermann, S. *Org. Biomol. Chem.* **2005,** *3,* 3184–3187. doi:10.1039/b507028g
38. Bauer, M.; Maurer, F.; Hoffmann, S. M.; Kazmaier, U. *Synlett* **2008,** 3203–3207. doi:10.1055/s-0028-1087366
39. Kazmaier, U.; Persch, A. *Org. Biomol. Chem.* **2010,** *8,* 5442–5447. doi:10.1039/c0ob00453g
40. Burkhart, J. L.; Kazmaier, U. *Synthesis* **2011,** 4033–4036. doi:10.1055/s-0031-1289594
41. Lehmann, J.; Linden, A.; Heimgartner, H. *Tetrahedron* **1998,** *54,* 8721–8736. doi:10.1016/S0040-4020(98)00506-7
42. Schmidt, U.; Lieberknecht, A.; Griesser, H.; Talbiersky, J. *J. Org. Chem.* **1982,** *47,* 3261–3264. doi:10.1021/jo00138a012
43. Micheel, F.; Flitsch, W. *Justus Liebigs Ann. Chem.* **1952,** *577,* 234–237. doi:10.1002/jlac.19525770306
44. Bredereck, H.; Gompper, R.; Seiz, H. *Chem. Ber.* **1957,** *90,* 1837–1843. doi:10.1002/cber.19570900922

License and Terms

Beilstein Journal of Organic Chemistry

Modulating the activity of short arginine-tryptophan containing antibacterial peptides with N-terminal metallocenoyl groups

H. Bauke Albada[1], Alina-Iulia Chiriac[2], Michaela Wenzel[3], Maya Penkova[1], Julia E. Bandow[3], Hans-Georg Sahl[2] and Nils Metzler-Nolte[*1]

Full Research Paper

Open Access

Address:
[1]Inorganic Chemistry I – Bioinorganic Chemistry, Faculty of Chemistry and Biochemistry, Ruhr University Bochum, Universitätsstraße 150, 44801 Bochum, Germany, [2]Institute for Medical Microbiology, Immunology, and Parasitology, Pharmaceutical Microbiology Section, University of Bonn, Meckenheimer Allee 168, 53115 Bonn, Germany and [3]Microbial Biology, Faculty of Biology and Biotechnology, Ruhr University Bochum, Universitätsstraße 150, 44801 Bochum, Germany

Email:
Nils Metzler-Nolte[*] - nils.metzler-nolte@rub.de.

* Corresponding author

Keywords:
antimicrobial peptides; arginine; medicinal organometallic chemistry; metallocenoyl; peptides; tryptophan

Beilstein J. Org. Chem. **2012,** *8,* 1753–1764.
doi:10.3762/bjoc.8.200

Received: 14 July 2012
Accepted: 06 September 2012
Published: 15 October 2012

This article is part of the Thematic Series "Antibiotic and cytotoxic peptides".

Guest Editor: N. Sewald

Abstract

A series of small synthetic arginine and tryptophan containing peptides was prepared and analyzed for their antibacterial activity. The effect of N-terminal substitution with metallocenoyl groups such as ferrocene (FcCO) and ruthenocene (RcCO) was investigated. Antibacterial activity in different media, growth inhibition, and killing kinetics of the most active peptides were determined. The toxicity of selected derivatives was determined against erythrocytes and three human cancer cell lines. It was shown that the replacement of an N-terminal arginine residue with a metallocenoyl moiety modulates the activity of WRWRW-peptides against Gram-positive and Gram-negative bacteria. MIC values of 2–6 μM for RcCO-W$(RW)_2$ and 1–11 μM for $(RW)_3$ were determined. Interestingly, W$(RW)_2$-peptides derivatized with ferrocene were significantly less active than those derivatized with ruthenocene which have similar structural but different electronic properties, suggesting a major influence of the latter. The high activities observed for the RcCO-W$(RW)_2$- and $(RW)_3$-peptides led to an investigation of the origin of activity of these peptides using several important activity-related parameters. Firstly, killing kinetics of the RcCO-W$(RW)_2$-peptide versus killing kinetics of the $(RW)_3$ derivative showed faster reduction of the colony forming units for the RcCO-W$(RW)_2$-peptide, although MIC values indicated higher activity for the $(RW)_3$-peptide. This was confirmed by growth inhibition studies. Secondly, hemolysis studies revealed that both peptides did not lead to significant destruction of erythrocytes, even up to 500 μg/mL for $(RW)_3$ and 250 μg/mL for RcCO-

W(RW)$_2$. In addition, toxicity against three human cancer cell lines (HepG2, HT29, MCF7) showed that the (RW)$_3$-peptide had an IC_{50} value of ~140 μM and the RcW(RW)$_2$ one of ~90 μM, indicating a potentially interesting therapeutic window. Both the killing kinetics and growth inhibition studies presented in this work point to a membrane-based mode of action for these two peptides, each having different kinetic parameters.

Introduction

New antibacterial agents need to be discovered since established antibiotics are increasingly losing ground against resistant bacteria and at the same time the pipeline that is supposed to produce new antibiotics is running dry [1]. For example, the number of methicillin-resistant *Staphylococcus aureus* (MRSA) infections in hospitals are still very high and new infectious agents like *Acinetobacter baumannii* are on the rise, both leading to increased numbers of mortality. In view of this, the discovery of host-defense and antimicrobial peptides with bacteria-specific membrane targeting modes of action (MOA) to which resistance cannot easily develop has led to high expectations in the treatment of bacterial infections [2-4]. Whereas host-defense peptides are found in many multicellular organisms as part of their innate immune system, the name "antimicrobial peptides" (abbreviated as AMPs) defines a larger group of peptides that also encompasses synthetic peptides, and peptidomimetics, for example. Among these, synthetic peptide-based antimicrobial agents are especially interesting because isolation and/or synthesis of traditional organic molecules is often time-consuming and costly [3,5]. In fact, already in World War II, peptides belonging to a certain group of antimicrobial peptides, i.e., the gramicidins, found application in the treatment of gunshot wounds [6]. Unfortunately, their general toxicity prevented widespread systemic administration in the clinic. However, during the past couple of decades a large number of peptides with very potent antimicrobial activity and lower general toxicity were discovered [7].

Inspired by these antimicrobial peptides, many synthetic derivatives of naturally occurring antimicrobial peptides have been studied [5]. In addition, chemical syntheses of a large number of peptides that do not have natural counterparts have furnished promising synthetic antimicrobial peptides (synAMPs) [8]. For example, peptide-dendrimers [9-13], lipidated short peptides [14], trivalent lipidated short peptides with antifungal activity [15], peptoids [16], peptides containing D-amino acids [17], and foldamers based on β-amino acid residues with antibacterial activity [18] have been described. Whereas nature has to stick to products compatible with biosynthetic pathways, the synthetic chemist is free to apply all available compounds and techniques, thereby introducing even the most exotic molecular entities. The most recent and exotic additions are conjugates of metallocenes with short synthetic antimicrobial peptides [19-22] and organometallic derivatives of platensimycin [23-28].

Among the synAMPs known to date, those based on arginine (Arg or R) and tryptophan (Trp or W) residues are amongst the smallest peptides that still possess significant antibacterial activity. For example, Strøm et al. [29] described short RW-based synAMPs with different N- and C-terminal substituents, which showed low micromolar antibacterial activity against various strains of Gram-positive bacteria and moderate activity against Gram-negative bacteria. Interestingly, head-to-tail cyclized RW-based synAMPs with clustered functionalities increased the activity against Gram-negative *Escherichia coli* much more than against Gram-positive *Bacillus subtilis* [30,31], and only slightly increased the hemolytic activity [32]. Moreover, the alkylation of tryptophan residues by *tert*-butyl groups resulted in increased activity and low hemolytic activity of the constructs [33]. Our group has previously shown that the covalent attachment of metal complexes to RW-based synAMPs yields more active derivatives with a changed activity profile for Gram-positive and Gram-negative bacteria. In this work, the attachment of the neutral ferrocenoyl group (ferrocene: dicyclopentadienyl iron, Cp_2Fe; ferrocenoyl: FcCO) was beneficial over the presence of the monocationic cobaltocenium (Cc^+CO) fragment [20].

To gain a better understanding of the origin of the activity of these RW-based synAMPs and of the effect exerted on it by a metallocene moiety, a set of peptides was synthesized and tested for antimicrobial activity. In this paper we add another metal to the spectrum of existing organometallic synAMPs and we provide a detailed assessment of the kinetic parameters of this peptide. Specifically, we describe the effect of the introduction of ruthenocenoyl (ruthenocene: dicyclopentadienyl ruthenium, Cp_2Ru; ruthenocenoyl: RcCO), an organometallic moiety that is almost isostructural to ferrocenoyl (FcCO) but has different electro- and physicochemical properties [34]. For example, the more extended d-orbitals of Rc form stronger hydrogen bonds with OH or NH groups than Fc [35]. The activities of the synAMPs (MIC values) were compared to those of GS($K_2\underline{Y}_2$) ($\underline{Y}$ = D-tyrosine), a gramicidin S analogue, and vancomycin, one of the last lines of defense against *Staphylococcus* infections. From the antibacterial activity screening, the two most active peptides were selected for further analysis, i.e., H-Arg-Trp-Arg-Trp-Arg-Trp-NH_2 (referred to as (RW)$_3$), and RcCO-Trp-Arg-Trp-Arg-Trp-NH_2 (referred to as RcCO-W(RW)$_2$). For these peptides, toxicity against three human

cancer cell lines was assessed, followed by determination of their killing kinetics and growth inhibition potential. Please note that underlined one-letter codes of the amino acid residues represent D-amino acids, not underlined one-letter codes of the residues are L-amino acids.

Results

Synthesis of the synAMPs

All peptides described in this study were prepared according to established or recently published procedures [36]. In short, Fmoc-protected amino acids were coupled in a solid-state synthesis scheme using HOBt, TBTU, and DiPEA under microwave irradiation. Using suitably protected amino acids, i.e., Fmoc-Arg(Pbf)-OH, Fmoc-Trp(Boc)-OH, and Fmoc-Lys(Boc)-OH, and polystyrene-based resin decorated with Fmoc-protected Rink linkers, a set of peptides were prepared (Table 1 and Figure 1). These peptides were obtained after acidic cleavage of the resin-bound protected precursors, purified by preparative HPLC, and the fractions containing the desired compound in high purity were lyophilized from the prep-HPLC buffers. All these peptides were obtained in high yields and close to 100% HPLC purity.

Table 1: Overview of the studied sequences and analysis thereof (retention times and *m*/*z* values). Underlined amino acids are D-enantiomers, not underlined residues are L-enantiomers; FcCO refers to ferrocenoyl and RcCO to ruthenocenoyl (Figure 1).

entry	sequence	t_R (min)	*m*/*z* found (calcd for $[M + H]^+$)
1	H-RWRWRW-NH_2	17.2	1044.25 (1044.58)
2	H-RWRWRW-NH_2	17.2	1044.27 (1044.58)
3	RcCO-WRWRW-NH_2	20.1	1146.27 (1146.44)
4	RcCO-WRWRW-NH_2	20.1	1146.11 (1146.44)
5	FcCO-WRWRW-NH_2	20.2	1100.36 (1100.47)
6	Ac-RWRWRW-NH_2	17.6	1086.45 (1086.59)
7	Ac-RWRWRW-NH_2	17.6	1086.37 (1086.59)
8	FcCO-RWRWRW-NH_2	19.0	1256.48 (1256.57)
9	FcCO-RWRWRW-NH_2	19.0	1256.46 (1256.59)
10	H-KWKWKW-NH_2	16.7	959.43 (959.55)
11	vancomycin[a]	11.7	1448.56 (1448.44)
12	GS(K_2Y_2)[b]	25.0	1201.46 (1201.73)

[a]Vancomycin was obtained from Sigma-Aldrich Fluka and purified by preparative HPLC using a C_{18}-reversered phase column; [b]GS(K_2Y_2) = cyclo([Pro-Val-Lys-Leu-D-Tyr]$_2$) was prepared according to [37].

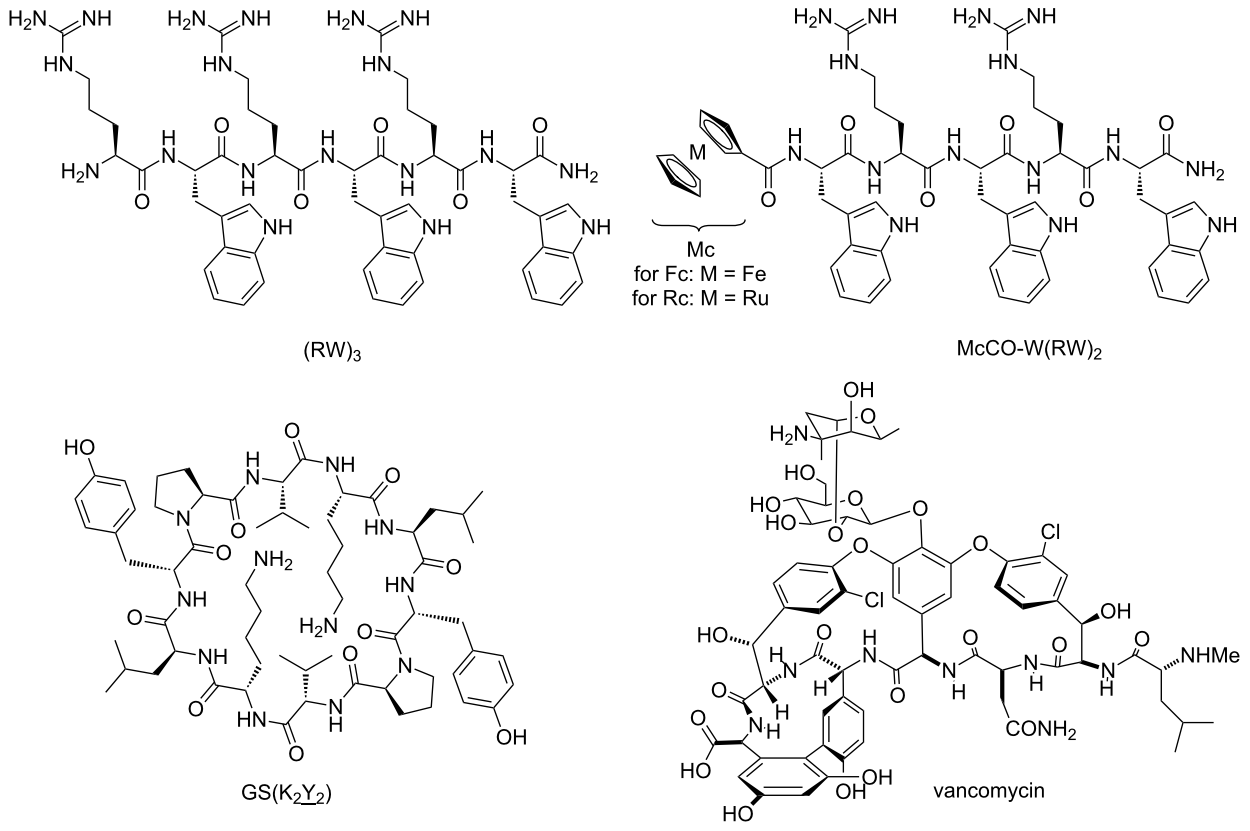

Figure 1: Structures of the most active peptides that have been used in this study. The top row shows two representative structures of the Arg-Trp based peptides (left) and their metallocene-derivatives (right); the lower row shows the structure of pore-forming gramicidin S derivative GS(K_2Y_2) (left) and lipid II-binding cell wall biosynthesis inhibitor vancomycin (right).

Biological activity

Minimum inhibitory concentration

The antibacterial activity of the peptides was first assessed by determining their minimum inhibitory concentration (MIC) value. This MIC value represents the lowest concentration of the antibacterial agent that is needed to hinder the growth of the bacteria [38]. For this, six standard bacterial strains – among them three Gram-negative and three Gram-positive pathogens – were incubated with increasing concentrations of the antibacterial peptide (Table 2). In order to put the activities of these RW-based synAMPs and their organometallic conjugates into perspective, two reference peptides were included, i.e., membrane-targeting gramicidin S derivative GS($K_2\underline{Y}_2$) and cell wall precursor lipid II-targeting vancomycin.

For the calculations of the MIC values in μM, molecular weights of the peptides together with one TFA-counterion for each basic amino acid residue were used. 'n.a.' means 'not active' (MIC > 100 μM), '–' indicates that these MIC values were not determined.

In general, the activity of these synAMPs against Gram-negative bacteria is lower than against Gram-positive pathogens. Even if differences can be seen in the Gram-negative values, none of the RW-peptides was very active. Unfortunately, none of the peptides showed significant activity against *Pseudomonas aeruginosa*, a prominent pathogen that causes infections in e.g., cystic fibrosis patients. However, activities of the synAMPs against Gram-positive bacteria are only slightly lower than those of gramicidin S derivative GS($K_2\underline{Y}_2$), a peptide that contains twice as many amino acids as RcCO-W$(RW)_2$. Interestingly, the replacement of the acetyl-group in Ac$(RW)_3$ with the ferrocenoyl moiety results in more active peptides, which is most likely due to the increased hydrophobicity of the FcCO-peptide (t_R 17.6 min (for Ac$(RW)_3$) vs 19.0 min (for FcCO-$(RW)_3$). Although hydrophobicity seems to be important for the activity of these synAMPs, it is not the dominant factor in the organometallic derivatives. For example, replacement of the ruthenium atom with iron, going from RcCO to FcCO, results in a 4-fold and 8-fold drop in activity against *B. subtilis* and *S. aureus* (MRSA), respectively, even though their hydrophobicity is very similar. Since Rc is slightly larger than Fc – i.e., metal–carbon bonds in the first are 221 ppm whereas those in the latter are 204 pm [39,40], a difference of about 0.17 Å – the difference in size of the two metallocene derivatives could contribute to the significant difference in activity. In addition, it has been described that ruthenocene is a stronger hydrogen bond acceptor than ferrocene [37], which originates from more extended d-orbitals of the Rc when compared to Fc [41].

The comparable activities of $(RW)_3$ and RcCO-W$(RW)_2$ are especially remarkable since the peptides have very different properties, i.e., the first peptide has four positive charges and three units of lipophilic bulk (t_R = 17.2 min) whereas the second peptide has only two positive charges and four units of lipophilic bulk (t_R = 20.1 min). Whereas it is known that tryptophan residues function as membrane anchors [42], details of the interaction between metallocene derivatives and bacterial membranes are far from being understood. Importantly, the activity of these peptides was comparable in two different media, namely the bacterial Mueller–Hinton (MH) and in the

Table 2: Minimum inhibitory concentrations (μM) in the cell culture medium of the synAMPs described in this study (according to CSLI guidelines). Peptides have C-terminal carboxamides and are not derivatized on the N-terminus except where noted, i.e., with acetyl (Ac), FcCO or RcCO. Values in brackets are determined in Mueller–Hinton (MH) medium. More details on the bacterial strains can be found in the experimental section.

synAMP	Gram-negative			Gram-positive		
	E. coli	*A. baumannii*	*P. aeruginosa*	*B. subtilis*	*S. aureus*	*S. aureus* (MRSA)
$(RW)_3$	21	21	n.a.	1.3	11 (11)	5.3 (11)
$(\underline{RW})_3$	21	21	n.a.	1.3	5.3	5.3
$(KW)_3$	n.a.	n.a.	n.a.	11–5.7	n.a.	n.a.
Ac$(RW)_3$	45	–	–	45	–	–
Ac$(\underline{RW})_3$	90	–	–	90	–	–
FcCO-$(RW)_3$	20	–	–	20	–	–
FcCO-$(\underline{RW})_3$	20	–	–	5	–	–
RcCO-W$(RW)_2$	47	23–12	n.a.	2.9	5.8 (5.8)	5.8 (5.8)
RcCO-$\underline{W}(\underline{RW})_2$	23	23–11	93	1.5	2.9	1.5
FcCO-W$(RW)_2$	>96	–	>96	12	–	48
vancomycin	76–38	38	n.a.	0.3	0.3	0.6
GS($K_2\underline{Y}_2$)	22–11	2.8–1.4	n.a.	1.4	1.4	2.8

richer cell culture medium. Interestingly, replacement of the arginine residues with lysine residues resulted in an almost completely inactive $(KW)_3$ peptide [43]. Although the center of the positive charge in both residues is found at five atoms from the backbone, the different structures of the functional groups and the hydrophobicity of the side chain seem to cause a significant difference in activity [44,45].

From the initial screening, four peptides were selected for further biological characterization. In view of the mentioned differences in structure, including the addition of a novel metal core in one of them, but rather similar activity the $(RW)_3$ and RcCO-$W(RW)_2$ peptides were chosen. Since both L- and D-amino acid versions of the $(RW)_3$ and RcCO-$W(RW)_2$ peptides are comparable in activity and represent the most promising synAMPs (Table 2), we next determined the MIC values of these four peptides against other Gram-positive bacteria in order to expand the panel of test strains (Table 3).

As can be inferred from this table, the L- and D-amino acid versions of these two synAMPs show comparable activity although small differences can be observed. For example, RcCO-$W(RW)_2$ is almost twice as active against *S. aureus* (SG511) as the D-amino acid isomer RcCO-$\underline{W}(\underline{RW})_2$, a difference that can be seen as a tendency against all but one of the bacterial strains. Since the biological world is chiral, it is not surprising to see some small differences between both chiral forms of the synAMPs. Similar differences in the interaction with chiral molecules and biological membranes have been described before [46-48], although only in a few examples and not without exceptions [49]. An opposite trend is seen for the $(RW)_3$-peptides, where the D-peptides show higher MIC values than the L-peptides. These values could have been corroborated, however, by preferential proteolytic degradation of the N-terminally unprotected $(RW)_3$-peptides [50].

In order to obtain more information on the antibacterial properties of these four peptides, we performed killing kinetics and growth inhibition studies. Finally, we assessed the selectivity of the RcCO-$W(RW)_2$ and $(RW)_3$ peptides towards bacteria by determining their activity against human red blood cells and several human cancer cell lines.

Killing kinetics

Killing kinetics experiments show the rate at which bacteria are killed over time and indicate whether an antibacterial agent has a bacteriostatic or bactericidal activity. The killing kinetics of the L-amino acid containing $(RW)_3$- and RcCO-$W(RW)_2$-peptides were determined against *S. aureus* and *B. megaterium* (Figure 2).

For this, peptides were added in various concentrations to bacterial cultures at the optical densities of 0.1 at OD_{600}. Aliquots of the mixture were taken at given time points, plated in duplicate on MH agar and incubated at 37 °C. Then, the number of colony forming units (CFU) was counted (see Experimental section for details).

The addition of the $(RW)_3$ peptide to the bacterial culture resulted in a strong inhibition and in an immediate reduction of CFUs by a factor of 10^3 after 1 min, for both *S. aureus* and *B. megaterium*. Similarly, treatment with RcCO-$W(RW)_2$ also decreased the number of CFUs and has shown increased potency since only one dose at the MIC value was needed to decrease the CFUs by 2–3 log units, whereas 5 × MIC of $(RW)_3$ was required for a similar drop of CFUs. The immediate drop in CFUs highlights the bactericidal nature of these synAMPs and typically occurs with membrane acting compounds [51,52].

Growth inhibition

Whereas the killing kinetics studies determine the number of viable cells as a function of time and thereby classify a compound as bacteriostatic or bactericidal, monitoring the optical density of a treated culture may give hints as to the lytic activity of a compound.

In this work, the growth inhibition of *Bacillus megaterium* was determined under the influence of the same four peptides used

Table 3: Detailed assessment of the MIC values (in μg/mL) of both L- and D-versions of the $(RW)_3$ and RcCO-$W(RW)_2$ synAMPs against several Gram-positive bacterial strains. More details on the bacterial strains can be found in the experimental section.

strain	$(RW)_3$	$(\underline{RW})_3$	RcCO-$W(RW)_2$	RcCO-$\underline{W}(\underline{RW})_2$
S. aureus (133)	2.1 ± 0.7	2.1 ± 0.7	3.3 ± 1.4	6.7 ± 2.9
S. simulans (22)	5.0 ± 0.0	3.3 ± 1.4	5.0 ± 0.0	6.7 ± 2.9
S. aureus (SG511)	6.7 ± 2.9	4.2 ± 1.4	4.2 ± 1.4	8.3 ± 2.9
B. subtilis	3.5 ± 1.8	3.8 ± 1.8	3.8 ± 1.8	3.8 ± 1.8
B. megaterium	0.8 ± 0.7	0.5 ± 0.2	1.9 ± 0.9	2.5 ± 0.0
M. luteus	0.6 ± 0.0	0.6 ± 0.0	0.9 ± 0.4	1.9 ± 0.9

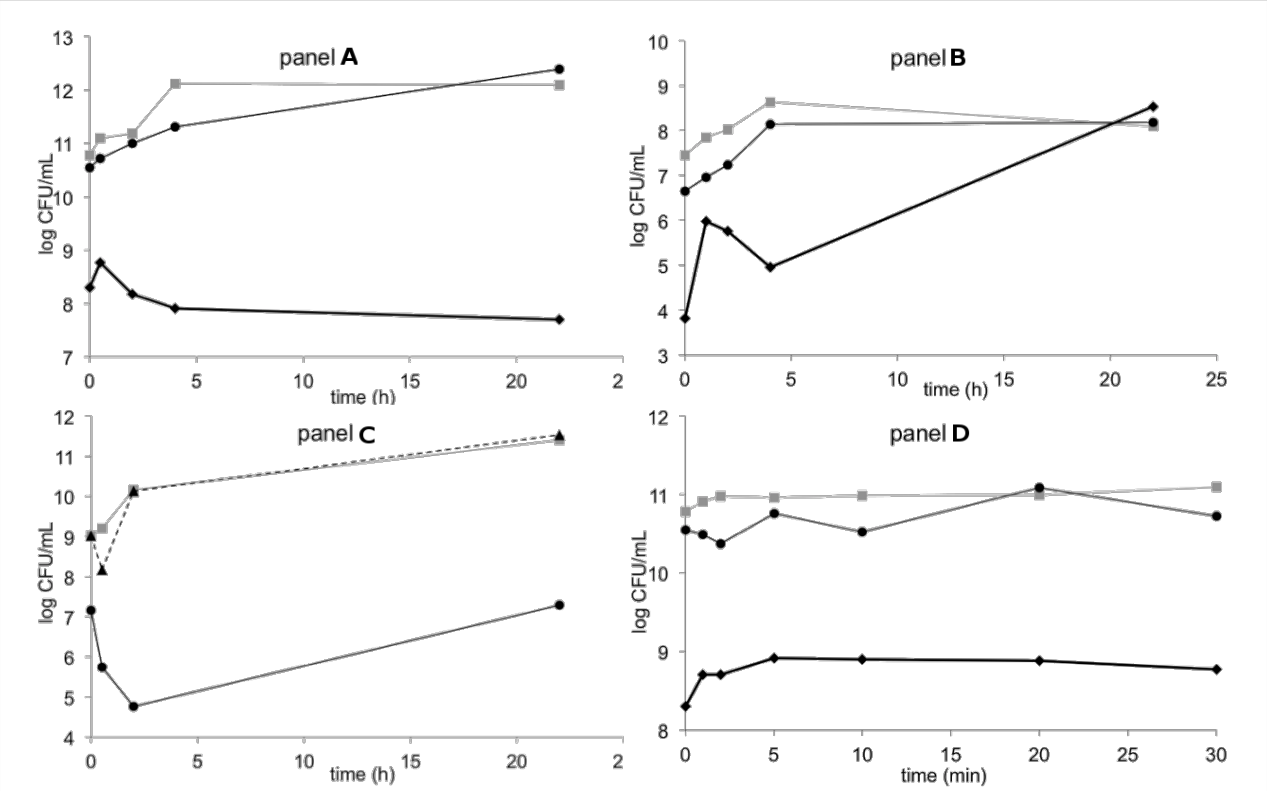

Figure 2: Bactericidal activity of $(RW)_3$ against *S. aureus* 133 (panel **A** and **D**) or *B. megaterium* (panel **B**) and of RcCO-W$(RW)_2$ (panel **C**) against *S. aureus* 133. Panel **D** shows the experiment on *S. aureus* 133 (as in panel **A**) using short-term intervals for sample collection (note that the time-scale is given in minutes). The first points in each graph are obtained after 1 min. Concentrations are denoted by: grey squares (for the control), black triangles with dotted line (only in panel **C**, 0.5 × MIC: 1.0 μg/mL for RcCO-W$(RW)_2$), black circles with narrow line (1 × MIC: 0.8 μg/mL for $(RW)_3$ and 1.9 μg/mL for RcCO-W$(RW)_2$), black diamonds with thick line (5 × MIC: 4 μg/mL for $(RW)_3$, only in panels **A**, **B**, and **D**).

in the killing kinetics studies described earlier (Figure 3). To determine this, *B. megaterium* was grown in half Mueller–Hinton (MH) medium and stressed with peptides $(RW)_3$ or RcCO-W$(RW)_2$ in their exponential growth phase. Three concentrations were used: 2 × MIC, 4 × MIC and 8 × MIC. As a positive control the potent naturally occurring pore-forming lantibiotic nisin was included.

At twice the MIC value, both of the D-amino acid containing derivatives are slightly inferior for inhibiting growth than the L-amino acid variants and the RcCO-W$(RW)_2$-peptides are more active than the $(RW)_3$-peptides (Figure 3). This is in line with our earlier observation, i.e., that the interaction of the bacterial target and D-peptides is slightly less favorable than that with L-peptides. Interestingly, the growth inhibition is more efficient with the RcCO-W$(RW)_2$ peptides than with the $(RW)_3$ peptides (Figure 3, panel **A**), although the cells treated with the RcCO-W$(RW)_2$ peptide recover faster than those treated with the $(RW)_3$ peptide. This is also reflected in the similar MIC values observed. It appears that the RcCO-W$(RW)_2$ peptides are faster acting than the $(RW)_3$ peptides but may produce cellular stress that can be better overcome by survivors in the course of an MIC determination experiment (which takes about 18 h). This difference in growth inhibition between the metalated and non-metalated peptide is even more pronounced at four times the MIC value. At this concentration it seems that the Rc-derivatized synAMPs are much more active than the non-derivatized counterparts (Figure 3, panel **B**). Moreover, at this concentration the RcCO-W$(RW)_2$-peptides display the same inhibition potency as nisin whereas the $(RW)_3$ peptides are much less active. At eight times the MIC value the bacterial growth inhibition was accompanied by cell lysis. For all compounds, the effect was equally strong so that a clear distinction could not be observed anymore and all the peptides exhibited the same effect on bacterial growth as nisin (Figure 3, panels **C** and **D**). These findings are in agreement with the killing kinetics in that RcCO-W$(RW)_2$ is faster in killing than $(RW)_3$.

Hemolytic activity against human red blood cells

After this, we assessed the hemolytic properties of these four most active peptides (Table 4). Although an HC_{50} value was reported for $(RW)_3$ [53], neither the D-amino acid peptide nor the organometallic derivatized peptides were studied with respect to their hemolytic capacity. Therefore, all peptides were

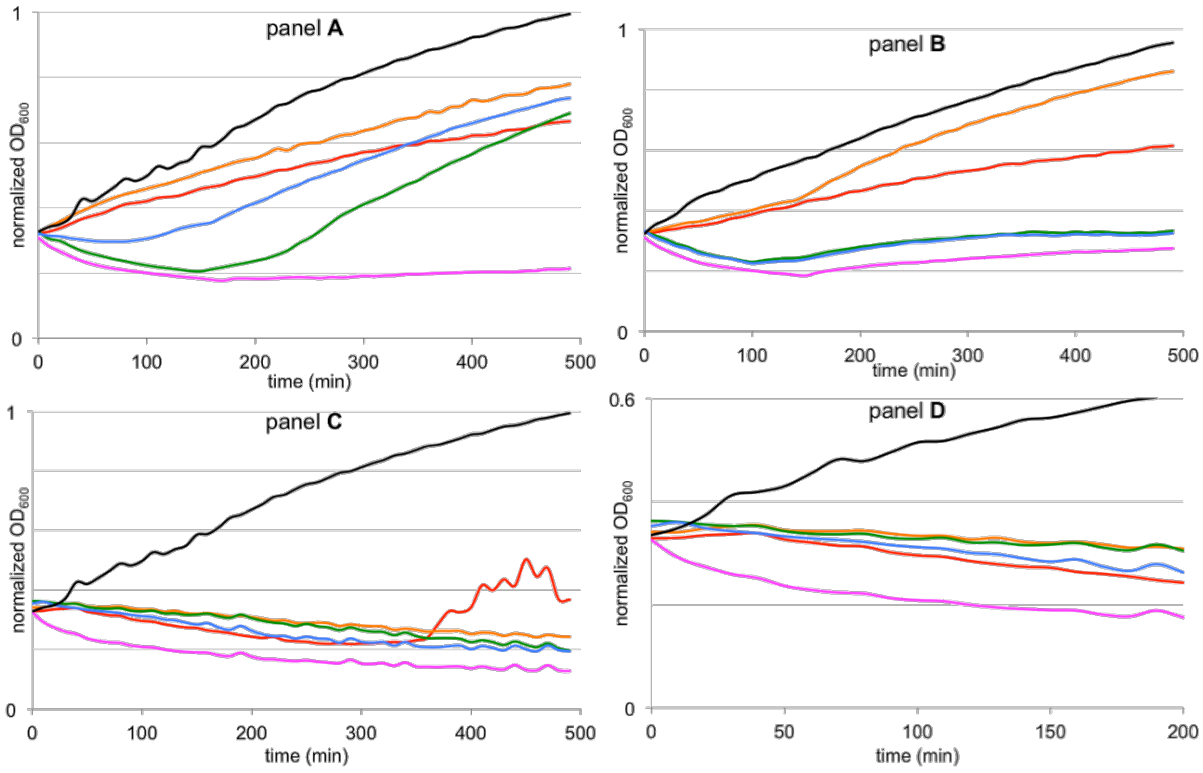

Figure 3: Growth kinetics of *B. megaterium* under the influence of different amounts of synAMP (red: $(RW)_3$; orange: $(\underline{RW})_3$; green: RcCO-W$(RW)_2$; blue: RcCO-$\underline{W}(\underline{RW})_2$), nisin (magenta), and a control (black). With 2 × MIC (1.6 µg/mL for $(RW)_3$ and 3.8 µg/mL for RcCO-W$(RW)_2$ panel **A**), 4 × MIC (3.2 µg/mL for $(RW)_3$ and 7.6 µg/mL for RcCO-W$(RW)_2$; panel **B**, note: The green line for RcCO-W$(RW)_2$ is under the blue line for RcCO-$\underline{W}(\underline{RW})_2$), and 8 × MIC (6.4 µg/mL for $(RW)_3$ and 15.2 µg/mL for RcCO-W$(RW)_2$; panel **C** and **D**). Gridlines at 0.2, 0.4, 0.6, and 0.8 normalized OD_{600} are shown.

tested in parallel to obtain HC_{50} values under identical conditions.

As can be seen from these results, none of these peptides is strongly hemolytic. For example, each of the two $(RW)_3$ compounds showed less than 50% hemolysis up to 500 µg/mL (333 µM). This value is higher from what has been reported before by Liu et al. (who reported 50% hemolysis at ~250 µM [53]). In fact, only the L-amino acid peptide $(RW)_3$ showed weak hemolysis at 333 µM with 17% of the hRBCs being destroyed as compared to Triton X-100. These low hemolytic properties for both $(RW)_3$-peptides, even up to 500 µg/mL, did not allow us to calculate their HC_{50}-values.

Table 4: Hemolytic activity of both L- and D-peptides of the $(RW)_3$ and RcCO-W$(RW)_2$ synAMPs against human red blood cells (hRBCs).

synAMP	hemolytic activity
$(RW)_3$	17% hemolysis at 500 µg/mL (333 µM)
$(\underline{RW})_3$	0% hemolysis up to 500 µg/mL (333 µM)
RcCO-W$(RW)_2$	64% hemolysis at 263 µg/mL (192 µM)
RcCO-$\underline{W}(\underline{RW})_2$	68% hemolysis at 263 µg/mL (192 µM)

The high concentrations of the ruthenocene derivatives required 50% DMSO/PBS-buffer mixtures for solubility. Using the appropriate blanks we found that >60% of the hRBCs were lysed using 195 µM of the peptide, with RcCO-$\underline{W}(\underline{RW})_2$ being more active than its L-amino acid counterpart. Using these directly observed values, approximate HC_{50} values of 153 µM (or 210 µg/mL) and 143 µM (or 196 µg/mL) were calculated for RcCO-W$(RW)_2$ and RcCO-$\underline{W}(\underline{RW})_2$, respectively.

Thus, the organometallic ruthenocenoyl-conjugated synAMPs are more hemolytic than the parent $(RW)_3$-peptides. Moreover, whereas the L-amino acid version of $(RW)_3$ was more active that the peptide containing only D-amino acids, the opposite was observed for the two RcCO-W$(RW)_2$ peptides. Nevertheless, none of the obtained values showed strong hemolytic activity of either of these peptides. This encouraged us to go ahead and test the activity of these peptides against several human cancer cell lines in order to assess in vitro cell-toxicity.

Toxicity against human cancer cell lines

Finally, to determine whether the peptides are selective for bacterial cells, we tested the toxicity against mammalian cells using three malignant cell lines: human liver carcinoma (HepG2), human colon adenocarcinoma grade II (HT29) and human breast adenocarcinoma (MCF7) cell lines (Table 5).

Table 5: IC_{50} values (in μM) of both $(RW)_3$ and RcCO-W$(RW)_2$ against human liver carcinoma (HepG2), human colon cancer (HT29) and human breast cancer (MCF7) cell lines.

synAMP	HepG2	HT29	MCF7
$(RW)_3$	143 ± 21	132 ± 12	159 ± 7
RcCO-W$(RW)_2$	92 ± 5	94 ± 6	90 ± 1

In general, we consider a peptide with an IC_{50} value higher than 100 μM to be inactive. As can be seen from Table 5, the peptides with the highest activity against Gram-positive bacteria are not toxic against the three selected human cancer cell lines. Based on average values from these cell lines, i.e., 142 μM for $(RW)_3$ and 92 μM for RcCO-W$(RW)_2$, a potential therapeutic window of about 7 and 4 can be calculated for Gram-negative pathogens using $(RW)_3$ and RcCO-W$(RW)_2$, respectively. Concerning the threatening Gram-positive *S. aureus* strains an even better window of >13 is calculated for $(RW)_3$ and RcCO-W$(RW)_2$. Interestingly, again the ruthenocenoyl-derivatized synAMP is more active than the $(RW)_3$ model peptide, as was seen in both the antibacterial and hemolysis studies.

Discussion

Ruthenium is one of the most promising metals in anticancer drug candidates [54-57], with two Ru-compounds even in clinical trials [58-62]. Surprisingly however, its potential in antibacterial research has not been explored so far. In this paper, we present the effects of the attachment of the organometallic ruthenocene (Rc) moiety to RW-based synthetic antimicrobial peptides (synAMPs). A comparison of the MIC values from a first screening of peptides that were N-terminally derivatized with a ruthenocenoyl (RcCO) group with that of the ferrocenoyl (FcCO)-derivatized peptides showed superior properties of the Rc-conjugated synAMPs (Table 2). Although both metallocenes have very similar hydrophobic properties, as confirmed herein again by their almost identical retention times on a C_{18}-column during HPLC-analysis, they have slightly different dimensions and very different physicochemical and electrochemical properties. Firstly, ferrocene derivatives have redox potentials that are within the realm of biological systems, but ruthenocene derivatives do not [41]. Secondly, while most ferrocene derivatives exhibit a reversible one-electron oxidation, ruthenocene and its derivatives typically undergo irreversible two-electron redox chemistry. Whether this difference in redox chemistry of the two metallocenes could interplay with the piezoelectric properties of phospholipid membranes [63] remains to be determined.

Ruthenocene is known to have more extended d-orbitals and is a stronger hydrogen-bond acceptor than ferrocene. In addition, ruthenocene is slightly larger than ferrocene, which might result in a possibly more disruptive interaction with bacterial membranes.

Small differences between the L- and D-amino acid versions of the peptides could be observed in their MIC values (Table 3) and within growth inhibition studies (Figure 3). Examples for this difference were found in other systems (see above) and points to a delicate contribution of the chirality of the peptides used. This effect was not observed in the first MIC values determined (Table 2), which indicates that this is a very subtle factor. Indeed, the quantification requires a more sophisticated analysis. This can be done using sensitive biophysical model systems like those used in quartz crystal microbalance (QCM) studies. This information can then be used to further optimize an active synAMP.

Fortunately, while retaining antibacterial activity in cell culture medium, the cellular toxicity of both the $(RW)_3$ and the RcCO-W$(RW)_2$ peptides is low, and only high peptide concentrations cause significant hemolysis. Apparently, these peptides have a strong preference for prokaryotic membranes over eukaryotic membranes, e.g., erythrocytes (Table 4 and Table 5). Nevertheless, it remains to be seen to what extent these short synAMPs can be used in vivo.

Concerning the antibacterial effect of these peptides, the killing kinetics showed rapid bactericidal properties of both the $(RW)_3$ and RcCO-W$(RW)_2$ peptides, and the growth kinetics showed growth arrest and also indicated bacteriolytic properties. Naturally occurring AMPs such as nisin and magainin typically have >20 amino acids and often have a specific target, like nisin, or are long enough to penetrate the membrane, like magainin. For these long peptides descriptions of their action mode with the “carpet-model”, the “toroidal pore model” or the “barrel stave model” [64] are quite suitable. Considering the rapid upon-contact killing and bacteriolytic properties, it appears that the small synAMPs studied herein interact with the bacterial membrane as well. The monomers of these peptides are, however, too short to penetrate a bacterial membrane in order to form pores, and therefore, probably act slightly different from the more or less well-established mechanisms for longer AMPs. We are currently undertaking efforts to uncover more details on the mode of action. Specifically, proteomic

analysis of the changes in the bacterial proteome as result of exposure to these synAMPs, and prokaryotic and eukaryotic membrane model systems will be used to precisely determine if it is simply a membrane-based mechanism or if there are more factors. While we attempt to elucidate the mode of action of these synAMPs, we are also interested in a detailed understanding of the effects of the organometallic fragment on the activity – for example by determining the contributions of hydrogen-bond forming processes in membrane environments – and the effect of the redox potential on the activity. We assume that the application of model systems will help us to determine the extent in which differences in chirality of the amino acids used to construct the peptides result in more or less favorable interactions.

Conclusion

We have shown that the replacement of the N-terminal arginine residue in non-toxic and non-hemolytic $(RW)_3$ peptides can modulate the kinetics of the peptide's antibacterial activity. Acetylation completely suppresses this activity. In comparison, replacement of the N-terminal arginine residue with the organometallic ferrocenoyl moiety reduces the activity only 5- to 10-fold, whereas the replacement with ruthenocene completely restores the level of activity. In summary, the data supports a metal-specific activity-enhancing effect of the added organometallic moiety. This effect is most likely due to the added lipophilic bulk together with intricate contributions from the electro- and physicochemical properties of the organometallic fragment. None of these peptides is hemolytic and both are hardly toxic against human cancer cell lines. Thereby, they represent an interesting group of synthetic antimicrobial peptides to be used in a therapeutic setting. Analysis of the antibacterial properties of these peptides showed that they are rapidly bactericidal and also bacteriolytic. Even though both peptides have similar MIC values, RcCO-W$(RW)_2$ is acting faster than $(RW)_3$, but is losing activity after 100–200 min, which is significantly faster compared to $(RW)_3$. Future studies on these peptides are directed towards a better understanding of their mode of action and attempts are being made for the improvement of their activity to increase the therapeutic window of these compounds.

Experimental

Minimal inhibitory concentration (results are shown in Table 2)

The minimal inhibitory concentrations (MIC) were tested against *Escherichia coli* DSM 30083, *Acinetobacter baumannii* DSM 30007, *Pseudomonas aeruginosa* DSM 50071, *Bacillus subtilis* DSM 402, *Staphylococcus aureus* DSM 20231 (type strain), and *Staphylococcus aureus* ATCC 43300 (MRSA) in a microtiter plate assay according to CLSI guidelines [65]. *E. coli*, *A. baumannii*, *S. aureus*, and *B. subtilis* were grown in Mueller–Hinton (MH) broth, *P. aeruginosa* in cation adjusted Mueller–Hinton II. Peptides were dissolved in DMSO to give 10 mg/mL stock solutions. Serial dilution in culture media was carried out automatically with the Tecan Freedom Evo 75 liquid handling workstation (Tecan, Männedorf, Switzerland) from 512 to 0.5 µg/mL. Peptide dilutions were inoculated with 10^5 bacteria/mL taken from late exponential cultures grown in the same media in a total volume of 200 µL per well. Cells were incubated for 16 h at 37 °C. The lowest peptide concentration inhibiting visible bacterial growth was taken as MIC.

For MIC determination in cell culture broth, the peptides were diluted manually in DMEM high glucose (with 4.5 g/L glucose, no penicillin). Only *S. aureus* DSM 20231 and ATCC 43300 were capable of growing in cell culture broth and were used for MIC determination. Cells were grown in DMEM until late exponential phase before using them for inoculation. Peptide concentrations, inoculation and incubation were performed as described above.

Minimum inhibitory concentration (results are shown in Table 3)

Determination of MIC values was performed in 96-well polypropylene microtiter plates (Life Technologies) in order to reduce the AMP binding [66]. A series of 2-fold dilutions of the peptides was prepared directly in the plate in half-concentrated MH broth. The tested strains were grown to an optical density (600 nm) of 0.5 in half-concentrated MH broth and diluted $1{:}10^5$ using the same medium. Then, 100 µL of this suspension was mixed with 100 µL of the peptide solution already prepared in the wells of the microtiter plate as mentioned earlier. After incubation for 18 h at 37 °C, the MIC value was read as the lowest concentration of antimicrobial agent that resulted in complete inhibition of visible growth. The results given are mean values of three or more independent determinations.

Killing kinetics

The cells were grown in half-concentrated MH broth up to an optical density of 0.5 and diluted in fresh medium to an optical density of 0.1. Peptides were added in concentrations corresponding to 0.5 to 5 × MIC. The viable count was monitored up to 18 h. Aliquots were taken at defined time intervals, diluted in 10 mM potassium phosphate buffer, and 100 µL of several decimal dilutions were plated in duplicate on MH agar. The plates were incubated at 37 °C and the plates containing 30–300 colony forming units (CFU) were counted after 24 h.

Kinetic growth inhibition

Growth kinetic experiments were performed in microtiter plates using 200 µL half concentrated MH broth. The cells were

grown to an optical density of up to 0.5 and diluted in fresh medium to an optical density of 0.25. After this, peptides were added in concentrations corresponding to 2 × MIC, 4 × MIC, and 8 × MIC and the optical density was registered for 8 h using a multichannel absorbance plate reader (SunriseTM, Tecan).

Hemolysis and in vitro cell toxicity studies

After drawing whole blood into anticoagulant containing tubes (BD Vacutainer®, K2 EDTA 3.6 mg, Ref 368841, Lot 1248213), its fractionation was executed with one volume whole blood added to nine volumes sterile 0.9% NaCl and centrifugation (800*g*, 10 min, 4 °C). Subsequently, the lowest fraction containing all hRBCs was washed twice with nine volumes 1 × PBS (PAA), triturating carefully. The concentrated hRBCs were re-suspended with 1 × PBS to an erythrocyte concentration of 5% (v/v). Wells of a 96-well plate were filled with 100 µL of the appropriate peptide solutions: The peptides were dissolved in 1 × PBS and DMSO (5% for $(RW)_3$ and 50% for RcCO-$W(RW)_2$). These were mixed with 100 µL of the 5% hRBCs solution and incubated under agitation on a flat shaker (170 rpm, 30 min, 37 °C). After sedimenting all probes under centrifugation (800*g*, 10 min, 4 °C), all supernatants were transferred into a clean 96-well plate. The release of hemoglobin was monitored by measuring the absorbance of the supernatant at 550 nm using an automated 96-well plate reader. Controls for 0 and 100% hemolysis consisted of hRBC 5% (v/v) suspended in PBS containing DMSO in appropriate concentrations and 1% Triton X-100, respectively. Toxicity on human cancer cell lines was determined according to previously described procedures [67,68].

Acknowledgements

We thank Annegret Knüfer for determining the IC_{50} values of the $RcW(RW)_2$ and $(RW)_3$ peptides. We also thank Vera Eßmann for preparing GS10($\underline{K_2Y_2}$), and Hung Bahn and Damla Yaprak for determining the MIC values of $Ac(RW)_3$ and $Fc(RW)_3$.

References

1. Wenzel, M.; Bandow, J. E. *Proteomics* **2011,** *11,* 3256–3268. doi:10.1002/pmic.201100046
2. Hancock, R. E. W.; Lehrer, R. *Trends Biotechnol.* **1998,** *16,* 82–88. doi:10.1016/S0167-7799(97)01156-6
3. Hancock, R. E. W.; Chapple, D. S. *Antimicrob. Agents Chemother.* **1999,** *43,* 1317–1323.
4. Hancock, R. E. W.; Sahl, H.-G. *Nat. Biotechnol.* **2006,** *24,* 1551–1557. doi:10.1038/nbt1267
5. Findlay, B.; Zhanel, G. G.; Schweizer, F. *Antimicrob. Agents Chemother.* **2010,** *54,* 4049–4058. doi:10.1128/AAC.00530-10
6. Gause, G. F.; Brazhnikova, M. G. *Nature* **1944,** *154,* 703. doi:10.1038/154703a0
7. Zasloff, M. *Nature* **2002,** *415,* 389–395. doi:10.1038/415389a
8. Fjell, C. D.; Hiss, J. A.; Hancock, R. E. W.; Schneider, G. *Nat. Rev. Drug Discovery* **2012,** *11,* 37–51. doi:10.1038/nrd3591
9. Kadam, R. U.; Bergmann, M.; Hurley, M.; Garg, D.; Cacciarini, M.; Swiderska, M. A.; Natici, C.; Sattler, M.; Smyth, A. R.; Williams, P.; Cámara, M.; Stocker, A.; Darbre, T.; Reymond, J.-L. *Angew. Chem., Int. Ed.* **2011,** *50,* 10631–10635. doi:10.1002/anie.201104342
10. Appelt, C.; Schrey, A. K.; Söderhäll, J. A.; Schmieder, P. *Bioorg. Med. Chem. Lett.* **2007,** *17,* 2334–2337. doi:10.1016/j.bmcl.2007.01.075
11. Young, A. W.; Liu, Z.; Zhou, C.; Totsingan, F.; Jiwrajka, N.; Shi, Z.; Kallenbach, N. R. *Med. Chem. Commun.* **2011,** *2,* 308–314. doi:10.1039/c0md00247j
12. Johansson, E. M. V.; Kadam, R. U.; Rispoli, G.; Crusz, S. A.; Bartels, K.-M.; Diggle, S. P.; Cámara, M.; Williams, P.; Jaeger, K.-E.; Darbre, T.; Reymond, J.-L. *Med. Chem. Commun.* **2011,** *2,* 418–420. doi:10.1039/c0md00270d
13. Stach, M.; Maillard, N.; Kadam, R. U.; Kalbermatter, D.; Meury, M.; Page, M. G. P.; Fotiadis, D.; Darbre, T.; Reymond, J.-L. *Med. Chem. Commun.* **2012,** *3,* 86–89. doi:10.1039/c1md00272d
14. Makovitzki, A.; Avrahami, D.; Shai, Y. *Proc. Natl. Acad. Sci. U. S. A.* **2006,** *103,* 15997–16002. doi:10.1073/pnas.0606129103
15. Arnusch, C. J.; Albada, H. B.; van Vaardegem, M.; Liskamp, R. M. J.; Sahl, H.-G.; Shadkchan, Y.; Osherov, N.; Shai, Y. *J. Med. Chem.* **2012,** *55,* 1296–1302. doi:10.1021/jm2014474
16. Chongsiriwatana, N. P.; Patch, J. A.; Czyzewski, A. M.; Dohm, M. T.; Ivankin, A.; Gidalevitz, D.; Zuckermann, R. N.; Barron, A. E. *Proc. Natl. Acad. Sci. U. S. A.* **2008,** *105,* 2794–2799. doi:10.1073/pnas.0708254105
17. Oren, Z.; Shai, Y. *Biochemistry* **1997,** *36,* 1826–1835. doi:10.1021/bi962507l
18. Tew, G. N.; Scott, R. W.; Klein, M. L.; DeGrado, W. F. *Acc. Chem. Res.* **2010,** *43,* 30–39. doi:10.1021/ar900036b
19. Chantson, J. T.; Verga Falzacappa, M. V.; Crovella, S.; Metzler-Nolte, N. *J. Organomet. Chem.* **2005,** *690,* 4564–4572. doi:10.1016/j.jorganchem.2005.07.007
20. Chantson, J. T.; Verga Falzacappa, M. V.; Crovella, S.; Metzler-Nolte, N. *ChemMedChem* **2006,** *1,* 1268–1274. doi:10.1002/cmdc.200600117
21. Fränzel, B.; Frese, C.; Penkova, M.; Metzler-Nolte, N.; Bandow, J. E.; Wolters, D. A. *J. Biol. Inorg. Chem.* **2010,** *15,* 1293–1303. doi:10.1007/s00775-010-0689-z
22. Patra, M.; Gasser, G.; Metzler-Nolte, N. *Dalton Trans.* **2012,** *41,* 6350–6358. doi:10.1039/c2dt12460b
23. Patra, M.; Gasser, G.; Pinto, A.; Merz, K.; Ott, I.; Bandow, J. E.; Metzler-Nolte, N. *ChemMedChem* **2009,** *4,* 1930–1938. doi:10.1002/cmdc.200900347
24. Patra, M.; Gasser, G.; Wenzel, M.; Merz, K.; Bandow, J. E.; Metzler-Nolte, N. *Eur. J. Inorg. Chem.* **2011,** 3295–3302. doi:10.1002/ejic.201100497
25. Patra, M.; Gasser, G.; Wenzel, M.; Merz, K.; Bandow, J. E.; Metzler-Nolte, N. *Organometallics* **2010,** *29,* 4312–4319. doi:10.1021/om100614c
26. Wenzel, M.; Patra, M.; Albrecht, D.; Chen, D. Y.-K.; Nicolau, K. C.; Metzler-Nolte, N.; Bandow, J. E. *Antimicrob. Agents Chemother.* **2011,** *55,* 2590–2596. doi:10.1128/AAC.00078-11
27. Patra, M.; Gasser, G.; Wenzel, M.; Merz, K.; Bandow, J. E.; Metzler-Nolte, N. *Organometallics* **2012,** *31,* 5760–5771. doi:10.1021/om201146c

28. Patra, M.; Merz, K.; Metzler-Nolte, N. *Dalton Trans.* **2012,** *41,* 112–117. doi:10.1039/c1dt10918a
29. Strøm, M. B.; Haug, B. E.; Skar, M. L.; Stensen, W.; Stiberg, T.; Svendsen, J. S. *J. Med. Chem.* **2003,** *46,* 1567–1570. doi:10.1021/jm0340039
30. Junkes, C.; Wessolowski, A.; Farnaud, S.; Evans, R. W.; Good, L.; Bienert, M.; Dathe, M. *J. Pept. Sci.* **2008,** *14,* 535–543. doi:10.1002/psc.940
31. Wessolowski, A.; Bienert, M.; Dante, M. *J. Pept. Res.* **2004,** *64,* 159–169. doi:10.1111/j.1399-3011.2004.00182.x
32. Dathe, M.; Nikolenko, H.; Klose, J.; Bienert, M. *Biochemistry* **2004,** *43,* 9140–9150. doi:10.1021/bi035948v
33. Haug, B. E.; Stensen, W.; Kalaaji, M.; Rekdal, Ø.; Svendsen, J. S. *J. Med. Chem.* **2008,** *51,* 4306–4314. doi:10.1021/jm701600a
34. Schatzschneider, U.; Metzler-Nolte, N. *Angew. Chem., Int. Ed.* **2006,** *45,* 1504–1507. doi:10.1002/anie.200504604
35. Shubina, E. S.; Krylov, A. N.; Kreindlin, A. Z.; Rybinskaya, M. I.; Epstein, L. M. *J. Mol. Struct.* **1993,** *301,* 1–5. doi:10.1016/0022-2860(93)80225-K
36. Kirin, S. I.; Noor, F.; Mier, W.; Metzler-Nolte, N. *J. Chem. Educ.* **2007,** *84,* 108–111. doi:10.1021/ed084p108
37. Wadhwani, P.; Afonin, S.; Ieronimo, M.; Buerck, J.; Ulrich, A. S. *J. Org. Chem.* **2006,** *71,* 55–61. doi:10.1021/jo051519m
38. *Mosby's Medical Dictionary,* 8th ed.; Elsevier: 2009.
39. Zanello, P. *Inorganic Electrochemistry, theory, practise and applications;* Royal Society of Chemistry: Cambridge, UK, 2003; pp 159–203.
40. Elschenbroich, C. *Organometallchemie;* B. G. Teubner Verlag: Wiesbaden, Germany, 2008; pp 457–458.
41. Mutoh, H.; Masuda, S. *J. Chem. Soc., Dalton Trans.* **2002,** 1875–1881. doi:10.1039/B111486G
42. Schibli, D. J.; Epand, R. F.; Vogel, H. J.; Epand, R. M. *Biochem. Cell Biol.* **2002,** *80,* 667–677. doi:10.1139/o02-147
43. Gopal, R.; Kim, Y. J.; Seo, C. H.; Hahm, K.-S.; Park, Y. *J. Pept. Sci.* **2011,** *17,* 329–334. doi:10.1002/psc.1369
44. Su, Y.; Doherty, T.; Waring, A. J.; Ruchala, P.; Hong, M. *Biochemistry* **2009,** *48,* 4587–4595. doi:10.1021/bi900080d
45. Kyte, J.; Doolittle, R. F. *J. Mol. Biol.* **1982,** *157,* 105–132. doi:10.1016/0022-2836(82)90515-0
46. Nandi, N. *J. Phys. Chem. A* **2003,** *107,* 4588–4591. doi:10.1021/jp030076s
47. Pathirana, S.; Neely, W. C.; Myers, L. J.; Vodyanoy, V. *J. Am. Chem. Soc.* **1992,** *114,* 1404–1405. doi:10.1021/ja00030a041
48. Alakoskela, J.-M.; Sabatini, K.; Jiang, X.; Laitala, V.; Covey, D. F.; Kinnunen, P. K. J. *Langmuir* **2008,** *24,* 830–836. doi:10.1021/la702909q
49. Alakoskela, J.-M.; Covey, D. F.; Kinnunen, P. K. J. *Biochim. Biophys. Acta* **2007,** *1768,* 131–145.
50. Nguyen, L. T.; Chau, J. K.; Perry, N. A.; de Boer, L.; Zaat, S. A. J.; Vogel, H. J. *PLoS One* **2010,** *5,* e12684. doi:10.1371/journal.pone.0012684
51. Pag, U.; Oedenkoven, M.; Sass, V.; Shai, Y.; Shamova, O.; Antcheva, N.; Tossi, A.; Sahl, H.-G. *J. Antimicrob. Chemother.* **2008,** *61,* 341–352. doi:10.1093/jac/dkm479
52. Sass, V.; Pag, U.; Tossi, A.; Bierbaum, G.; Sahl, H.-G. *Int. J. Med. Microbiol.* **2008,** *298,* 619–633. doi:10.1016/j.ijmm.2008.01.011
53. Lui, Z.; Brady, A.; Young, A.; Rasimick, B.; Chen, K.; Zhou, C.; Kallenbach, N. R. *Antimicrob. Agents Chemother.* **2007,** *51,* 597–603. doi:10.1128/AAC.00828-06
54. Page, S. M.; Ross, S. R.; Barker, P. D. *Future Med. Chem.* **2009,** *1,* 541–559. doi:10.4155/fmc.09.25
55. Schluga, P.; Hartinger, C. G.; Egger, A.; Reisner, E.; Galanski, M.; Jakupec, M. A.; Keppler, B. K. *Dalton Trans.* **2006,** 1796–1802. doi:10.1039/b511792e
56. Therrien, B.; Süss-Fink, G.; Govindaswamy, P.; Renfrew, A. K.; Dyson, P. J. *Angew. Chem., Int. Ed.* **2008,** *47,* 3773–3776. doi:10.1002/anie.200800186
57. Gasser, G.; Ott, I.; Metzler-Nolte, N. *J. Med. Chem.* **2011,** *54,* 3–25. doi:10.1021/jm100020w
58. Rademaker-Lakhai, J. M.; van den Bongard, D.; Pluim, D.; Beijnen, J. H.; Schellens, J. H. M. *Clin. Cancer Res.* **2004,** *10,* 3717–3727. doi:10.1158/1078-0432.CCR-03-0746
59. Lentz, F.; Drescher, A.; Lindauer, A.; Henke, M.; Hilger, R. A.; Hartinger, C. G.; Scheulen, M. E.; Dittrich, C.; Keppler, B. K.; Jaehde, U. *Anti-Cancer Drugs* **2009,** *20,* 97–103. doi:10.1097/CAD.0b013e328322fbc5
60. Hartinger, C. G.; Zorbas-Seifried, S.; Jakupec, M. A.; Kynast, B.; Zorbas, H.; Keppler, B. K. *J. Inorg. Biochem.* **2006,** *100,* 891–904. doi:10.1016/j.jinorgbio.2006.02.013
61. Hartinger, C. G.; Jakupec, M. A.; Zorbas-Seifried, S.; Groessl, M.; Egger, A.; Berger, W.; Zorbas, H.; Dyson, P. J.; Keppler, B. K. *Chem. Biodiversity* **2008,** *5,* 2140–2155. doi:10.1002/cbdv.200890195
62. Groessl, M.; Reisner, E.; Hartinger, C. G.; Eichinger, R.; Semenova, O.; Timerbaev, A. R.; Jakupec, M. A.; Arion, V. B.; Keppler, B. K. *J. Med. Chem.* **2007,** *50,* 2185–2193. doi:10.1021/jm061081y
63. Harden, J.; Diorio, N.; Petrov, A. G.; Jakli, A. *Phys. Rev. E* **2009,** *79,* 011701. doi:10.1103/PhysRevE.79.011701
64. Brogden, K. A. *Nat. Rev. Microbiol.* **2005,** *3,* 238–250. doi:10.1038/nrmicro1098
65. M07-A8, Vol. 29, No. 2; *Methods for Dilution Antimicrobial Susceptibility Tests for Bacteria That Grow Aerobically; Approved Standard* – 8th edition, Clinical and Laboratory Standards Institute, Wayne, Pennsylvania, USA, 2009.
66. Giacometti, A.; Cirioni, O.; Barchiesi, F.; Del Prete, M. S.; Fortuna, M.; Caselli, F.; Scalise, G. *Antimicrob. Agents Chemother.* **2000,** *44,* 1694–1696. doi:10.1128/AAC.44.6.1694-1696.2000
67. Bernhardt, G.; Reile, H.; Birnböck, H.; Spruß, T.; Schönenberger, H. *J. Cancer Res. Clin. Oncol.* **1992,** *118,* 35–43. doi:10.1007/BF01192309
68. Neukamm, M. J.; Pinto, A.; Metzler-Nolte, N. *Chem. Commun.* **2008,** 232–234. doi:10.1039/b712886j

Beilstein Journal of Organic Chemistry

Dimerization of a cell-penetrating peptide leads to enhanced cellular uptake and drug delivery

Jan Hoyer[1,2], Ulrich Schatzschneider[3], Michaela Schulz-Siegmund[4] and Ines Neundorf[*2]

Full Research Paper

Open Access

Address:
[1]Institute of Biochemistry, Faculty of Biosciences, Pharmacy and Psychology, University of Leipzig, Brüderstraße 34, D-04103 Leipzig, Germany, [2]Institute for Biochemistry, Department of Chemistry, University of Cologne, Zülpicher Straße 47, D-50674 Cologne, Germany, [3]Institute of Inorganic Chemistry, Julius-Maximilians-Universität Würzburg, Am Hubland, D-97074 Würzburg, Germany and [4]Institute of Pharmaceutical Technology, Faculty of Biosciences, Pharmacy and Psychology, University of Leipzig, Eilenburger Straße 15A, D-04317 Leipzig, Germany, University of Leipzig

Email:
Ines Neundorf[*] - ines.neundorf@uni-koeln.de

* Corresponding author

Keywords:
anti-tumor agents; cell-penetrating peptides; drug delivery; internalization studies; organometallic complexes; peptides

Beilstein J. Org. Chem. **2012,** *8,* 1788–1797.
doi:10.3762/bjoc.8.204

Received: 01 July 2012
Accepted: 17 September 2012
Published: 18 October 2012

This article is part of the Thematic Series "Antibiotic and cytotoxic peptides".

Guest Editor: N. Sewald

Abstract

Over the past 20 years, cell-penetrating peptides (CPPs) have gained tremendous interest due to their ability to deliver a variety of therapeutically active molecules that would otherwise be unable to cross the cellular membrane due to their size or hydrophilicity. Recently, we reported on the identification of a novel CPP, sC18, which is derived from the C-terminus of the 18 kDa cationic antimicrobial protein. Furthermore, we demonstrated successful application of sC18 for the delivery of functionalized cyclopentadienyl manganese tricarbonyl (cymantrene) complexes to tumor cell lines, inducing high cellular toxicity. In order to increase the potential of the organometallic complexes to kill tumor cells, we were looking for a way to enhance cellular uptake. Therefore, we designed a branched dimeric variant of sC18, $(sC18)_2$, which was shown to have a dramatically improved capacity to internalize into various cell lines, even primary cells, using flow cytometry and fluorescence microscopy. Cell viability assays indicated increased cytotoxicity of the dimer presumably caused by membrane leakage; however, this effect turned out to be dependent on the specific cell type. Finally, we could show that conjugation of a functionalized cymantrene with $(sC18)_2$ leads to significant reduction of its IC_{50} value in tumor cells compared to the respective sC18 conjugate, proving that dimerization is a useful method to increase the drug-delivery potential of a cell-penetrating peptide.

Introduction

A substantial problem concerning promising drug candidates is often their incapacity to reach their full therapeutic potential due to limited bioavailability and cellular uptake. In recent years, cell-penetrating peptides (CPPs) emerged as an encouraging tool to overcome this obstacle owing to their ability to autonomously cross the cellular membrane in a receptor-independent manner. This enables them to deliver a large variety of cargo molecules for therapy and diagnosis, as could be successfully shown for, e.g., cytostatics [1], proteins [2], oligonucleotides [3,4] and nanoparticles [5]. A common feature of CPPs is their typically high content in basic arginine and lysine residues, leading to a positive net charge of the peptides, which is considered to be crucial for initial membrane interaction through binding to negatively charged phospholipids and glycosaminoglycans [6]. Endocytic and non-endocytic processes have been proposed to be involved in cellular uptake; however, the exact mechanism triggering internalization is still under debate and was shown to depend on several factors such as structure and concentration of the CPP as well as the cargo to be transported and the specific cell line [7].

Recently, we identified a novel cell-penetrating peptide, sC18 [8], derived from the C-terminal domain of CAP18 (18 kDa antimicrobial protein), which is found in rabbit leukocytes and was shown to bind to negatively charged lipopolysaccharides of Gram-negative bacteria to inhibit their pathogenic activity [9]. We were able to successfully apply sC18 for tumor imaging by conjugation with a metal chelator and a tumor-homing agent, which accumulates in hypoxic tissue [10]. Furthermore, we reported on the delivery of functionalized cyclopentadienyl manganese tricarbonyl (cymantrene) complexes with the help of sC18, which lead to significant induction of cytotoxicity in tumor cells [11-13], which was even more pronounced after introduction of an enzymatic cleavage site [12]. However, the aim of the present study was to investigate whether the cytotoxic effect of these organometallic complexes can be further increased by conjugating them to a dimeric variant of sC18, $(sC18)_2$, since previous studies demonstrated improvement of the delivery of various kinds of cargo by CPP oligomerization [14,15].

Results and Discussion

Uptake studies

We reasoned that dimerization of sC18 would be beneficial for cellular uptake since the local concentration of the monomeric unit at the membrane would be increased. Instead of simply synthesizing a linear peptide with two consecutive sC18 sequences, we opted for a branched version of $(sC18)_2$ by introducing the second unit at the side chain of Lys^4. This ensures that both N-termini of the monomeric units remain free and hence the general structure of the dimer is unaltered upon symmetric introduction of N-terminal modifications. To test the hypothesis of improved internalization behavior of the dimer, we conducted flow-cytometric cellular uptake studies with sC18 versus $(sC18)_2$ in various cell lines after N-terminal labeling with carboxyfluorescein (labeling of the dimer occurred at the N-terminus of the first sC18 unit). A dramatic increase of intracellular fluorescence that was 10-fold or higher in all cell lines was observed (Figure 1). Even at a peptide concentration as low as 1 μM significant uptake of $(sC18)_2$ after 1 h incubation was achieved, whereas the parent peptide sC18 almost failed to internalize at this concentration. In human embryonic kidney (HEK-293) cells and MCF-7 cells (human breast adenocarcinoma) the uptake rate of $(sC18)_2$ at 1 μM was significantly higher even when compared to sC18 at a concentration of 10 μM ($p \leq 0.05$). When comparing the different cell lines, the uptake rate of $(sC18)_2$ at 1 μM decreases in the order HEK-293 > MCF-7 > HT-29 ($p \leq 0.05$). Similarly, at 10 μM, the amount of $(sC18)_2$ taken up by HT-29 cells (human colon adenocarcinoma) is still less than half compared to the other cell lines; however, no statistically significant difference between HEK-293 and MCF-7 was observed.

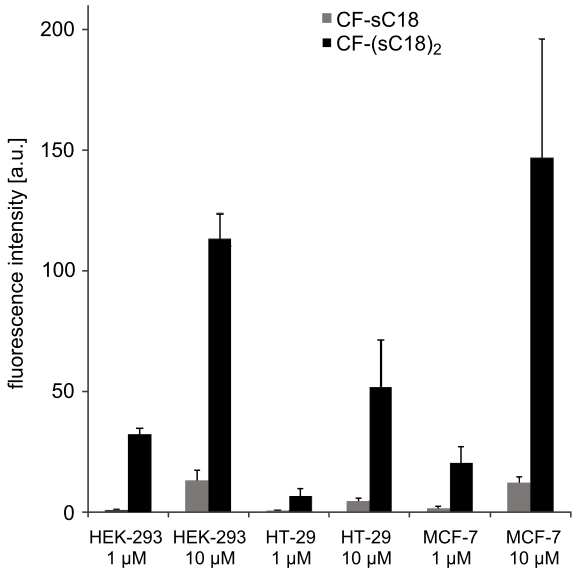

Figure 1: Flow cytometric uptake studies of carboxyfluorescein-labeled $(sC18)_2$ in HEK-293 (human embryonic kidney) cells, HT-29 cells (human colon adenocarcinoma) and MCF-7 cells (human breast adenocarcinoma) with sC18 as reference after 1 h incubation. Experiments were conducted in duplicate with $n = 2$. Error bars represent the standard deviation.

The drastically enhanced uptake of the dimer compared to the monomeric peptide is in contrast to previous studies with the

TAT peptide, which is similar to sC18 with respect to the number of arginine and lysine residues and the overall charge of the peptide. Dimerization of TAT turned out to have no or little effect on translocation through cellular [14,16] or model [17] membranes. Only a branched trimeric variant of TAT was observed to have a major impact on the internalization behavior [14].

In order to gain insight into the mechanism of cell entry of $(sC18)_2$, we investigated the intracellular distribution pattern of the fluorescently-labeled peptide in HEK-293 by fluorescence microscopy (Figure 2). The punctate uptake pattern speaks in favor of an endocytic internalization mode and is also observed for sC18, which is in line with previous reports [8]. Therefore, the general uptake mechanism in this cell line seems not to be altered upon dimerization.

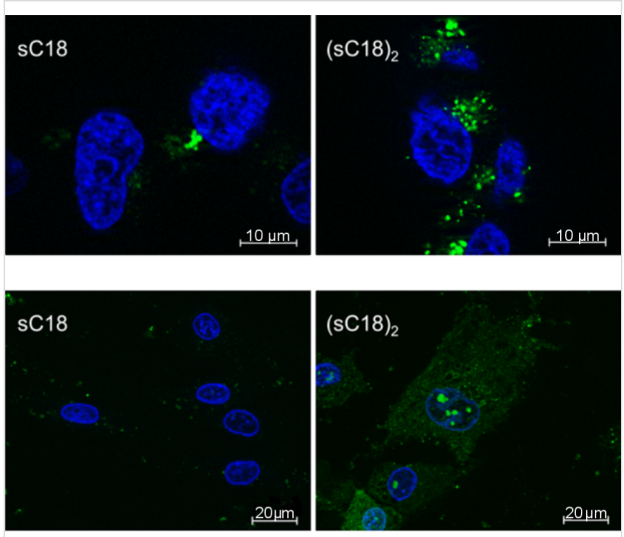

Figure 2: Top: Fluorescence microscopic images of unfixed HEK-293 cells after 30 min incubation with 1 µM CF-sC18 and CF-$(sC18)_2$. Bottom: Fluorescence microscopic images of unfixed hADSC after 1 h incubation with 25 µM CF-sC18 and CF-$(sC18)_2$. Blue: Hoechst33342 nuclear dye, green: carboxyfluorescein-labeled peptides. Images taken with a 63× oil immersion objective.

With this potent cell-penetrating peptide at hand, we were interested as to whether it is also able to internalize into primary cells, which are much less susceptible to CPP-based intracellular delivery than immortalized or tumor cell lines. We indeed observed bright intracellular fluorescence when incubating human adipose tissue-derived stem cells for 1 h with $(sC18)_2$ at 25 µM as opposed to sC18, which shows hardly any detectable uptake (Figure 2). Interestingly, the peptide is evenly distributed throughout the cells, indicating that a large fraction of $(sC18)_2$ was able to reach the cytosol. Whether this is due to a different mechanism of uptake or to improved endosomal escape requires further investigation. Importantly, no effect on cell morphology is apparent and, thus, no cytotoxicity at a concentration that is sufficient for very efficient peptide internalization.

Cytotoxicity of $(sC18)_2$

The effect of the dimeric sC18 on the survival of HEK-293, HT-29 and MCF-7 cells was determined by means of a resazurin-based cell viability assay. After 24 h incubation, a cell-type-dependent cytotoxicity profile of $(sC18)_2$ was observed (Figure 3). While HEK-293 cells remained unharmed even at high peptide concentrations up to 100 µM, a steady decrease of cell viability was induced in the tumor cell lines, which was particularly obvious in MCF-7 cells. At least for HEK-293 and MCF-7, this effect seemed to be in no way related to different intracellular amounts of peptide since both cell lines showed equal propensity to take up $(sC18)_2$ as was shown above. The significant induction of cytotoxicity in MCF-7 and HT-29 is in plain contrast to the monomeric peptide, which did not cause any loss of cell viability in previous studies [8].

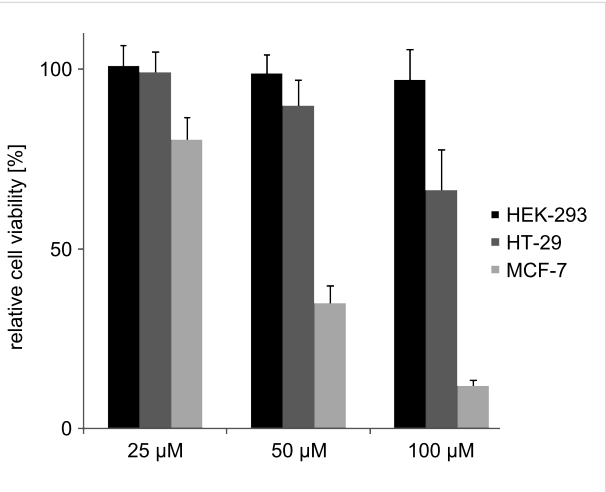

Figure 3: Cell viability of different cell lines after 24 h incubation with $(sC18)_2$ at different concentrations as determined by a resazurin-based cell viability assay. Experiments were conducted in triplicate with $n = 2$. Error bars represent the standard deviation.

Since $(sC18)_2$ possesses a net charge of +17 and due to the fact that it has been shown for oligoarginines that the higher the number of positive charges, the higher is the propensity of the peptide to induce pore formation in the cellular membrane [18], we performed membrane integrity assays measuring the amount of lactate dehydrogenase (LDH) released from the cells when the membrane becomes prone to leaking. In the case of MCF-7, high levels of extracellular LDH even after 1 h incubation with 30 µM $(sC18)_2$ attested to a high extent of membrane destabilization, which eventually leads to cell death (Figure 8), suggesting membrane disruption as the cause for the cellular

toxicity of the dimeric peptide owing to its high number of basic residues. Extracellular LDH levels in HT-29 were much smaller, which is in line with the results of the resazurin-based cell viability assay, as well as the observation that HEK-293 cells only show a little membrane leakage even at elevated $(sC18)_2$ concentrations (Figure 4). It can thus be hypothesized that the cytotoxic behavior of the peptide is related to the individual membrane composition of each cell line.

The finding that the dimer exhibits significant cytotoxic effects while the monomer does not is consistent with previous studies that demonstrated the increase of membrane leakage and cytotoxicity with the number of arginine residues in oligoarginines [19] as well as increased cytotoxicity for oligomeric CPPs in general [20].

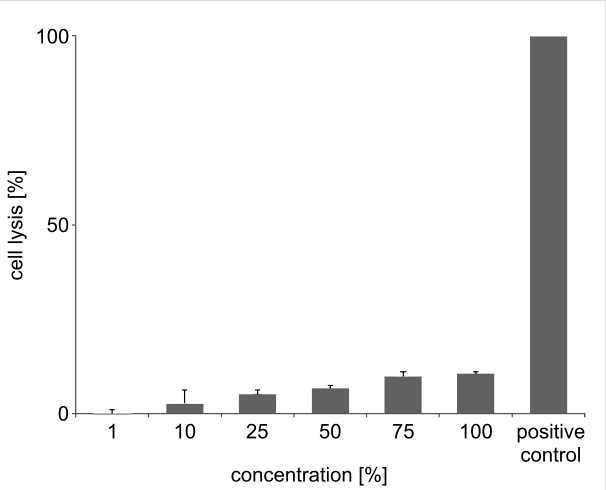

Figure 4: Cell lysis of HEK-293 cells induced by $(sC18)_2$ after 1 h incubation. Experiments were conducted in triplicate with $n = 2$. Error bars represent the standard deviation.

Synthesis and characterization of $(sC18)_2$ bioconjugates

In order to evaluate the potential of the sC18 dimer to effectively deliver cytotoxic drugs into cells and even enhance the cytotoxicity of functionalized cymantrenes, the synthesis of which has previously been reported [11], we synthesized a single (**1**) and a double conjugate (**2**) of $(sC18)_2$ and Cym2 (Table 1, Scheme 1). For comparison, we also synthesized bioconjugates with known cytostatic agents: the common DNA

Table 1: Peptide sequences.[a]

Peptide	Sequence
sC18	GLRKRLRKFRNKIKEK-NH_2
$(sC18)_2$	GLRKRLRKFRNKIKEK-NH_2 GLRKRLRKFRNKIKEK
Cym2-GFL-$(sC18)_2$ (**1**)	Cym2-GFLGLRKRLRKFRNKIKEK-NH_2 GLRKRLRKFRNKIKEK
(Cym2-GFL)2-$(sC18)_2$ (**2**)	Cym2-GFLGLRKRLRKFRNKIKEK-NH_2 Cym2-GFLGLRKRLRKFRNKIKEK
(Cbl-GFL)2-$(sC18)_2$ (**3**)	Cbl-GFLGLRKRLRKFRNKIKEK-NH_2 Cbl-GFLGLRKRLRKFRNKIKEK
PAD-GFL-$(sC18)_2$ (**4**)	KLAKLAKKLAKLAKGFLGLRKRLRKFRNKIKEK-NH_2 GLRKRLRKFRNKIKEK
PAD	KLAKLAKKLAKLAK-NH_2

[a]Cbl: chlorambucil.

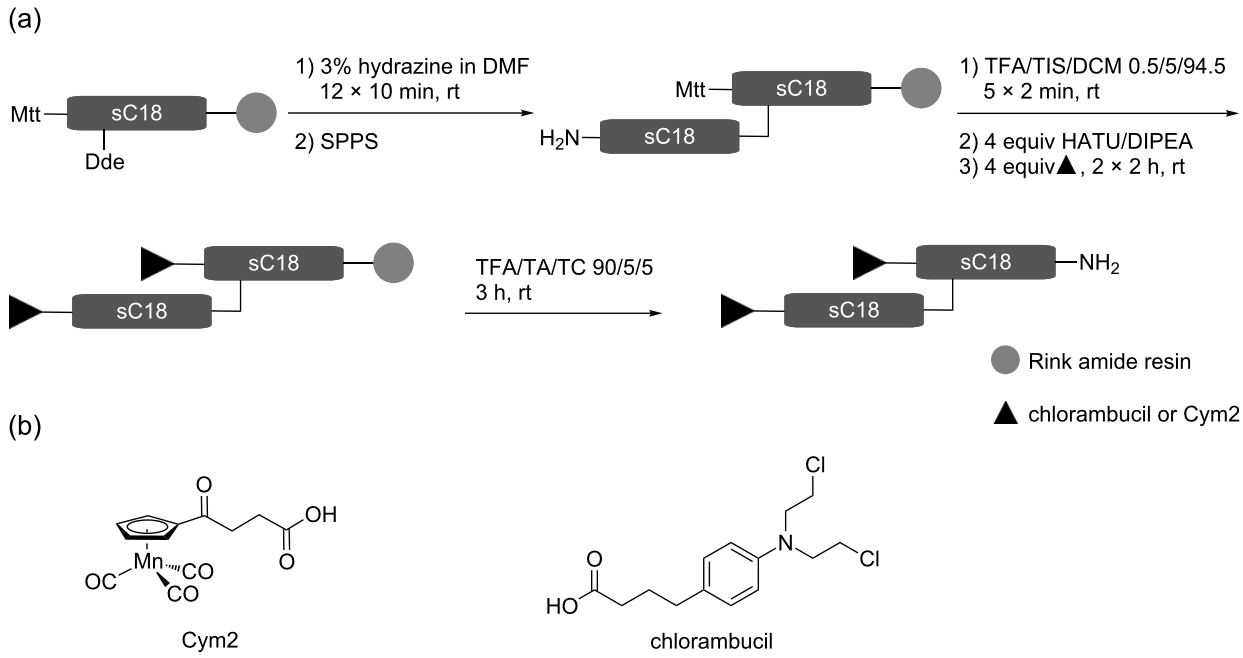

Scheme 1: Synthesis of $(sC18)_2$ bioconjugates (a) and chemical structures of the coupled anti-tumor agents (b). Mtt: 4-methyltrityl chloride; Dde: 1-(4,4-dimethyl-2,6-dioxocyclohex-1-ylidene)ethyl; SPPS: solid-phase peptide synthesis; TFA: trifluoroacetic acid; TIS: triisopropylsilane; HATU: *O*-(7-azabenzotriazol-1-yl)-1,1,3,3-tetramethyluronium hexafluorophosphate; DIPEA: diisopropylethylamine; TA: thioanisole; TC: *p*-thiocresol.

alkylating anticancer therapeutic chlorambucil (Cbl, **3**), which may induce apoptosis, and the cell impermeable proapoptotic peptide $(KLAKLAK)_2$ (PAD, proapoptotic domain peptide) [21] **4**. All conjugates were synthesized with an enzymatic cleavage site for the peptidase cathepsin B (Gly-Phe-Leu-Gly), the expression of which is up-regulated in tumor cells [22,23], since this approach has been shown to improve intracellular release of the cargo [12,24]. Peptides were obtained in high purity as determined by analytical HPLC, and their identity was confirmed by mass spectrometry (Table 2). However, for compound **2** a partial loss of one $Mn(CO)_3$ unit of the organometallic complex was observed to some extent, which was considered to be negligible for the biological testing. An exemplary HPLC chromatogram and ESI-MS spectrum is shown in Figure 5. Double conjugates were synthesized by an orthogonal protecting-group strategy involving highly acid-labile 4-methyltrityl (Mtt) protection (Scheme 1), which can be cleaved in the presence of *tert*-butyloxycarbonyl (Boc). Indeed, we did not observe concomitant deprotection of lysine side chains, which was favored by the fact that Mtt groups situated at the N-terminus are even more acid-sensitive than N^{ε}-Mtt groups [25].

The structural analysis of the $(sC18)_2$ conjugates by circular dichroism spectroscopy did not reveal any change of the secondary structure with respect to the parent peptide (Figure 6). They all exhibit a random coil structure in phosphate buffer with transition to an α-helical structure in the helix-inducing environment of trifluoroethanol, which has already been shown for monomeric sC18 [8]. Thus, in this case, no significant influence of the cargo on the uptake of $(sC18)_2$ is expected, since this is largely determined by the structure of the CPP.

Table 2: Analytical data and IC_{50} values of the $(sC18)_2$ bioconjugates.[a]

Peptide	MW_{calc}	MW_{exp}	Purity [%]	IC_{50} [μM]	
				HT-29	MCF-7
1	4722.8	4725.4[b]	>95	33.2 ± 2.2	11.8 ± 0.4
2	5326.0	5328.9[b]	>90	21.1 ± 2.0	6.2 ± 0.9
3	5324.1	5324.1[c]	>95	26.0 ± 1.2	8.9 ± 0.3
4	5941.9	5941.0[c]	>99	14.3 ± 1.4	3.6 ± 1.5

[a]Monoisotopic masses given, purity determined by analytical HPLC; [b]ESI-MS; [c]MALDI-MS.

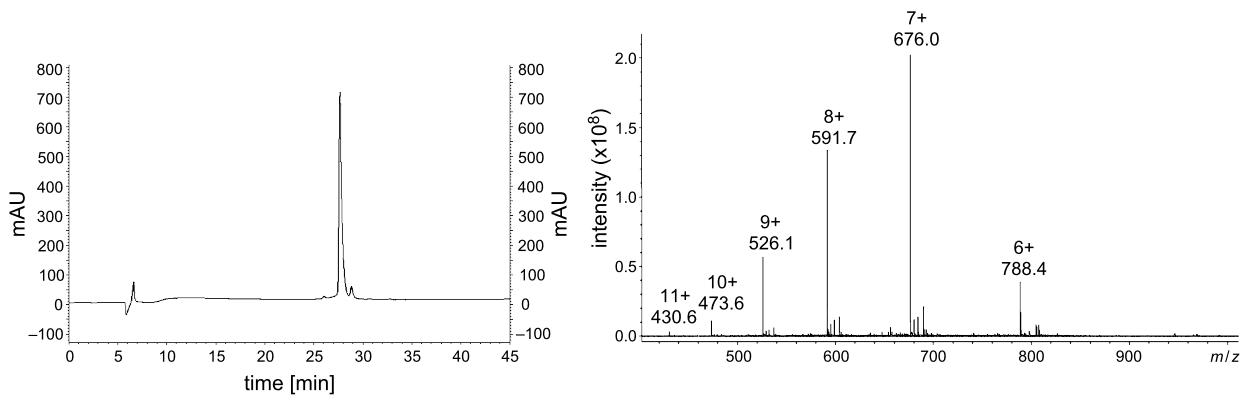

Figure 5: Chromatogram and ESI-MS of purified Cym2-GFL-$(sC18)_2$. The gradient was 10→60% acetonitrile in water over 45 min.

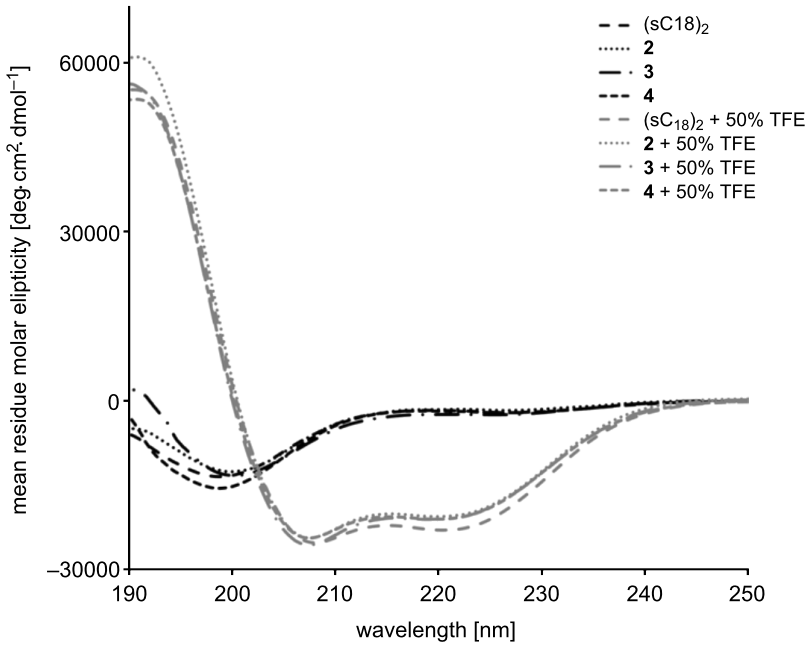

Figure 6: Circular dichroism spectra of the $(sC18)_2$ conjugates. Spectra were acquired in 10 mM phosphate buffer with or without 50% trifluoroethanol (TFE), as indicated.

The bioconjugates were tested for cytotoxicity in MCF-7 and HT-29 in the presence of serum by using a resazurin-based cell viability assay. These are well-established tumor cell lines that allow for direct comparison of the results with previous studies. All substances were shown to exhibit significant cytotoxicity in both cell lines (Figure 7). IC_{50} values are given in Table 2. Importantly, the unconjugated cytostatic compounds did not have any effect on cell viability at any of the concentrations tested, which is confirmed by microscopic images of HT-29 that do not reveal any morphological aberration except in the case of incubation with the bioconjugates. This is in agreement with previous studies for Cym2 [12] and Cbl [26] and is also plausible for PAD, since it was shown to interact with mitochondrial membranes; however, it does not cause cell death unless it is internalized into the cytosol [27]. The failure of the cytostatic compounds to induce cytotoxicity is due to their limited capability to cross the cellular membrane. Likewise, the CPP alone did not affect cell viability of HT-29 cells over the whole concentration range tested, while in MCF-7 the IC_{50} values of **1**–**4** are still well below the onset of cytotoxic effects, which were only observed to some extent above a concentration of 15 μM. Compound **2** showed significantly increased cytotoxicity compared to **1**, demonstrating the advantage of the double conjugate approach. Importantly, when using the dimer instead of monomeric sC18, which was used in previous studies [12], the IC_{50} values of the functionalized cymantrene could be

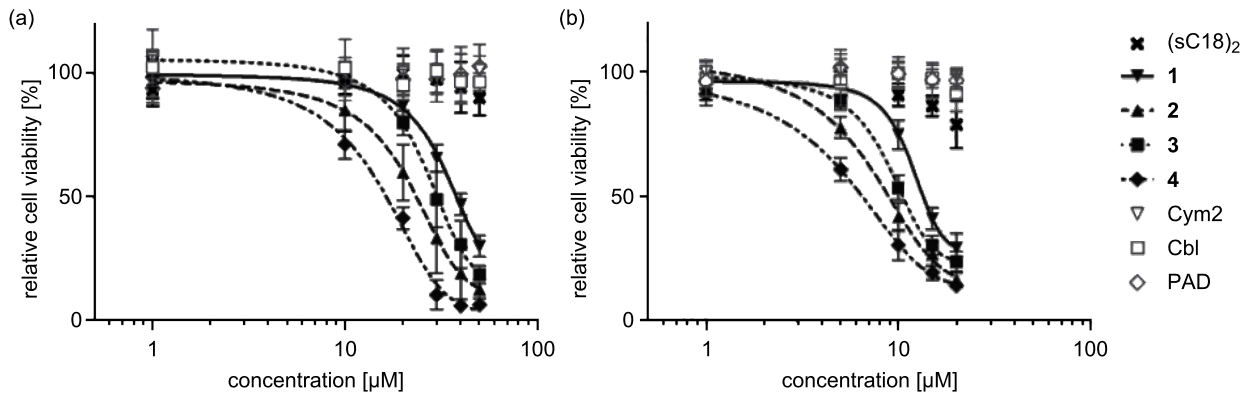

Figure 7: Cell viability of (a) HT-29 and (b) MCF-7 cells after 24 h incubation with the $(sC18)_2$ conjugates at different concentrations, as determined by a resazurin-based cell viability assay. Experiments were conducted in triplicate with $n = 2$. Error bars represent standard deviation. Curves obtained by nonlinear regression (sigmoidal dose–response). For IC_{50} values see Table 2.

significantly reduced to 21 µM in HT-29 and 6 µM in MCF-7. Interestingly, Cym2 and Cbl were shown to be similarly effective in both cell lines, whereas the highest cytotoxicity was induced by the PAD conjugate.

The mechanism that eventually leads to cell death has not yet been elucidated for the functionalized cymantrenes; however, it was observed that it is mainly induced by necrosis, albeit apoptosis could also be demonstrated to some extent [12]. The high degree of membrane leakage even after 1 h and, thus, the rapidly occurring induction of cell death again speak in favor of mostly necrotic cell death. This is also true for compounds **3** and **4**, which exert the same effect on cell morphology (Figure 8) and induce an equal amount of LDH release (Figure 9). This is surprising at least for compound **4**, since several PAD–CPP conjugates were shown to induce apoptosis upon cytosolic delivery [28,29]. It is possible, though, that the even higher positive net charge (+23) of **4** due to the additional lysine residues of the cargo peptide leads to further membrane destabilization, which eventually becomes irreversible and induces cell death. Thus, $(sC18)_2$ may not be suitable for the delivery of positively charged cargo.

In conclusion, we could demonstrate that dimerization of a cell-penetrating peptide, sC18, leads to dramatically enhanced cellular uptake in various cell lines, but also increases cytotoxicity in a cell-type-dependent manner. The dimer also turned out to efficiently internalize into primary cells that are commonly less susceptible to standard delivery methods. Furthermore, we were able to effectively transport cytostatic compounds into

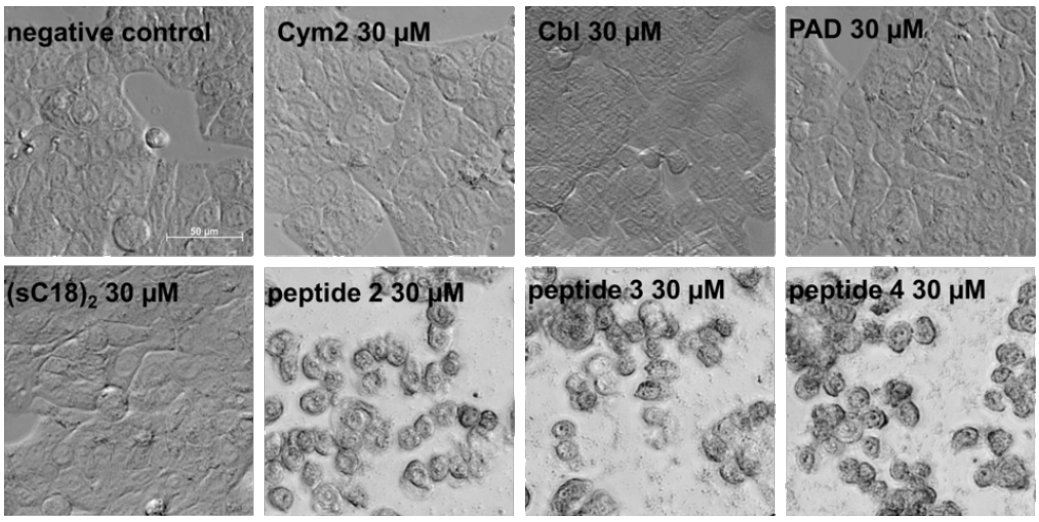

Figure 8: Brightfield microscopic images of unfixed HT-29 cells after 24 h incubation with the $(sC18)_2$ conjugates at 30 µM. Scale bar: 50 µm.

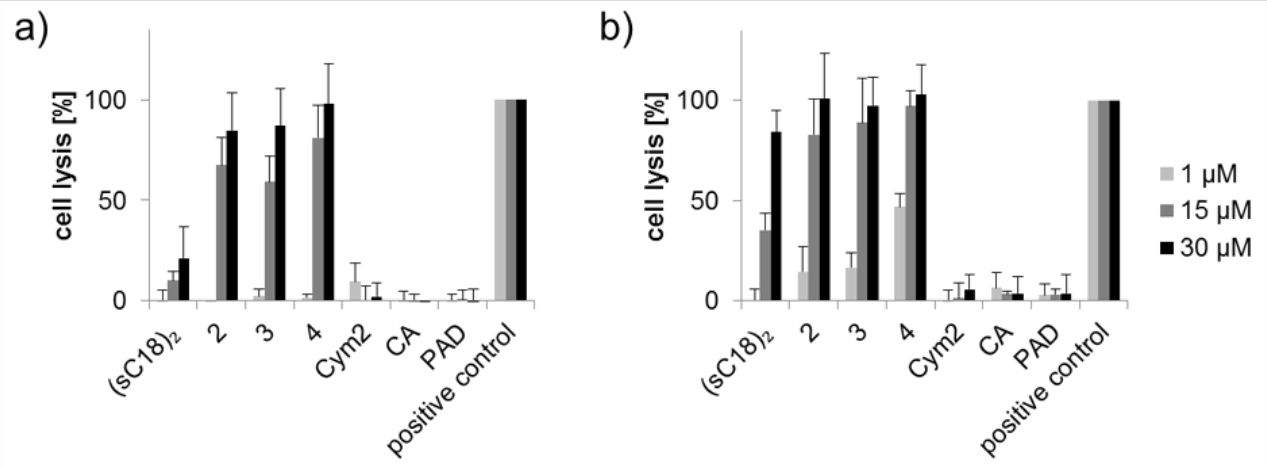

Figure 9: Cell lysis of (a) HT-29 and (b) MCF-7 cells induced by the $(sC18)_2$ conjugates at different concentrations after 1 h incubation. Experiments were conducted in triplicate with $n = 2$. Error bars represent the standard deviation.

tumor cell lines, observing a significant decrease of the IC_{50} values of Cym2 compared to previous studies, further increasing the therapeutic potential of functionalized cymantrenes.

Experimental

Materials

N^{α}-Fmoc-protected amino acids were purchased from IRIS Biotech (Marktredwitz, Germany), the following side-chain protecting groups were chosen: *tert*-butyloxy (*t*-BuO) for Glu; *tert*-butyloxycarbonyl (Boc) and 1-(4,4-dimethyl-2,6-dioxocyclohex-1-ylidene)ethyl (Dde) for Lys. 4-(2',4'-Dimethoxyphenyl-Fmoc-aminomethyl)phenoxy (Rink amide) resin and 4-methyltrityl chloride were obtained from Novabiochem (Darmstadt, Germany). *O*-(7-Azabenzotriazol-1-yl)-1,1,3,3-tetramethyluronium hexafluorophosphate (HATU), *N*,*N*-diisopropylethylamine (DIEA), thioanisole, *p*-thiocresole, piperidine, trifluoroacetic acid, trypan blue, 5(6)-carboxyfluorescein (CF) and 2,2,2-trifluoroethanol were purchased from Fluka (Taufkirchen, Germany). Chlorambucil (Cbl) and the resazurin-based in vitro toxicology assay kit were purchased from Sigma-Aldrich (Taufkirchen, Germany). *N*,*N*-Dimethylformamide (DMF), dichloromethane, and diethyl ether were obtained from Biosolve (Valkenswaard, Netherlands). Acetonitrile was obtained from Merck (Darmstadt, Germany). The CytoTox-One homogeneous membrane integrity assay was from Promega. For cell culture, the following media and supplements were used: Dulbecco's modified Eagle's medium (DMEM), Ham's F12 (without L-glutamine), OptiMEM, Dulbecco's phosphate buffered saline (PBS) without calcium and magnesium, fetal bovine serum (FBS), L-glutamine and trypsin/EDTA (all purchased from PAA, Linz, Austria, or Gibco Life Technologies, Karlsruhe, Germany). Cell culture flasks (75 cm^2) and 96-well plates were from TPP (Trasadingen, Switzerland), 48-well plates were purchased from Greiner Bio-One (Frickenhausen, Germany) and 8-well µ-slides were from ibidi (Martinsried, München Germany). MCF-7, HT-29 and HEK-293 cell lines were kindly provided by Prof. Dr. A. G. Beck-Sickinger.

Peptide synthesis

The peptides used were synthesized as described previously [30] by automated solid-phase peptide synthesis (SPPS) on a multiple Syro II peptide synthesizer (MultiSynTech, Witten, Germany) following Fmoc/*t*-Bu-strategy utilizing a double-coupling procedure and in situ activation with Oxyma/DIC. Synthesis of branched $(sC18)_2$ was achieved by N-terminal coupling of Dde-Lys(Fmoc)-OH to sC18(5-16) and subsequent automated elongation of the peptide chain at the lysine side chain by using N^{α}-Boc protected glycine at the terminal position. Cleavage of the Dde group was achieved by treatment with a 3% solution of hydrazine in DMF for 12 × 10 min. Subsequently, the peptide was elongated to its final length by automated SPPS. *N*-terminal coupling of Cym2 or 5(6)-carboxyfluorescein was carried out by using 2 equiv of the substance to be coupled and activation with 2 equiv of HATU/DIPEA in DMF under vigorous shaking for 2 × 2 h. CF-polymers were cleaved by treatment with 20% piperidine for 45 min.

For the synthesis of double conjugates of $(sC18)_2$ with Cym2 or Cbl (Scheme 1), the N-terminus of the first sC18 unit was protected by using 10 equiv of Mtt and 1 equiv of DIPEA in DCM under vigorous shaking for 18 h at room temperature. After cleavage of the Dde group at the side chain of Lys^4 and automated elongation of the peptide chain, the Mtt group was selectively removed by treatment with 0.5% TFA and 5% TIS in DCM for 5 × 2 min. Coupling of the cytostatic compound was carried out by using 4 equiv of either Cym2 or Cbl, and ac-

tivation with 4 equiv of HATU/DIPEA in DMF under vigorous shaking for 2 × 2 h. All peptides were purified by preparative reversed-phase HPLC using a binary eluent system consisting of 0.1% TFA in water and 0.08% TFA in acetonitrile and analyzed by MALDI or ESIMS, and analytical RP-HPLC. For the peptide sequences see Table 1.

Circular dichroism spectroscopy

Circular dichroism spectra were recorded on a Jasco spectropolarimeter J 715 at 20 °C in 10 mM phosphate buffer (pH 7.0) with or without addition of 50% trifluoroethanol, respectively. The concentration of the peptides was 20 μM.

Cell culture

HEK-293 cells (human embryonic kidney epithelium transformed with adenovirus 5 DNA) were grown to subconfluency in 75 cm^2 culture flasks at 37 °C and 5% CO_2 in a humidified atmosphere by using DMEM/Ham's F12 (without L-glutamine), which contained 15% heat-inactivated FBS. MCF-7 cells (human breast adenocarcinoma) were grown under the same standard growth conditions in DMEM/Ham's F12 containing 2 mM L-glutamine and 10% FBS. HT-29 cells (human colon adenocarcinoma) were grown in RPMI 1640 supplemented with 10% FBS. Freshly isolated human-adipose-tissue-derived stem cells (hADSC) were grown in DMEM high glucose (4.5 g/L) containing 1% penicillin/streptomycin and 10% FBS.

Internalization studies

For peptide-uptake studies by flow cytometry, cells were seeded in a 48-well plate and grown to 60–70% confluence. After incubation at 37 °C for 1 h with 5(6)-carboxyfluorescein-labeled peptides in OptiMEM, the cells were treated with 150 μM trypan blue for 0.5 min to quench extracellular fluorescence and washed twice with PBS, trypsinized and resuspended in standard cell-culture medium. Analyses were performed on a Partec CyFlow ML flow cytometer. Cellular autofluorescence was subtracted. The experiments were carried out with *n* (number of experiments) = 2 in duplicate.

For fluorescence microscopic uptake studies, cells were seeded in an 8-well ibidi plate and grown to 60–70% confluence. The cells were then incubated with CF-labeled peptides in OptiMEM for 30 min at 37 °C. Ten minutes prior to the end of incubation, the nuclei were stained by addition of Hoechst33342 nuclear dye. Finally, the solution was removed, and the cells were treated with a 150 μM trypan blue solution for 0.5 min. After washing twice with PBS, images were taken by using a Zeiss Observer Z1 fluorescence microscope equipped with an ApoTome unit using a 63× oil immersion objective.

Cell viability assay

Cytotoxicity was determined by means of a resazurin-based cell-viability assay. Cells were seeded in a 96-well plate, grown to subconfluency and incubated with the substances at different concentrations for 24 h in the presence of serum under standard growth conditions. For the positive control, cells were treated with 70% ethanol for 10 min. After washing, the cell viability was determined relative to untreated cells by using the In Vitro Toxicology Assay Kit from Sigma-Aldrich according to the manufacturer's protocol. Measurement was performed fluorimetrically at 595 nm (λ_{ex} = 550 nm) on a Tecan SpectraFluor Plus plate reader. Untreated cells were set to 100%. IC_{50} values were calculated by using nonlinear regression (sigmoidal dose–response) with GraphPad Prism. Experiments were carried out with n = 2 in triplicate. Microscopic images were taken with a 20× objective on a Zeiss Observer Z1 microscope.

LDH release assay

For the membrane leakage assay utilizing the Promega CytoTox-One kit, cells were seeded in a 96-well plate, grown to subconfluency, and incubated with the substances at different concentrations for 1 h in the presence of serum under standard growth conditions. Afterwards, the assay was conducted according to the manufacturer's protocol including the provided cell lysis positive control. Measurement was performed fluorimetrically at 595 nm (λ_{ex} = 550 nm) on a Tecan SpectraFluor Plus plate reader. The negative control served as blank value, and data were normalized to the positive control. Experiments were carried out with n = 2 in triplicate.

Acknowledgements

This work was supported by the Bundesministerium für Bildung und Forschung (BMBF, PtJ-Bio, 0313909) and by the Deutsche Forschungsgemeinschaft (DFG) within the project FOR 630 "Biological function of organometallic compounds". We thank Prof. A. G. Beck-Sickinger for generous access to all facilities of the institute.

References

1. Krauss, U.; Kratz, F.; Beck-Sickinger, A. G. *J. Mol. Recognit.* **2003,** *16,* 280–287. doi:10.1002/jmr.638
2. Looi, C. Y.; Imanishi, M.; Takaki, S.; Sato, M.; Chiba, N.; Sasahara, Y.; Futaki, S.; Tsuchiya, S.; Kumaki, S. *PLoS One* **2011,** *6,* e23640. doi:10.1371/journal.pone.0023640
3. El Andaloussi, S.; Lehto, T.; Mäger, I.; Rosenthal-Aizman, K.; Oprea, I. I.; Simonson, O. E.; Sork, H.; Ezzat, K.; Copolovici, D. M.; Kurrikoff, K.; Viola, J. R.; Zaghloul, E. M.; Sillard, R.; Johansson, H. J.; Said Hassane, F.; Guterstam, P.; Suhorutšenko, J.; Moreno, P. M. D.; Oskolkov, N.; Hälldin, J.; Tedebark, U.; Metspalu, A.; Lebleu, B.; Lehtiö, J.; Smith, C. I.; Langel, Ü. *Nucleic Acids Res.* **2011,** *39,* 3972–3987. doi:10.1093/nar/gkq1299

4. Trabulo, S.; Resina, S.; Simões, S.; Lebleu, B.; Pedroso de Lima, M. C. *J. Controlled Release* **2010,** *145,* 149–158. doi:10.1016/j.jconrel.2010.03.021
5. Yukawa, H.; Kagami, Y.; Watanabe, M.; Oishi, K.; Miyamoto, Y.; Okamoto, Y.; Tokeshi, M.; Kaji, N.; Noguchi, H.; Ono, K.; Sawada, M.; Baba, Y.; Hamajima, N.; Hayashi, S. *Biomaterials* **2010,** *31,* 4094–4103. doi:10.1016/j.biomaterials.2010.01.134
6. Ziegler, A. *Adv. Drug Delivery Rev.* **2008,** *60,* 580–597. doi:10.1016/j.addr.2007.10.005
7. Madani, F.; Lindberg, S.; Langel, Ü.; Futaki, S.; Gräslund, A. *J. Biophys.* **2011,** *2011,* 414729. doi:10.1155/2011/414729
8. Neundorf, I.; Rennert, R.; Hoyer, J.; Schramm, F.; Löbner, K.; Kitanovic, I.; Wölfl, S. *Pharmaceuticals* **2009,** *2,* 49–65. doi:10.3390/ph2020049
9. Larrick, J. W.; Hirata, M.; Balint, R. F.; Lee, J.; Zhong, J.; Wright, S. C. *Infect. Immun.* **1995,** *63,* 1291–1297.
10. Splith, K.; Bergmann, R.; Pietzsch, J.; Neundorf, I. *ChemMedChem* **2012,** *7,* 57–61. doi:10.1002/cmdc.201100401
11. Splith, K.; Neundorf, I.; Hu, W.; Peindy N'Dongo, H. W.; Vasylyeva, V.; Merz, K.; Schatzschneider, U. *Dalton Trans.* **2010,** *39,* 2536–2545. doi:10.1039/b916907e
12. Splith, K.; Hu, W.; Schatzschneider, U.; Gust, R.; Ott, I.; Onambele, L. A.; Prokop, A.; Neundorf, I. *Bioconjugate Chem.* **2010,** *21,* 1288–1296. doi:10.1021/bc100089z
13. Hu, W.; Splith, K.; Neundorf, I.; Merz, K.; Schatzschneider, U. *J. Biol. Inorg. Chem.* **2012,** *17,* 175–185. doi:10.1007/s00775-011-0840-5
14. Angeles-Boza, A. M.; Erazo-Oliveras, A.; Lee, Y.-J.; Pellois, J.-P. *Bioconjugate Chem.* **2010,** *21,* 2164–2167. doi:10.1021/bc100130r
15. Said Hassane, F.; Ivanova, G. D.; Bolewska-Pedyczak, E.; Abes, R.; Arzumanov, A. A.; Gait, M. J.; Lebleu, B.; Gariépy, J. *Bioconjugate Chem.* **2009,** *20,* 1523–1530. doi:10.1021/bc900075p
16. Chugh, A.; Eudes, F. *Biochim. Biophys. Acta, Biomembr.* **2007,** *1768,* 419–426. doi:10.1016/j.bbamem.2006.11.012
17. Zhu, W. L.; Shin, S. Y. *J. Pept. Sci.* **2009,** *15,* 345–352. doi:10.1002/psc.1120
18. Cahill, K. *Phys. Biol.* **2010,** *7,* 16001. doi:10.1088/1478-3975/7/1/016001
19. Tünnemann, G.; Ter-Avetisyan, G.; Martin, R. M.; Stöckl, M.; Herrmann, A.; Cardoso, M. C. *J. Pept. Sci.* **2008,** *14,* 469–476. doi:10.1002/psc.968
20. Park, S.-H.; Doh, J.; Park, S. I.; Lim, J. Y.; Kim, S. M.; Youn, J.-I.; Jin, H.-T.; Seo, S.-H.; Song, M.-Y.; Sung, S. Y.; Kim, M.; Hwang, S. J.; Choi, J. M.; Lee, S.-K.; Lee, H. Y.; Lim, C. L.; Chung, Y. J.; Yang, D.; Kim, H.-N.; Lee, Z. H.; Choi, K. Y.; Jeun, S.-S.; Sung, Y. C. *Gene Ther.* **2010,** *17,* 1052–1061. doi:10.1038/gt.2010.58
21. Javadpour, M. M.; Juban, M. M.; Lo, W.-C. J.; Bishop, S. M.; Alberty, J. B.; Cowell, S. M.; Becker, C. L.; McLaughlin, M. L. *J. Med. Chem.* **1996,** *39,* 3107–3113. doi:10.1021/jm9509410
22. Foekens, J. A.; Kos, J.; Peters, H. A.; Krasovec, M.; Look, M. P.; Cimerman, N.; Meijer-van Gelder, M. E.; Henzen-Logmans, S. C.; van Putten, W. L.; Klijn, J. G. *J. Clin. Oncol.* **1998,** *16,* 1013–1021.
23. Ebert, M. P. A.; Krüger, S.; Fogeron, M.-L.; Lamer, S.; Chen, J.; Pross, M.; Schulz, H.-U.; Lage, H.; Heim, S.; Roessner, A.; Malfertheiner, P.; Röcken, C. *Proteomics* **2005,** *5,* 1693–1704. doi:10.1002/pmic.200401030
24. Miller, K.; Erez, R.; Segal, E.; Shabat, D.; Satchi-Fainaro, R. *Angew. Chem., Int. Ed.* **2009,** *48,* 2949–2954. doi:10.1002/anie.200805133
25. Aletras, A.; Barlos, K.; Gatos, D.; Koutsogianni, S.; Mamos, P. *Int. J. Pept. Protein Res.* **1995,** *45,* 488–496. doi:10.1111/j.1399-3011.1995.tb01065.x
26. Myrberg, H.; Zhang, L.; Mäe, M.; Langel, Ü. *Bioconjugate Chem.* **2008,** *19,* 70–75. doi:10.1021/bc0701139
27. Takeuchi, T.; Kosuge, M.; Tadokoro, A.; Sugiura, Y.; Nishi, M.; Kawata, M.; Sakai, N.; Matile, S.; Futaki, S. *ACS Chem. Biol.* **2006,** *1,* 299–303. doi:10.1021/cb600127m
28. Kwon, M.-K.; Nam, J.-O.; Park, R.-W.; Lee, B.-H.; Park, J.-Y.; Byun, Y.-R.; Kim, S.-Y.; Kwon, I.-C.; Kim, I.-S. *Mol. Cancer Ther.* **2008,** *7,* 1514–1522. doi:10.1158/1535-7163.MCT-07-2009
29. Futaki, S.; Niwa, M.; Nakase, I.; Tadokoro, A.; Zhang, Y.; Nagaoka, M.; Wakako, N.; Sugiura, Y. *Bioconjugate Chem.* **2004,** *15,* 475–481. doi:10.1021/bc034181g
30. Rennert, R.; Wespe, C.; Beck-Sickinger, A. G.; Neundorf, I. *Biochim. Biophys. Acta, Biomembr.* **2006,** *1758,* 347–354. doi:10.1016/j.bbamem.2005.10.006

License and Terms

Beilstein Journal of Organic Chemistry

Peptides presenting the binding site of human CD4 for the HIV-1 envelope glycoprotein gp120

Julia Meier[1], Kristin Kassler[2], Heinrich Sticht[2] and Jutta Eichler[*1]

Full Research Paper

Open Access

Address:
[1]Department of Chemistry and Pharmacy, Universität Erlangen-Nürnberg, Schuhstrasse 19, 91052 Erlangen, Germany and [2]Institute of Biochemistry, Universität Erlangen-Nürnberg, Fahrstrasse 17, 91054 Erlangen, Germany

Email:
Jutta Eichler[*] - jutta.eichler@medchem.uni-erlangen.de

* Corresponding author

Keywords:
biomimetic synthesis; CD4; HIV entry; peptide; protein binding site

Beilstein J. Org. Chem. **2012,** *8,* 1858–1866.
doi:10.3762/bjoc.8.214

Received: 08 July 2012
Accepted: 24 September 2012
Published: 31 October 2012

This article is part of the Thematic Series "Antibiotic and cytotoxic peptides".

Guest Editor: N. Sewald

Abstract

Based on the structure of the HIV-1 glycoprotein gp120 in complex with its cellular receptor CD4, we have designed and synthesized peptides that mimic the binding site of CD4 for gp120. The ability of these peptides to bind to gp120 can be strongly enhanced by increasing their conformational stability through cyclization, as evidenced by binding assays, as well as through molecular-dynamics simulations of peptide–gp120 complexes. The specificity of the peptide–gp120 interaction was demonstrated by using peptide variants, in which key residues for the interaction with gp120 were replaced by alanine or D-amino acids.

Introduction

Synthetic molecules that have the ability to mimic binding and/or functional sites of proteins are useful tools for exploring and modulating protein function, as they interfere with binding events underlying the protein function. Furthermore, such mimetic molecules are promising candidates for the inhibition of protein–protein interactions. Synthetic peptides can be produced as direct reproductions of protein fragments and by diverse chemical modification, including the integration of non-proteinogenic amino acids, and the modification of the peptide backbone. Such modifications widen the chemical and structural diversity exhibited by peptides, as well as improve their proteolytic stability, increasing their prospects for pharmaceutical use. Therefore, peptides are excellent candidates as protein binding site mimics. We have previously developed strategies for the design and generation of scaffolded and assembled peptides to generate protein binding site mimics [1].

The interaction of the HIV-1 envelope glycoprotein gp120 with its cellular receptor CD4 is the first step in the process of entry of the virus HIV-1 into its host cell. A range of crystal structures of the gp120–CD4 complex [2-6] have provided information on the structural details of the gp120–CD4 interaction and,

thus, the basis for a rational design of inhibitors. Later on, it was found that the epitopes of a range of broadly neutralizing anti-HIV-1 antibodies, such as mAb b12 [7] and mAb VRC01 [8], overlap the CD4 binding site (CD4bs) of gp120, making this region of gp120 an important target for immunogen design. Therefore, we have previously designed and generated a synthetic peptide that presents the CD4bs fragments of gp120 [9]. This peptide is recognized by CD4, as well as by mAbs b12 and VRC01.

The receptor glycoprotein CD4 is composed of four extracellular immunoglobulin domains (D1–D4), a short cytoplasmatic tail, and a single transmembrane helix [10]. Gp120 contacts the CD4 D1 domain, which forms a stable eight-stranded beta-sheet [3] (Figure 1). The 22 residues of CD4 that contact 26 amino acids of gp120 [3] are located in the N-terminus of CD4 D1 (residues 22–64). Hot spots of CD4 for its interaction with gp120 include F43 at the tip of the CDR2-like loop, which contacts the CD4 binding site of gp120. Ionic interactions of R59 of CD4 with D368 of gp120 stabilize this interaction [3] (Figure 1). Mutation of F43 and R59 to alanine or glycine [11-14] dramatically impairs binding to gp120, corroborating the importance of F43 and R59 for the interaction of CD4 with gp120.

Molecules that are capable of inhibiting the CD4–gp120 interaction are promising candidates for HIV-1-entry inhibitors, an upcoming class of AIDS therapeutics that offer an alternative to the clinically established anti-HIV-1 drugs, which are mainly inhibitors of HIV-1-encoded enzymes (protease, reverse transcriptase and integrase). During recent years, a range of structurally different CD4 mimetic molecules have been presented. These include small molecules [15-18] as well as stably folded miniproteins, which were mutated to present a putative binding site for gp120 [19-21].

We have recently shown that synthetic peptides mimicking the gp120 binding sites of human and murine CD4 can be used as molecular tools to elucidate the structural basis for the species selectivity of the CD4–gp120 interaction [22]. We have now focused on peptides mimicking the binding site of human CD4, and on their interaction with gp120.

Results and Discussion

Peptide design and synthesis

Based on the resolved 3D structure of the gp120–CD4 complex, we have designed peptides that present the binding site of CD4 for gp120, i.e., residues 22–64 (Table 1). Apart from the peptides covering this complete CD4 stretch (CD4-M1), we generated a truncated peptide presenting only the CDR2-like loop of CD4 (residues 34–48, CD4-M4). Since the N- and C-termini of CD4-M1 and CD4-M4 are in fairly close proximity in the CD4-gp120 complex [3], as evidenced by the short distances between S23 and D63 (4.6 Å) as well as between I34

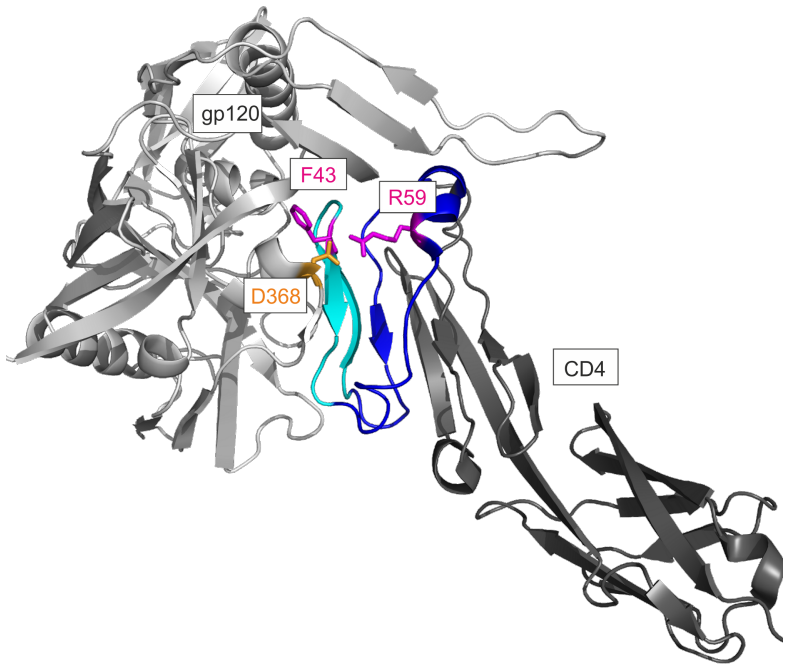

Figure 1: Structural details of the CD4–gp120 complex (pdb 1rzj). The binding site of CD4 for gp120 is shown in blue (residues 22–33 and 49–64) and in cyan (CDR2-like loop, residues 34–48). The key residues for the interaction with gp120 (F43 and R59) are depicted in purple, and the contact residue D368 of gp120 in yellow.

Table 1: Peptide sequences.

Peptide	CD4-residues	Sequence
CD4-M1	22–64, linear	Ac-His_6[a]-X[b]KSIQFHWKNSNQIKILGNQGSFLTKGPSKLNDRADSRRSLWDQ-NH_2
CD4-M2	22–64, cyclic, S23C, D63C	Ac-His_6-XK[CIQFHWKNSNQIKILGNQGSFLTKGPSKLNDRADSRRSLWC]Q-NH_2
CD4-M3	22–64, cyclic, F43A, R58A, R59A, S23C, D63C	Ac-His_6-XK[CIQFHWKNSNQIKILGNQGSALTKGPSKLNDRADSRASLWC]Q-NH_2
CD4-M4	34–48, linear	Ac-His_6-XIKILGNQGSFLTKGP-NH_2
CD4-M5	34–48, cyclic	Ac-His_6-X[CB[c]IKILGNQGSFLTKGPBC]-NH_2
CD4-M6	34–48, cyclic, F43A	Ac-His_6-X[CBIKILGNQGSALTKGPBC]-NH_2
CD4-M7	34–48, cyclic, F43-D-Phe	Ac-His_6-X[CBIKILGNQGS-DPhe-LTKGPBC]-NH_2

[a]His_6, hexahistidine tag; [b]X, ε-aminohexanoic acid; [c]B, β-alanine. Brackets indicate a disulfide bridge between cysteine residues. All residues that are part of CD4 are shown in bold face and blue (residues 22–33 and 49–64) or cyan (CDR2-like loop). The hot spot residues F43 and R59, or their substitutes, are shown in red.

and P48 (10.6 Å), we also generated peptides in which this proximity is covalently stabilized. This was achieved by means of a disulfide bridge between cysteine residues, which were introduced either by replacing S23 and D63 with cysteine (CD4-M2 and CD4-M3), or by being added to either side of the CD4 sequence (CD4-M5, CD4-M6 and CD4-M7). Furthermore, variants CD4-M2 and CD4-M5 were synthesized in which the key amino acids for the interaction with gp120 (F43 and R59) were replaced by alanine (CD4-M3 and CD4-M6). In CD4-M3, we also replaced the adjacent R58 by alanine in order to avoid functional compensation for the loss of R59 by R58. Finally, we probed the stereoselectivity of the peptide–gp120 interaction by replacing F43 in CD4-M5 by D-phenylalanine (CD4-M7). All peptides were equipped with an N-terminal hexahistidine tag for directed attachment to Ni-NTA assay plates. The tag, as well as the additional cysteine residues in CD4-M5, CD4-M6 and CD4-M7, was separated from the CD4 sequences by the spacer amino acids ε-aminohexanoic acid (X) and β-alanine (B). All peptides were generated through solid-phase synthesis and purified by preparative HPLC (Figure 2 and Experimental section).

Peptide binding to gp120

The seven CD4-derived peptides (Table 1) were tested in an ELISA type binding assay for their ability to bind to recombinant gp120 from HIV-1 strain IIIB (Figure 3, left). Of the two linear peptides (CD4-M1 and CD4-M4), only the longer peptide CD4-M1 is recognized by gp120, illustrating the importance of the salt bridge R59 for the stabilization of the interaction of the CDR2-like loop of CD4 with gp120, as CD4-M4 lacks this residue. Covalent stabilization of the spatial proximity between the N- and C-termini of peptides CD4-M1 and CD4-M4 through a disulfide bridge in the cyclic peptides CD4-M2 and CD4-M5 appears to stabilize the gp120-bound conformation, since binding of both peptides to gp120 was strongly enhanced, as compared to their linear, more flexible counterparts. The specificity of this interaction could be demonstrated by using analogues of CD4-M2 and CD4-M5, in which the key residues for the interaction with gp120, (F43 and R59), were replaced by alanine (CD4-M3 and CD4-M6, respectively). Binding of these alanine variants to gp120 was largely abrogated, indicating that the mode of binding of CD4-M2 and CD4-M5 to gp120 is related to that of CD4. Likewise, an analogue of CD4-M5, in which F43 was replaced by D-phenylalanine (CD4-M7), did not bind to gp120, most likely because the incorrect orientation of the phenyl side chain of this amino acid precludes its interaction with D368 and E370 of gp120, which are key residues of the CD4 binding site of gp120. The differences in affinity to gp120 between the cyclic peptides CD4-M2 and CD4-M5 on

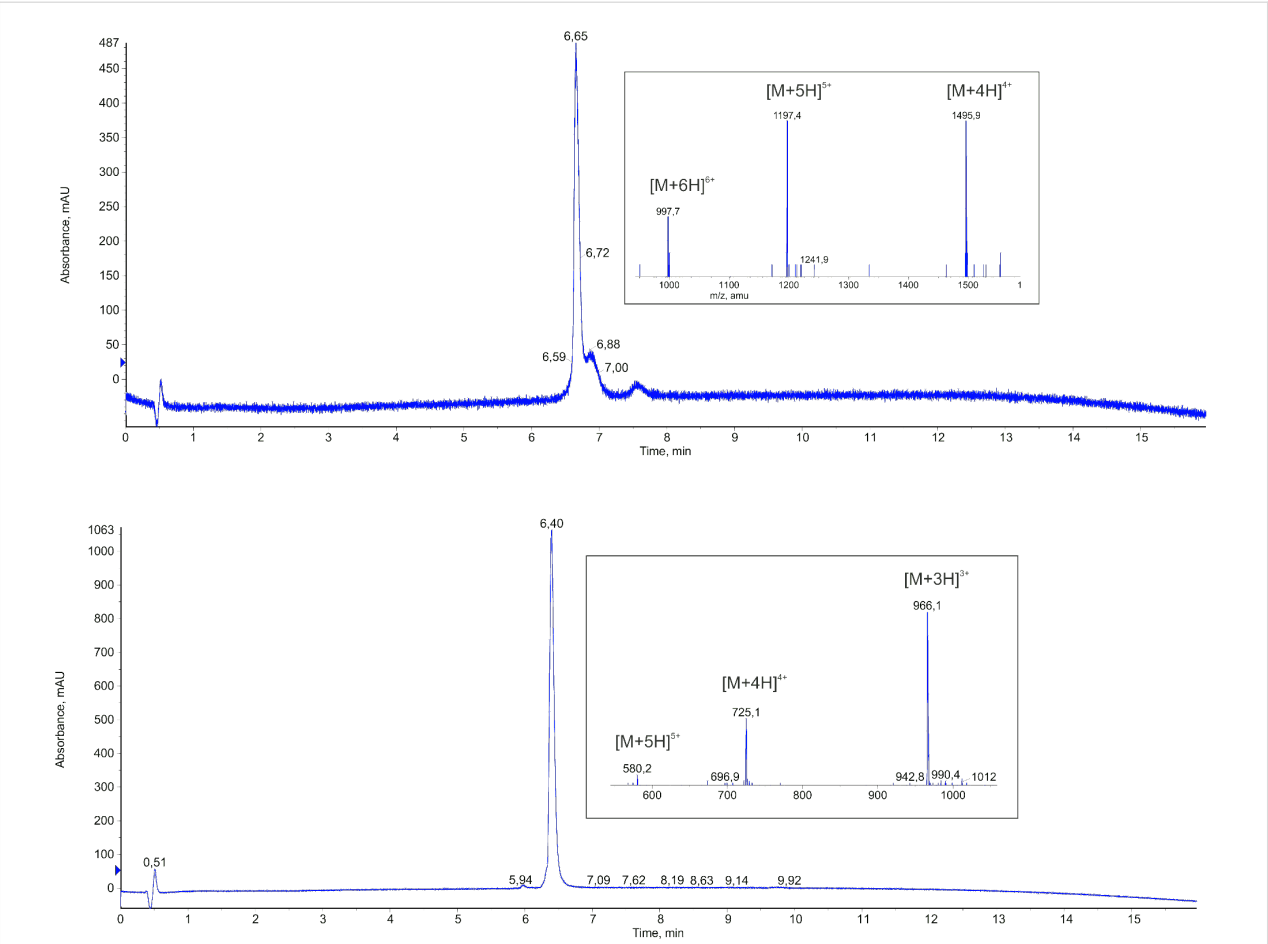

Figure 2: HPLC chromatograms and ion masses from the ESI-mass spectra (insets) of purified CD4-M2 (M = 5979.83, top) and CD4-M5 (M = 2896.4, bottom).

one hand, and their alanine substitution variants CD4-M3 and CD4-M6 on the other hand, could also be shown in a more quantitative fashion by dose-dependent binding of gp120 (Figure 3, left).

In a separate binding assay, we addressed the interaction of HIV-1 with cellular coreceptors. This interaction is induced by binding of gp120 to cellular CD4, which triggers a conformational rearrangement of gp120, resulting in the exposure

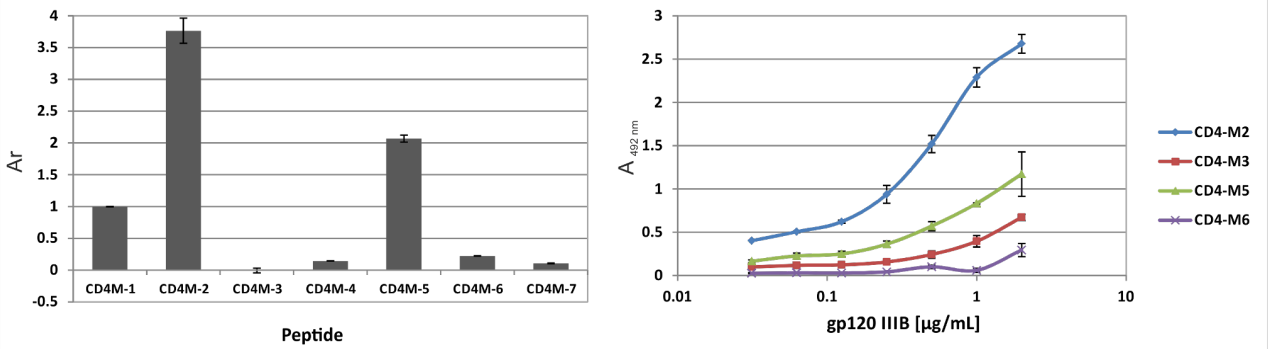

Figure 3: Left: Relative affinities (A_r, CD4-M1 = 1) to gp120(IIIB) of peptides. Right: Concentration-dependent binding of gp120 to peptides. Absorbance values (A) are corrected for the respective blanks (wells without peptide). See Table 1 for peptide sequences and Experimental section for details of the binding assay.

of its coreceptor binding site [23]. Such binding enhancement could also be demonstrated in binding assays involving recombinant proteins, i.e., gp120, and soluble CD4 (sCD4) presenting the extracellular CD4 domains, in conjunction with the use of antibodies that recognize the coreceptor binding site of gp120 (CD4i antibodies) as coreceptor surrogates [8]. Similar to sCD4, the cyclic peptide CD4-M5, which presents the CDR2-like loop of CD4, is able to enhance binding of gp120 to the CD4i antibody mAb X5 [24] (Figure 4), providing further indication of a functional mimicry of CD4 by the mimetic peptides.

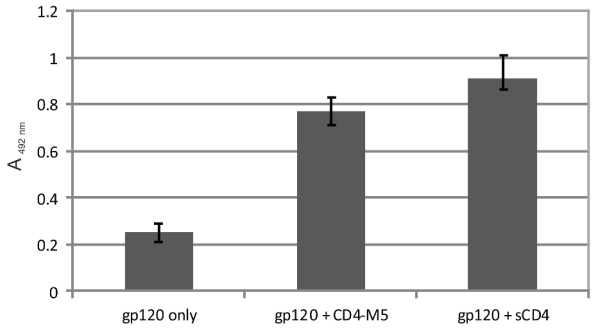

Figure 4: Enhancement of binding of gp120(MN) to the CD4i antibody X5 by CD4-M5 and sCD4, respectively. See Experimental section for details of the binding assay.

Comformational stability of gp120-peptide complexes

To investigate the conformational stability and binding properties of CD4-M1 and CD4-M2, molecular dynamics (MD) simulations of the peptides in complex with gp120 were carried out and compared to a simulation of the CD4–gp120 complex. Analysis confirmed that the linear peptide CD4-M1 is more flexible than the respective region in CD4 (Figure 5A) because it lacks the stabilizing interactions contributed by the remaining parts of intact CD4 (Figure 1).

Interestingly, the introduction of a disulfide bridge between C23 and C63 in CD4-M2 re-establishes the rigidity present in the CD4–gp120 complex. This is evident from the conformational stability shown in Figure 5A and the per-residue fluctuations shown in Figure 5B. In both types of analysis, the cyclic peptide CD4-M2 is significantly more stable than the linear peptide CD4-M1, with a conformational stability similar to the respective region in CD4. The larger flexibility of CD4-M1 also becomes evident from a visual analysis of the structures over time (Figure 6). Regions of enhanced fluctuation comprise the CC'-loop, both termini, and the C-terminal stretch containing two short 3_{10}-helices (Figure 5B and Figure 6A). Hence, it appears that the introduction of a disulfide bridge between the N- and C-terminus in CD4-M2 stabilizes not only the termini but also other flexible regions of the peptide, suggesting a global stabilization of the peptide (Figure 6B). The overlays shown in Figure 6B and Figure 6C again demonstrate that the conformational rigidity of gp120-bound CD4-M2 is similar to that of the respective region in CD4.

Another observation from the binding assay was the complete loss of binding of the triple alanine mutants (F43A, R58A, R59A) of CD4-M2 (peptide CD4-M3). Analysis of the interactions formed by these residues over the simulation time shows that F43 and R59 preserve the stable interactions with gp120

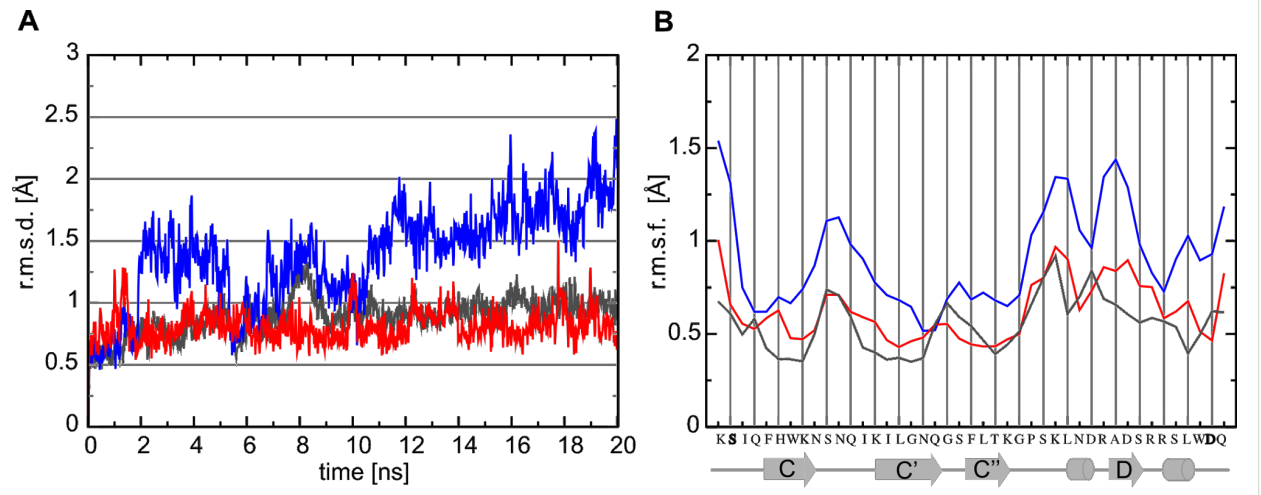

Figure 5: Conformational stability of CD4 mimetic peptides in complex with gp120 during 20 ns of MD simulation. Results are shown in blue (CD4-M1) and red (CD4-M2), respectively. For comparison, the respective sequence region has also been analysed for the CD4–gp120 complex (black). (A) Root-mean-square deviation of the peptides and CD4 over simulation time. (B) Root-mean-square fluctuation of individual residues measured for backbone atoms averaged over time. Residues replaced by cysteine in CD4-M2 are indicated in bold face. Secondary structure elements are assigned below the plot.

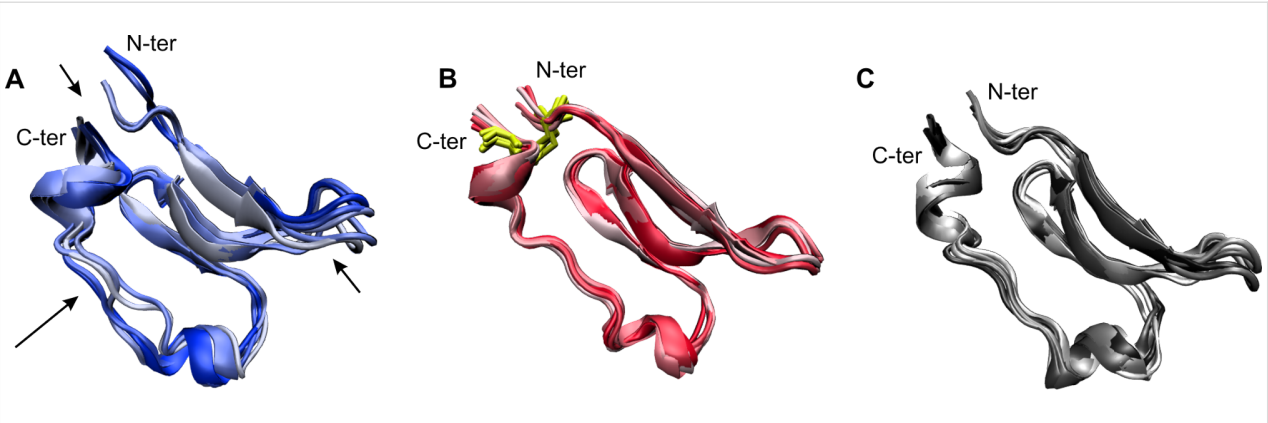

Figure 6: Structural presentation of peptide motions in the gp120-bound state during the MD simulation. (A) CD4-M1, (B) CD4-M2, (C) respective sequence stretch of CD4 (the remaining part of CD4 has been omitted for simplicity in this plot). The disulfide bridge that fixes N- and C-termini in CD4-M2 is represented by yellow sections. Arrows indicate regions in CD4-M1 that show enhanced fluctuation during simulation, namely the N- and C-termini, the CC'-loop and the stretch between the short 3_{10}-helixes upstream of the C-terminus.

that are present in the gp120–CD4 complex (Figure 1), while R58 does not significantly contribute to binding in any of the simulations. The importance of F43 and R59 for peptide binding also supports the notion that both peptides bind specifically to the CD4 binding site of gp120.

Conclusion

The binding behaviour of synthetic CD4 mimetic peptides was shown to be strongly related to their conformational flexibility, as demonstrated by binding assays in conjunction with molecular-dynamics simulations. These results illustrate the utility of peptide mimics of protein binding sites as molecular tools to explore the molecular and structural basis of protein–protein interactions. Furthermore, this strategy may be potentially useful for the structure-based design of synthetic protein-binding-site mimics by improving the conformational stability of the mimetic peptides, which in turn will increase their affinity to the complementary protein, and, consequently, their ability to interfere with the native protein–protein interaction.

Experimental

Peptide synthesis

Peptides were synthesized as C-terminal amides by Fmoc/*t*-Bu-based solid-phase synthesis on 100 mg TentaGel S RAM resin (0.23 mmol/g) by using an automated multiple peptide synthesizer (SYRO from MultiSynTech), as previously described [25]. In a standard coupling cycle, five equiv of Fmoc-amino acid/*N*,*N*'-diisopropylcarbodiimide/*N*-hydroxybenzotrialzole in DMF were coupled twice for 60 min, followed by a capping step using a mixture of acetic anhydride/pyridine/DMF (1:2:3; 30 min). The Fmoc group was removed by using 20% piperidine/DMF (20 min). After completing the sequence, the N-terminal amino group was acetylated. Peptides were cleaved from the resin by using Reagent K (TFA/water/phenol/thioanisole/1,2-ethanedithiol; 82.5:5:5:5:2.5), precipitated in a cold 1:1 mixture of cyclohexane and tert-butyl methyl ether, extracted with water, lyophilized twice, and purified by preparative HPLC (conditions: column: Dr. Maisch Reprosil 100, 250 × 20 mm, flow rate: 9 mL/min, gradient: 35–45% ACN in H_2O (both containing 0.1% TFA) in 40 min and UV detection at 216 nm). Disulfide bridges were formed by oxidizing the peptides (0.25 mg/mL in 50% ACN in 0.1 M ammonium acetate, pH 8) at room temperature with slight shaking until free thiol groups were no longer detectable by Ellman's reagent. Oxidized peptides were purified again as described above. Peptides were characterized by analytical HPLC with online ESI mass spectrometry detection (LC–MS). Conditions: column: Phenomenex Kinetex 2.6 µM C18 100 Å, 50 × 2.1 mm, flow rate: 0.4 mL/min, gradient: 5–95% ACN in H_2O (both containing 0.05% TFA) in 15 min (see Table 2 for mass spectrometry data).

Binding assays

Direct ELISA (Figure 3): The following buffers were used: Coupling buffer: 0.01 M KCl; blocking buffer: 5% BSA in 0.1 M phosphate buffer pH 7.2; sample buffer: 0.1% BSA and 0.01% Tween 20 in 0.1 M phosphate buffer pH 7.2; washing buffer: phosphate buffer pH 7.2 containing 0.01% Tween 20. Antibody buffer: Phosphate buffer pH 7.2 containing 1% BSA and 0.1% Tween 20. The wells of 96-well Ni-Chelate plates from Thermo Scientific were coated overnight at 4 °C with peptide solution (100 µL, 4 µM in coupling buffer). After unspecific binding had been blocked with a blocking buffer (1 h at room temperature, gentle agitation), the plates were washed twice. Plates were then incubated for 2 h with 100 µL/well gp120(IIIB) from ImmunoDiagnostics at 0.25 µg/mL (Figure 3, left), or in serial dilutions starting at 2 µg/mL (Figure 3, right) in sample buffer, and washed four times. Following incubation

Table 2: ESI-mass spectrometry data of peptides.

Peptide	M_{calc}	$[M + 2H]^{2+}$	$[M + 3H]^{3+}$	$[M + 4H]^{4+}$	$[M + 5H]^{5+}$	$[M + 6H]^{6+}$	$[M + 7H]^{7+}$	$[M + 8H]^{8+}$
CD4-M1	5977.72			1494.9	1196.0	996.8	854.3	748.1
CD4-M2	5979.83			1495.9	1197.4	997.7	855.3	748.6
CD4-M3	5733.51			1433.5	1147.1	956.2		
CD4-M4	2550.0	1275.7	851.0	638.3	510.8			
CD4-M5	2896.4	1448.4	966.1	725.1	580.2			
CD4-M6	2707.14	1354.6	903.4	677.8	542.9			
CD4-M7	2896.4	1448.6	966.3	725.1	580.4			

with 100 µL/well sheep-anti-HIV-1-gp120 (D7324) from Aalto Bio Reagents (1:5000 in antibody buffer) for 1 h at room temperature, plates were washed four times with washing buffer, incubated for 1 h at room temperature with 100 µL/well rabbit-anti-sheep-IgG peroxidase conjugate from Dianova (diluted 1:5000 with antibody buffer), and washed four times with washing buffer. Plates were developed with 100 µL/well substrate solution (1 mg/mL OPD in 0.03% H_2O_2/H_2O) in the dark (approx. 20 min), and the reaction was stopped by addition of 2 M sulfuric acid (50 µL/well). Absorbances (A) were read at 492 nm by using a multichannel photometer (Infinite F200 from Tecan).

Relative Affinities (A_r) were calculated according to the following formula:

$$A_r = (A_{peptide} - A_{blank}) / (A_1 - A_{blank})$$

in which A_1 is the absorbance of a well coated with CD4-M1, and A_{blank} is the absorbance of a well without any peptide.

Enhancement Assay (Figure 4): The following buffers were used: Coating buffer: 0.1 M Na_2CO_3, pH 9.5; blocking buffer: 1% BSA in 0.1 M phosphate buffer pH 7.2; sample buffer: 0.1% BSA and 0.01% Tween 20 in 0.1 M phosphate buffer pH 7.2; washing buffer: phosphate buffer pH 7.2 containing 0.01% Tween 20. The wells of 96-well Immulon 2HB plates from Thermo Labsystems were coated overnight at 4 °C with 100 µL mAb X5 (0.25 µg/mL in coating buffer). After unspecific binding had been blocked with blocking buffer (1 h at room temperature), the plates were washed twice. CD4-M5 (50 µL, 60 µM) or sCD4 from SinoBiologicals (50 µL, 0.4 µg/mL) was pre-incubated with gp120(MN) from Immune Technology (50 µL, 0.5 µg/mL) for 10 min. Then the pre-incubated mixture of gp120(MN) with CD4-M5 or sCD4 was added to the X5-coated plate, incubated for 2 h, washed four times, and developed as described above. Absorbances (A) were read at 492 nm, and corrected for the respective blanks (wells without X5). All binding assays were performed at least twice, each time in duplicate.

MD simulation

Computational analysis included modelling of peptide–gp120 complexes followed by molecular dynamics simulation to study the stability and dynamics of the respective complexes. Three gp120-complexes were investigated: gp120 in complex with CD4-M1 and CD4-M2, as well as with CD4. All protein structures were derived from the crystal structure [3], which was treated as explained in the following. First, the gp120-CD4 part was extracted and the nonresolved V4 loop of gp120 was added by using SwissModel [26]. Shortened loops V1, V2 and V3 of gp120 were treated according to the crystal structure. This procedure yielded the setup structure for the full length CD4–gp120 complex, from which all CD4 residues except 22–64 were deleted to obtain the starting structure for the linear peptide CD4-M1. To obtain the complex for CD4-M2, mutations of S23C and D63C and the connecting disulfide bridge were additionally introduced by using Sybyl 7.3 [27]. Final system preparation and MD simulation were carried out according to standard approaches [22,28] by using the software package AMBER [29-31] with the ff99SB force field [32]. Following neutralization with an appropriate number of chloride ions, each protein complex was placed in a standard TIP3P water box [33] with at least 12 Å space to the box boundaries. Energy minimization, heating and equilibration were carried out as explained previously [22]. Subsequently, all complexes were subjected to 100 ns simulation at 310 K with boundary conditions and a 2 fs time step by using SHAKE [34]. Analysis was based on a total of 1000 structures taken from the final 20 ns of the MD simulation at an interval of 20 ps.

Acknowledgements

This work was supported by SFB 796 (Projects A2 and A5) from the German Research Foundation (DFG). We thank Dennis Burton (Scripps Research Institute, La Jolla) for kindly providing mAb X5.

References

1. Eichler, J. *Curr. Opin. Chem. Biol.* **2008,** *12,* 707–713. doi:10.1016/j.cbpa.2008.09.023
2. Kwong, P. D.; Wyatt, R.; Robinson, J.; Sweet, R. W.; Sodroski, J.; Hendrickson, W. A. *Nature* **1998,** *393,* 648–659. doi:10.1038/31405
3. Huang, C.-c.; Venturi, M.; Majeed, S.; Moore, M. J.; Phogat, S.; Zhang, M.-Y.; Dimitrov, D. S.; Hendrickson, W. A.; Robinson, J.; Sodroski, J.; Wyatt, R.; Choe, H.; Farzan, M.; Kwong, P. D. *Proc. Natl. Acad. Sci. U. S. A.* **2004,** *101,* 2706–2711. doi:10.1073/pnas.0308527100
4. Kwong, P. D.; Wyatt, R.; Majeed, S.; Robinson, J.; Sweet, R. W.; Sodroski, J.; Hendrickson, W. A. *Structure* **2000,** *8,* 1329–1339. doi:10.1016/S0969-2126(00)00547-5
5. Pancera, M.; Majeed, S.; Ban, Y.-E.; Chen, L.; Huang, C. C.; Kong, L.; Kwon, Y. D.; Stuckey, J.; Zhou, T.; Robinson, J. E.; Schief, W. R.; Sodroski, J.; Wyatt, R.; Kwong, P. D. *Proc. Natl. Acad. Sci. U. S. A.* **2010,** *107,* 1166–1171. doi:10.1073/pnas.0911004107
6. Huang, C.-c.; Tang, M.; Zhang, M.-Y.; Majeed, S.; Montabana, E.; Stanfield, R. L.; Dimitrov, D. S.; Korber, B.; Sodroski, J.; Wilson, I. A.; Wyatt, R.; Kwong, P. D. *Science* **2005,** *310,* 1025–1028. doi:10.1126/science.1118398
7. Zhou, T.; Xu, L.; Dey, B.; Hessell, A. J.; Van Ryk, D.; Xiang, S. H.; Yang, X.; Zhang, M. Y.; Zwick, M. B.; Arthos, J.; Burton, D. R.; Dimitrov, D. S.; Sodroski, J.; Wyatt, R.; Nabel, G. J.; Kwong, P. D. *Nature* **2007,** *445,* 732–737. doi:10.1038/nature05580
8. Wu, X.; Yang, Z.-Y.; Li, Y.; Hogerkorp, C. M.; Schief, W. R.; Seaman, M. S.; Zhou, T.; Schmidt, S. D.; Wu, L.; Xu, L.; Longo, N. S.; McKee, K.; O'Dell, S.; Louder, M. K.; Wycuff, D. L.; Feng, Y.; Nason, M.; Doria-Rose, N.; Connors, M.; Kwong, P. D.; Roederer, M.; Wyatt, R. T.; Nabel, G. J.; Mascola, J. R. *Science* **2010,** *329,* 856–861. doi:10.1126/science.1187659
9. Franke, R.; Hirsch, T.; Overwin, H.; Eichler, J. *Angew. Chem., Int. Ed.* **2007,** *46,* 1253–1255. doi:10.1002/anie.200603274
10. Ryu, S.-E.; Kwong, P. D.; Truneh, A.; Porter, T. G.; Arthos, J.; Rosenberg, M.; Dai, X.; Xuong, N.-H.; Axel, R.; Sweet, R. W.; Hendrickson, W. A. *Nature* **1990,** *348,* 419–426. doi:10.1038/348419a0
11. Ryu, S.-E.; Truneh, A.; Sweet, R. W.; Hendrickson, W. A. *Structure* **1994,** *1,* 59–74. doi:10.1016/S0969-2126(00)00008-3
12. Arthos, J.; Deen, K. C.; Chaikin, M. A.; Fornwald, J. A.; Sathe, G.; Sattentau, Q. J.; Clapham, P. R.; Weiss, R. A.; McDougal, J. S.; Pietropaolo, C.; Axel, R.; Trumeh, A.; Maddon, P. J.; Sweet, R. W. *Cell* **1989,** *57,* 469–481. doi:10.1016/0092-8674(89)90922-7
13. Moebius, U.; Clayton, L. K.; Abraham, S.; Harrison, S. C.; Reinherz, E. L. *J. Exp. Med.* **1992,** *176,* 507–517. doi:10.1084/jem.176.2.507
14. Ashkenazi, A.; Presta, L. G.; Marsters, S. A.; Camerato, T. R.; Rosenthal, K. A.; Fendly, B. M.; Capon, D. J. *Proc. Natl. Acad. Sci. U. S. A.* **1990,** *87,* 7150–7154. doi:10.1073/pnas.87.18.7150
15. Madani, N.; Schön, A.; Princiotto, A. M.; Lalonde, J. M.; Courter, J. R.; Soeta, T.; Ng, D.; Wang, L.; Brower, E. T.; Xiang, S.-H.; Kwon, Y. D.; Huang, C.-c.; Wyatt, R.; Kwong, P. D.; Freire, E.; Smith, A. B., III; Sodroski, J. *Structure* **2008,** *16,* 1689–1701. doi:10.1016/j.str.2008.09.005
16. LaLonde, J. M.; Kwon, Y. D.; Jones, D. M.; Sun, A. W.; Courter, J. R.; Soeta, T.; Kobayashi, T.; Princiotto, A. M.; Wu, X.; Schön, A.; Freire, E.; Kwong, P. D.; Mascola, J. R.; Sodroski, J.; Madani, N.; Smith, A. B., 3rd. *J. Med. Chem.* **2012,** *55,* 4382–4396. doi:10.1021/jm300265j
17. Narumi, T.; Ochiai, C.; Yoshimura, K.; Harada, S.; Tanaka, T.; Nomura, W.; Arai, H.; Ozaki, T.; Ohashi, N.; Matsushita, S.; Tamamura, H. *Bioorg. Med. Chem. Lett.* **2010,** *20,* 5853–5858. doi:10.1016/j.bmcl.2010.07.106
18. Yoshimura, K.; Harada, S.; Shibata, J.; Hatada, M.; Yamada, Y.; Ochiai, C.; Tamamura, H.; Matsushita, S. *J. Virol.* **2010,** *84,* 7558–7568. doi:10.1128/JVI.00227-10
19. Vita, C.; Drakopoulou, E.; Vizzavona, J.; Rochette, S.; Martin, L.; Menez, A.; Roumestand, C.; Yang, Y. S.; Ylisastigui, L.; Benjouad, A.; Gluckman, J. C. *Proc. Natl. Acad. Sci. U. S. A.* **1999,** *96,* 13091–13096. doi:10.1073/pnas.96.23.13091
20. Martin, L.; Stricher, F.; Misse, D.; Sironi, F.; Pugniere, M.; Barthe, P.; Prado-Gotor, R.; Freulon, I.; Magne, X.; Roumestand, C.; Menez, A.; Lusso, P.; Veas, F.; Vita, C. *Nat. Biotechnol.* **2003,** *21,* 71–76. doi:10.1038/nbt768
21. Huang, C.-c.; Stricher, F.; Martin, L.; Decker, J. M.; Majeed, S.; Barthe, P.; Hendrickson, W. A.; Robinson, J.; Roumestand, C.; Sodroski, J.; Wyatt, R.; Shaw, G. M.; Vita, C.; Kwong, P. D. *Structure* **2005,** *13,* 755–768. doi:10.1016/j.str.2005.03.006
22. Kassler, K.; Meier, J.; Eichler, J.; Sticht, H. *Adv. Bioinf.* **2011,** Article ID 736593. doi:10.1155/2011/736593
23. Berger, E. A.; Murphy, P. M.; Farber, J. M. *Annu. Rev. Immunol.* **1999,** *17,* 657–700. doi:10.1146/annurev.immunol.17.1.657
24. Darbha, R.; Phogat, S.; Labrijn, A. F.; Shu, Y.; Gu, Y.; Andrykovitch, M.; Zhang, M. Y.; Pantophlet, R.; Martin, L.; Vita, C.; Burton, D. R.; Dimitrov, D. S.; Ji, X. *Biochemistry* **2004,** *43,* 1410–1417. doi:10.1021/bi035323x
25. Franke, R.; Hirsch, T.; Eichler, J. *J. Recept. Signal Transduction* **2006,** *26,* 453–460. doi:10.1080/10799890600923179
26. Arnold, K.; Bordoli, L.; Kopp, J.; Schwede, T. *Bioinformatics* **2006,** *22,* 195–201. doi:10.1093/bioinformatics/bti770
27. *Sybyl,* 7.3; Tripos: St. Louis, Missouri, USA, 2008.
28. Meiselbach, H.; Sticht, H.; Enz, R. *Chem. Biol.* **2006,** *13,* 49–59. doi:10.1016/j.chembiol.2005.10.009
29. *AMBER,* 10; University of California: San Francisco, 2008.
30. *AMBER,* 9; University of California: San Francisco, 2006.
31. *AMBER,* 11; University of California: San Francisco, 2010.
32. Hornak, V.; Abel, R.; Okur, A.; Strockbine, B.; Roitberg, A.; Simmerling, C. *Proteins: Struct., Funct., Bioinf.* **2006,** *65,* 712–725. doi:10.1002/prot.21123
33. Jorgensen, W. L.; Chandrasekhar, J.; Madura, J. D.; Impey, R. W.; Klein, M. L. *J. Chem. Phys.* **1983,** *79,* 926–935. doi:10.1063/1.445869
34. Ryckaert, J.-P.; Ciccotti, G.; Berendsen, H. L. C. *J. Comput. Phys.* **1977,** *23,* 327–341. doi:10.1016/0021-9991(77)90098-5

Beilstein Journal of Organic Chemistry

Total synthesis and biological evaluation of fluorinated cryptophycins

Christine Weiß, Tobias Bogner, Benedikt Sammet and Norbert Sewald*

Full Research Paper

Open Access

Address:
Organic and Bioorganic Chemistry, Department of Chemistry, Bielefeld University, PO Box 100131, 33501 Bielefeld, Germany

Email:
Norbert Sewald* - norbert.sewald@uni-bielefeld.de

* Corresponding author

Keywords:
antimitotic drug; cytotoxicity; depsipeptide; fluorinated natural product analogues; structure-activity relationship

Beilstein J. Org. Chem. **2012,** *8,* 2060–2066.
doi:10.3762/bjoc.8.231

Received: 04 September 2012
Accepted: 09 November 2012
Published: 23 November 2012

This article is part of the Thematic Series "Antibiotic and cytotoxic peptides".

Associate Editor: D. Dixon

Abstract

Cryptophycins are cytotoxic natural products that exhibit considerable activities even against multi-drug-resistant tumor cell lines. As fluorinated pharmaceuticals have become more and more important during the past decades, fluorine-functionalized cryptophycins were synthesized and evaluated in cell-based cytotoxicity assays. The unit A trifluoromethyl-modified cryptophycin proved to be highly active against KB-3-1 cells and exhibited an IC_{50} value in the low picomolar range. However, the replacement of the 3-chloro-4-methoxyphenyl-substituent in unit B by a pentafluorophenyl moiety resulted in a significant loss of activity.

Introduction

Cryptophycins form a class of cytotoxic sixteen-membered macrocyclic depsipeptides. Cryptophycin-1 (**1**) was isolated for the first time in 1990 from cyanobacteria *Nostoc* sp. ATCC 53789 [1] (Figure 1). Moore et al. isolated cryptophycin-1 from the related *Nostoc* strain GSV 224, investigated the stereochemistry, and described the cytotoxicity [2]. At the same time Kobayashi et al. succeeded in a full structural analysis and described the first total synthesis of another member of the cryptophycin family [3,4]. Twenty-eight naturally occurring cryptophycins have been isolated up to this day [5-7], while numerous synthetic analogues have been synthesized in the frame of structure–activity-relationship studies [8,9]. Crypto-

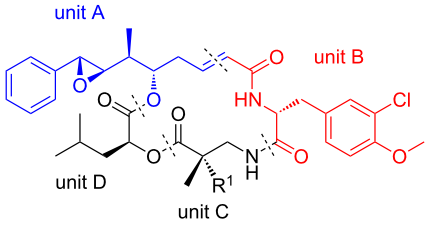

R^1 = H: cryptophycin-1 (**1**)
R^1 = Me: cryptophycin-52 (**2**)

Figure 1: Structures of cryptophycin-1 (**1**) and -52 (**2**).

phycins display remarkable biological activity against multi-drug-resistant (MDR) tumor cells. Such tumor cells express a P-glycoprotein, a drug efflux pump that transports xenobiotics out of the cell. A synthetic analogue, cryptohycin-52 (**2**, LY355703), has been investigated in clinical trials. However, this development was discontinued because of neurotoxic side effects and lacking efficacy in vivo [10,11].

Fluorinated drugs are gaining increasing importance, and currently about 20% of all pharmaceuticals on the world market contain fluorine substituents [12,13]. Fluorination is supposed to enhance bioavailability and receptor selectivity. The van der Waals-radius of a fluorine substituent (1.47 Å) lies between the value of a hydrogen substituent (1.20 Å) and an oxygen substituent (1.52 Å). However, despite this similarity in size, a fluorine substituent exerts considerable electronic effects due to the high electronegativity. A trifluoromethyl substituted analogue of epothilone, another important tubulin-binding cytotoxic drug, was shown to retain the cytotoxic activity of the parent compound. At the same time nonspecific side effects due to oxidative degradation were prevented by the introduction of the CF_3 group [14,15]. Likewise, partially fluorinated taxoids, analogues of paclitaxel and docetaxel, displayed biological activity even exceeding that of the parent nonfluorinated compounds [16]. The interesting biological profile of fluorinated cytotoxic agents prompted us to synthesize partially fluorinated analogues of cryptophycins.

The depsipeptidic character of the cryptophycins suggests four different fragments to be assembled in the total synthesis, named unit A–D (Figure 1). Unit A is an α,β-unsaturated δ-hydroxy acid that usually also contains a benzylic epoxide or a benzylic double bond. Unit B represents a chlorinated *O*-methyl-D-tyrosine derivative, while unit C is a β^2-amino acid, usually β^2-homoalanine. Finally, unit D is leucic acid, the hydroxy analogue of leucine. Numerous synthetic analogues have been obtained in the frame of structure–activity-relationship studies (SAR-studies), as reviewed in [17,18].

Unit A *para*-alkoxymethyl derivatives of cryptophycin-52 have been synthesized and were shown to retain cytotoxicity even against MDR tumor cell lines [19]. The introduction of a fluorine substituent in the same position also provides a cytotoxic analogue, albeit with decreased biological activity by a factor of 5 [8].

In unit B the chlorine and the methoxy substituents at the D-tyrosine residue were crucial for high antimitotic activity [17,18]. Moore et al. patented the synthesis of fluorinated analogues of cryptophycin-1 and cryptophycin-52 [20]. In particular, derivative **3** was shown to retain biological activity (IC_{50} = 39 pM) and was active against the tumor cell line KB-3-1 [21] (Figure 2). The chlorohydrin derived from **4** that also contained a fluorine substituent in the *para*-position of the unit A phenyl ring was patented as a promising candidate [22].

In the frame of our on-going SAR studies on cryptophycins [19,23-30], we envisaged the synthesis of analogues of cryptophycin-52 with a *para*-trifluoromethyl substituent at the unit A aryl ring. In addition, we targeted the replacement of the unit B by a D-pentafluorophenylalanine residue.

Results and Discussion

Cryptophycin-52 with a *para*-trifluoromethyl substituted unit A

The synthesis of the *para*-trifluoromethyl substituted unit A started with a modified Knoevenagel condensation [23,31]. The required aldehyde **9** was obtained by DIBAL-H reduction of the corresponding methyl ester **8** and was found to decompose upon chromatographic purification (Scheme 1). However, it can usually be employed in the Knoevenagel condensation without purification. Reaction of **9** with malonic acid in the presence of piperidine/acetic acid gave the β,γ-unsaturated carboxylic acid **10**. The latter compound was transformed into the methyl ester by treatment with $SOCl_2$ in methanol. The resulting ester **11** could then be directly employed without purification in the

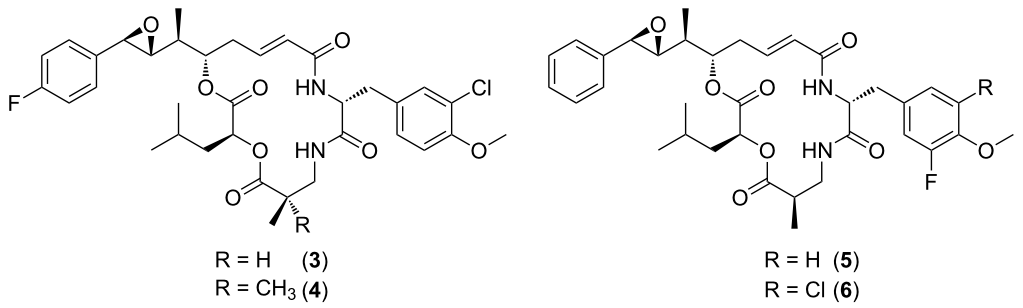

Figure 2: Fluorinated derivatives of cryptophycin-1 and -52 [20-22].

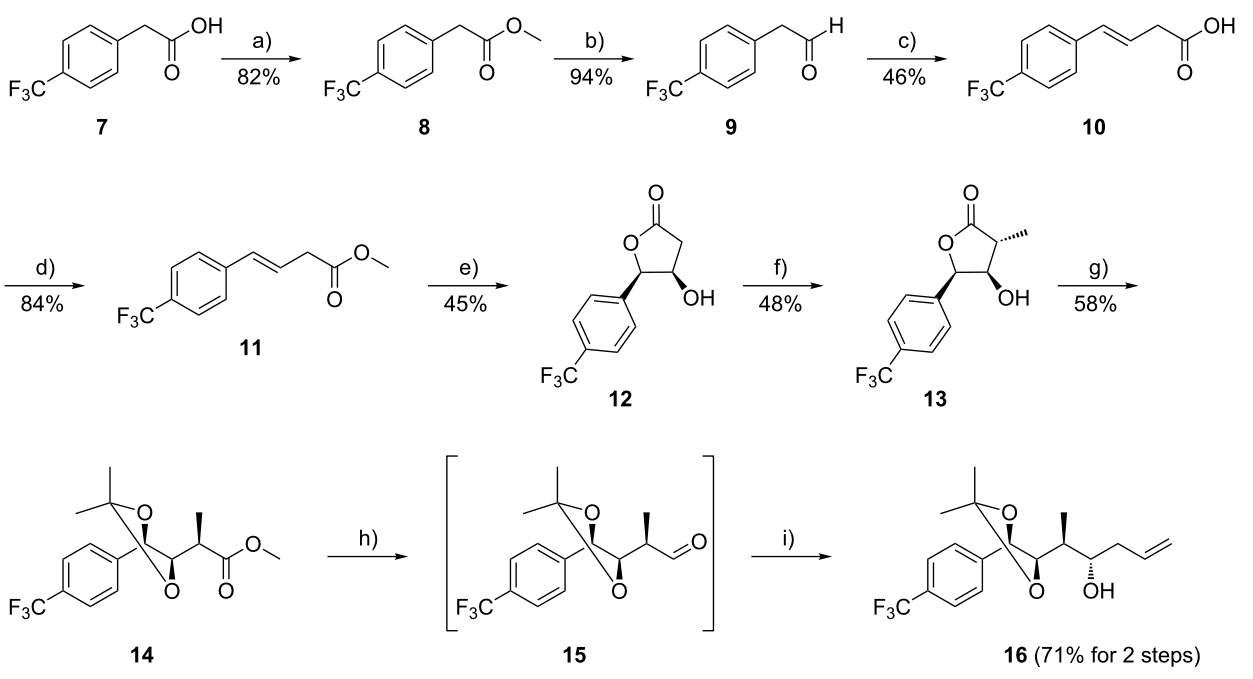

Scheme 1: Access to the trifluoromethyl substituted unit A-building block **16**. Reagents and conditions: (a) $SOCl_2$, MeOH, 0 °C → rt, 16 h; (b) DIBAL-H, CH_2Cl_2, −78 °C, 3.5 h; (c) malonic acid, piperidine, AcOH, DMSO, 65 °C, 1.5 h; (d) $SOCl_2$, MeOH, 0 °C → rt, 1 h; (e) K_2CO_3, $K_2OsO_4{\cdot}2H_2O$, $K_3[Fe(CN)_6]$, $(DHQD)_2$-PHAL, $CH_3SO_2NH_2$, *t*-BuOH/H_2O, 0 °C, 42 h; (f) LDA, MeI, THF, −78 °C, 3 d; (g) $(CH_3)_2C(OCH_3)_2$, MeOH, Amberlyst-15®, rt, 8 d; (h) DIBAL-H, CH_2Cl_2, −78 °C, 4.5 h; (i) $AllylSnBu_3$, $MgBr_2{\cdot}Et_2O$, CH_2Cl_2, −78 °C, 15 h.

asymmetric dihydroxylation with osmium tetroxide and $(DHQD)_2PHAL$, in close analogy to a previously published procedure [23]. The initially formed vicinal diol cyclizes under the reaction conditions to give lactone **12** in enantiomerically pure form (chiral HPLC: Chiralpak OD®). Deprotonation of **12** with 2.5 equiv of LDA, followed by treatment with iodomethane furnished the α-methyl substituted lactone **13**. Treatment of this compound with acetone dimethyl acetal in methanol in the presence of an acidic ion exchanger resulted in acetonide protection of the vicinal diol, accompanied by methyl ester formation. The methyl ester **14** was subsequently reduced with DIBAL-H to give the aldehyde **15**. In order to avoid epimerisation, this aldehyde was not purified, but filtered through Celite only and then reacted with allyl-tri-*n*-butyltin to give the homoallyl alcohol **16**. The magnesium bromide diethyl etherate mediated allylation proceeded under substrate control and with complete diastereoselectivity [23,32].

Cross-metathesis of homoallyl alcohol **16** with the unit B derived acrylamide **17** provided the α,β-unsaturated δ-hydroxy carboxamide **18** (Scheme 2). In order to bring about complete metathesis of **16**, the acrylamide **17** had to be employed in 1.2-fold excess, which resulted in a contamination of the cross-metathesis product **18** with minor amounts of the homo-coupling product **23**. The latter could not be separated by flash chromatography on this stage, but did not interfere with the subsequent Yamaguchi esterification of **18** with the unit C–D segment **19** and was removed on this stage [33]. Fmoc cleavage of the *seco*-depsipeptide **20** liberated the free amino group of unit C, which under the reaction conditions displaced the trichloroethylester of unit B resulting in macrocyclization according to Moher et al. [34]. In the final steps the dioxolane ring of **21** was cleaved with trifluoroacetic acid in the presence of water. The resulting vicinal diol was not purified, but reacted with a large excess of trimethyl orthoformate. The cyclic orthoester resulting from this transformation was directly subjected to reaction with acetyl bromide to form a bromohydrin formate. This was then treated with a potassium carbonate/ethylene glycol/dimethoxyethane-emulsion to bring about cleavage of the formyl ester accompanied by epoxide formation as previously described by us [19]. The trifluoromethyl substituted cryptohycin-52 analogue **22** was obtained in a yield of 39% over the final four steps. It was purified by column chromatography, followed by lyophilization.

Cryptophycin-52 with D-pentafluorophenylalanine as unit B

The *N*-acryloyl derivative **26** of D-pentafluorophenylalanine was obtained by carbodiimide esterification of commercially available Boc-D-pentafluorophenylalanine (**24**) with trichloroethanol, followed by cleavage of Boc and reaction with acryloylchloride in the presence of base [19] (Scheme 3).

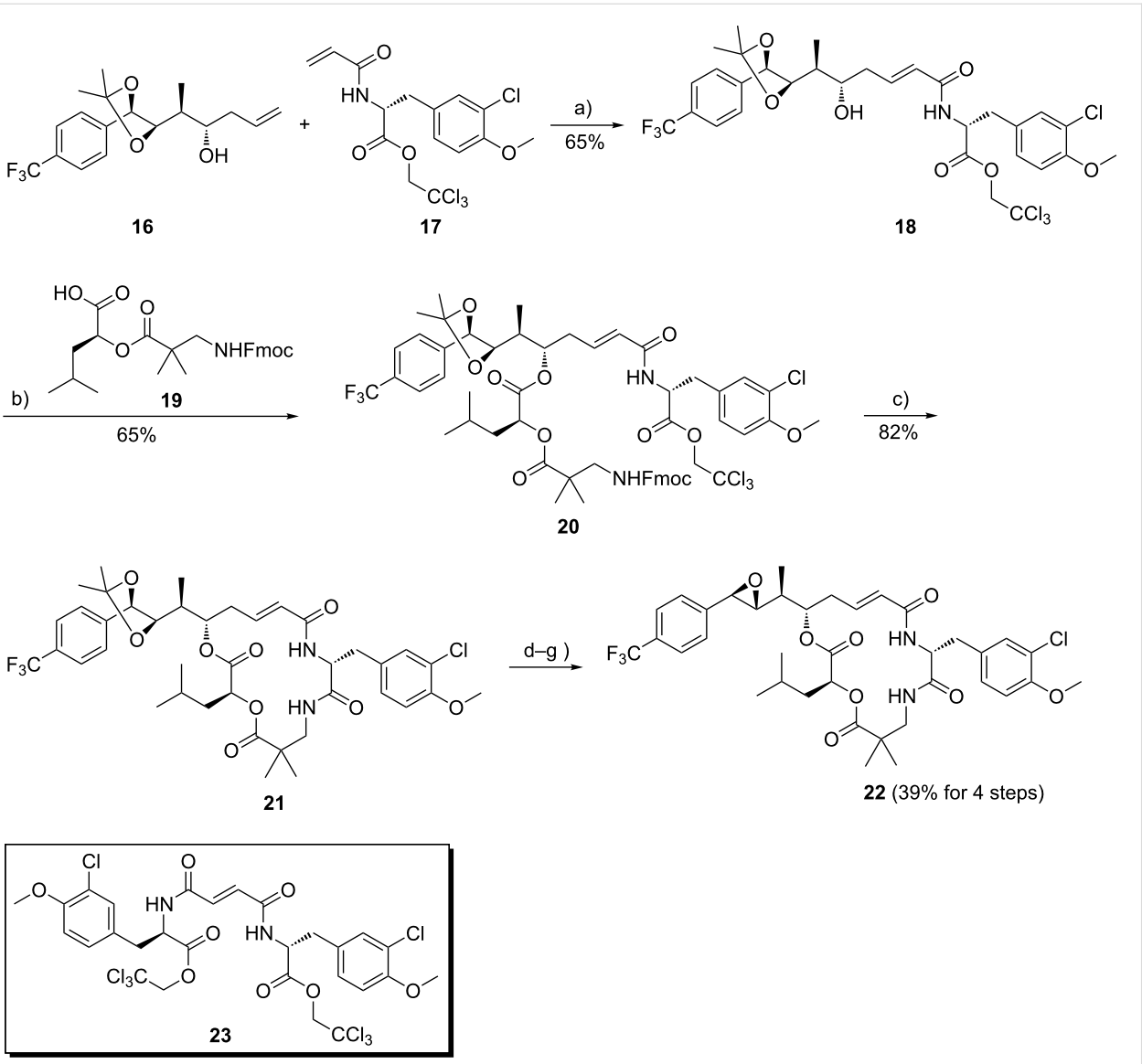

Scheme 2: Assembly of units A–D and macrocyclization, followed by diol-epoxide transformation to give the trifluoromethyl substituted analogue **22** of cryptophycin-52. Reagents and conditions: (a) Grubbs II catalyst, CH_2Cl_2, reflux, 16 h; (b) **19**, DMAP, NEt_3, 2,4,6-trichlorobenzoylchloride, THF, 0 °C, 1 h; (c) piperidine, DMF, rt, 16 h; (d) TFA, CH_2Cl_2, H_2O, 0 °C, 3 h; (e) $(CH_3O)_3CH$, PPTS, CH_2Cl_2, rt, 2 h; (f) AcBr, CH_2Cl_2, rt, 4 h; (g) K_2CO_3, DME, ethylene glycol, rt, 3 min.

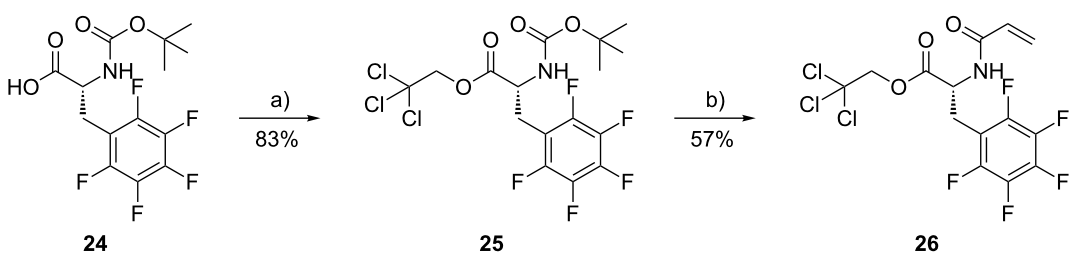

Scheme 3: Synthesis of the pentafluorophenylalanine building block **26**. Reagents and conditions: (a) pyridine, trichloroethanol, DCC, CH_2Cl_2, 0 °C, 20 h; (b) 1. TFA, rt, 2 h; 2. NEt_3, acryloylchloride, CH_2Cl_2, 0 °C, 7 h.

The cryptophycin analogue with D-pentafluorophenylalanine as unit B was synthesized by the same convergent route as described for derivative **22**. Homoallyl alcohol **27** [23] was reacted with the D-pentafluorophenylalanine derivative **26** in a cross-metathesis reaction in the presence of Grubbs II catalyst (Scheme 4). The resulting α,β-unsaturated δ-hydroxy carboxamide **28**, representing units A and B was then esterified with **19** under Yamaguchi conditions with 2,4,6-trichlorobenzoylchloride and triethylamine in the presence of catalytic amounts of DMAP. Macrocyclization was brought about by cleavage of the Fmoc protecting group from the unit C amino group, which concomitantly displaced the trichloroethylester at unit B to result in the macrocyclic product **30** [34]. Cleavage of the dioxolane liberated the vicinal diol, which was then subjected to the final diol-epoxide transformation to provide the cryptophycin-52 analogue **31** in a yield of 14% over the final four steps.

The biological activities of the fluorine-functionalized cryptophycin analogues were determined in a resazurin assay with the tumor cell line KB-3-1 and its MDR correlate KB-V1. The IC_{50} values of the fluorinated cryptophycins **22** and **31** were compared to cryptophycin-52 in Table 1 [17]. While the cytotoxicity of the unit A-modified analogue **22** against the tumor cell line KB-3-1 was only by about a factor of 4 decreased compared to cryptophycin-52, the pentafluorophenylalanine-containing derivative **31** was much less active. A significant loss in activity of both analogues against the MDR cell line KB-V1 was observed. The degree of activity against MDR tumor cells can be described by the resistance factor F_R, which

Table 1: Cytotoxicity of the fluorinated cryptophycins **22** and **31** in comparison to cryptophycin-52 (**2**).

	IC_{50} [pM] (KB-3-1)	IC_{50} [nM] (KB-V1)	F_R
2	15.5	0.26	16.7
22	66.0	10.1	153
31	2970	98.4	33

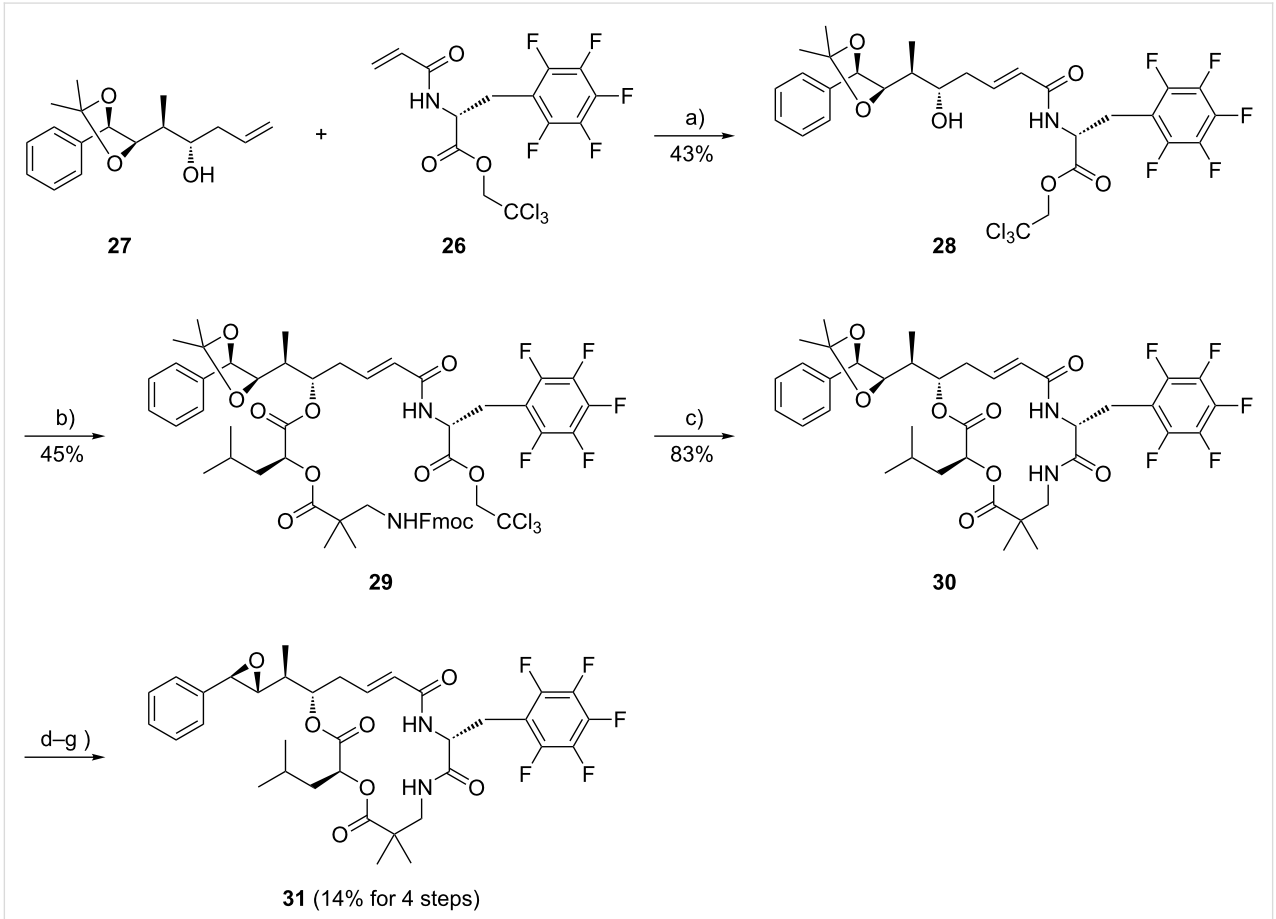

Scheme 4: Convergent synthesis of the pentafluorinated cryptophycin **31**. Reagents and conditions: (a) Grubbs II catalyst, CH_2Cl_2, reflux, 16 h; (b) **19**, DMAP, NEt_3, 2,4,6-trichlorobenzoylchloride, THF, 0 °C, 1 h; (c) piperidine, DMF, rt, 16 h; (d) TFA, CH_2Cl_2, H_2O, 0 °C, 3 h; (e) $(CH_3O)_3CH$, PPTS, CH_2Cl_2, rt, 2 h; (f) AcBr, CH_2Cl_2, rt, 4 h; (g) K_2CO_3, DME, ethylene glycol, rt, 3 min.

is defined as the ratio of the IC_{50} value for the MDR cell line and the value for the nonresistant cell line. A high F_R means a high loss of activity due to the cellular resistance mechanisms. Analogue **22** exhibited a high F_R value whereas compound **31** showed a lower loss of activity.

Conclusion

The synthesis of selectively fluorinated cryptophycin-52 analogues succeeded and both target compounds could be obtained. The two analogues were less active, both against the tumor cell line KB-3-1 and its MDR subclone KB-V1. This fact was quite surprising because the fluorinated cryptophycins were expected to display higher lipophilicity compared to the parent compound cryptophycin-52 and, therefore, exhibit equal or even higher activities. In contrast, more amphiphilic or polar compounds are usually good substrates for the P-glycoprotein efflux pump resulting in a decreased bioactivity.

Supporting Information

Supporting Information File 1

Full experimental procedures and detailed analytical data for the synthesis of all compounds.
[http://www.beilstein-journals.org/bjoc/content/supplementary/1860-5397-8-231-S1.pdf]

Acknowledgements

We thank A. Nieß, L. Ahlers, and C. Michalek for technical assistance. Financial support from Deutsche Forschungsgemeinschaft (DFG) is gratefully acknowledged.

References

1. Schwartz, R. E.; Hirsch, C. F.; Sesin, D. F.; Flor, J. E.; Chartrain, M.; Fromtling, R. E.; Harris, G. H.; Salvatore, M. J.; Liesch, J. M.; Yudin, K. *J. Ind. Microbiol. Biotechnol.* **1990,** *5,* 113–123. doi:10.1007/BF01573860
2. Trimurtulu, G.; Ohtani, I.; Patterson, G. M. L.; Moore, R. E.; Corbett, T. H.; Valeriote, F. A.; Demchik, L. *J. Am. Chem. Soc.* **1994,** *116,* 4729–4737. doi:10.1021/ja00090a020
3. Kobayashi, M.; Kurosu, M.; Ohyabu, N.; Wang, W.; Fujii, S.; Kitagawa, I. *Chem. Pharm. Bull.* **1994,** *42,* 2196–2198. doi:10.1248/cpb.42.2196
4. Kobayashi, M.; Aoki, S.; Ohyabu, N.; Kurosu, M.; Wang, W.; Kitagawa, I. *Tetrahedron Lett.* **1994,** *35,* 7969–7972. doi:10.1016/S0040-4039(00)78398-5
5. Golakoti, T.; Ogino, J.; Heltzel, C. E.; Le Husebo, T.; Jensen, C. M.; Larsen, L. K.; Patterson, G. M. L.; Moore, R. E.; Mooberry, S. L. *J. Am. Chem. Soc.* **1995,** *117,* 12030–12049. doi:10.1021/ja00154a002
6. Subbaraju, G. V.; Golakoti, T.; Patterson, G. M. L.; Moore, R. E. *J. Nat. Prod.* **1997,** *60,* 302–305. doi:10.1021/np960700a
7. Chaganty, S.; Golakoti, T.; Heltzel, C.; Moore, R. E.; Yoshida, W. Y. *J. Nat. Prod.* **2004,** *67,* 1403–1406. doi:10.1021/np0499665
8. Eggen, M.; Georg, G. I. *Med. Res. Rev.* **2002,** *22,* 85–101. doi:10.1002/med.10002
9. Hamel, E.; Covell, D. G. *Curr. Med. Chem.* **2002,** *2,* 19–53. doi:10.2174/1568011023354263
10. Edelman, M. J.; Gandara, D. R.; Hausner, P.; Israel, V.; Thornton, D.; DeSanto, J.; Doyle, L. A. *Lung Cancer* **2003,** *39,* 197–199. doi:10.1016/S0169-5002(02)00511-1
11. Sessa, C.; Weigang-Köhler, K.; Pagani, O.; Greim, G.; Mora, O.; De Pas, T.; Burgess, M.; Weimer, I.; Johnson, R. *Eur. J. Cancer* **2002,** *38,* 2388–2396. doi:10.1016/S0959-8049(02)00489-6
12. Müller, K.; Faeh, C.; Diederich, F. *Science* **2007,** *317,* 1881–1886. doi:10.1126/science.1131943
13. Thayer, A. M. *Chem. Eng. News* **2006,** *84* (33), 29–31.
14. Rivkin, A.; Chou, T.-C.; Danishefsky, S. J. *Angew. Chem.* **2005,** *117,* 2898–2910. doi:10.1002/ange.200461751
15. Chou, T.-C.; Dong, H.; Rivkin, A.; Yoshimura, F.; Gabarda, A. E.; Cho, Y. S.; Tong, W. P.; Danishefsky, S. J. *Angew. Chem.* **2003,** *115,* 4910–4915. doi:10.1002/ange.200352361
16. Ojima, I.; Inoue, T.; Chakravarty, S. *J. Fluorine Chem.* **1999,** *97,* 3–10. doi:10.1016/S0022-1139(99)00058-5
17. Eißler, S.; Stončius, A.; Nahrwold, M.; Sewald, N. *Synthesis* **2006,** 3747–3789. doi:10.1055/s-2006-950332
18. Nahrwold, M.; Eißler, S.; Sewald, N. *Chim. Oggi – Chem. Today (Suppl. Focus on Peptides)* **2008,** *26,* 13–16.
19. Eißler, S.; Bogner, T.; Nahrwold, M.; Sewald, N. *Chem.–Eur. J.* **2009,** *15,* 11273–11287. doi:10.1002/chem.200901750
20. Al-Awar, R. S.; Ehlhardt, W. J.; Gottumukkala, S. V.; Martinelli, M. J.; Moher, E. D.; Moore, R. E.; Munroe, J. E.; Norman, B. H.; Patel, V. F.; Shih, C.; Toth, J. E.; Vasudevan, V.; Ray, J. E. (Eli Lilly and Company, University of Hawaii, Wayne State University) Pharmaceutical Compounds. WO9808505A1, March 3, 1998.
21. Moore, R. E.; Hemscheidt, T. K. (University of Hawaii, Wayne State University), Cryptophycins From Aberrant Biosynthesis. WO9708334A1, March 6, 1997.
22. Shih, C.; Williams, D. C. (Eli Lilly and Company). EP870510A2, 1998.
23. Eißler, S.; Nahrwold, M.; Neumann, B.; Stammler, H.-G.; Sewald, N. *Org. Lett.* **2007,** *9,* 817–819. doi:10.1021/ol063032l
24. Mast, C. A.; Eißler, S.; Stončius, A.; Stammler, H.-G.; Neumann, B.; Sewald, N. *Chem.–Eur. J.* **2005,** *11,* 4667–4677. doi:10.1002/chem.200500282
25. Eißler, S.; Neumann, B.; Stammler, H.-G.; Sewald, N. *Synlett* **2007,** 273–277. doi:10.1055/s-2007-1000868
26. Sammet, B.; Radzey, H.; Neumann, B.; Stammler, H.-G.; Sewald, N. *Synlett* **2009,** 417–420. doi:10.1055/s-0028-1087541
27. Nahrwold, M.; Bogner, T.; Eissler, S.; Verma, S.; Sewald, N. *Org. Lett.* **2010,** *12,* 1064–1067. doi:10.1021/ol1000473
28. Sammet, B.; Bogner, T.; Nahrwold, M.; Weiß, C.; Sewald, N. *J. Org. Chem.* **2010,** *75,* 6953–6960. doi:10.1021/jo101563s
29. Sammet, B.; Brax, M.; Sewald, N. *Beilstein J. Org. Chem.* **2011,** *7,* 243–245. doi:10.3762/bjoc.7.32
30. Nahrwold, M.; Weiß, C.; Bogner, T.; Mertink, F.; Sammet, B.; Palmisano, R.; Royo Gracia, S.; Preuße, T.; Sewald, N. *J. Med. Chem.* **2012**. In revision.
31. Ragoussis, N.; Ragoussis, V. *J. Chem. Soc., Perkin Trans. 1* **1998,** 3529–3534. doi:10.1039/A806173D
32. Eißler, S. Synthese von Cryptophycinen für SAR-Studien. Ph.D. Thesis, Bielefeld University, Bielefeld, Germany, 2008.

33. Weiß, C. Synthese von Cryptophycin-Analoga für SAR- und subzelluläre Lokalisationsstudien. Ph.D. Thesis, Bielefeld University, Bielefeld, Germany, 2012.
34. Hoard, D. W.; Moher, E. D.; Martinelli, M. J.; Norman, B. H. *Org. Lett.* **2002,** *4,* 1813–1815. doi:10.1021/ol025933+

License and Terms

Beilstein Journal of Organic Chemistry

Chemical modification allows phallotoxins and amatoxins to be used as tools in cell biology

Jan Anderl[1], Hartmut Echner[2] and Heinz Faulstich[*3]

Full Research Paper

Open Access

Address:
[1]Heidelberg Pharma GmbH, Schriesheimer Str. 101, 68526 Ladenburg, Germany, [2]University of Tübingen, Medical School, Hoppe-Seyler-Str. 3, 72076 Tübingen, Germany, and [3]Max-Planck Institute for Medical Research, Jahnstr. 29, 69120 Heidelberg, Germany

Email:
Heinz Faulstich[*] - hfaulstich@web.de

* Corresponding author

Keywords:
amatoxins; cellular uptake; endocytosis; peptides; phalloidin; phallotoxins

Beilstein J. Org. Chem. **2012,** *8,* 2072–2084.
doi:10.3762/bjoc.8.233

Received: 24 August 2012
Accepted: 09 November 2012
Published: 27 November 2012

This article is part of the Thematic Series "Antibiotic and cytotoxic peptides".

Guest Editor: N. Sewald

Abstract

Phallotoxins inhibit the dynamics of microfilaments in cells and lead to apoptosis. Due to poor cellular uptake these effects cannot be studied in live cells, even at millimolar toxin concentrations, nor can phalloidin be used for the elimination of tumor cells. Uptake is greatly enhanced by conjugation of phallotoxins to either lipophilic or polycationic moieties, such as oleic acid, polylysine, or Tat-peptide. These conjugates were lethally toxic for cells, e.g., mouse fibroblasts or Jurkat leukemia cells, in the micromolar range. Uptake into cells starts with the attachment of the toxin conjugates to the plasma membrane, followed by endocytosis and, in most cases, cleavage of the toxin from the carrier. Interestingly, the internalization rate of phalloidin into cells was also significantly increased by the fluorescent moiety tetramethylrhodaminyl, as well as by high molecular weight methoxy-polyethyleneglycol, two compounds unknown so far for their uptake-mediating activity. Conjugation to carriers as investigated in this work will allow the use of phallotoxins in experimental cell biology and possibly in tumor therapy. The findings obtained with phallotoxins could be applied also to the family of amatoxins, where α-amanitin, for example, when conjugated to oleic acid was more than 100-fold more toxic for cells than the native toxin. This suggests the possibility of a more general use of the moieties examined here to enhance the uptake of hydrophilic peptides, or drugs, into live cells.

Introduction

Phallotoxins and amatoxins, the two families of toxic cyclopeptides produced by the green death cap *Amanita phalloides*, have been the subject of intense biochemical research for decades [1]. Although produced by the same mushroom and of similar structure, the two peptide families have totally different cellular targets. Phallotoxins, such as phalloidin, bind to polymeric actin, thus stabilizing microfilaments and decreasing the amount of monomeric actin in equilibrium with the filaments. This

interaction is in the nanomolar range and highly specific: no other targets for phalloidin in the cell are known. Amatoxins, such as the main toxin α-amanitin, bind to RNA-polymerases II of eukaryotic cells, thus inhibiting the transcription process at nanomolar concentrations. Also this interaction is specific, since RNA-polymerases I are not inhibited at all, whereas RNA-polymerases III are inhibited at amanitin concentrations ca. 1000 times higher than for RNA-polymerases II [2,3]. The fact that both the cytoskeleton and the eukaryotic transcription machine are complex structures and still under investigation, may explain the continuing interest in these two kinds of specific inhibitors.

Phalloidin has been used to study actin dynamics in vitro [1], and in microscopic studies after microinjection into single cells [4]. Beside such experiments phalloidin conjugated to fluorescent moieties is widely used for visualizing filamentous actin in fixed cells [5,6]. In all these applications, cell-free systems were used, allowing direct access of phallodin to its target. Similarly, α-amanitin was mainly used with isolated nuclei or the solubilized enzyme, as recently reported for stabilizing yeast RNA-polymerase II in an X-ray analysis [7].

For both phallotoxins and amatoxins, experience with live cells is limited by the fact that the peptides cross the plasma membrane barrier only very slowly. Poor uptake rates of phallotoxins and amatoxins have been observed for most mammalian cells. Mammalian hepatocytes are an exception: they display transporting proteins on their sinusoidal surface (such as OATP1B1 and OATP1B3 of human hepatocytes [8-10]), which internalize phallotoxins and amatoxins. It is through the presence of the transporting protein OATP1B3 on human hepatocytes, for example, that amatoxins are feared as liver toxins causing the majority of fatal human mushroom poisonings worldwide.

The aim of this study was to explore known lipophilic and polycationic internalization-mediating moieties for their applicability with phallotoxins and amatoxins, and to find novel internalization-mediating moieties and investigate the potential of their conjugates with toxins as specific inhibitors in cultured cells. The internalization-mediating moieties used in this study were either lipophilic in nature (such as oleic acid), or multicationic (such as polylysine and octarginine): two features applying also to so-called membrane-transducing peptides [11,12].

Results

Preparation of phallotoxin derivatives

Attachment sites in phalloidin (Figure 1) for conjugation with uptake-mediating moieties were chosen based on our knowledge of structure–activity relationships in phalloidin [1]: As the side chains in the small heterodet peptide ring are known to be involved in actin binding they were not used for derivatization. In the larger peptide ring, on the other hand, the dihydroxylated leucine moiety is juxtaposed to the actin binding site and thus appeared as most promising for derivatization. Accordingly, all residues investigated in this study were attached to the Cδ-atom of the dihydroxylated leucine moiety, either as esters or amides (Table 1). Large residues, which might disturb the interaction of a phalloidin derivative with actin through steric hindrance, were coupled via disulfide-containing linkers, which would be reduced inside the cell so as to release a defined thiol derivative of phalloidin (Table 1).

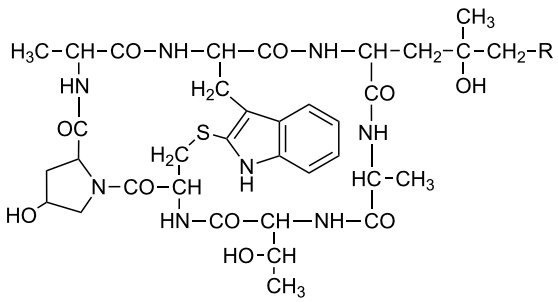

Figure 1: Chemical structure of phalloidin with the attachment site (R) used for conjugation to uptake-mediating moieties.

Actin binding

All phalloidin derivatives were tested for their affinity to muscle actin (α-actin), which is used as a model for β-actin present in nonmuscle cells. This parameter was important, since cytotoxicity depends not only on membrane permeability but also on actin affinity. Moreover, this parameter will hint on whether phalloidin was cleaved from its carrier inside the cell, in cases where low actin affinity of a phalloidin derivative was combined with high cytotoxicity. Relative affinity values of the phalloidin derivatives to muscle actin are shown in Table 1.

Growth inhibition of mouse fibroblasts

By using the MTT cell proliferation assay, each phalloidin conjugate was examined for its capacity to inhibit the growth of mouse fibroblasts in vitro after 72 h incubation time (Table 1). Phalloidin displayed no antiproliferative activity up to a concentration of 10^{-3} M in the culture medium. In contrast, the most lipophilic ester derivative, phalloidin oleate (**1e**), showed an IC_{50} value of proliferation inhibition of 2.5×10^{-6} M, and was thus ca. 1000 times more active than phalloidin. Other esters (**1a**–**1d**) exhibited increasing cytotoxic activities with increasing hydrophobicity (Figure 2). In order to examine a possible relationship between cytotoxicity and hydrophobicity we determined the octanol/water equilibrium distribution coefficient of the ester derivatives (log P_{ow} values) and found a linear rela-

Table 1: Structures of phalloidin derivatives, their relative affinity values for α-actin as compared to phalloidin and their IC_{50} values of cell growth inhibition after incubation for 72 h as determined by MTT cell proliferation assay (n.a.: not assayed).

	R	Name/designation	Relative affinity to α-actin [%]	IC_{50} values NIH 3T3 fibroblasts [μM]	IC_{50} values Jurkat cells [μM]
1	OH	phalloidin	100	ca. 1,000	ca. 1,000
1a	$OCOC_6H_5$	(**1**)-benzoate	76	92	94
1b	$OCOC_6H_4$*o*-OH	(**1**)-salicylate	81	364	96
1c	$OCOC_7H_{15}$	(**1**)-octanoate	12	44	37
1d	$OCOC_{13}H_{27}$	(**1**)-myristate	7	11	9
1e	$OCO(CH_2)_7CHCH(CH_2)_7CH_3$	(**1**)-oleate	4	3	2
2	NH_2	aminophalloidin	2	ca. 1,000	ca. 1,000
2a	$NHCOC_6H_5$	*N*-benzoyl-(**2**)	74	693	599
2b	$NHCO(CH_2)_7CHCH(CH_2)_7CH_3$	*N*-oleoyl-(**2**)	5	883	630
2c	$NHCO(CH_2)_2SS(Ac)CysGlyTyrGly$-$Arg(Lys)_2(Arg)_2Glu(Arg)_3OH$	(**2**)-Tat-peptide	3	4	3
2d	$NHCO(CH_2)_2SS(Ac)CysGly(Arg)_8OH$	(**2**)-octarginine	2	11	7
2e	$NHCO(CH_2)_6CONH(Lys)_{210}$	(**2**)-poly-(L)-lysine$_{28,000}$	40	5	4
		(**2**)-poly-(D)-lysine$_{28,000}$	38	54	37
2f	$NHCO(CH_2)_2SS(CH_2)_2CONH(Lys)_{210}$	(**2**)-(SS) poly-(L)-lysine$_{28,000}$	39	3	2
		(**2**)-(SS) poly-(D)-lysine$_{28,000}$	39	4	2
2g	$NH(CH_2)_2SS(CH_2)_2CONH(PEG)_{800}$	(**2**)-(SS) PEG_{800}	8	167	98
2h	$NH(CH_2)_2SS(CH_2)_2CONH(PEG)_{5.200}$	(**2**)-(SS) $PEG_{5,200}$	4	77	50
2i	$NH(CH_2)_2SS(CH_2)_2CONH(PEG)_{23.000}$	(**2**)-(SS) $PEG_{23,000}$	1	10	10
2f +DTT	$NH(CH_2)_2SH$	*N*-(2-mercaptoethyl)-(**2**)-SH	37	n.a.	n.a.
3	for structure see Figure 6a	dithiolanoaminophalloidin TRITC labeled	25	11	n.a

tionship between log P_{ow} and IC_{50} values of cellular cytotoxicity (Figure 3). The ester derivatives of phalloidin are probably hydrolyzed inside the cell, e.g., by esterases or proteases, as suggested by the fact that the ester **1e** and the corresponding amide **2b** possess comparable affinities to actin (Table 1), but differ in their IC_{50} values by a factor of ca. 300. The effect is presumably a consequence of the faster hydrolysis of esters over amides by intracellular hydrolases.

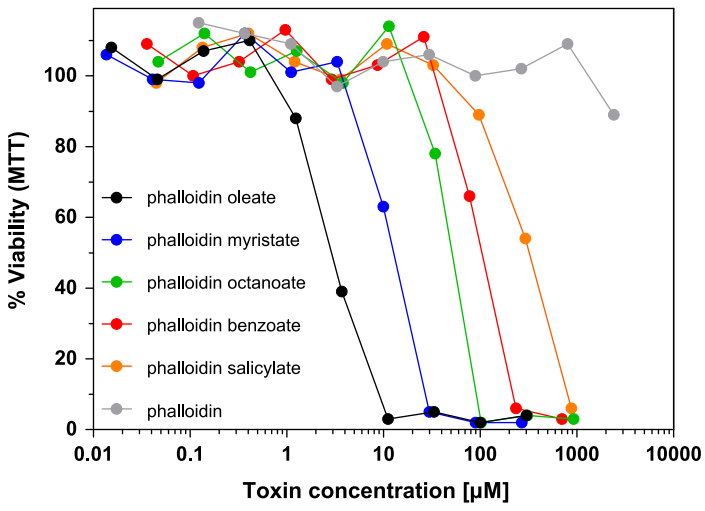

Figure 2: Cytotoxicity of phalloidin derivatives. NIH 3T3 mouse fibroblasts were incubated with various concentrations of phalloidin and phalloidin derivatives. Cell viability was determined after 72 h incubation time by MTT assay.

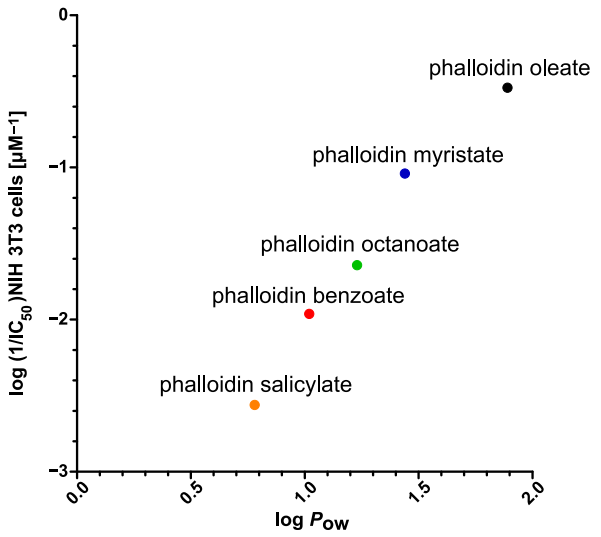

Figure 3: *n*-Octanol/water distribution coefficients (log P_{ow}) of the hydrophobic phalloidin derivatives of Figure 2 plotted versus cell toxicity (log (1/IC_{50}) in NIH 3T3 mouse fibroblasts.

Polycationic derivatives of phalloidin, such as the polylysine conjugates, were highly toxic for mouse fibroblasts, and their antiproliferative activity was comparable to the most lipophilic derivative, phalloidin oleate (Figure 4a). Their toxicity was found to be dependent on the configuration of the polymer, since phalloidin bound to D-configurated polylysine was about 10 times less toxic than when bound to poly-(L)-lysine. This suggests that the release of a toxic phalloidin species inside the cell includes the enzymatic breakdown of the carrier. In agreement with this we found no difference between the L-configurated and the D-configurated carrier when the linker contained a disulfide bridge, arguing for the presence of a disulfide-reducing compartment inside the cells.

Likewise, high cytotoxicity was found for the octarginine conjugate (Figure 4a). From the fact that the cytotoxic activities of the polylysine derivative (ca. 150 residues) and the oligoarginine derivative (8 residues) are comparable, we argue that arginine residues are more effective in mediating internalization of phalloidin than are lysine residues.

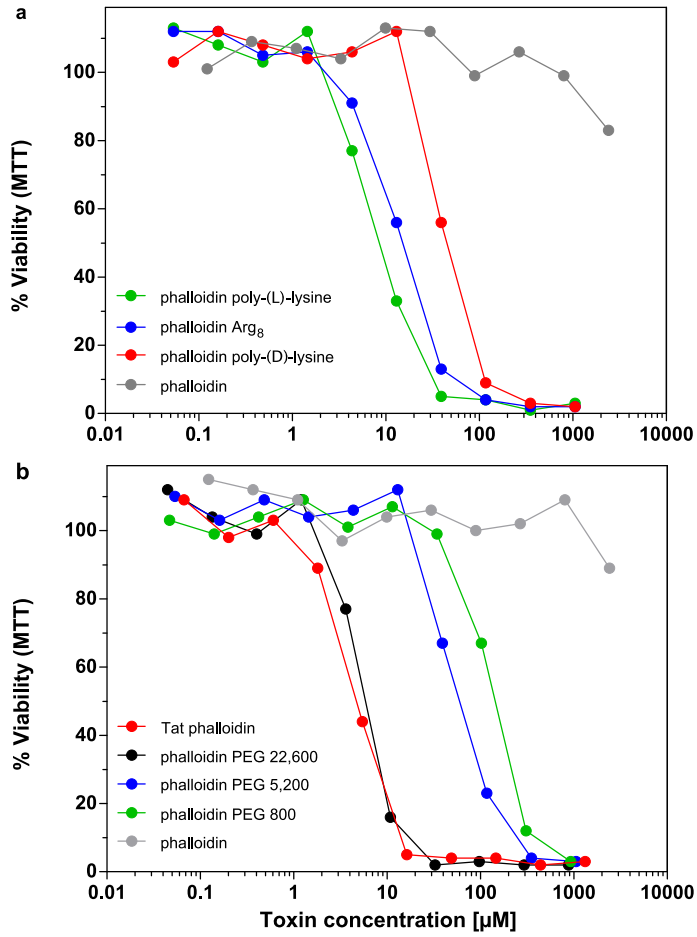

Figure 4: (a) and (b): NIH 3T3 mouse fibroblasts were incubated with various concentrations of phalloidin and phalloidin derivatives. Cell viability was determined after 72 h incubation time by MTT assay.

For phalloidin bound to methoxy-polyethylene-glycol we found that cytotoxicity strictly depended on the molecular weight of the polymer chain (Figure 4b). Most active was the conjugate with the longest chain (M_r = 22,600). Cytotoxicity fell strikingly when the polymer chain was shortened (Table 1).

Coupling to Tat-peptide was also very effective in enhancing the cytotoxicity of phalloidin (Figure 4b), while the phalloidin conjugate with the Kaposi protein fragment (likewise claimed to enhance membrane permeability) was much less effective (data not shown).

Beside mouse fibroblasts, we investigated the phalloidin derivatives in several human leukemia and lymphoma cell lines, in order to find possible specificities for one or the other kind of tumor cell. However, Jurkat cells (Table 1) and all other cell lines tested (K562 cells, HL-60 cells, and Daudi cells) showed sensitivities comparable to mouse fibroblasts (see Supporting Information File 1).

Uptake kinetics

Since the toxic effects of phalloidin develop slowly, growth inhibition was measured only after 72 h. During this period several partial processes must occur such as binding to the plasma membrane, internalization, processing and toxin release, etc., which cannot be distinguished. However, replacement of the toxin medium by toxin-free medium after various times of incubation would provide information on the time required for each of the toxin derivatives to bind to the cell surface. We compared the three most effective phalloidin conjugates, phalloidin oleate (**1e**), phalloidin-Tat conjugate (**2c**), and phalloidin polylysine (**2e**) (Figure 5) and found that the exposure times necessary to achieve, e.g., a 50% growth inhibition by a given toxin concentration after 72 h indeed varied considerably, from 2 h to 24 h. The results show that the polycationic derivative was bound much more rapidly than the lipophilic conjugate.

A fluorescent residue that enhances uptake of phalloidin into cells

Tetramethylrhodaminyl-phalloidin (Figure 6a) has been used to visualize actin fibers in fixed cells for 30 years. Here we show that the rhodamine residue also strongly enhanced cellular uptake, making this phalloidin derivative a tool for cell biology. With an IC_{50} value of 11 µM its toxicity is comparable to those of the most toxic phalloidin derivatives, phalloidin oleate (**1e**) and phalloidin-poly-(L)-lysine (**2e**). More importantly, rhodaminyl-phalloidin seems not to be cleaved inside the cell and, through its fluorescence, can report on the structure of its target protein, the actin filaments, albeit under toxic conditions.

Using rhodamine-labeled phalloidin, we could also study how membrane-permeable peptides are incorporated into the cell. Immediately after exposure the toxin was located on the plasma membrane of the cells as shown by fluorescence microscopy (Figure 6c), while after 6 h increasing amounts of the toxin were found in endocytotic vesicles. After 24 h most of the rhodamine-labeled toxin was still in endosomes, while some of it had found its target, as concluded from the decoration of filaments.

Phalloidin causes apoptosis of cells

Under the microscope, cells treated with membrane-permeable phalloidin derivatives appeared shrunken and developed blebs, as described for cells undergoing apoptosis. Treatment with

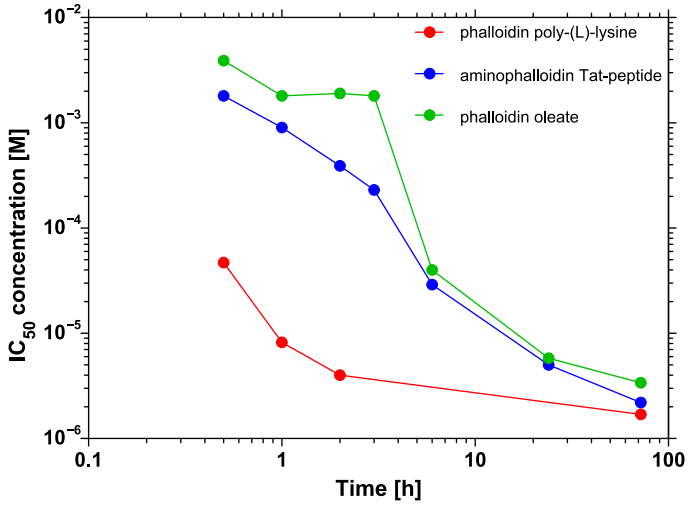

Figure 5: Time course of uptake in NIH 3T3 cells of three phalloidin derivatives as measured by the cytotoxicity after 72 h incubation during which the toxins were washed off after various exposure times.

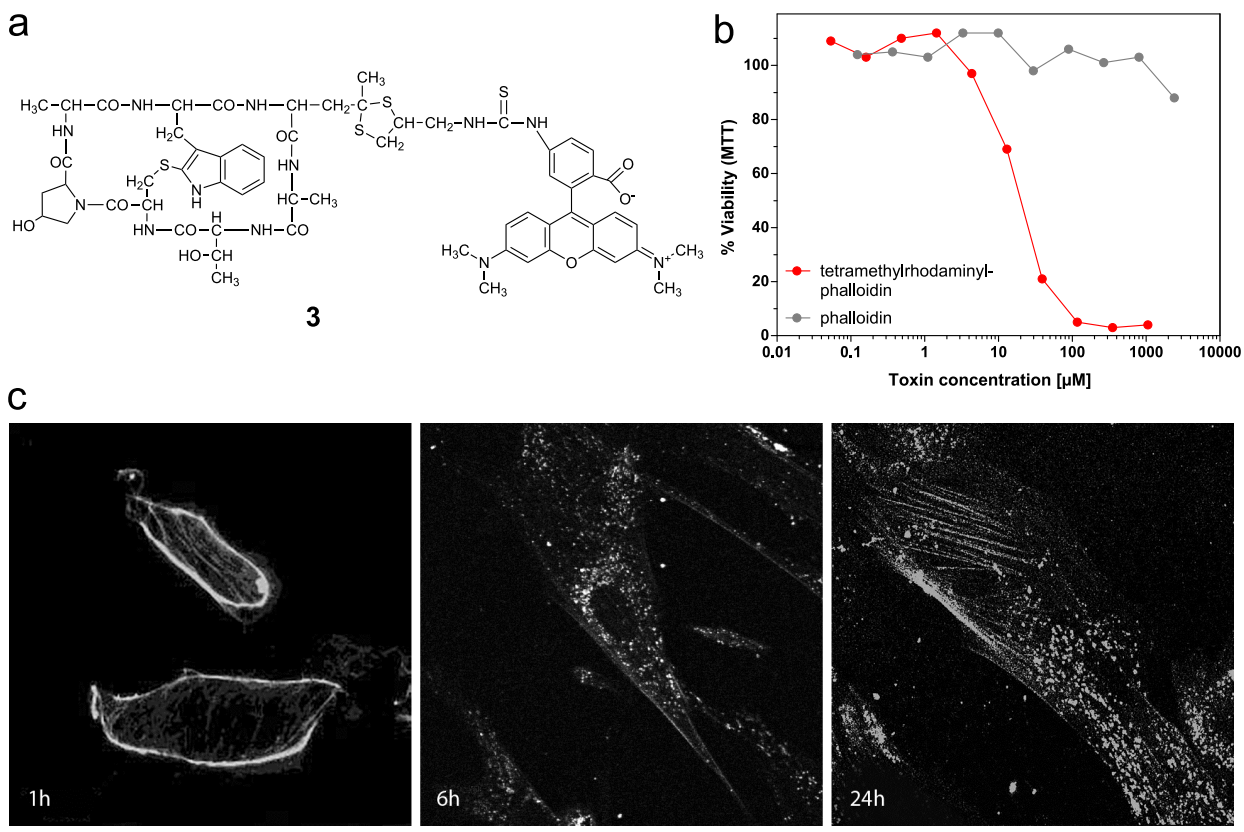

Figure 6: (a) Chemical structure of tetramethylrhodaminyl-phalloidin (**3**). (b) Growth inhibition of NIH 3T3 mouse fibroblasts by tetramethylrhodaminyl-phalloidin (**3**) versus phalloidin (**1**) after 72 h incubation time. (c) Binding and uptake of tetramethylrhodaminyl-phalloidin (**3**) in NIH 3T3 mouse fibroblasts after 1, 6 and 24 h, as documented by fluorescence microscopy.

annexin followed by flow cytometric analysis showed a fluorescence distribution typical for apoptosis and similar to that induced by camptothecin. Cells treated with native phalloidin were indistinguishable from controls [13].

Growth inhibition by amatoxin derivatives

Unlike the phallotoxins, the natural amatoxins are toxic in cell cultures, exhibiting IC_{50} values around 10^{-6} M. As amatoxins are more hydrophilic than phallotoxins, it seems unlikely that their membrane permeation capacity is larger than that of phallotoxins. The more likely explanation is that for amatoxins the threshold concentration lethal for cells is much lower than for phallotoxins (see Discussion).

Two of the internalization-mediating residues investigated in the phallotoxin series, oleic acid and polylysine, were also tested for their uptake capacity in the amatoxin series. Structure–activity studies had shown that the primary OH group of the dihydroxy-isoleucine moiety (Figure 7) is not involved in RNA polymerase II binding and, hence, may be used for derivatization with oleic acid chloride (Table 2). In order to avoid concurrent acylation of the 6'-OH of tryptophan, the phenolic OH was methylated before acetylation. For coupling to polylysine the natural carboxy group of aspartic acid as present in β-amanitin was used, which after activation as *N*-hydroxysuccinimide ester reacted with ε-amino groups in polylysine. Since

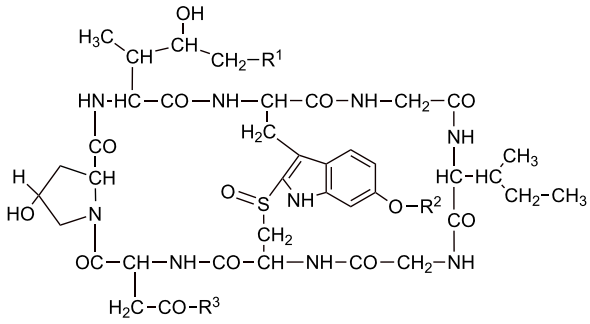

Figure 7: Chemical structure of amanitin with attachment site for conjugation to internalization-mediating moieties (R^1, R^3).

Table 2: Structures of amanitin derivatives and IC_{50} concentrations of growth inhibition in mouse fibroblasts after 72 h incubation time (MTT cell proliferation assay).

	R^1	R^2	R^3		IC_{50} values NIH 3T3 fibroblasts [nM]
4	OH	OH	NH_2	α-amanitin	6,200
4a	$OCO(CH_2)_7CHCH(CH_2)_7CH_3$	OCH_3	NH_2	α-amanitin oleate	39
5	OH	OH	OH	β-amanitin	1,000
5a	OH	OH	$CO(Lys)_mOH$ $^{\varepsilon}NH(CH_2)_4-CH$ $NH(Lys)_nH$	β-amanitin poly-(L)-lysine	10
5b	OH			β-amanitin poly-(D)-lysine	18,000

the polymeric carrier may be broken down inside the cell by proteases, we investigated both poly-(L)-lysine and poly-(D)-lysine as carriers, in order to study whether the biological availability of the amatoxin depended on the configuration of lysine in the polymeric carrier.

Conjugation of amanitin to oleic acid increased the cytotoxicity by a factor of 150 (see Table 2). In analogy with the phallotoxins, we conclude that the oleic acid ester is hydrolysed inside the cell. β-Amanitin, when conjugated to poly-(L)-lysine, became 100-fold more toxic for mouse fibroblasts than the native toxin, showing IC_{50} values in the nanomolar range (Figure 8). As in the phallotoxin series, toxicity of β-amanitin conjugates depends on the cleavage of the toxin from the polymeric carrier, as shown by the fact that β-amanitin coupled to the (L)-polymer was 1800 times more toxic than when coupled to the (D)-polymer (Table 2).

Discussion

Growth inhibition as a parameter of internalization

Phallotoxins as well as amatoxins find their targets inside the cell. Thus, if growth inhibition by these toxins occurs the toxins must have penetrated the cell. Moreover, the extent of the toxic lesions will mirror the amount of toxin that penetrated the cell and, hence, can be used to estimate the amount of toxin taken up. Although some of the steps involved in the uptake process became evident in this study it was not our aim to investigate

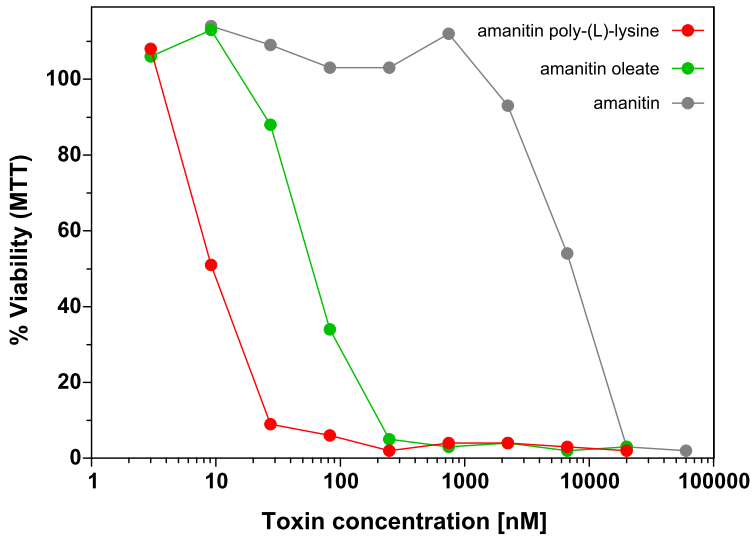

Figure 8: NIH 3T3 mouse fibroblasts were incubated with various concentrations of α-amanitin and amanitin derivatives. Cell viability was determined after 72 h incubation time by MTT assay.

details of internalization, but to gather experience with moieties that may help to overcome the plasma membrane barrier and to shift hydrophilic peptides into a cell.

Previous experience with internalization-mediating moieties

Lipid acids have been used by various researchers to enhance the uptake of peptides and proteins into cells. For example Honeycutt et al. [14] used palmitic acid to deliver a protease inhibitor into cells, and Bradley et al. [15] used docosahexanoic acid to improve the uptake of paclitaxel into tumor cells. For a review see Wong and Toth [16]. Of particular interest was the incorporation of anti-sense oligonucleotides into cells by coupling them to lipophilic ligands as reported by Boutorin et al. [17], Letsinger et al. [18], and Shea et al. [19].

Polycationic carriers such as polylysine and polyarginine represent another, and possibly even more effective technique for delivering drugs into cells. Ryser and Shen [20] reported the internalization by polylysine of methothrexate and horse radish peroxidase; Leonetti et al. [21] the internalization of oligonucleotides; and Mulders et al. [22] the internalization of adenovirus into cells. A polylysine peptoid derivative was used by Murphy et al. [23] for "gene delivery", and Emi et al. [24] used polyarginine as a carrier for gene transfer.

Protein transduction domains such as Tat-peptide, usually consisting of 10–30 amino acids, have been used to transport enzymes, drugs, liposomes and supermagnetic particles into cells [25-29]. In the meantime it has been shown that nona-arginine is many times more efficient than Tat-peptide, suggesting that the internalization effect of Tat-peptide is mainly due to its eight cationic side chains [30].

Attachment to plasma membrane determines the rate of internalization

Plasma membranes of cells in culture represent a lipophilic phase in an aqueous medium, and amphiphilic compounds brought into this system will distribute between the two phases according to their nature. This process is similar to the distribution the substance will take between *n*-octanol and water, an idea that has been suggested by Palm et al. [31].

Compounds **1a**–**1e** represent a series of phalloidin derivatives with increasing log P_{ow} values. At the same time they represent a series of phalloidin derivatives with increasing cytotoxic activity. Since the two parameters are linearly related (Figure 3), we conclude that the amount of toxin attached to the membrane determines the extent of the toxic effects observed. Clearly, this conclusion is valid only under the condition that, as in our case, all derivatives belong to the same chemical class, esters for example, and that processing inside the cell will yield the same toxic product, here native phalloidin, set free in all cases.

Attachment to the plasma membrane can also occur by electrostatic forces and, thus, may be behind the internalization effect observed with polylysine or oligoarginine as well. Plasma membranes expose numerous negatively charged components that can attract oligo- or polycationic molecules. As already pointed out, arginine residues as in **2d** are more effective than lysine residues in **2e**, as 120 lysine groups are required to match the internalization increase caused by eight arginine residues.

Concerning Tat-peptide, we believe that its eight cationic side chains interacting with the plasma membrane represent the more likely explanation for its internalization than other models proposed in the past.

Finally, tight attachment to the plasma membrane may also explain why the methoxy-polyethyleneglycol residue mediates internalization, since polyethyleneglycols are soluble not only in water but also in diethylether, i.e., can adopt a conformation capable of anchoring to the phospholipids in the plasma membrane. Lipophilic interaction of the aromatic part of tetramethylrhodamine with the plasma membrane is also thought to be the main cause of the internalization capacity of this fluorescent residue, beside its delocalized cationic charge on the two nitrogen atoms.

Although proved for a lipophilic phalloidin derivative only, we postulate that attachment to the plasma membrane also provides the first step in entering cells for the polycationic and the pegylated toxin derivatives presented in this study.

Internalization and processing

The uptake process following the binding step of the phalloidin derivative **3** to the plasma membrane was identified as endocytosis. As shown in Figure 6c, the fluorescent phalloidin is bound on the plasma membrane of mouse fibroblasts after 1 h, while after 6 h most of the fluorescent material resides in endocytotic vesicles. This finding confirms the earlier observation [6] that TRITC-phalloidin **3** enters isolated mouse hepatocytes by endocytosis and not through a phalloidin-transporting protein, such as the OATP1B1 present on human hepatocytes. The type of endocytosis seen here remains, however, to be elucidated. Likewise, we have no data on whether lipophilic or polycationic phallotoxins enter cells in the same way as the fluorescent toxin, but this seems likely since proteolytic enzymes present in endosomal-lysosomal compartments were found to be involved in the processing, and the difference in de-

gradation after arrival in endosomes is the most likely explanation for the difference found in the toxicities of phalloidin when bound to either poly-(L)- or to poly-(D)-lysine (**2e**).

There is no evidence so far about how phalloidin released from the carrier finds its way out of the endosomal-lysosomal compartments into cytoplasm, where the target, the actin filaments, is located.

Conclusions

With IC_{50} values of >10 mM (8 mg/mL; M_r 789 g/mol), phalloidin has so far been of no benefit for research on living cells, unless it was microinjected. This is regrettable, since the molecular mechanism of phalloidin action, the immobilization of the microfilament system, has been investigated in great detail. Moreover, phalloidin action is comparable to that of taxol, which induces comparable immobilization of the microtubular system and has been widely employed in cell research and even in tumor therapy [32,33]. One difference is that taxol is a lipophilic compound, and is thus active on cells at much lower concentrations. We balanced this disadvantage by coupling phalloidin, e.g., to oleic acid, allowing studies of the molecular toxicity of phalloidin on cells in the micromolar range and encouraging its use in tumor therapy.

The internalization-mediating effect observed with phalloidin was seen also with amatoxins. Although amanitin is active on cells in the micromolar range, it may be advantageous to use it bound to oleic acid or polylysine and thus decrease the medium concentration necessary to achieve growth inhibition down to the nanomolar range. Amanitin as a drug bound to tumor monoclonal antibodies, has recently been described for the therapy of adenocarcinomas [34].

Coupling to methoxypolyethyleneglycol has been described as a method to improve the solubility of drugs, prolong their half-lives in plasma, or modulate their pharmacokinetics [35]. An effect not described to our knowledge so far is that pegylation can enhance, several hundred-fold, the penetration of a hydrophilic drug into cells. Linkers with the drug should contain a disulfide bridge, as in compound (**2i**), to make sure that after internalization the drug is released in a defined and active form.

Likewise new, is the observation that the red fluorescent tetramethylrhodaminyl residue can facilitate internalization, e.g., of phalloidin, by a factor of >100. Linked by a thiourea moiety, as in compound **3**, the fluorescent moiety is not cleaved inside the cell, as concluded from the observation that this phalloidin derivative still decorates filaments in the cell. This property of rhodamine-labeled phalloidin seems useful as a tool for studying the kinetics of phalloidin-induced disturbances in the actin system of a cell in correlation with, for example, the development of apoptosis in the cell.

Experimental

Fatty acid esters of phalloidin

Ten micromoles of phalloidin was dissolved in 0.1 mL dry pyridine and reacted with 0.3 µmol of benzoyl chloride, salicyl chloride, octoyl chloride, myristoyl chloride, or oleoyl chloride for 2 h at rt. Under these conditions, the reaction proceeded predominantly at the primary OH group of the γ,δ-dihydroxyleucine residue in position 7 of phalloidin, with ca. 10–20% of esterification at the secondary OH groups. The reaction was stopped with 2 mL of methanol, and solvents were removed in vacuo at 60 °C. Purification of the esters was achieved by preparative TLC on silica (Merck HF_{254}, Darmstadt; Germany) in chloroform/methanol/2 N acetic acid (65:25:4), followed by further purification of the methanolic extract of the silica on a Sephadex-LH20 column developed with methanol. Yields of the esters were 43% for benzoyl phalloidin, 35% for salicyl phalloidin, 46% for octoyl phalloidin, 50% for myristoyl phalloidin and 44% for oleoyl phalloidin; purities were 88 to 95% by HPLC.

Aminophalloidin

Ten micromoles of toluene-4-sulfonyl chloride in 2 mL chloroform were added to 0.6 µmol of phalloidin in 5 mL dry pyridine and allowed to react for 30 min on ice. The reaction was stopped by the addition of 50 mL of dry diethyl ether, and the sediment was isolated by centrifugation, washed twice with 50 mL diethyl ether, and dissolved in 5 mL methanol for separation on a Sephadex-LH20 (60 × 3 cm) column developed with methanol/H_2O (1:1). Yield of the monotosylphalloidin was 65%; purity 94%. The vacuum-dried monotosylphalloidin was dissolved in 40 mL of methanol containing 2.5 N ammonia and reacted for 2 h. After evaporation in vacuo at 60 °C, the aminophalloidin was purified on a Sephadex-LH20 column with methanol as eluant. Yield of aminophalloidin was 80%, purity 89% by HPLC.

Fatty acid amides of phalloidin

Aminophalloidin and the fatty acid chlorides were reacted as described for the synthesis of phalloidin esters.

Linear peptides linked to aminophalloidin

Linear peptides such as Ac-Cys-Gly-Tyr-Gly-Arg-Lys-Lys-Arg-Arg-Gln-Arg-Arg-Arg-OH (Tat peptide), and Ac-Cys-Gly-Arg_8-OH (Arg_8) were synthesized on an Eppendorf Ecosyn P solid-phase synthesizer by using 9-fluorenylmethoxycarbonyl (Fmoc)-Arg(Pbf)SPHB resin (Rapp Polymere, Tübingen, Germany). For the Kaposi sequence Ac-Cys-Gly-Ala-Ala-Val-

Ala-Leu-Leu-Pro-Ala-Val-Leu-Leu-Ala-Leu-Leu-Ala-Pro-OH an Fmoc-Pro-Trt-Tentagel resin was used. All amino acids were incorporated with the α-amino functions protected with the Fmoc group. Side chain functions were protected as *tert*-butyl ethers (tyrosine), *tert*-butyloxycarbonyl derivatives (lysine), trityl derivatives (cysteine, glutamine), and as (2,2,4,6,7-pentamethyl)dihydrobenzofuran-5-sulfonyl derivative (arginine). Coupling was performed by using a 4-fold excess of each of the protected amino acids and the coupling reagent 2-(1*H*-benzotriazole-1-yl)-1,1,3,3-tetramethyluronium tetrafluoborate (TBTU) and 2 equiv of diisopropylethylamine (DIEA) over the resin loading. Before the coupling steps the Fmoc groups were removed from the last amino acid of the growing peptide fragment by using 25% piperidine in dimethylformamide. After cleavage of the N-terminal Fmoc group, the peptide was removed from the resin under simultaneous cleavage of the amino-side-chain protecting groups by incubation for 3 h in a mixture of trifluoroacetic acid (TFA) (12 mL), ethanedithiol (0.6 mL), anisole (0.3 mL), water (0.3 mL), and triisopropylsilane (0.15 mL). The mixture was filtered, and washed with TFA and anhydrous diethyl ether. The crude products were further purified by HPLC on a Nucleosil 100 C18 (7 µm) column (250 × 10 mm, Macherey & Nagel, Düren, Germany) by using a gradient from 10–90% B in 32 min (solution A: 0.07% TFA/H_2O; solution B: 0.059% TFA in 80% acetonitrile). The elution was monitored at 214 nm. The peptides were assayed for purity by analytical HPLC and ESIMS. The peptides were coupled to aminophalloidin through the heterobifunctional cross-linking agent SPDP (3-(2-pyridyldithio)propionic acid *N*-hydroxysuccinimide ester). Thus, the activated ester end of excess SPDP was reacted with the primary amine group in aminophalloidin to form an amide linkage. In general, 63 µmol aminophalloidin were dissolved in 3.4 mL H_2O and 1.7 equiv SPDP, dissolved in 900 µL dimethylformamide, were added. The solution was adjusted to pH 7.5 with 1 N NaOH; reaction time was 1 h. Separation of the products was performed by Sephadex-LH20 column developed with methanol. The purity of PDP-aminophalloidin was 93%; the yield was about 65%. The 2-pyridyldithiol group at the other end of the linker was reacted with the sulfhydryl in the amino terminal Ac-Cys-Gly moiety of the linear peptides to form a disulfide group. The reaction conditions of the three linear peptides varied slightly and were as follows: 33 µmol Tat-peptide, dissolved in 1.0 mL PBS was added to 40 µmol of PDP-aminophalloidin dissolved in 0.5 mL methanol; 13.6 µmol Arg_8-peptide, dissolved in 1.5 mL PBS was added to 28 µmol of PDP-aminophalloidin dissolved in 0.25 mL methanol; 12 µmol Kaposi-peptide, dissolved in 0.8 mL PBS was added to 36 µmol of PDP-aminophalloidin dissolved in 0.2 mL methanol. Reaction time was in all cases 16 h at rt. Separation was achieved on Sephadex-LH20 with H_2O/methanol (4:1) as solvent. Yield for Tat-phalloidin was 52%, for Arg_8-phalloidin 43% and for Kaposi-peptide 39%. Purity of all conjugates was >90% as shown by HPLC (Table 1) and MALDI–TOF analysis. The HPLC analysis conditions were as follows: Column Knauer RP Nucleosil-100 C18 (250 × 4 mm); mobile phase was a linear gradient of buffer A H_2O, 0.05% TFA and buffer B acetonitrile/H_2O (9:1), 0.05% TFA.; flow rate, 1.2 mL/min.

General

MALDI–TOF analysis was performed in the linear, high-mass, positive-ion mode with pulsed (time-delayed) extraction on a Kratos Maldi IV instrument (Shimadzu Deutschland, Duisburg, Germany). Samples (usually in 0.1% TFA) were either applied by a sandwich technique (in which 0.7 µL of matrix was dried onto the sample spot, followed by 0.7 µL of sample and then another 0.7 µL of matrix) or, for more concentrated samples, were simply mixed 1:10 with the matrix solution and 0.7 µL of this mixture was dried onto the stainless-steel sample holder. Matrix solutions were usually α-cyano-4-hydroxycinnamic acid [dissolved at 10 mg/mL in 50% acetonitrile, 50% 0.1% TFA (all % v/v)]. Spectra were calibrated by using near-external standards consisting of a mixture of fragment 1–4 of substance P ([M + H] *m*/*z* 497.6); angiotensin II ([M + H] *m*/*z* 1047.2); angiotensin I ([M + H] *m*/*z* 1297.5); fragment 1–13 of angiotensinogen ([M + H] *m*/*z* 1646.9); and oxidized insulin B chain ([M + H] *m*/*z* 3496.9). Absolute *m*/*z* values occasionally varied up to 1 Da depending on the individual calibration and the distance and time between the individual measurements; for these samples, spectra were recalibrated by using known *m*/*z* values of the largest peak(s). Spectra were collected and analyzed by using standard Kratos software (Sun OS, Release 5.4, OpenWindows Ver. 3.4, Kratos Kompact Software Ver. 5.2.0) and were usually the average of 50–100 individual laser shots across the width of the sample spot. Data were smoothed and baseline-corrected, generally with a window width of 30 channels.

Polymers linked to aminophalloidin

Poly-(L)-lysine (hydrobromide; M_r = 27500), and monomethoxy-polyethyleneglycolamine (M_r = 810, 5200, 22600) were coupled to aminophalloidin by the amine-reactive homobifunctional cross-linking reagents DSP (dithiobis(succinimidylpropionate); Lomant's reagent) with cleavable disulfide group, or DSS (disuccinimidyl suberate) containing a hydrocarbon chain instead of the disulfide group. DSP or DSS (248 µmol) were dissolved in 1.0 mL of *N*,*N*-dimethylformamide and added to 63 µmol dried aminophalloidin. The reaction was started with 2 µL triethylamine and allowed to proceed under magnetic stirring for 16 h at rt. The reaction was stopped with 10 mL diethyl ether and the mixture was centrifuged; after a second wash with ether, the sediment was dissolved in 5 mL

methanol and separated on a Sephadex-LH20 column with methanol as solvent. Yield of DSP-, and DSS-phalloidin was about 80%, purity >90% for both.

Seven milligrams DSP-, or DSS-phalloidin were dissolved in 0.5 mL *N*,*N*-dimethylformamide and 5 equiv of poly-(L)-lysine hydrobromide or poly-(D)-lysine hydrobromide added in 0.5 mL PBS. After reaction for 16 h at rt, high-molecular-weight products were separated by gel-filtration chromatography with Sephadex G-25 with 0.1% NaCl as eluant. After lyophilisation, the amount of phalloidin coupled to the polymer was determined from the characteristic absorption of phalloidin at 300 nm (ε = 10,100). We found that ca. 1 out of ca.10 lysine residues was spiked with aminophalloidin, independent of the molecular weight of the polymer. For modification of DSP-phalloidin and DSS-phalloidin with methoxypolyethyleneglycolamine, monomethoxypolyethyleneglycol was tosylated and reacted with ammonia to yield monomethoxy-PEG with a reactive amino group: 100 mg monomethoxy-PEG 810, 5,200 and 22,600 were dissolved in 1.0 mL of dry pyridine in a round-bottom flask on ice, and 5 equiv toluol-4-sulfonylchloride in 0.4 mL chloroform were added dropwise. After being stirred for 30 min, the reaction was stopped with 20 mL of diethyl ether. Sediment was dried in a rotation evaporator and reacted with 20 mL of methanol/2.5 N ammonia. After 1 h, the solvent was evaporated in vacuo and the aminomonomethoxy-PEG purified by Sephadex-LH20 chromatography. Ten milligrams DSP- or DSS-aminophalloidin were dissolved in 0.5 mL *N*,*N*-dimethylformamide and added to 1 equiv dry aminomonomethoxy-PEG. After reaction for 16 h at rt, phalloidin PEG 22,600 and phalloidin PEG 5,200 were purified on a Sephadex G25 column by using 0.1% NaCl as solvent, and phalloidin PEG 810 was purified on a Sephadex-LH20 column developed with methanol. The yield was 37% for phalloidin PEG 22,600, 34% for phalloidin PEG 5,200 and 45% for phalloidin PEG 810.

Affinity to rabbit muscle actin

Actin was prepared from rabbit muscle as described previously [36]. The binding assay was used with the following modifications: Freshly prepared G-actin solution was diluted in Tris-ATP buffer (2 mM of Tris; 0.2 mM ATP; 0.1 mM $CaCl_2$; 0.02% NaN_3; pH 7.8) to an extinction of 0.28 at 290 nm (null balance at 310 nm). Typically, 18 µL of a [^{3}H]-demethylphalloin methanolic solution (specific activity 9 Ci/mmol) was evaporated in a scintillation tube by a hot-air dryer, and 1.5 mL of G-actin solution was added. Polymerisation was initiated by addition of 12.5 µL 0.2 M $MgCl_2$. After 30 min incubation at room temperature the solution was filled up to ten volumes with Tris-ATP buffer and gently homogenized. Hydrophilic toxin derivatives were dissolved in potassium Tris-buffer (100 mM KCl, 1 mM Tris, pH 7.4). The concentration was determined spectrophotometrically at 300 nm (ε (300 nm) = 10100 M^{-1} cm^{-1}). Hydrophobic toxin derivatives, because of low solubility in aqueous solvents, were dissolved in methanol. Concentration was determined spectophotometrically at 300 nm. The methanolic solution was filled up to three volumes with potassium Tris-buffer, and a dilution series established down to a concentration of 10^{-7} M. Fifty microliters of this solution was added to 450 µL of the above actin solution and allowed to equilibrate for 1 h. Samples of 180 µL of this solution were transferred to Ti 42.2 centrifugation tubes (Beckman) and centrifuged at 40.000 rpm for 50 min at 10 °C. Twenty microliter aliquots of the supernatant were counted, and affinity values based on phalloidin = 1 were calculated from those concentrations of phallotoxins required for a 50% substitution of the [^{3}H]-demethylphalloin.

MTT proliferation assay

Mouse fibroblasts NIH 3T3 (generous donation from Prof. Traub, MPI Ladenburg), K562, HL-60 and Jurkat cells (ATCC) maintained in RPMI 1640 medium containing 10% fetal calf serum and 0.05 mM β-mercaptoethanol, were cultured at 37 °C in a humidified 95% air/5% CO_2 incubator. The cytotoxicity of phallotoxins was assessed by using the 3-(4,5-dimethylthiazol-2-yl)-2,5-diphenyltetrazolium bromide (MTT) assay. Exponentially growing cells were plated at a density of 2×10^4 cells/well in 96-well plates 24 h before the toxin was added in medium with up to 1% DMSO, with a volume equal to the volume of medium in the culture dish. The final concentrations of toxins in the media were between 10^{-3} and 10^{-9} M. At 72 h, the medium was replaced by serum-free medium containing 25 µL MTT solution (5 mg/mL in PBS), and the incubation was continued at 37 °C for 4 h. Then, lysis buffer (100 µL 20% SDS in 50% dimethylformamide) was added to each well and incubated for another 16–20 h. Viability of cells was determined by measuring the 570 nm absorbance of each well using a microplate reader (Molecular Devices). IC_{50} values were calculated as the concentration of toxin required to reduce the absorbance to 50% of the control cultures.

Microscopic studies

Exponentially growing fibroblasts were plated at a density of 2 × 104 cells/well in glass-bottom dishes 24 h before the fluorescently labeled peptides were added. The final concentration of the peptides was 10^{-5} M. After different incubation times the cells were washed with fresh medium, and microscopic studies were performed by using a confocal laser scanning microscope TCS SP2 (Leica Microsystems, Heidelberg/Mannheim, Germany), equipped with an inverted microscope DMIRE2 and an incubation chamber (Pe-Con Erbach, Germany). Image data stacks and time-lapse studies of the live cells were obtained at 37 °C and in 5% CO_2 atmosphere with a 100×/1.4 N.A.

oil immersion objective and CLSM software (Leica Microsystems). The data were processed with ImageJ software, optimizing images in brightness and contrast, and visualization of the fluorescing structures was performed on serial confocal optical sections.

Supporting Information

Supporting Information File 1

Structures of phalloidin derivatives and IC_{50} concentration values of cell growth inhibition.
[http://www.beilstein-journals.org/bjoc/content/supplementary/1860-5397-8-233-S1.pdf]

References

1. Wieland, T. *Peptides of Poisonous Amanita Mushrooms;* Springer Series in Molecular and Cell Biology; Springer: Berlin, Heidelberg, Germany, 1986.
2. Roeder, R. G.; Rutter, W. J. *Nature* **1969,** *224,* 234–237. doi:10.1038/224234a0
3. Chambon, P.; Gissinger, F.; Kedinger, C.; Mandel, J. L.; Meilhac, M. *The Cell Nucleus;* Academic Press: New York, 1974; Vol. III.
4. Wehland, J.; Weber, K. *Eur. J. Cell Biol.* **1981,** *24,* 176–183.
5. Wulf, E.; Deboben, A.; Bautz, F. A.; Faulstich, H.; Wieland, T. *Proc. Natl. Acad. Sci. U. S. A.* **1979,** *76,* 4498–4502. doi:10.1073/pnas.76.9.4498
6. Faulstich, H.; Trischmann, H.; Mayer, D. *Exp. Cell Res.* **1983,** *144,* 73–82. doi:10.1016/0014-4827(83)90443-3
7. Bushnell, D. A.; Cramer, P.; Kornberg, R. D. *Proc. Natl. Acad. Sci. U. S. A.* **2002,** *99,* 1218–1222. doi:10.1073/pnas.251664698
8. Fehrenbach, T.; Cui, Y.; Faulstich, H.; Keppler, D. *Naunyn Schmiedebergs Arch. Pharmacol.* **2003,** *368,* 415–420. doi:10.1007/s00210-003-0814-4
9. Meier-Abt, F.; Faulstich, H.; Hagenbuch, B. *Biochim. Biophys. Acta* **2004,** *1664,* 64–69. doi:10.1016/j.bbamem.2004.04.004
10. Letschert, K.; Faulstich, H.; Keller, D.; Keppler, D. *Toxicol. Sci.* **2006,** *91,* 140–149. doi:10.1093/toxsci/kfj141
11. Heitz, F.; Morris, M. C.; Divita, G. *Br. J. Pharmacol.* **2009,** *157,* 195–206. doi:10.1111/j.1476-5381.2009.00057.x
12. Jones, A. T.; Sayers, E. J. *J. Control. Release* **2012,** *161,* 582–591. doi:10.1016/j.jconrel.2012.04.003
13. Anderl, J. *Synthesis and cytotoxicity of membrane-permeable phallotoxins*, Doctoral Thesis, Heidelberg University, Germany, 2003.
14. Honeycutt, L.; Wang, J.; Ekrami, H.; Shen, W.-C. *Pharm. Res.* **1996,** *13,* 1373–1377. doi:10.1023/A:1016078118033
15. Bradley, M. O.; Swindell, C. S.; Anthony, F. H.; Witman, P. A.; Devanesan, P.; Webb, N. L.; Baker, S. D.; Wolff, A. C.; Donehower, R. C. *J. Control. Release* **2001,** *74,* 233–236. doi:10.1016/S0168-3659(01)00321-2
16. Wong, A.; Toth, I. *Curr. Med. Chem.* **2001,** *8,* 1123–1136. doi:10.2174/0929867013372535
17. Boutorin, A. S.; Gus'kova, L. V.; Ivanova, E. M.; Kobetz, N. D.; Zarytova, V. F.; Ryte, A. S.; Yurchenko, L. V.; Vlassov, V. V. *FEBS Lett.* **1989,** *254,* 129–132. doi:10.1016/0014-5793(89)81023-3
18. Letsinger, R. L.; Zhang, G. R.; Sun, D. K.; Ikeuchi, T.; Sarin, P. S. *Proc. Natl. Acad. Sci. U. S. A.* **1989,** *86,* 6553–6556. doi:10.1073/pnas.86.17.6553
19. Shea, R. G.; Masters, J. C.; Bischofberger, N. *Nucleic Acids Res.* **1990,** *18,* 3777–3783. doi:10.1093/nar/18.13.3777
20. Ryser, H. J.-P.; Shen, W.-C. *Proc. Natl. Acad. Sci. U. S. A.* **1978,** *75,* 3867–3870. doi:10.1073/pnas.75.8.3867
21. Leonetti, J. P.; Degols, G.; Lebleu, B. *Bioconj. Chem.* **1990,** *1,* 149–153. doi:10.1021/bc00002a010
22. Mulders, P.; Pang, S.; Dannull, J.; Kaboo, R.; Hinkel, A.; Michel, K.; Tso, C.-L.; Roth, M.; Belldegrun, A. *Cancer Res.* **1998,** *58,* 956–961.
23. Murphy, J. E.; Uno, T.; Hamer, J. D.; Cohen, F. E.; Dwarki, V.; Zuckermann, R. N. *Proc. Natl. Acad. Sci. U. S. A.* **1998,** *95,* 1517–1522. doi:10.1073/pnas.95.4.1517
24. Emi, N.; Kidoaki, S.; Yoshikawa, K.; Saito, H. *Biochem. Biophys. Res. Commun.* **1997,** *231,* 421–424. doi:10.1006/bbrc.1997.6125
25. Fawell, S.; Seery, J.; Daikh, Y.; Moore, C.; Chen, L. L.; Pepinsky, B.; Barsoum, J. *Proc. Natl. Acad. Sci. U. S. A.* **1994,** *91,* 664–668. doi:10.1073/pnas.91.2.664
26. Anderson, D. C.; Nichols, E.; Manger, R.; Woodle, D.; Barry, M.; Fritzberg, A. R. *Biochem. Biophys. Res. Commun.* **1993,** *194,* 876–884. doi:10.1006/bbrc.1993.1903
27. Allinquant, B.; Hantraye, P.; Mailleux, P.; Moya, K.; Bouillot, C.; Prochiantz, A. *J. Cell Biol.* **1995,** *128,* 919–927. doi:10.1083/jcb.128.5.919
28. Rothbard, J. B.; Garlington, S.; Lin, Q.; Kirschberg, T.; Kreider, E.; McGrane, P. L.; Wender, P. A.; Khavari, P. A. *Nat. Med.* **2000,** *6,* 1253–1257. doi:10.1038/81359
29. Torchilin, V. P.; Rammohan, R.; Weissig, V.; Levchenko, T. S. *Proc. Natl. Acad. Sci. U. S. A.* **2001,** *98,* 8786–8791. doi:10.1073/pnas.151247498
30. Wender, P. A.; Mitchell, D. J.; Pattabiraman, K.; Pelkey, E. T.; Steinman, L.; Rothbard, J. B. *Proc. Natl. Acad. Sci. U. S. A.* **2000,** *97,* 13003–13008. doi:10.1073/pnas.97.24.13003
31. Palm, K.; Luthman, K.; Ungell, A.-L.; Strandlund, G.; Artursson, P. *J. Pharm. Sci.* **1996,** *85,* 32–39. doi:10.1021/js950285r
32. Schiff, P. B.; Horwitz, S. B. *Proc. Natl. Acad. Sci. U. S. A.* **1980,** *77,* 1561–1565. doi:10.1073/pnas.77.3.1561
33. Perez, E. A. *Mol. Cancer Ther.* **2009,** *8,* 2086–2095. doi:10.1158/1535-7163.MCT-09-0366
34. Moldenhauer, G.; Salnikov, A. V.; Lüttgau, S.; Herr, I.; Anderl, J.; Faulstich, H. *J. Natl. Cancer Inst.* **2012,** *104,* 622–634. doi:10.1093/jnci/djs140
35. Veronese, F. M.; Mero, A. *BioDrugs* **2008,** *22,* 315–329. doi:10.2165/00063030-200822050-00004
36. Spudich, J. A.; Watt, S. *J. Biol. Chem.* **1971,** *246,* 4866–4871.

Beilstein Journal of Organic Chemistry

The multicomponent approach to *N*-methyl peptides: total synthesis of antibacterial (–)-viridic acid and analogues

Ricardo A. W. Neves Filho[1], Sebastian Stark[1,2], Bernhard Westermann[1,2] and Ludger A. Wessjohann[*1,2]

Full Research Paper

Open Access

Address:
[1]Department of Bioorganic Chemistry, Leibniz Institute of Plant Biochemistry, Weinberg 3, 06120 Halle (Saale), Germany, Tel: +49 345 5582 1301, Fax: +49 345 5582 1309 (Address for correspondence) and [2]Martin-Luther-University Halle-Wittenberg, Institute of Organic Chemistry, Kurt-Mothes-Str. 2, 06120 Halle (Saale), Germany

Email:
Ludger A. Wessjohann[*] - wessjohann@ipb-halle.de.

* Corresponding author

Keywords:
antibiotic; anticancer; Gram negative bacteria; natural product; peptide coupling; peptides; peptoid; toxin; Ugi reaction

Beilstein J. Org. Chem. **2012,** *8,* 2085–2090.
doi:10.3762/bjoc.8.234

Received: 10 August 2012
Accepted: 30 October 2012
Published: 28 November 2012

This article is part of the Thematic Series "Antibiotic and cytotoxic peptides".

Guest Editor: N. Sewald

Abstract

Two syntheses of natural viridic acid, an unusual triply *N*-methylated peptide with two anthranilate units, are presented. The first one is based on peptide-coupling strategies and affords the optically active natural product in 20% overall yield over six steps. A more economical approach with only four steps leads to the similarly active racemate by utilizing a Ugi four-component reaction (Ugi-4CR) as the key transformation. A small library of viridic acid analogues is readily available to provide first SAR insight. The biological activities of the natural product and its derivatives against the Gram-negative bacterium *Aliivibrio fischeri* were evaluated.

Introduction

Viridic acid (**1**) is a tetrapeptide produced by several fungi of the genus *Penicillium*, including *P. viridicatum*, *P. nordicum*, and *P. aurantiogriseum* among others [1-4]. It was first isolated from the basic fraction of the chloroform/methanol extract of *P. viridicatum* Westling [5], and it was assumed to be responsible for the toxicity of this extract due to its metal-chelating properties [6]. Later, this (putative) mycotoxin was also found in cultures of *P. nordicum* cultivated on cheese agar medium. The crude extracts from these cultures displayed pronounced cytotoxicity in a MTT assay on an undisclosed cell line [7].

Albeit that these two reports on the toxicity of extracts containing constituent **1** were very intriguing, no further biological screening of the pure substance has been performed to date. The connection between compound **1** and the bioactivity of the extract containing it is thus purely correlative, i.e., speculative. No causal relationship between the compound and the MTT results is proven.

The structure of compound **1** was determined as the peptide $N(Me)_2$Ant-Gly-(N-Me)Val-Ant (Ant = anthranilic acid) in 1986, based on a series of degradation experiments, NMR, and IR measurements as well as a first total synthesis [5]. Thus, it was revealed that **1** belongs to the small group of natural peptides that contain anthranilic acid residues in the peptidic backbone [8-10]. Furthermore, to the best of our knowledge, viridic acid is unique in its N-terminus, which bears a *N*,*N*-dimethyl anthranilic amide moiety of still unknown biosynthetic origin. The previously reported synthetic strategy toward **1** was based upon a series of peptide couplings employing DCC reagent [5]. The necessity of difficult-to-perform peptide couplings with phenyl carboxylates and *N*-methylated amino groups demanded harsher than usual conditions, upon which the desired viridic acid (**1**) was obtained in just 5% overall yield.

The lack of sufficient amounts of isolated materials from natural sources did not allow for reliable bioactivity tests, and the demand for higher quantities and derivatives of viridic acid (**1**), required the development of a more efficient and milder approach. In this endeavor we envisioned two routes. The first one uses improved peptide-coupling protocols, leading to the natural enantiomer (Scheme 1) [11]. The blueprint of the synthesis was planned as a bidirectional sequence from the least- to the most-reactive amine (NMe-Val < H-Ant-OBn < H-Gly) to yield the protected tetrapeptide **2** (Scheme 1a). Alternatively, a multicomponent (MCR) approach based on a Ugi four-component reaction (Ugi-4CR) of dipeptide **3**, isobutyraldehyde, methylamine and isonitrile **4** as the key transformation was envisioned to yield racemic viridic acid (±)-**1** (Scheme 1b) [12]. Besides furnishing the desired natural product in only four steps, the MCR approach allows a ready access to analogues endowed with a proteolysis-resistant peptoid moiety [13]. Recently, we demonstrated that chemically more stable peptoid analogues of tubulysins, named tubugis, present cytotoxicity against cancer cell lines comparable to the native natural product [14]. Thus, it was hoped that some viridic acid analogues readily accessible by MCR may also display enhanced biological activity or at least stability.

Results and Discussion

The 2-CR approach based on the peptide coupling of Boc-Gly and NMe-Val-OMe in the presence of EDCl and HOAt gave the central dipeptide **5** in 73% yield (Scheme 2) [15].The use of even more activating coupling reagents, such as HATU and BOP, was also investigated and resulted in increased formation of side products [11]. After saponification of intermediate **5** to dipeptide **6**, the latter was coupled with benzyl anthranilate. This reaction was particularly challenging due to the very poor

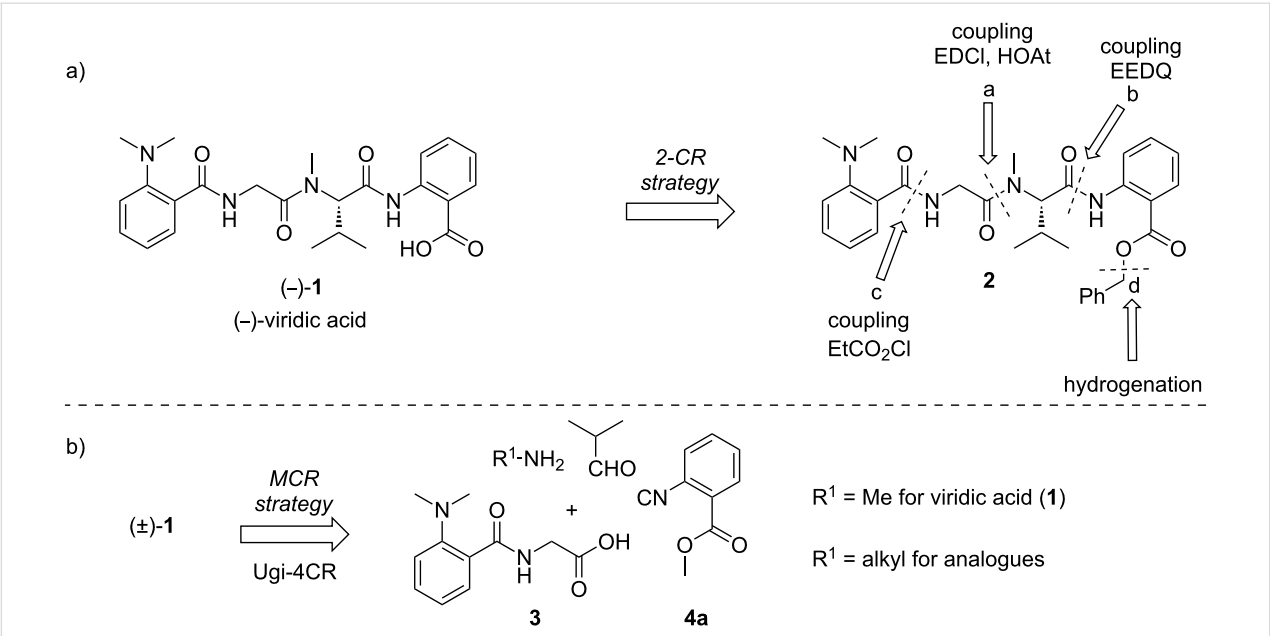

Scheme 1: Retrosynthetic strategies for (−)-viridic acid (**1**) and analogues by (a) a bidirectional peptide-coupling sequence, and (b) a novel MCR approach.

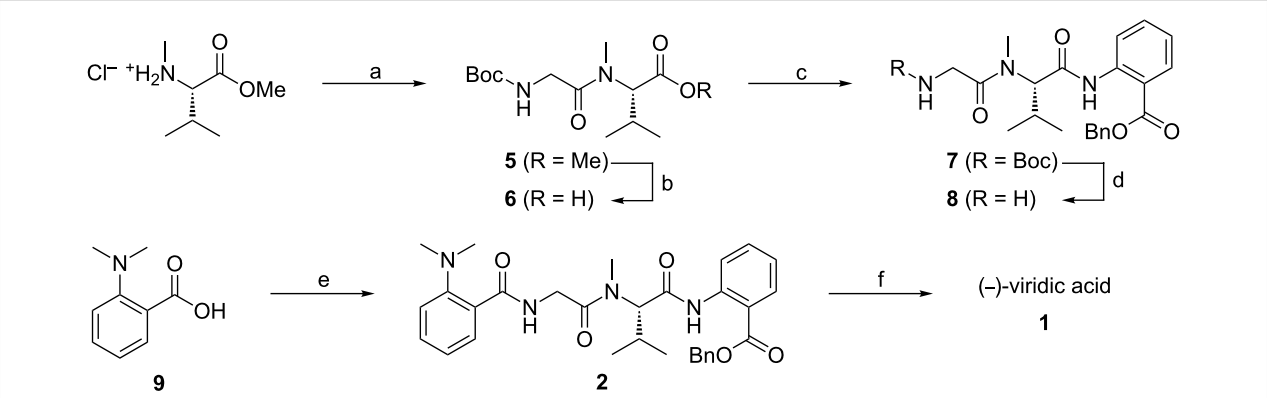

Scheme 2: Reactions and conditions: (a) Boc-Gly-OH, EDCI, HOAt, TEA, CH_2Cl_2, rt, 20 h, 73%. (b) LiOH, THF/H_2O (1:1), rt, 3 h, 97%. (c) Benzyl anthranilate, EEDQ, $CHCl_3$, rt, 20 h, 51%. (d) TFA, CH_2Cl_2, rt, 5 h. quant. (e) **8**, NMM, ethyl chloroformate, $CHCl_3$, rt, 20 h, 85%. (f) H_2, 10% Pd/C, MeOH, rt, 16 h, 92%.

reactivity of this combination [10]. All attempts to perform this coupling with carbodiimides, HBTU, HATU, and PyBroP failed or resulted in very low conversions. The addition of a catalytic amount of DMAP to the carbodiimide-mediated reactions improved the conversions, but resulted in severe racemization. The best result was obtained by employing *N*-ethoxycarbonyl-2-ethoxy-1,2-dihydroquinoline (EEDQ) as coupling reagent, which gave the optically active tripeptide **7** in 51% yield [16,17]. Intermediate **7** was converted into amine **8** under acidic conditions, and coupled directly to *N*,*N*-dimethylanthranilic acid (**9**). It was already reported that carbodiimide-mediated couplings involving aromatic carboxylic acids such as **9** can result in the formation of *N*-acylurea adducts through competitive N–O rearrangement [18,19]. In order to overcome this problem the mixed-carbonate method was used [20]. The reaction resulted in the desired optically active key intermediate **2** in 85% yield. Its hydrogenation afforded the desired (−)-viridic acid (**1**) in quantitative conversion and >92% isolated yield, i.e., in 20% overall yield. Analytical data such as the HRMS, ^{1}H NMR, melting point, and optical rotation of synthetic compound **1** are consistent with the data reported for the natural substance (Scheme 2) [5].

In order to more rapidly access derivatives for biological activity screens, we decided to investigate the suitability of a MCR approach utilizing the Ugi reaction. Due to the character of the Ugi-4CR, the racemate of viridic acid and congeners is easily available, and assaying with (±)-**1** can give an estimation of the relevance or effect of the configuration of the asymmetric center on the biological activity. With this goal in mind, the Ugi-4CR between methylamine, isobutyraldehyde, dipeptide **3**, and the anthranilate-derived isonitrile **4a** was planned (Scheme 1) [21]. For the synthesis of the N-terminal dipeptide **3**, amino acid **9** was coupled with benzyl glycinate in the presence of ethyl chloroformate to give **10** in 88% yield. This intermediate was hydrogenated to afford the dipeptide acid **3** quantitatively. An alternative multicomponent approach to dipeptide **3** requires the use of ammonia or an ammonia equivalent, such as 2,4-dimethoxybenzylamine (DMB-NH_2), as amino component, formaldehyde as oxo-component, and a convertible isonitrile [22-25]. Although many convertible isonitriles are reported in the literature [24,26], the recently developed 4-isocyanopermethylbutane-1,1,3-triol (IPB) was chosen due to its ease of preparation, better reactivity, and mild conversion conditions [27]. The Ugi-4CR involving carboxylic acid **9**, DMB-NH_2, formaldehyde and IPB resulted in intermediate **11** in 35% yield. A tandem DMB group cleavage/pyrrole-formation sequence under acidic conditions followed by saponification afforded the desired carboxylic acid **3** in 21% yield over the two steps (Scheme 3). The MCR approach to building block **3** with two convertible components gives lower yields compared to the classical amide formation, but it carries the diversity-generating ability inherent in Ugi-4CRs, and the potential to synthesize derivatives where classical methods are less suitable.

The key Ugi-4CR combining isobutyraldehyde, methylamine (**12a**), dipeptidic carboxylate **3** and anthranilic isonitrile **4a**, to form the final tetrapeptide backbone was performed by using standard protocols, with imine preformation in methanol, to give **13a** in 51% yield. Finally, saponification of **13a** afforded the racemic viridic acid (±)-**1** in 83% yield. Attempts to improve the MCR yield with conventional or microwave heating, or by employing trifluoroethanol or DMF as solvents resulted in poor conversions, with competitive Passerini reaction in the latter case [28,29]. With the general process in place, the MCR approach was employed to generate a library of synthetic derivatives of **1** with the hope of gaining a first glimpse of structure–activity relationships (SAR), and to give hints for further applications, as for example for attachment points for

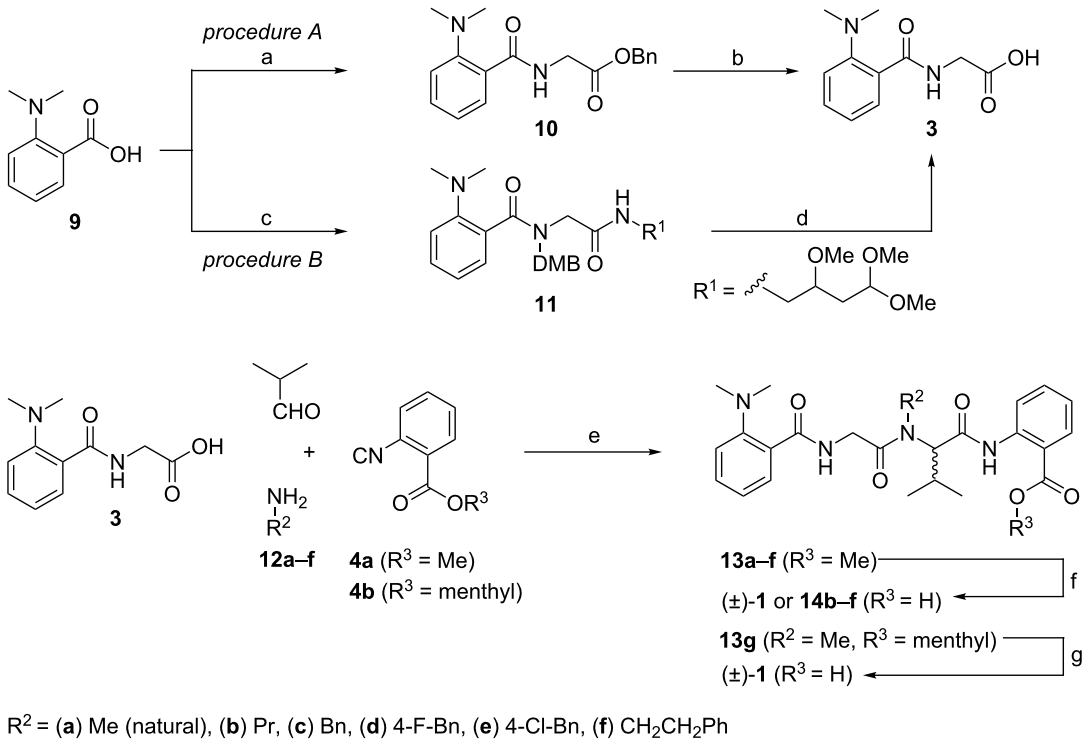

Scheme 3: Reactions and conditions: (a) H-Gly-OBn·HCl, NMM, ethyl chloroformate, $CHCl_3$, 18 h, rt, 88%. (b) H_2, 10% Pd/C, MeOH, rt, 16 h, 98%. (c) 2,4-Dimethoxybenzylamine, formaldehyde, IPB, MeOH, rt, 18 h, 35%. (d) TFA, CH_2Cl_2, 0 °C to rt, 48 h, then LiOH, THF/H_2O (1:1), rt, 3 h, 21% (over two steps). (e) MeOH, rt, 20 h, 51–70%. (f) LiOH, THF/H_2O, rt, 8 h, 81–91%. (g) KOH, MeOH/H_2O (3:1), rt, 8 h, 70%.

probe design and experiments [30,31]. Thus, methylamine was substituted by **12b**–**f** in the key Ugi-4CR to yield the intermediates **13b**–**f** (55–70% yields) [16], which afforded the desired peptoid analogues **14b**–**f** after saponification. Compared to simple peptides, N-alkylated ones (peptoid moieties) allow different low-energy conformations, and contrary to common belief they are more restricted in conformational space [32]. Moreover, they commonly possess a higher lipophilicity and protease stability, and this combination seems to improve their antibiotic properties (Scheme 3) [13].

Since the MCR results in racemates, we decided to investigate the applicability of a chiral auxiliary MCR approach for the asymmetric synthesis of viridic acid (**1**). The Ugi-4CR is not specifically prone to asymmetric induction, but at least some auxiliaries are known to result in preferential formation of a diastereoisomer [33,34]. Therefore, the isonitrile **4b** was synthesized from menthyl anthranilate. The Ugi-4CR of **4b** in analogy to the reaction of **4a** with methylamine (**12a**) gave the desired peptoid–peptide adduct **13g** in 47% yield, albeit as a 1:1 diastereomeric mixture. Unfortunately, even a separation of the epimers failed by using thin- or thick-layer or conventional column chromatography or HPLC, under varied conditions of different column types, methods, mobile-phase compositions, etc. This is in accordance with earlier results, where also no or only negligible diastereoselection could be achieved [35,36]. Saponification of the menthyl ester **13g** afforded the racemic viridic acid (**1**) again in 70% yield (Scheme 3) [37].

To our knowledge no biological screening of pure (−)-viridic acid or its analogues has been performed, and due to the potential of natural peptides and peptoids as antibacterial agents [13,38-47], it was decided to investigate their activity against the Gram-negative bacterium *Aliivibrio fischeri* [48]. Compounds (−)-**1** and (±)-**1** were the most active ones with IC_{50} values of 45.0 ± 4.4 and 38.4 ± 5.8 μM, respectively. In this test system, derivatives **14b**–**f** displayed IC_{50} values above 100 μM and can be considered as inactive. Although (−)-viridic acid (**1**) was isolated thirty years ago, this is the first unambiguous report concerning its biological activity. Based upon the results presented above, it seems that the configuration of the stereogenic center has almost no influence on the antibacterial effect of **1**. The lack of activity of the derivatives **14b**–**f** is difficult to rationalize without knowing the target, but it demonstrates that the size of the group attached to the nitrogen of the Val residue has a clear influence. This fact suggests that **1** does not act just by engaging bacterial membranes as most antibacterial peptides do [49], but that it may bind to a specific target.

Conclusion

These results highlight the usefulness of the Ugi-4CR for the diversity-oriented synthesis of natural *N*-methyl peptides, such as viridic acid and its derivatives. Considering the attractiveness of the anthranilic acid moiety as a promising building block for drug-like molecules and the diverse properties exhibited by natural products containing it [8,50], further biological trials involving such components are currently being pursued. The advantages of the MCR protocol are speed, variability, insensitivity to steric crowding, safe peptoid-moiety formation, and access to equally distributed stereoisomers (which can be a disadvantage though, once the most active isomer is identified).

The improved classical approach gave the natural product in much lower overall yield and more steps but, after careful choice of conditions, in optically pure form. A set of N-alkylated derivatives were screened against *Aliivibrio fischeri*, but only the (*N*-methylated) natural product displayed noteworthy activity of ca. 40 μM IC_{50}, independent of stereochemistry.

Supporting Information

Supporting Information File 1

Complete experimental procedures and characterization.
[http://www.beilstein-journals.org/bjoc/content/supplementary/1860-5397-8-234-S1.pdf]

Supporting Information File 2

Figures of ^{1}H and ^{13}C NMR spectra.
[http://www.beilstein-journals.org/bjoc/content/supplementary/1860-5397-8-234-S2.pdf]

Acknowledgements

The authors acknowledge support from the state of Saxony-Anhalt (MK-LSA, WZW project “Lipopeptide”). We thank Dr. Jürgen Schmidt and Ms. Annett Werner for HRMS and HPLC support, respectively. R.A.W.N.F. is grateful to Brazilian funds from CNPq for a Ph.D. fellowship.

References

1. Bräse, S.; Encinas, A.; Keck, J.; Nising, C. F. *Chem. Rev.* **2009,** *109,* 3903–3990. doi:10.1021/cr050001f
2. Filtenborg, O.; Frisvad, J. C.; Thrane, U. *Int. J. Food Microbiol.* **1996,** *33,* 85–102. doi:10.1016/0168-1605(96)01153-1
3. Frisvad, J. C.; Smedsgaard, J.; Larsen, T. O.; Samson, R. A. *Stud. Mycol.* **2004,** 201–241.
4. Lund, F.; Frisvad, J. C. *Mycol. Res.* **1994,** *98,* 481–492. doi:10.1016/S0953-7562(09)80466-8
5. Holzapfel, C. W.; Koekemoer, J. M.; van Dyk, M. S. *S. Afr. J. Chem.* **1986,** *39,* 75–80.
6. Burkhard, R. *Angew. Chem., Int. Ed. Engl.* **1967,** *6,* 885. doi:10.1002/anie.196708851
7. Larsen, T. O.; Gareis, M.; Frisvad, J. C. *J. Agric. Food Chem.* **2002,** *50,* 6148–6152. doi:10.1021/jf020453i
8. Komatsu, K.; Shigemori, H.; Kobayashi, J. *J. Org. Chem.* **2001,** *66,* 6189–6192. doi:10.1021/jo0156767
9. Lan, H.-Q.; Ye, J.-L.; Wang, A.-E.; Ruan, Y.-P.; Huang, P.-Q. *Chem.–Eur. J.* **2011,** *17,* 958–968. doi:10.1002/chem.201002063
10. Nakao, K.; Hamada, Y.; Shioiri, T. *Chem. Pharm. Bull.* **1989,** *37,* 930–932. doi:10.1248/cpb.37.930
11. Han, S.-Y.; Kim, Y.-A. *Tetrahedron* **2004,** *60,* 2447–2467. doi:10.1016/j.tet.2004.01.020
12. De Moliner, F.; Banfi, L.; Riva, R.; Basso, A. *Comb. Chem. High Throughput Screening* **2011,** *14,* 782–810. doi:10.2174/138620711796957099
13. Miller, S. M.; Simon, R. J.; Ng, S.; Zuckermann, R. N.; Kerr, J. M.; Moos, W. H. *Drug Dev. Res.* **1995,** *35,* 20–32. doi:10.1002/ddr.430350105
14. Pando, O.; Stark, S.; Denkert, A.; Porzel, A.; Preusentanz, R.; Wessjohann, L. A. *J. Am. Chem. Soc.* **2011,** *133,* 7692–7695. doi:10.1021/ja2022027
15. Boger, D. L.; Lee, J. K. *J. Org. Chem.* **2000,** *65,* 5996–6000. doi:10.1021/jo000382r
16. Belleau, B.; Malek, G. *J. Am. Chem. Soc.* **1968,** *90,* 1651–1652. doi:10.1021/ja01008a045
17. Akazome, M.; Enzu, M.; Takagi, K.; Matsumoto, S. *Chirality* **2011,** *23,* 568–573. doi:10.1002/chir.20972
18. Ślebioda, M. *Tetrahedron* **1995,** *51,* 7829–7834. doi:10.1016/0040-4020(95)00400-3
19. Neves Filho, R. A. W.; de Oliveira, R. N.; Srivastava, R. M. *J. Braz. Chem. Soc.* **2007,** *18,* 1410–1414. doi:10.1590/S0103-50532007000700018
20. Joullie, M. M.; Lassen, K. M. *ARKIVOC* **2010,** No. viii, 189–250.
21. Kobayashi, K.; Nakashima, T.; Mano, M.; Morikawa, O.; Konishi, H. *Chem. Lett.* **2001,** 602–603. doi:10.1246/cl.2001.602
22. Abbas, M.; Wessjohann, L. *Org. Biomol. Chem.* **2012,** *10,* 9330–9333. doi:10.1039/c2ob26552d
23. de Greef, M.; Abeln, S.; Belkasmi, K.; Dömling, A.; Orru, R. V. A.; Wessjohann, L. A. *Synthesis* **2006,** 3997–4004. doi:10.1055/s-2006-950335
24. Pick, R.; Bauer, M.; Kazmaier, U.; Hebach, C. *Synlett* **2005,** 757–760. doi:10.1055/s-2005-863722
25. Nenajdenko, V. G., Ed. *Isocyanide Chemistry: Applications in Synthesis and Material Science;* Wiley-VCH: Weinheim, Germany, 2012. doi:10.1002/9783527652532
26. Kreye, O.; Westermann, B.; Wessjohann, L. A. *Synlett* **2007,** 3188–3192. doi:10.1055/s-2007-990912
27. Neves Filho, R. A. W.; Stark, S.; Morejon, M. C.; Westermann, B.; Wessjohann, L. A. *Tetrahedron Lett.* **2012,** *53,* 5360–5363. doi:10.1016/j.tetlet.2012.07.064
28. Barreto, A. D. F.; Vercillo, O. E.; Birkett, M. A.; Caulfield, J. C.; Wessjohann, L. A.; Andrade, C. K. Z. *Org. Biomol. Chem.* **2011,** *9,* 5024–5027. doi:10.1039/c1ob05471f
29. Rhoden, C. R. B.; Rivera, D. G.; Kreye, O.; Bauer, A. K.; Westermann, B.; Wessjohann, L. A. *J. Comb. Chem.* **2009,** *11,* 1078–1082. doi:10.1021/cc900106u
30. Brauch, S.; Henze, M.; Osswald, B.; Naumann, K.; Wessjohann, L. A.; van Berkel, S. S.; Westermann, B. *Org. Biomol. Chem.* **2012,** *10,* 958–965. doi:10.1039/c1ob06581e

31. Neves Filho, R. A. W.; Westermann, B.; Wessjohann, L. A. *Beilstein J. Org. Chem.* **2011,** *7,* 1504–1507. doi:10.3762/bjoc.7.175
32. Brandt, W.; Herberg, T.; Wessjohann, L. *Biopolymers* **2011,** *96,* 651–668. doi:10.1002/bip.21620
33. van Berkel, S. S.; Bögels, B. G. M.; Wijdeven, M. A.; Westermann, B.; Rutjes, F. P. J. T. *Eur. J. Org. Chem.* **2012,** 3543–3559. doi:10.1002/ejoc.201200030
34. Dömling, A.; Beck, B.; Eichelberger, U.; Sakamuri, S.; Menon, S.; Chen, Q.-Z.; Lu, Y.; Wessjohann, L. A. *Angew. Chem., Int. Ed.* **2006,** *45,* 7235–7239. doi:10.1002/anie.200601259
35. Pirrung, M. C.; Ghorai, S.; Ibarra-Rivera, T. R. *J. Org. Chem.* **2009,** *74,* 4110–4117. doi:10.1021/jo900414n
36. Zhdanko, A. G.; Nenajdenko, V. G. *J. Org. Chem.* **2009,** *74,* 884–887. doi:10.1021/jo802420c
37. Er, M.; Coskun, N. *ARKIVOC* **2009,** No. xii, 153–160.
38. Boman, H. G. *J. Int. Med.* **2003,** *254,* 197–215. doi:10.1046/j.1365-2796.2003.01228.x
39. Mejías, X.; Feliu, L.; Planas, M.; Bardají, E. *Tetrahedron Lett.* **2006,** *47,* 8069–8071. doi:10.1016/j.tetlet.2006.09.057
40. Ryge, T. S.; Hansen, P. R. *Bioorg. Med. Chem.* **2006,** *14,* 4444–4451. doi:10.1016/j.bmc.2006.02.034
41. Shuey, S. W.; Delaney, W. J.; Shah, M. C.; Scialdone, M. A. *Bioorg. Med. Chem. Lett.* **2006,** *16,* 1245–1248. doi:10.1016/j.bmcl.2005.11.075
42. Long Zhu, W.; Park, Y.; Park, I.-S.; Sun Park, Y.; Kim, Y.; Hahm, K.-S.; Yub Shin, S. *Protein Pept. Lett.* **2006,** *13,* 719–725. doi:10.2174/092986606777790575
43. Hoffmann, B.; Ast, T.; Polakowski, T.; Reineke, U.; Volkmer, R. *Protein Pept. Lett.* **2006,** *13,* 829–833. doi:10.2174/092986606777841299
44. Wessjohann, L. A.; Andrade, C. K. Z.; Vercillo, O. E.; Rivera, D. G. *Targets Heterocycl. Syst.* **2006,** *10,* 24–53.
45. Lim, S. S.; Yoon, S.-P.; Park, Y.; Zhu, W. L.; Park, I.-S.; Hahm, K.-S.; Shin, S. Y. *Biotechnol. Lett.* **2006,** *28,* 1431–1437. doi:10.1007/s10529-006-9107-6
46. Au, V. S.; Bremner, J. B.; Coates, J.; Keller, P. A.; Pyne, S. G. *Tetrahedron* **2006,** *62,* 9373–9382. doi:10.1016/j.tet.2006.07.059
47. Chongsiriwatana, N. P.; Patch, J. A.; Czyzewski, A. M.; Dohm, M. T.; Ivankin, A.; Gidalevitz, D.; Zuckermann, R. N.; Barron, A. E. *Proc. Natl. Acad. Sci. U. S. A.* **2008,** *105,* 2794–2799. doi:10.1073/pnas.0708254105
48. Backhaus, T.; Froehner, K.; Altenburger, R.; Grimme, L. H. *Chemosphere* **1997,** *35,* 2925–2938. doi:10.1016/S0045-6535(97)00340-8
49. Horne, S. *Expert Opin. Drug Discovery* **2011,** *6,* 1247–1262. doi:10.1517/17460441.2011.632002
50. Congiu, C.; Cocco, M. T.; Lilliu, V.; Onnis, V. *J. Med. Chem.* **2005,** *48,* 8245–8252. doi:10.1021/jm050711d

License and Terms